

**OBSERVATION AND CATALYTIC PROMISCUITY OF  
RETAINING GLYCOSIDASE INTERMEDIATES**

By

DAVID LOUIS ZECHEL

B.Sc., The University of Toronto, 1995

A THESIS SUBMITTED IN PARTIAL FULFILLMENT OF  
THE REQUIREMENTS FOR THE DEGREE OF

DOCTOR OF PHILOSOPHY

in

THE FACULTY OF GRADUATE STUDIES

(Department of Chemistry)

We accept this thesis as conforming  
to the required standard

THE UNIVERSITY OF BRITISH COLUMBIA

July 2001

© David Louis Zechel, 2001

In presenting this thesis in partial fulfilment of the requirements for an advanced degree at the University of British Columbia, I agree that the Library shall make it freely available for reference and study. I further agree that permission for extensive copying of this thesis for scholarly purposes may be granted by the head of my department or by his or her representatives. It is understood that copying or publication of this thesis for financial gain shall not be allowed without my written permission.

Department of Chemistry

The University of British Columbia  
Vancouver, Canada

Date July 6/01

## Abstract

This thesis is divided into two parts. The first addresses basic issues of retaining glycosidase mechanism. This includes the use of a new technique, time-resolved electrospray mass spectrometry, to directly monitor changes in the mass of *Bacillus circulans*  $\beta$ -xyylanase during its catalytic cycle. This enabled the pre-steady state kinetic parameters for the reaction it catalyses to be determined, which were in turn validated by traditional stopped-flow spectrophotometry. This study is followed by the characterization of the *Cellulomonas fimi*  $\beta$ -mannosidase (Man2A) by site-directed mutagenesis, pH-rate dependencies, Brønsted relationships and kinetic isotope effects. The contribution of the substrate 2-hydroxyl to catalysis in Man2A is also evaluated. The second part of this thesis describes the development of 'glycosynthases' from nucleophile mutants of Man2A, *Agrobacterium* sp.  $\beta$ -glucosidase (Abg) and *Streptomyces lividans* endoglucanase (CelB). When provided with  $\alpha$ -glycosyl fluoride donors and glycoside acceptors these mutant glycosidases synthesize glycosidic bonds. In all three cases higher glycosylation activity is observed with serine nucleophile mutants than with the corresponding alanine mutants. This is ascribed to stabilization of the departing fluoride in the glycosylation transition state by the serine hydroxyl group, most likely through a hydrogen bond. Glycosidic bond cleaving activity can be restored to these nucleophile mutants by providing a small exogenous anion such as azide or formate. In addition to recovering bond cleaving activity with azide and formate, Abg and Man2A nucleophile mutants are also rescued by halides, including fluoride. This is an exceedingly rare form of enzymatic catalysis, as well as a dramatic example of how a variety of chemistries, or catalytic promiscuity, can develop from a single enzyme active site.

# Table of Contents

<b>OBSERVATION AND CATALYTIC PROMISCUITY OF RETAINING GLYCOSIDASE INTERMEDIATES .....</b>	<b>1</b>
Abstract .....	ii
Table of Contents .....	iii
List of Figures .....	vi
List of Tables.....	x
Abbreviations .....	xi
Acknowledgments.....	xii
Dedication.....	xiii
<b>CHAPTER 1 INTRODUCTION TO RETAINING GLYCOSIDASE MECHANISMS</b>	<b>1</b>
The Legacy of David Phillips .....	2
Emerging From the Shadow of Lysozyme.....	3
<i>Structural biology of glycosidases</i> .....	6
<i>Defining rate-determining steps</i> .....	7
<i>Transition state structure</i> .....	8
<i>Acid-base catalysis</i> .....	12
<i>Substrate distortion</i> .....	15
<i>Covalent intermediates</i> .....	16
Objectives of This Thesis: Glycosidase Mechanisms.....	19
<b>CHAPTER 2 APPLICATION OF MASS SPECTROMETRY TO ENZYME KINETICS</b>	<b>21</b>
.....	
Introduction to ESI-MS and Time-Resolved ESI-MS .....	22
Application of Time-resolved ESI-MS to <i>Agrobacterium</i> sp. $\beta$ -glucosidase.....	26
Application of Time-resolved ESI-MS to <i>Bacillus circulans</i> Xylanase .....	30
<i>Steady-state kinetics and stopped-flow spectroscopy</i> .....	31
<i>Observation of the covalent intermediate by time-resolved ESI-MS</i> .....	32
<i>Pre-steady state kinetic analysis by time-resolved ESI-MS</i> .....	34
<i>Non-covalent enzyme-substrate complexes</i> .....	35
<i>Stopped-flow UV-Vis spectroscopy vs time-resolved ESI-MS</i> .....	36
Conclusions and Epilogue.....	37
<b>CHAPTER 3 MECHANISTIC INVESTIGATIONS INTO THE RETAINING <math>\beta</math>-MANNOSIDASE <i>CELLULOMONAS FIMI</i> MAN2A.....</b>	<b>39</b>
<i>Cellulomonas fimi</i> $\beta$ -mannosidase Man2A .....	40
Synthesis of Substrates for Man2A.....	41
Brønsted Analysis of Man2A.....	44
pH-Rate Dependence of Man2A .....	48
Identification of the General Acid-Base Catalyst in Man2A .....	49
Kinetic Isotope Effects .....	53
Evaluating the Role of the 2-Hydroxyl in Catalysis .....	54

Conclusions .....	55
<b>CHAPTER 4 INTRODUCTION TO GLYCOSYL TRANSFER REACTIONS AND GLYCOSYNTHASES .....</b>	<b>56</b>
Glycosides in Biology .....	57
'Chemical' Synthesis of Glycosidic Bonds.....	59
Glycosyltransferases .....	61
Glycosidases.....	65
<i>Inverting glycosidases</i> .....	65
<i>Retaining glycosidases</i> .....	66
Glycosynthases.....	70
Objectives of This Thesis: Glycosynthases.....	76
<b>CHAPTER 5 ENGINEERING ENHANCED GLYCOSYNTHASE ACTIVITY IN AGROBACTERIUM SP. <math>\beta</math>-GLUCOSIDASE .....</b>	<b>77</b>
Improving Glycosynthase Activity .....	78
Transglycosylation Kinetics with Abg E358 mutants.....	80
Synthesis of Oligosaccharides With Abg E358S .....	82
Chemical Rescue of Abg E358 Mutants .....	83
Brønsted Analysis of Abg E358G.....	88
Contribution of the Substrate 2-Hydroxyl to Chemical Rescue and Transglycosylation .....	89
Donor Interactions in the Glycosynthase Transition State.....	89
Acceptor Interactions with Glycosynthases .....	92
A Kinetic Model for Chemical Rescue of Retaining Glycosidase Nucleophile Mutants .....	93
Prediction of Glycosynthase Activity .....	96
Conclusions .....	98
<b>CHAPTER 6 DEVELOPMENT OF A MANNOSYNTHASE FROM <i>CELLULOMONAS</i> <i>FIMI</i> <math>\beta</math>-MANNOSIDASE MAN2A.....</b>	<b>100</b>
Chemical and Enzymatic Synthesis of $\beta$ -Mannosides .....	101
Engineering a $\beta$ -Mannosynthase.....	102
Transglycosylation Kinetics with Man2A E519A and E519S.....	104
Azide rescue of Man2A E519A and E519S.....	106
Conclusions .....	108
<b>CHAPTER 7 DEVELOPMENT OF A 'CELLULOSYNTHASE' FROM <i>STREPTOMYCES LIVIDANS</i> ENDOGLUCANASE CELB.....</b>	<b>109</b>
Introduction .....	110
Steady-State and Inactivation Kinetics of CelB.....	111
Identification of the Catalytic Nucleophile of CelB .....	114
Structural Features of Family 12 Glycosidases.....	116
Glycosynthase Activity of CelB Nucleophile Mutants.....	118
Conclusions .....	121

<b>CHAPTER 8 ENZYMATIC SYNTHESIS OF CARBON-FLUORINE BONDS .....</b>	<b>122</b>
Mechanisms of Enzymatic Halogenation.....	123
Nucleophilic Fluorination by Glycosynthases .....	125
Hydrogen Bonding to Fluoride .....	128
Kinetic Isotope Effects .....	129
Glycosynthases as Halogenases .....	129
Fluorination Activity of a General Acid-Base Mutant.....	131
Conclusions .....	133
Catalytic Promiscuity .....	134
<b>EXPERIMENTAL METHODS.....</b>	<b>136</b>
Chapter 2: Application of Mass Spectrometry to Enzyme Kinetics .....	137
Chapter 3: Mechanistic Investigations into the Retaining $\beta$ -Mannosidase <i>Cellulomonas fimi</i> Man2A .....	140
Chapter 5: Engineering Enhanced Glycosynthase Activity in <i>Agrobacterium</i> sp. $\beta$ -glucosidase .....	159
Chapter 6: Development of a Mannosynthase from <i>Cellulomonas fimi</i> Man2A.....	172
Chapter 7: Development of a 'Cellulosynthase' from <i>Streptomyces lividans</i> endoglucanase CelB.....	199
Chapter 8: Enzymatic Synthesis of Carbon-Fluorine Bonds .....	205
<b>APPENDIX A .....</b>	<b>209</b>
<b>APPENDIX B.....</b>	<b>211</b>
<b>APPENDIX C .....</b>	<b>214</b>
<b>APPENDIX D .....</b>	<b>215</b>
<b>REFERENCES .....</b>	<b>218</b>

# List of Figures

Figure 1-1: The venerable lysozyme mechanism proposed by David Phillips.....	2
Figure 1-2: Generalized mechanisms for inverting and retaining glycosidases. ....	5
Figure 1-3: Mechanism for HEWL proposed by Lowe involving substrate assisted catalysis. ....	6
Figure 1-4: Brønsted relationship for a series of aryl $\beta$ -glucosides with <i>Agrobacterium</i> sp. $\beta$ -glucosidase.....	7
Figure 1-5: Examples of naturally occurring and synthetic glucosidase inhibitors.....	10
Figure 1-6: Illustration of <i>anti</i> -protonation by triazole and imidazole inhibitors.....	11
Figure 1-7: Glycosylation of the Abg acid-base mutant (E170G) with 2,4-dinitrophenyl glucoside or by substrate assisted catalysis .....	14
Figure 1-8: Nature's version of substrate assisted catalysis and chemical rescue. Hydrolysis of sinigrin by <i>Sinapis alba</i> myrosinase .....	14
Figure 1-9: Thiosugar substrate analogue bound in the active site of <i>Fusarium oxysporum</i> endoglucanase I with the -1 sugar distorted to a ${}^1S_3$ conformation .....	16
Figure 1-10: Examples of fluorosugar inactivators. ....	17
Figure 1-11: Turnover of a 2-fluoro glycosyl enzyme by transglycosylation. ....	17
Figure 1-12: Retaining glycosidase transition state involving a short hydrogen bond between the 2-hydroxyl and the nucleophile.....	18
Figure 1-13: Bcx trapped as a covalent intermediate and implications for the transition state. The corresponding transition state for <i>Bacillus circulans</i> cyclodextrin glucanotransferase.....	19
Figure 2-1: Simplified scheme of ESI-MS.....	23
Figure 2-2: ESI-MS of cytochrome <i>c</i> denatured at pH 2.4 and in the native fold at pH 3.0 .....	24
Figure 2-3: Experimental apparatus for time-resolved ESI-MS.....	25
Figure 2-4: Mechanism for the reaction of Abg with D-glucal .....	26
Figure 2-5: ESI mass spectrum of Abg under 'native' conditions .....	27
Figure 2-6: Analysis of the $10^+$ charge state in the Abg ESI mass spectrum before and after reaction with D-glucal to form the 2-deoxy glucosyl enzyme intermediate .....	28
Figure 2-7: Monitoring the reaction of Abg with D-glucal in the pre-steady state with time-resolved ESI-MS .....	30
Figure 2-8: Mechanism and kinetic scheme for the hydrolysis of 2,5-dinitrophenyl $\beta$ -D-xylobioside (2,5-DNPX <sub>2</sub> ) by <i>Bacillus circulans</i> xylanase (Bcx).....	31
Figure 2-9: Hydrolysis of 2,5-DNPX <sub>2</sub> by Bcx Y80F, monitoring the release of 2,5-DNP in the pre-steady state by stopped-flow UV-Vis spectroscopy .....	32
Figure 2-10: Detection of a transient enzyme intermediate with time-resolved ESI-MS. ESI mass spectra of wild type Bcx recorded before and after mixing with 2,5-DNPX <sub>2</sub> .....	33
Figure 2-11: ESI mass spectra recorded after mixing a solution of Bcx Y80F with the substrate 2,5-DNPX <sub>2</sub> .....	34
Figure 2-12: Relative contribution of the $8^+$ ion generated from the covalent xylobiosyl-enzyme intermediate (E-X <sub>2</sub> ) in the ESI mass spectrum as a function of time .....	35
Figure 2-13: Validation of time-resolved ESI-MS by stopped-flow UV-Vis spectroscopy.....	37
Figure 3-1: Enzymes involved in the degradation of galactomannan by <i>Cellulomonas fimi</i> .....	40

Figure 3-2: Labeling of the nucleophile E519 of Man2A with 2-deoxy-2-fluoro $\beta$ -D-mannosyl fluoride .....	41
Figure 3-3: Synthesis of aryl $\beta$ -D-mannopyranosides.....	42
Figure 3-4: Synthesis of 2,5-dinitrophenyl $\beta$ -D-[1- $^2$ H]-mannopyranoside .....	43
Figure 3-5: Synthesis of 4-nitrophenyl 2-deoxy- $\beta$ -D- <i>arabino</i> -hexopyranoside (3-8) .....	44
Figure 3-6: Plots of reaction velocity ( $V_0/E_0$ ) versus substrate concentration for Man2A catalyzed hydrolyses of 4-nitrophenyl $\beta$ -mannoside (PNPMan) and phenyl $\beta$ -mannoside (PhMan).....	45
Figure 3-7: Simplified kinetic scheme for substrate inhibition. ....	46
Figure 3-8: Dependence of $\log k_{cat}$ and $\log (k_{cat}/K_M)$ on $pK_a^{lg}$ for wild type Man2A catalysed hydrolyses of aryl $\beta$ -mannosides.....	47
Figure 3-9: Dependence of the reaction rate of Man2A wt with saturating substrate and added ethylene glycol ...	48
Figure 3-10: Dependence of $k_{cat}/K_M$ on pH for the reaction of 4-nitrophenyl $\beta$ -mannoside and phenyl $\beta$ -mannoside with Man2A .....	49
Figure 3-11: Alignment of the amino acid sequence of Man2A with selected Family 2 glycosidases. ....	49
Figure 3-12: Reaction rate versus substrate concentration for the reaction of Man2A E429A with 2,5-dinitrophenyl $\beta$ -mannoside.....	50
Figure 3-13: Dependence of $k_{cat}$ on pH for the reaction of 2,5DNPMan with Man2A E429A .....	51
Figure 3-14: Mechanism for azide rescue of Man2A E429A.....	52
Figure 3-15: Reaction rate of Man2A E429A with 2,5DNPMan as a function of azide concentration .....	52
Figure 3-16: A comparison of the role of the 2-hydroxyl in the transition states of a $\beta$ -glucosidase and a $\beta$ -mannosidase .....	54
Figure 4-1: Examples of oligosaccharides of biological significance. ....	58
Figure 4-2: Molecular orbital representation of the anomeric effect.....	59
Figure 4-3: Trans and cis glycosidic linkages. ....	60
Figure 4-4: Neighbouring group effects .....	60
Figure 4-5: Representative structures of glycosyltransferase donor sugars. ....	61
Figure 4-6: Synthesis of sialyl Lewis X using glycosyltransferases and in-situ generation of sugar nucleotide donors with coupling enzymes.....	63
Figure 4-7: Postulated mechanism for the retaining $\alpha$ -galactosyltransferase from <i>Neisseria meningitidis</i> and mechanism for in situ generation of UDP-galactose from $\alpha$ -galactosyl fluoride and UDP.....	64
Figure 4-8: Synthesis of $\alpha$ -cyclodextrin by cyclodextrin glucanotransferase. ....	65
Figure 4-9: Hehre mechanism for inverting glycosidases .....	66
Figure 4-10: Transglycosylation and hydrolysis pathways for partitioning of a covalent intermediate.....	66
Figure 4-11: Examples of the thermodynamic approach to glycoside synthesis with retaining glycosidases.....	67
Figure 4-12: Examples of the kinetic approach to oligosaccharide synthesis using retaining glycosidases with activated donor substrates .....	68
Figure 4-13: Kinetic transfer of a single glucose unit with an <i>endo</i> -glycosidase, <i>Humicola insolens</i> Cel7B, using $\beta$ -lactosyl fluoride as a donor and subsequent cleavage with $\beta$ -galactosidase.....	69
Figure 4-14: Mechanism for transglycosylation by the T4 phage lysozyme mutant T26H.....	69

Figure 4-15: Synthesis of 2-deoxy glycosides using Abg and D-glucal as donor.....	70
Figure 4-16: Mechanism for <i>Agrobacterium</i> sp. $\beta$ -glucosidase mutant E358A acting as an inverting glucosidase in the presence of azide and as a 'glycosynthase' with $\alpha$ -glucosyl fluoride.....	71
Figure 4-17: Reaction schemes for Abg E358A using $\alpha$ -glucosyl fluoride and $\alpha$ -galactosyl fluoride as donors....	72
Figure 4-18: Synthesis of cellulase inactivators with Abg E358A.....	73
Figure 4-19: Synthesis of spin and isotopically labelled oligosaccharides with Abg E358A .....	73
Figure 4-20: <i>Sulfolobus solfataricus</i> E387G glycosynthase (Ss- $\beta$ -Gly) .....	74
Figure 4-21: <i>Bacillus licheniformis</i> E134A glycosynthase .....	75
Figure 4-22: <i>Humicola insolens</i> Cel7B E197A 'cellulosynthase' .....	75
Figure 4-23: Chemical rescue and transglycosylation as complementary glycosynthase probes.....	76
Figure 5-1: pH dependence of $k_{cat}/K_M$ for the reaction of $\alpha$ -galactosyl fluoride with Abg E358A and Abg E358S using PNP $\beta$ -glucoside as acceptor .....	82
Figure 5-2: Plots of reaction rate vs anion concentration for the reaction of Abg E358S with 2,4-dinitrophenyl $\beta$ -glucoside and formate or azide .....	84
Figure 5-3: pH dependence for the reaction of Abg E358G with 2 M azide and 2,4-dinitrophenyl $\beta$ -glucoside. ....	85
Figure 5-4: Plots of rate versus substrate concentration for the reaction of Abg E358 nucleophile mutants with 2,4-dinitrophenyl $\beta$ -glucoside and 2 M azide.....	87
Figure 5-5: Plots of rate versus substrate concentration for the reaction of Abg E358 nucleophile mutants with 2,4-dinitrophenyl $\beta$ -glucoside and formate .....	87
Figure 5-6: Brønsted relationships for the reaction of Abg E358G with formate and aryl $\beta$ -glucosides.....	88
Figure 5-7: Proposed transitions states for the solvolysis of $\alpha$ -glucosyl fluoride and $\beta$ -glucosyl fluoride in alcohol mixtures.....	90
Figure 5-8: A comparison of the hypothetical glycosylation transition state for Abg E358S and the transition state for the wild type enzyme.....	91
Figure 5-9: Active site residues in <i>Bacillus circulans</i> sp. $\beta$ -glucosidase that are conserved in Abg. ....	92
Figure 5-10: A minimal kinetic scheme for chemical rescue of a retaining glycosidase nucleophile mutant followed by transfer of the $\alpha$ -glycosyl donor to a second equivalent of substrate .....	93
Figure 5-11: Simulated plot of substrate concentration versus reaction rate for chemical rescue of a glycosynthase using equation 5-1.....	95
Figure 5-12: Simulations of chemical rescue using equation 5-1.....	96
Figure 5-13: Kinetic scheme for inactivation and reactivation of a retaining glycosidase.....	97
Figure 6-1: Examples of 'chemical' $\beta$ -mannosylation methods.....	101
Figure 6-2: Synthesis of branched oligosaccharide products with Man2A E519S from PNP $\beta$ -gentiobioside and $\alpha$ -mannosyl fluoride. ....	104
Figure 6-3: Reaction of Man2A E519S with $\alpha$ -ManF and PNPC as a function of pH .....	106
Figure 6-4: Reaction rate versus 2,4-dinitrophenyl $\beta$ -mannoside concentration for the reaction with Man2A E519S and E519A in the presence of 1 M azide .....	107
Figure 6-5: pH dependence of the reaction of 2,4-dinitrophenyl $\beta$ -mannoside with Man2A E519S and azide.....	108

Figure 7-1: Plot of reaction velocity vs substrate concentration for the reaction of DNPC with <i>Streptomyces lividans</i> CelB .....	111
Figure 7-2: Inactivation of CelB by 2FDNPC.....	112
Figure 7-3: Protection against inactivation with cellobiose.....	113
Figure 7-4: Turnover of the 2-deoxy-2-fluorocellobiosyl CelB intermediate via hydrolysis or transglycosylation. ....	113
Figure 7-5: Detection of the 2-deoxy-2-fluorocellobiosyl labeled peptide by ESI-MS/MS .....	115
Figure 7-6: Daughter ion mass spectrum for the 2-deoxy-2-fluorocellobiosyl labeled peptide produced by ESI-MS/MS.....	116
Figure 7-7: Alignment of the sequence regions containing the labeled nucleophile and the putative general acid-base catalyst of CelB with other Family 12 endoglucanases .....	117
Figure 7-8: Structure of 2-fluorocellobiosyl labeled CelB.....	118
Figure 7-9: CelB E120S acting as a 'cellulosynthase'. .....	120
Figure 8-1: Examples of fluorinated natural products: fluoroacetate and nucleocidin.....	123
Figure 8-2: Simplified scheme for a haloperoxidase reaction. ....	124
Figure 8-3: Nucleophilic halogenation mechanisms .....	125
Figure 8-4: Plot of reaction rate versus fluoride concentration for the reaction of Abg E358S with 2,4-dinitrophenyl $\beta$ -glucoside.....	126
Figure 8-5: Abg E358S catalyzing nucleophilic fluorination of 2,4-dinitrophenyl $\beta$ -glucoside and subsequent transfer of $\alpha$ -glucosyl fluoride to a second equivalent of substrate. Abg E358S synthesizing $\alpha$ -galactosyl fluoride.....	126
Figure 8-6: Plots of reaction velocity vs substrate concentration for the reaction of Abg and Man2A nucleophile mutants with 2,4-dinitrophenyl glycosides and fluoride.....	128
Figure 8-7: $^1\text{H}$ NMR spectra of the reaction of Abg E358G with 2,4-dinitrophenyl $\beta$ -galactoside in the presence of 2 M NaCl.....	130
Figure 8-8: Reaction rates versus 2,4-dinitrophenyl $\beta$ -glucoside concentration for Abg E358A and E358G in the presence of chloride .....	131
Figure 8-9: Man2a E429A catalysing nucleophilic fluorination of the mannosyl-enzyme covalent intermediate, forming $\beta$ -D-mannosyl fluoride.....	132
Figure 8-10: $^{19}\text{F}$ NMR spectrum of the reaction of Man2A E429A with 2,5-dinitrophenyl $\beta$ -mannoside in the presence of 1 M KF.....	132
Figure 8-11: Plots of initial rates versus salt concentration for the reaction of Man2A E429A with 2,5-dinitrophenyl $\beta$ -mannoside.....	133

## List of Tables

Table 3-1: Yields and anomeric selectivity of Mitsunobu mannosylation of substituted phenols. ....	43
Table 3-2: Kinetic parameters for the reaction of Man2A with substituted aryl $\beta$ -mannosides.....	46
Table 3-3: $^1\text{H}$ NMR data for aryl 2,3:4,6-di- <i>O</i> -cyclohexylidene $\beta$ -D-mannopyranosides (400 MHz, $\text{CDCl}_3$ ).....	148
Table 3-4: $^{13}\text{C}$ NMR data for aryl 2,3:4,6-di- <i>O</i> -cyclohexylidene $\beta$ -D-mannopyranosides (100 MHz, $\text{CDCl}_3$ ).....	149
Table 3-5: $^1\text{H}$ NMR data for aryl $\beta$ -D-mannopyranosides (400 MHz, $\text{CD}_3\text{OD}$ ).....	150
Table 5-1: Apparent kinetic parameters for transglycosylation reactions of Abg E358 mutants .....	82
Table 5-2: Yields of transglycosylation reactions with Abg E358S using $\alpha$ -galactosyl fluoride as a donor .....	83
Table 5-3: Yields of transglycosylation reactions with Abg E358S using $\alpha$ -glucosyl fluoride as a donor.....	83
Table 5-4: Kinetic parameters for the reaction of Abg E358 mutants with 2,4-dinitrophenyl $\beta$ -glucoside and anions at pH 7, 37°C.....	86
Table 5-5: Kinetic parameters for the reaction of Abg E358 mutants with 2,4-dinitrophenyl $\beta$ -glucoside and anions at pH 6, 25°C.....	86
Table 5-6: Kinetic parameters for the reaction of Abg E358G with aryl $\beta$ -glucosides and 2 M formate .....	88
Table 5-7: Kinetic parameters for reactivation of 2-fluoro glycosyl enzyme intermediates. ....	98
Table 6-1: Products synthesized with Man2A E519S using $\alpha$ -mannosyl fluoride as donor. ....	103
Table 6-2: Apparent transglycosylation kinetic parameters for Man2A E519S and E519A.....	105
Table 6-3: Kinetic parameters for the reaction of Man2A nucleophile mutants with 2,4-dinitrophenyl $\beta$ -mannoside and azide .....	107
Table 7-1: Kinetic parameters for the reaction of CelB nucleophile mutants with $\alpha$ -cellobiosyl fluoride .....	120
Table 8-1: Kinetic parameters for Abg and Man2A nucleophile mutants catalyzing glycosidic bond cleavage of 2,4- dinitrophenyl $\beta$ -glycosides using halides as nucleophiles .....	127

## Abbreviations

Abg	<i>Agrobacterium</i> sp. $\beta$ -glucosidase
amu	atomic mass units
Bcx	<i>Bacillus circulans</i> xylanase
CelB	<i>Streptomyces lividans</i> endoglucanase B
Cex	<i>Cellulomonas fimi</i> exoglycanase
DCM	dichloromethane
DEAD	diethylazodicarboxylate
DMF	dimethylformamide
2,4DNPGlu	2,4-dinitrophenyl $\beta$ -D-glucopyranoside
DNPC	2,4-dinitrophenyl $\beta$ -cellobioside
2,5DNPMan	2,5-dinitrophenyl $\beta$ -D-mannopyranoside
2,5-DNPX <sub>2</sub>	2,5-dinitrophenyl $\beta$ -xylobioside
ESI-MS	electrospray ionisation mass spectrometry
2FDNPC	2,4-dinitrophenyl 2-deoxy-2-fluoro- $\beta$ -cellobioside
GC	gas chromatography
HEWL	Hen egg white lysozyme
HPLC	high performance liquid chromatography
Hz	Hertz
MALDI	matrix assisted laser desorption ionisation
Man2A	<i>Cellulomonas fimi</i> $\beta$ -mannosidase 2A
MW	molecular weight
<i>m/z</i>	mass-to-charge ratio
NAG	<i>N</i> -acetyl glucosamine
NAM	<i>N</i> -acetyl muramic acid
PE	petroleum ether (30-60°C)
PNPC	<i>para</i> -nitrophenyl $\beta$ -cellobioside
PNPMan	<i>para</i> -nitrophenyl $\beta$ -D-mannopyranoside
THF	tetrahydrofuran
TLC	thin layer chromatography
TsOH	toluene-4-sulphonic acid
UV-Vis	ultra-violet, visible

## Acknowledgments

A good teacher offers more questions than answers to his students. For this I am indebted to my supervisor, Steve Withers, for without his questions this thesis would not have been written. I am also thankful to Steve for his unflinching support over the years, in addition to the numerous opportunities he has provided me to develop as scientist. I would like to specifically thank Drs. Christoph Mayer, Dominik Stoll, Oyekanmi Nashiru and David Jakeman, as well as Professor Claude Dupont, for their efforts which provided all of the glycosidase mutants used in this work. Likewise, I am grateful to Professors Don Douglas and Lars Konnerman for offering me the opportunity to participate in their exciting adventure with ‘time-resolved’ ESI mass spectroscopy. My thanks goes to Professor R. Antony J. Warren for access to his ‘Cellulase’ lab and resources over the years, as well as to Melanie Mah for her cheerful assistance in enzyme mutagenesis and expression. I also had the privilege of working with two summer students, Stephen Reid and Teraneh Mohammadzadeh, who made substantial contributions to this work, for which I am grateful. I reserve a special thanks for Karen Rupitz, for her friendship and invaluable guidance, as well as for tolerating my numerous thefts of her lab equipment and stationary. My thanks also goes to Lianne Diarge, Marietta Austria and Dr. Nick Burlinson for their guidance through the mysteries of NMR spectroscopy, and to Shouming He for his diligent handling of my innumerable mass spectrometry samples. I wish to thank Dr. Gideon Davies for many inspired discussions over the years as well as for bringing the CelB project to my attention. Likewise, I thank Professor Martin Tanner for his critical reading of this thesis, as well as for being an inspiring character and scientist. Of course, a very special thanks goes to Corina for pushing me out West in the first place and holding our world together ever since. Finally, I gratefully acknowledge all the members and visitors of the ‘Withers group’, who laboured in the trenches by my side since 1996 and made this rambling trip a most memorable one.

Jan Blanchard	Bonnie May	Jacqueline Wicki	Dr. Jakob Tolberg
Tim Hiebert	Renee Mosi	Alex Wong	Dr. Chris Tarling
Omid Hekmat	Shin Numao	Dr. Harry Brumer	Dr. Spencer Williams
Seung Lee	Lars Pedersen	Dr. Steve Howard	Professor Robert Stick
Yunsong Li	Edwin Rydberg	Dr. Michael Jahn	
Hoa Ly	Carl Rye	Dr. Heiko Padre	
Lloyd Mackenzie	Dave Vocadlo	Dr. Hannes Schloegl	

For Corina, Maks and Anni

# **Chapter 1 Introduction to Retaining Glycosidase Mechanisms**

## The Legacy of David Phillips

The most stable of the linkages within naturally occurring biopolymers is the glycosidic bond, with half lives for spontaneous hydrolysis of cellulose and starch being in the range of 5 million years.<sup>1</sup> The fact that glycosidases are capable of hydrolysing these materials with rate constants up to  $1000 \text{ sec}^{-1}$  marks these enzymes as some of the most proficient of catalysts. The first enzyme X-ray crystal structure determined happened to be that of a glycosidase, lysozyme,<sup>2</sup> and the following 34 years of research into the catalytic prowess of glycosidases, for better or for worse, has largely been interpreted through the lens of that work. Indeed, David Phillips' original proposal for the mechanism of hen egg white lysozyme (HEWL) has become a paradigm in enzymology, and is standard fare in all undergraduate biochemistry textbooks.

HEWL serves a defensive role by cleaving the glycosidic bond between the *N*-acetylglucosamine (NAG) and *N*-acetyl muramic acid (NAM) residues that comprise the peptidoglycan in bacterial cell walls. Model building studies by Phillips suggested that the *N*-acetylglucosamine residue of the scissile bond would be distorted from a normal chair conformation to a half chair, placing the glycosidic oxygen in a pseudo-axial position near the proposed general acid-base catalyst, Glu 35 (Figure 1-1). The Phillips mechanism also holds that this distortion would favour a fully formed oxocarbenium ion intermediate, stabilized electrostatically by an ionized Asp 52, following general acid catalysed expulsion of the glycosidic bond by Glu 35. Subsequent general-base catalyzed attack of water at the  $\beta$  face of the oxocarbenium-ion intermediate would produce a hydrolyzed product with retained stereochemistry.

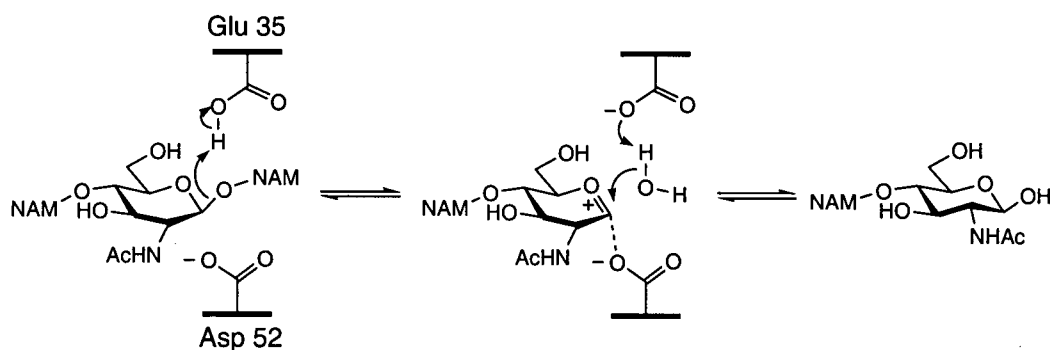


**Figure 1-1:** The venerable lysozyme mechanism proposed by David Phillips.

Controversial even until recently, the concept of substrate distortion received support in Phillips' time from measurements of sub-site affinities, which indicated a negative contribution

from the binding site,<sup>3</sup> and later from stereoelectronic arguments which require such distortion in order to place the lone pair on the endocyclic oxygen anti-periplanar to the scissile bond.<sup>4</sup> More recent structural work with HEWL lent support to the distortion model,<sup>5</sup> but ambiguity remained because these results were based on the structure of an enzyme-product complex, not that of a substrate spanning the cleavage site. However, the most distressing part of this mechanism was the formidable challenge of stabilizing the highly reactive oxocarbenium ion for a length of time sufficient to allow diffusion of the aglycone from the active site and the return of a water molecule to complete hydrolysis. Solvolysis studies of acetals and glycosides have established that the oxocarbenium ion is too unstable to exist as a real intermediate in the presence of a nucleophile, such as Asp 52.<sup>6-10</sup> However, for over 30 years kinetic evidence for or against the existence of an ion pair in HEWL has been impossible to obtain because there are no known substrates for which hydrolysis of the glycosyl-enzyme intermediate (Figure 1-1, second step) is rate determining.<sup>11-14</sup> Thus it has never been possible to isolate the oxocarbenium intermediate on any timescale, and the Phillips mechanism has remained inviolable to the passage of time. That is until recently, as will be discussed below.

### **Emerging From the Shadow of Lysozyme**

The Phillips mechanism for HEWL is all the more curious when one considers that Daniel Koshland, 14 years earlier, had proposed two possible mechanisms for the enzymatic hydrolysis of a glycosidic bond.<sup>15</sup> Koshland recognized that because the anomeric carbon of a glycosidic bond is stereogenic, glycosidase-catalyzed hydrolysis of a glycosidic bond could proceed through retention or inversion of the stereochemistry, or anomeric configuration, at that carbon. Each stereochemical outcome demands entirely different mechanisms, and two general schemes were proposed, as shown in Figure 1-2. The inversion mechanism for glycoside hydrolysis was envisioned as a simple S<sub>N</sub>2 like displacement of the glycosidic oxygen by a water nucleophile (Figure 1-2a). Although at the time Koshland did not know the identity of the catalytic residues, today it is known that two carboxyl residues in the active site function as general acid-base catalysts. In the retaining mechanism, Koshland circumvented the issue of an unstable oxocarbenium ion by proposing a double displacement reaction in which a covalent intermediate was transiently formed (Figure 1-2b). Once again, two carboxyl residues are employed for this purpose, one as the nucleophile, the other as a general acid-base catalyst in the glycosylation and deglycosylation steps. In both mechanisms, each displacement reaction passes through a transition state with substantial oxocarbenium ion character, involving sp<sup>2</sup> hybridization of the

anomeric carbon as well as delocalization of partial positive charge between the anomeric carbon and the endocyclic oxygen. Features of these transition states, as well as the covalent intermediate, will be discussed in more detail below.

Remarkably, a covalent catalysis mechanism had been proposed for HEWL by Lowe at the same time as Phillips proposed his oxocarbenium mechanism.<sup>16,17</sup> Lowe's mechanism was a variation on Koshland's scheme and called for the *N*-acetamido group on *N*-acetyl glucosamine to function as a nucleophile, forming a relatively stable cyclic oxazoline intermediate (Figure 1-3). In this case an ionized Asp 52 would stabilize the positive charge of the oxazoline. Substrate assisted catalysis is well-precedented in the spontaneous hydrolysis of *N*-acetyl  $\beta$ -hexosaminides,<sup>18,19</sup> and is actually used by certain *N*-acetyl  $\beta$ -hexosaminidases (those from Family 18 and 20).<sup>20,21</sup> However, this mechanism was discarded for HEWL in favour of the Phillips' version on the basis of the relatively rapid turnover of substrates lacking the *N*-acetyl group.<sup>22,23</sup>

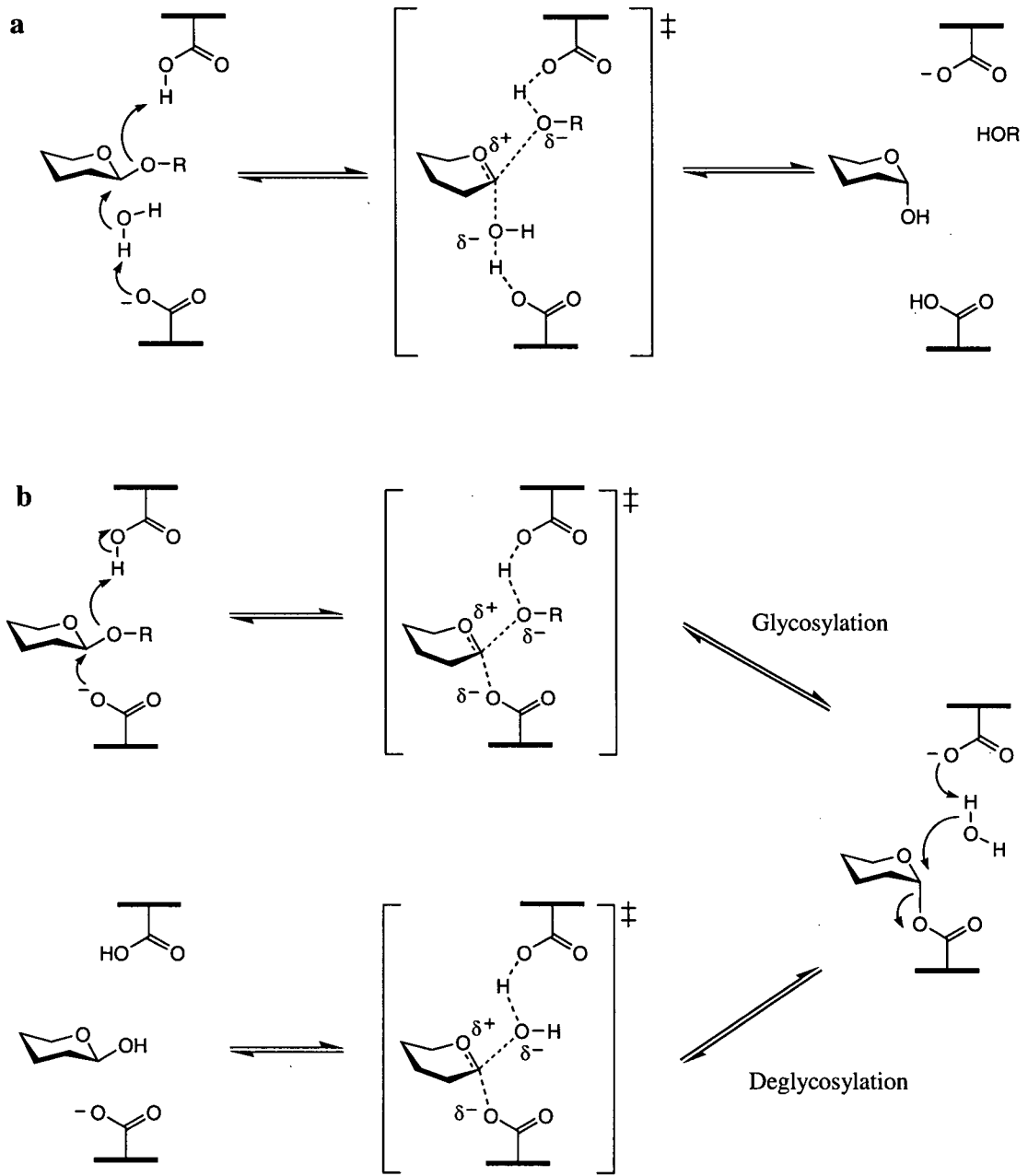


**Figure 1-2:** Generalized mechanisms for inverting (a) and retaining glycosidases (b).

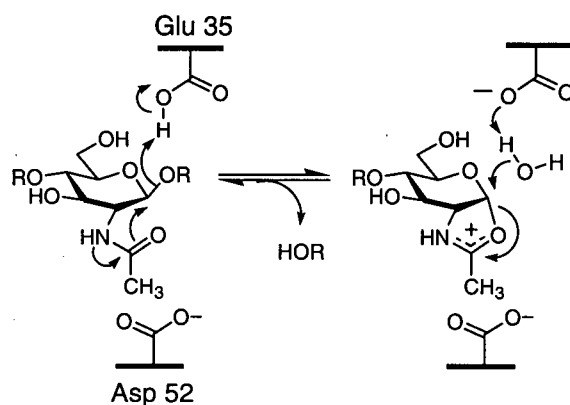


**Figure 1-3:** Mechanism for HEWL proposed by Lowe involving substrate assisted catalysis.

### *Structural biology of glycosidases*

Until 1990, HEWL was one of a handful of glycosidases with a known three-dimensional structure. However, following advances in molecular biology in the last decade there has been an explosion of structural information on glycosidases in terms of sequences and three-dimensional structures. The predicted amino acid sequences of well over 2000 different glycosidases are now available, these being divided into over 80 different families on the basis of sequence similarities.<sup>24</sup> Now a necessity in the post-genomic era, this information is maintained and continually updated on a web-site (<http://afmb.cnrs-mrs.fr/~pedro/CAZY/db.html>). Three-dimensional structures have now been determined for representatives of at least 30 of these families, revealing stunning structural diversity despite the fact that all these enzymes catalyse the same reaction, hydrolysis of an acetal.<sup>25</sup> Nonetheless some families adopt similar folds and on this basis have been assigned to so called 'clans.'<sup>24,26,27</sup> However, many active site features, such as the pair of carboxyl groups, are retained throughout. Likewise, although glycosidic bond cleavage can occur with inversion or retention, all enzymes within a sequence-related family appear to catalyse reaction with the same stereochemical outcome (Figure 1-2).<sup>28</sup> Predictably, there are fundamental differences in the active site geometries of inverters and retainers. The two carboxyl groups in inverting glycosidases that serve as general acid and general base catalysts are suitably placed, some 10.5 Å apart on average,<sup>29,30</sup> to allow the substrate *and* a water molecule to bind between them (Figure 1-2a). By contrast the carboxyl groups in retaining glycosidases are only 5.5 Å apart, consistent with a double-displacement mechanism involving a covalent glycosyl-enzyme intermediate (Figure 1-2b).<sup>26,29,30</sup> Glycosidase structures have also revealed two basic active site shapes, corresponding to two forms of polysaccharide cleavage.

Pocket shaped active sites are found on *exo*-glycosidases, or those that cleave sugar residues from the end of a polysaccharide chain. Cleft shaped (or possibly, in some cases, tunnel shaped) active sites are found on *endo*-glycosidases, which cleave glycosidic bonds anywhere along the length of the polysaccharide chain. In order to bind a polymeric substrate, glycosidases typically have a number of sugar ring binding sites. By convention, subsites that bind the glycone portion of the substrate are designated -1, -2, -3 etc., while the aglycone or 'leaving group' binding sites are designated +1, +2, etc.

### *Defining rate-determining steps*

In order to fully characterise each step in the retaining mechanism, it is necessary to first identify a number of substrates for which different steps are rate-limiting. The aryl glycosides have proved ideal for this purpose with a number of  $\beta$ -glycosidases, early studies being performed on the almond  $\beta$ -glucosidase<sup>31</sup> and *E. coli*  $\beta$ -galactosidase.<sup>32</sup> In the case of *Agrobacterium* sp.  $\beta$ -glucosidase (Abg) a plot of  $\log k_{cat}$  values for the hydrolysis of a series of aryl glucoside substrates versus the aglycone  $pK_a$  values produces a biphasic, concave-downward Brønsted relationship, indicating a change in rate-determining step as the aglycone leaving group ability increases (Figure 1-4).<sup>33</sup> The glycosylation step is rate-limiting for substrates to the right of the break as indicated by the strong dependence ( $\beta_{lg} = -0.7$ ) in this region. Below the break the  $k_{cat}$  value is independent of the leaving group, indicating that some other step is rate-limiting. This was shown to be the deglycosylation step through nucleophilic competition studies and the observation of 'burst' kinetics in the pre-steady state.<sup>33,34</sup>

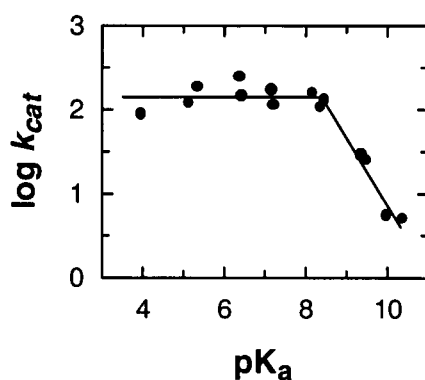


**Figure 1-4:** Brønsted relationship for a series of aryl  $\beta$ -glucosides with *Agrobacterium* sp.  $\beta$ -glucosidase.

### *Transition state structure*

Substantial oxocarbenium ion character has been shown to be present at the anomeric centre in the transition states of both inverting and retaining mechanisms, as is also the case for the spontaneous hydrolysis mechanism.<sup>34,35</sup> Perhaps the best evidence is that derived from measurements of alpha secondary deuterium kinetic isotope effects ( $\alpha$ DKIE). Such measurements on glycosidases have a long history<sup>11,36</sup> and are illustrated here in studies with Abg. The  $\alpha$ DKIE values measured<sup>33</sup> for two substrates for which deglycosylation was rate-limiting averaged  $k_H/k_D = 1.11$ , while  $\alpha$ DKIE values for the glycosylation step averaged  $k_H/k_D = 1.06$ . The larger  $\alpha$ DKIE values measured for deglycosylation suggest that this step has more oxocarbenium ion character than does glycosylation, thus it involves a more dissociative transition state. More importantly, because the  $\alpha$ DKIE for deglycosylation is normal (i.e.  $\alpha$ DKIE > 1), indicating a  $sp^3$  to  $sp^2$  rehybridization of the anomeric carbon, the existence of a *covalent* intermediate prior to the transition state is required. Had the intermediate been an oxocarbenium ion, an inverse isotope effect would be expected ( $\alpha$ DKIE < 1) as the result of  $sp^2$  to  $sp^3$  rehybridization. In all retaining glycosidases where this measurement has been possible on the deglycosylation step a normal isotope has been observed, indicating the formation of a covalent intermediate.

A significant component of catalysis in most enzymes derives from non-covalent enzyme-substrate interactions that are optimised at the transition state. In order to probe the importance of hydrogen bonding interactions at each sugar hydroxyl position for each step along the reaction coordinate with Abg, a series of deoxygenated and deoxyfluorinated derivatives of the substrate 2,4-dinitrophenyl  $\beta$ -glucoside were synthesised and subjected to detailed kinetic analysis.<sup>34</sup> Key conclusions from this study were that binding interactions at the 3, 4, and 6-positions individually contribute 3-10  $\text{kJ} \cdot \text{mol}^{-1}$  to each transition state, whereas contributions in the ground state are much weaker ( $\leq 3 \text{kJ} \cdot \text{mol}^{-1}$ ). However, the most interesting interactions are those at the 2-position which contribute substantially (18-22  $\text{kJ} \cdot \text{mol}^{-1}$ ) to stabilization of the glycosylation and deglycosylation transition states. This appears to be a common phenomenon with  $\beta$ -glycosidases with interactions at this position in some enzymes reaching 45  $\text{kJ} \cdot \text{mol}^{-1}$ .<sup>34</sup> This feature is examined further in Chapter 3 of this thesis in the context of a  $\beta$ -mannosidase.

Further information on the structure of the glycosidase transition state can be derived from inhibition studies with transition state mimics.<sup>37</sup> The flattened half-chair conformation and the development of positive charge at the position of the endocyclic oxygen, anomeric carbon

and glycosidic oxygen are favourite features that are incorporated into transition state analogues (Figure 1-5). Nature was the first to incorporate these features into secondary metabolites such as acarbose (**1-1**), 1-deoxynojirimycin (**1-2**)<sup>38</sup> and castanospermine (**1-3**)<sup>39</sup>, all potent inhibitors of certain glucosidases. Synthetic efforts in the last two decades have produced numerous nojirimycin analogues as well as other nitrogen substituted 'aza-sugars',<sup>40,41</sup> including isofagomines (**1-4**)<sup>42,43</sup>, 1-azafagomines (**1-5**)<sup>44</sup>, the bicyclo[4.1.0]heptane compound **1-6**<sup>45</sup> and cyclic imines (**1-7**),<sup>46</sup> all attempting to mimic positive charge development and the half-chair conformation. Others, such as the hydroximolactam (**1-8**) and norjiritetrazole (**1-9**) derivatives attempt to mimic the flattened half chair as well as interact with the acid-base catalyst.<sup>47</sup> In a recent diversion from these themes, the non-basic lactam xylobiose derivative (**1-10**) was designed to take advantage of the strong interactions ( $\sim 10 \text{ kcal} \cdot \text{mol}^{-1}$ ) developed at the 2-hydroxyl position by *Cellulomonas fimi* exoglycanase (Cex), and indeed proved to be a potent inhibitor of this enzyme.<sup>48</sup>

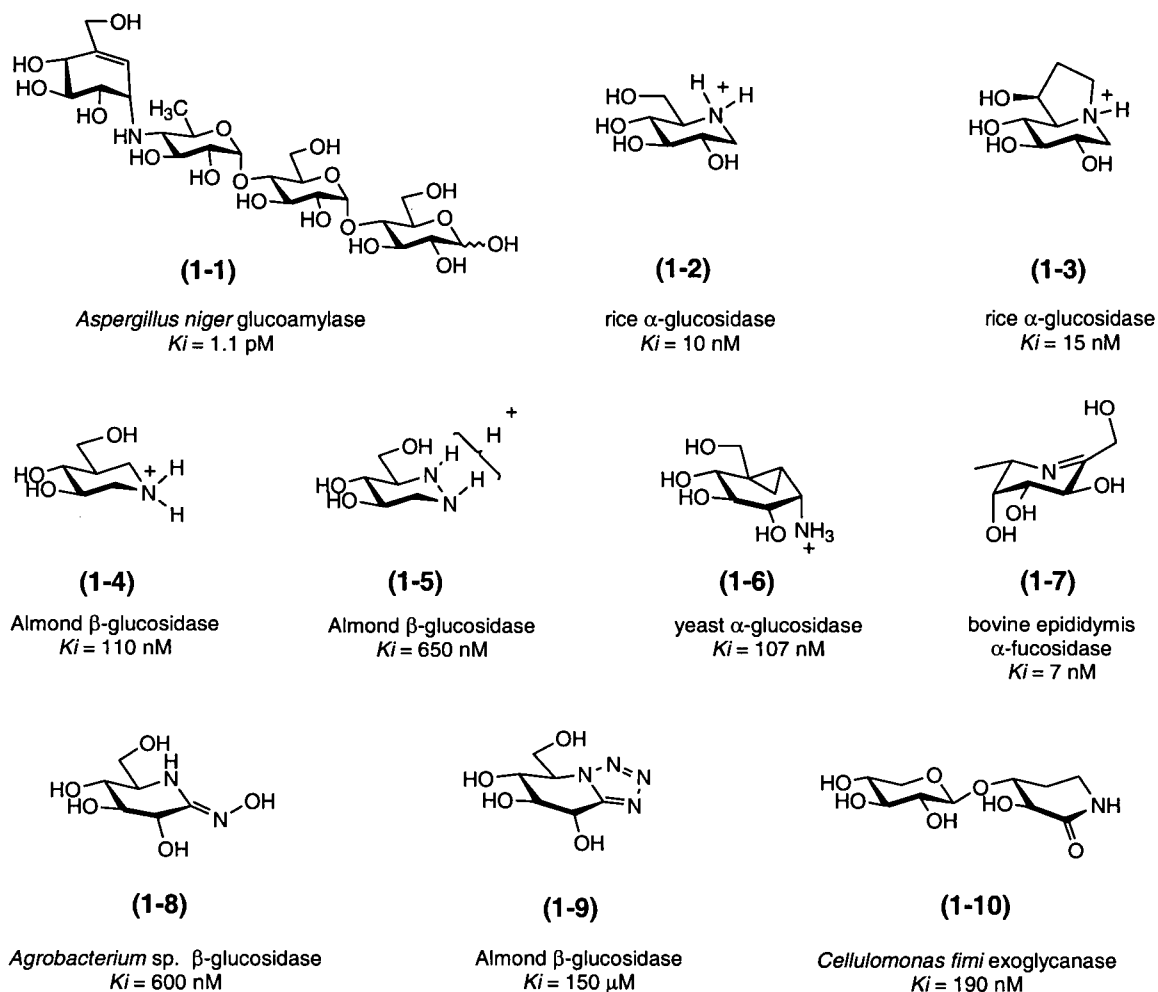


**Figure 1-5:** Examples of naturally occurring and synthetic glucosidase inhibitors.

Significant differences in the transition state structure have been inferred from transition state mimics. This includes the observation that retaining  $\alpha$ -glucosidases are potently inhibited by nojirimycin derivatives (1-2), whereas retaining  $\beta$ -glucosidases are more potently inhibited by isofagomine derivatives (1-4), implying that markedly different localization of positive charge (at O5 or C1) occurs in the respective transition states.<sup>42,49,50</sup> This parallels the relative effectiveness of 5-fluoro and 2-fluoro glycoside inactivators on these enzymes, as well as the opposite positions of their nucleophiles.<sup>49</sup> Likewise, significant differences in the transition states of two xylanases, Cex and Bcx, have been inferred from strong inhibition of the former by imidazole, lactam, and isofagomine xylobioside derivatives, but not the latter.<sup>51,52</sup> This appears to correlate with the dramatically different structures that are observed for the corresponding covalent intermediates (see below). The development of protonation site-specific transition state

analogue inhibitors has elegantly revealed a subtlety in the positioning of the acid-base catalyst.<sup>47</sup> The vastly reduced potency of 1,2,3-triazoles (**1-11**) relative to hydroximolactams (**1-8**), tetrazoles (**1-9**) and imidazoles (**1-12**) with glycosidases belonging to clan GH-A implies that protonation of the glycosidic oxygen occurs within the plane of the sugar ring and *anti* to the O5-C1 bond (Figure 1-6). Recent structural analyses of imidazole and hydroximolactam complexes with a cellulase<sup>53</sup> and Cex<sup>52</sup> has confirmed this mode of binding. Examination of other glycosidase structures has revealed that the opposite protonation trajectory, *syn* to the O5-C1 bond, also exists.<sup>47</sup>

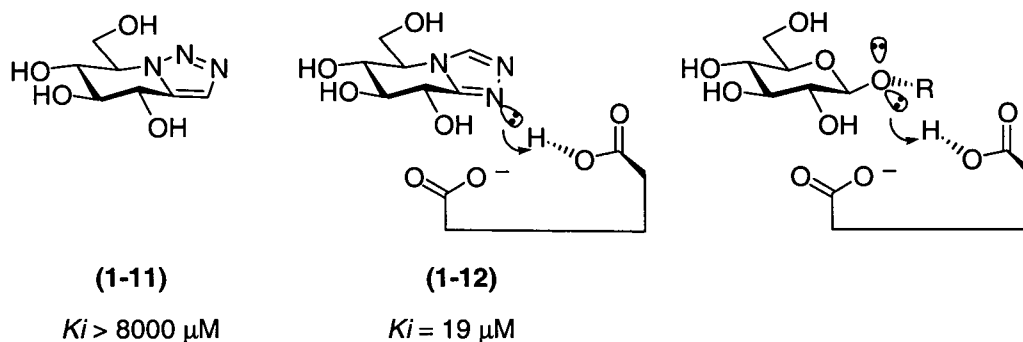


**Figure 1-6:** Illustration of *anti*-protonation by triazole (**1-11**) and imidazole (**1-12**) inhibitors.  $K_i$  values are for Almond  $\beta$ -glucosidase.

It is essential to note that potent inhibition of an enzyme may merely be the result of fortuitous binding, and not transition state analogy.<sup>37</sup> A more rigorous approach to assessing the transition state mimicry of an inhibitor was developed by Wolfenden<sup>54</sup> and Bartlett.<sup>55</sup> This involves testing a series of 'mutant' variants of an inhibitor (e.g. deoxy or fluorinated analogues) with an enzyme, or the converse, testing a series of active site mutants of the enzyme with a single inhibitor. If an inhibitor is an accurate transition state mimic, then these mutations will affect the binding of the inhibitor ( $K_i$ ) and transition state binding ( $k_{cat}/K_M$ ) in equivalent ways, and the following relationship will hold:

$$\log K_i \propto \log(K_M / k_{cat}) \quad (1-1)$$

This criterion was used to establish that acarbose (**1-1**) was a transition state mimic for *Aspergillus niger* glucoamylase<sup>56</sup> and *Bacillus circulans* cyclodextrin glucanotransferase.<sup>57</sup> Likewise, *manno*- and *gluco*-nojiritetrazoles such as (**1-9**) were determined to be transition state

mimics for glucosidases and mannosidases.<sup>58</sup> In contrast, this correlation did not hold for a series of deoxynojirimycins (**1-2**) and castanospermines (**1-3**) with *Agrobacterium* sp.  $\beta$ -glucosidases, marking these as fortuitous binders with this enzyme.<sup>37</sup>

### *Acid-base catalysis*

Cleavage of a glycosidic bond between two sugar residues requires substantial general acid catalytic assistance, as well as general base catalysis to assist the attack of the nucleophilic water molecule. Three-dimensional structures generally provide good clues regarding the identities of the acid-base catalysts. Alternatively, candidates identified through sequence alignments can be investigated by detailed kinetic analysis of mutants modified at those conserved residues.<sup>59</sup> However, simple measurement of activities can lead to mis-assignments.

Replacement of the acid-base catalyst carboxyl group with a methyl group (Ala) or amide functionality (Asn or Gln) should yield a mutant with kinetic parameters that vary widely with the leaving group ability of the substrate aglycone. Thus the glycosylation step, as measured through  $k_{cat}/K_M$  values or pre-steady state kinetics, is drastically slowed for substrates such as disaccharides with poor leaving groups that need protonic assistance for departure, but is affected relatively little for substrates such as dinitrophenyl glycosides or glycosyl fluorides that need no such assistance (Figure 1-7, upper pathway). However the deglycosylation step is slowed equally (typically 200-2000 fold) for all substrates of the same glycone structure, due to removal of general base catalytic assistance. This results in accumulation of the covalent intermediate when reactive substrates are employed, as suggested by unusually low substrate  $K_M$  values and 'burst' kinetics in the pre-steady state.<sup>60-64</sup>

The kinetic characteristics described above are necessary, but not sufficient, indicators of mutation of the acid-base catalyst. Changes in the pH-rate profile should also be observed, ideally involving complete removal of the ionization from the profile,<sup>62</sup> though in many cases this can be masked by other proton transfer events. A more definitive and rapid diagnostic test for having mutated the acid-base catalyst is the observation of a large increase in rate of cleavage of substrates for which deglycosylation is rate-limiting upon addition of nucleophilic anions such as azide, formate or acetate. This is accompanied by the formation of a new product with retained anomeric configuration (Figure 1-7, upper pathway). These effects are due to the anion reacting more rapidly with the glycosyl-enzyme than does water in the absence of general base catalysis. No such effect is seen with wild type enzymes, charge screening by the base catalyst

presumably denying access to the anions in that case. This approach allows relatively facile identification of the acid-base catalyst and appears to be general.<sup>59</sup>

Catalytic activity has also been restored to the acid-base mutant of Abg (E170G) by the inclusion of a suitably positioned carboxyl group into the substrate.<sup>65</sup> Thus the  $k_{cat}/K_M$  value for cleavage of *ortho*-carboxyphenyl  $\beta$ -glucoside by this mutant (in the presence of azide to ensure that deglycosylation is not rate-limiting) is some  $10^7$  fold greater than that for its *para*-substituted isomer, due to intramolecular delivery of a proton (Figure 1-7, lower pathway). Remarkably, *Sinapis alba* myrosinase has evolved to use a similar rescue strategy. This enzyme has a Gln residue in the position normally occupied by Glu in Family 1 glycosidases.<sup>66</sup> To compensate, the myrosinase relies on the the good leaving group ability of the sinigrin aglycone to perform the glycosylation step. Even more striking is that L-ascorbate ( $pK_1 = 4.17$ ) provides general base assistance in the deglycosylation step (Figure 1-8).<sup>67</sup>

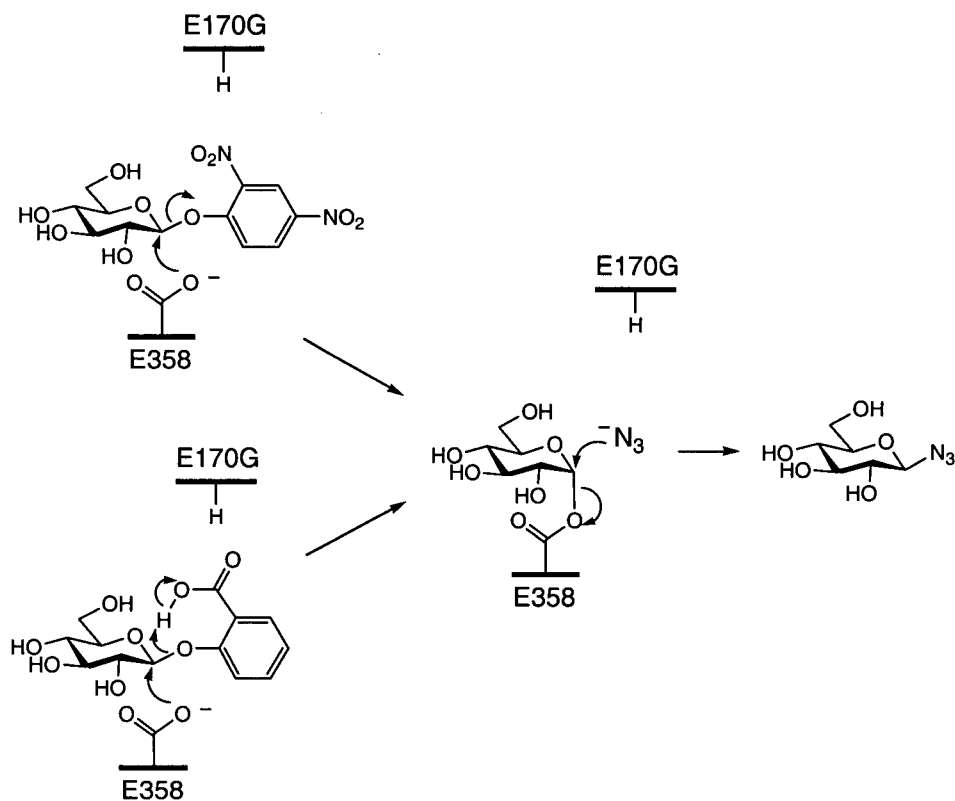


**Figure 1-7:** Glycosylation of the Abg acid-base mutant (E170G) with 2,4-dinitrophenyl glucoside (upper pathway) or by substrate assisted catalysis (lower pathway). Azide assists deglycosylation, forming a retained product.

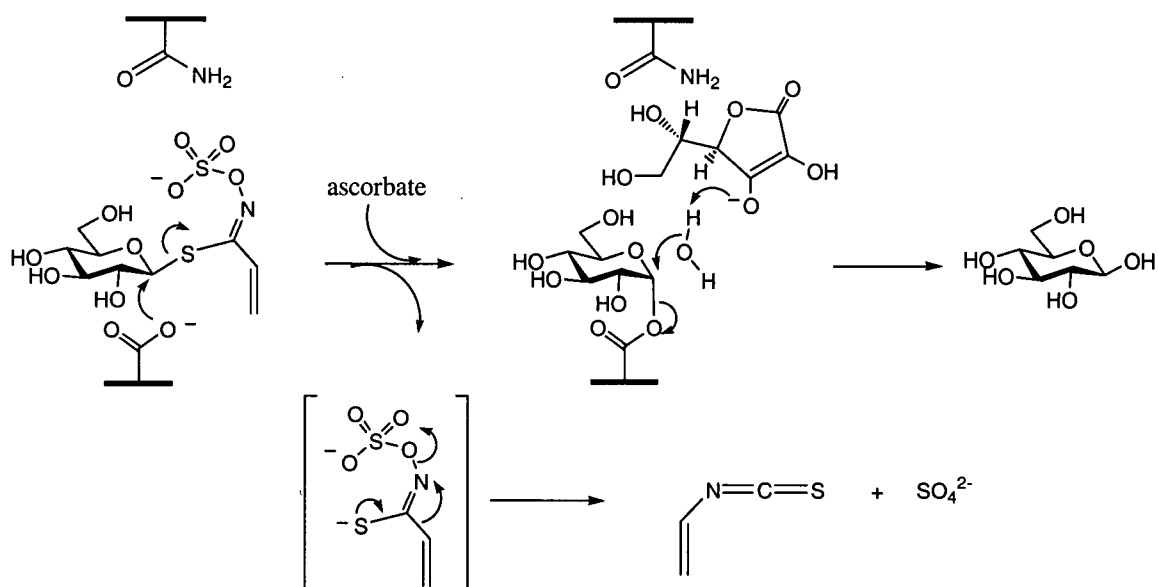


**Figure 1-8:** Nature's version of substrate assisted catalysis and chemical rescue. Hydrolysis of sinigrin by *Sinapis alba* myrosinase (Family 1).<sup>67</sup>

These examples point to a surprising tolerance to the chemical identity of the acid-base catalyst. Indeed, in a remarkable study the general base (Glu400) of the inverting glucoamylase from *Aspergillus awamori* was replaced by cysteine then oxidized to cysteinesulfinic acid. The pKa of this sulphinate residue was determined to be merely 0.5 pKa units lower than the wild type Glu400.<sup>68</sup> However, the  $k_{cat}$  value of the mutant towards maltose was 700 times higher than that of the wild type enzyme, and the  $K_M$  was unchanged. Likewise, changes in the position of the acid-base catalyst in Bcx were demonstrated to have modest effects on catalysis.<sup>63</sup>

Another intriguing feature of the acid-base catalyst in a retaining glycosidase is a dynamic pKa. This was first demonstrated by <sup>13</sup>C NMR titrations performed on Bcx that had been specifically <sup>13</sup>C-labeled in the side chain carboxyl groups of the nucleophile (Glu78) and the acid-base catalyst (Glu172).<sup>69</sup> pKa values of 4.6 and 6.7 were measured for Glu78 and Glu172 respectively. However, when the 2-fluoroxyllobiosyl-enzyme intermediate was titrated it was seen that the pKa of Glu172 had dropped some 2.5 units, thereby producing the ionisation state required for the subsequent deglycosylation step. This drop in pKa also drives the formation of the covalent intermediate by creating a thermodynamically favourable proton transfer from the strongly acidic glutamic acid side chain to the strongly basic alkoxide leaving group.<sup>70</sup> Such 'pKa cycling' is ascribed to changes in the active site environment arising from the presence and absence of charge on Glu78 and is most likely a general feature of the mechanisms of retaining glycosidases.

### *Substrate distortion*

The role of substrate distortion in the mechanism of  $\beta$ -glycosidases is a contentious issue with a long history. First posited for HEWL on the basis of models of bound oligosaccharides, this concept has received support from measurements of sub-site affinities, which indicated a negative contribution from the -1 site, and from stereoelectronic arguments which require such distortion in order to place the lone pair on the endocyclic oxygen anti-periplanar to the scissile bond.<sup>3,4</sup> Structural evidence for such distortion has been ambiguous, possibly because the complexes under investigation in many cases had no sugar filling the +1 site. Recently, however, there have been three separate structure determinations of  $\beta$ -glycosidases with uncleaved substrates spanning the active sites, in which large distortions of the pyranoside ring bound in the -1 site into a <sup>1</sup>S<sub>3</sub> skew boat have been seen (Figure 1-9).<sup>71-73</sup> Such distortion, which is likely driven by interactions between the enzyme and the substrate in the +1 site, can assist

bond cleavage in several ways. Firstly it permits an in-line attack of the enzymic nucleophile at the anomeric centre, unencumbered by the repulsive 1,3-diaxial interactions otherwise present when displacing an equatorial leaving group. It also moves the substrate closer to the conformation of the oxocarbenium ion transition state, as well as placing the glycosidic oxygen in an appropriate position for protonation by the general acid catalyst. Finally it is consistent with the dictates of stereoelectronic theory, which favours the endocyclic oxygen lone pair to align with the developing  $sp^2$  orbital on the anomeric carbon in the transition state.<sup>4</sup>

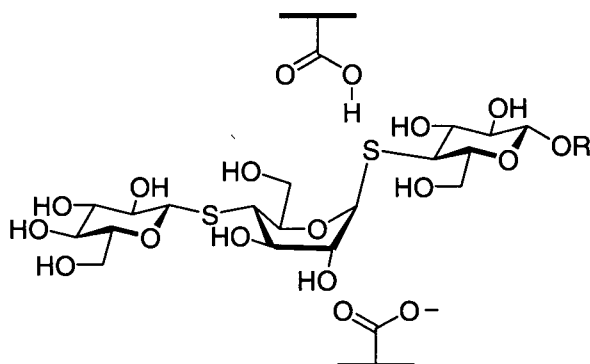


**Figure 1-9:** Thiosugar substrate analogue bound in the active site of *Fusarium oxysporum* endoglucanase I with the -1 sugar distorted to a  ${}^1S_3$  conformation.<sup>72</sup>

### *Covalent intermediates*

The covalent intermediate is now firmly established for a large number of retaining glycosidases, including HEWL.<sup>74</sup> As noted above, important evidence has been provided by  $\alpha$ DKIE's of  $k_H/k_D > 1.0$  measured on the deglycosylation step, which are consistent *only* with a covalent intermediate reacting through an oxocarbenium ion-like transition state. Direct trapping of the covalent intermediate has been achieved in several different ways. One approach involves the introduction of a fluorine substituent into the 2 or 5 position of the substrate (Figure 1-10) to slow the reaction by destabilising the positive charge that develops at the transition state and removing the important transition state hydrogen bonding interactions which develop at the 2 position.<sup>75-77</sup> Since such substitutions slow both the glycosylation and deglycosylation steps a good leaving group, typically fluoride or dinitrophenolate, is generally incorporated into the analogue to ensure that the glycosylation step is faster than the deglycosylation, and thus that the intermediate accumulates.

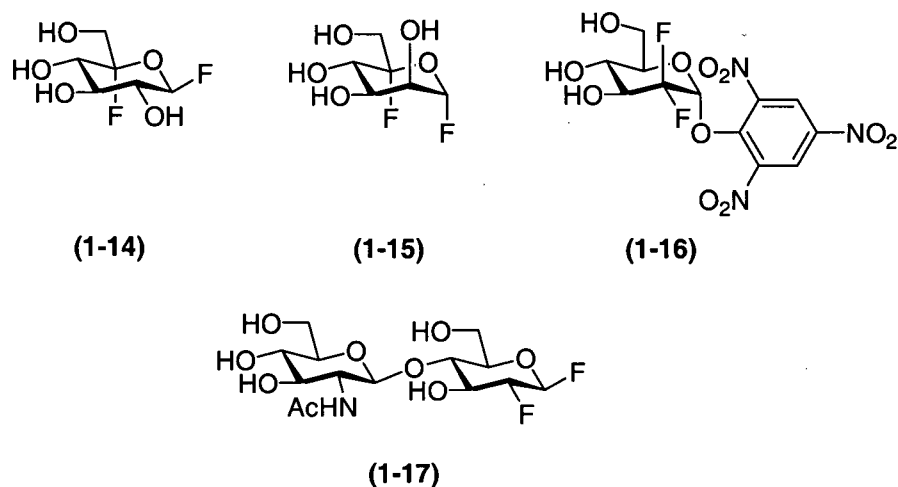


**Figure 1-10:** Examples of fluorosugar inactivators.

Inactivation of the enzyme is accompanied by the release of one full equivalent of aglycone per equivalent of enzyme. The formation of a covalent intermediate is now trivially demonstrable by electrospray mass spectrometric analysis<sup>78</sup> and <sup>19</sup>F NMR studies have provided good evidence for the stereochemistry of the linkage.<sup>79,80</sup> The catalytic competence of these intermediates (with typical lifetimes of days) has been evidenced by their accelerated turnover in the presence of acceptor sugars, via transglycosylation (Figure 1-11):

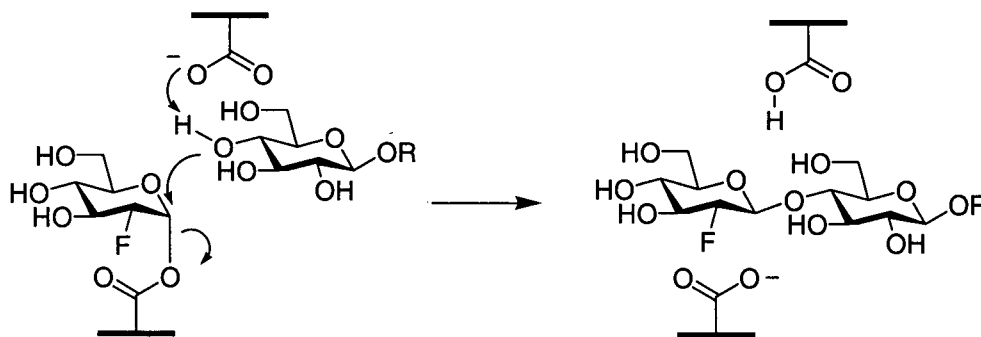


**Figure 1-11:** Turnover of a 2-fluoro glycosyl enzyme by transglycosylation.

The identity of the nucleophilic amino acid residue involved in intermediate formation has been determined in a number of cases by proteolytic cleavage of the labeled protein, followed by isolation and sequencing of the glycosylated peptide. This process has been significantly accelerated by the use of LC/MS/MS protocols.<sup>78</sup> Using this or closely related

approaches the active site nucleophiles of 21 glycosidases have been identified, including a hexosaminidase,<sup>81</sup> representing approximately half of the retaining glycosidase families.<sup>82</sup>

Certainly the best insight into the nature of the glycosyl-enzyme intermediate has come from X-ray crystallographic analysis of trapped complexes. Structures of several such complexes have now been solved,<sup>50,66,71,80,83-85</sup> including the acid-base mutant of HEWL using the 2-fluoro chitobiosylfluoride inactivator **1-17**.<sup>74</sup> In one study a true cellobiosyl moiety was trapped on Cex by deletion of both the acid-base catalyst (E127A) and a histidine (H205N), then reacting the double mutant with 2,4-dinitrophenyl  $\beta$ -cellobioside.<sup>85</sup> In the resulting structure the 2-hydroxyl of the -1 sugar had formed a single, unusually short hydrogen bond (2.4 Å) to the E233 oxygen. This strongly implies that the substantial contribution of the 2-hydroxyl to catalysis with this enzyme ( $10 \text{ kcal} \cdot \text{mol}^{-1}$ ) arises from a strong hydrogen bond, possibly of the low-barrier type,<sup>86</sup> in the transition state. The interaction observed would become shorter and stronger at the transition state through flattening of the sugar ring *and* approach of the carboxylate. In addition, positive charge developed at the anomeric centre would transiently increase the acidity of the 2-hydroxyl, making it a better hydrogen bond donor as shown in Figure 1-12. As noted above (and Chapter 3 of this thesis) this may be a general phenomenon for retaining glycosidases with appropriately configured 2-hydroxyls.<sup>34</sup>

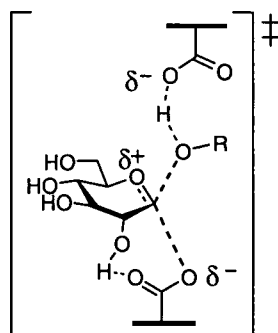


**Figure 1-12:** Retaining glycosidase transition state involving a short hydrogen bond between the 2-hydroxyl and the nucleophile.

A remarkably different substrate conformation was observed for 2-deoxy-2-fluoroxyllobiosyl-enzyme intermediate formed on Bcx.<sup>87</sup> In this case the covalently linked -1 xylosyl moiety was distorted into a <sup>2,5</sup>B boat conformation (Figure 1-13) whereas the corresponding 2-deoxy-2-fluoroxyllobiosyl-enzyme intermediate in Cex accommodated the -1 sugar ring in an undistorted <sup>4</sup>C<sub>1</sub> chair.<sup>84</sup> As proposed earlier for yeast  $\alpha$ -glucosidase,<sup>88</sup> such

distortion places C5, O5, C1 and C2 in a planar array, ideally set up for stabilisation of oxocarbenium ion character at the transition state. Also observed in the Bcx structure was a bifurcated hydrogen bond formed by the Y69 hydroxyl group to the covalently linked oxygen of E78 and the sugar ring endocyclic oxygen (Figure 1-13a). Upon bond cleavage and positive charge development at O5 the symmetry of this arrangement will be broken and a hydrogen bond will develop to the partially negatively charged E78 oxygen. Simultaneously, a stabilizing electrostatic or dipolar interaction could develop with the ring oxygen, as shown in Figure 1-13b. A very similar interaction was observed in the covalent intermediate for *Bacillus circulans* cyclodextrin glucanotransferase, but in this case the nucleophile carboxyl oxygen had the appropriate orientation to donate negative charge to an electropositive endocyclic oxygen in the transition state (Figure 1-13c).<sup>50</sup>

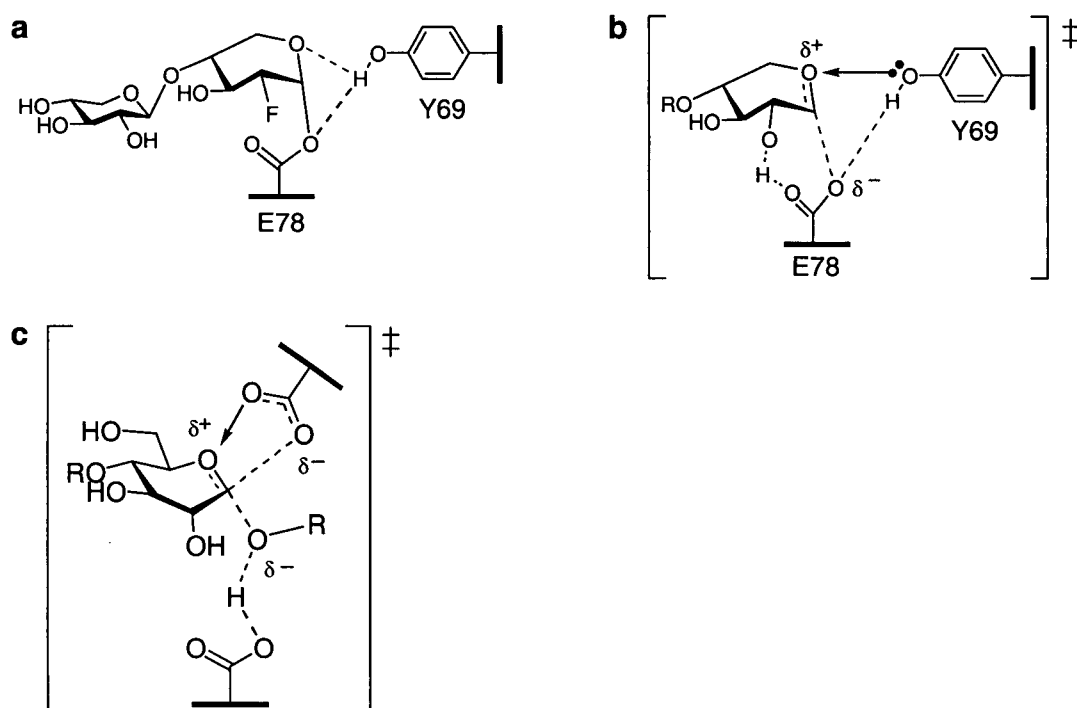


**Figure 1-13:** Bcx trapped as a covalent intermediate (a) and implications for the transition state (b). The corresponding transition state for *Bacillus circulans* cyclodextrin glucanotransferase (c).

### Objectives of This Thesis: Glycosidase Mechanisms

The first component of this thesis explores basic questions in enzyme mechanism. Chapter 2 describes the development of a new technique, called time-resolved ESI-MS, as a means of

detecting transient enzyme intermediates and measuring the rate constants for their formation and decomposition. The covalent intermediates formed by retaining glycosidases present an ideal system with which to develop this method. Chapter 3 explores the catalytic features of a retaining  $\beta$ -mannosidase, with particular attention dedicated to the role of the substrate 2-hydroxyl in catalysis and features of the acid-base catalyst.

## **Chapter 2 Application of Mass Spectrometry to Enzyme Kinetics**

## Introduction to ESI-MS and Time-Resolved ESI-MS

Reaction kinetic analysis is a study of mass balance as a function of time. In this regard a mass spectrometer would appear to be the ideal instrument with which to monitor a chemical reaction. However, prior to the development of 'soft' ionisation techniques in the 1980's, namely matrix assisted laser desorption ionisation (MALDI) and electrospray ionisation (ESI), the accurate quantification of large chemical species as a function of time without the complication of fragmentation was impossible. This was particularly true for delicate structures such as enzymes and oligonucleotides. This chapter will focus on the use of ESI-MS for enzyme kinetics.

During the ESI process, intact molecular ions are generated directly from solution at atmospheric pressure by rapid vaporization of the surrounding solvent (Figure 2-1). A high voltage (3-6 kV) is applied to a metal capillary through which the analyte solution flows at 1-10  $\mu\text{L min}^{-1}$ . In the positive ion mode of ESI operation, the capillary is biased positively and positive ions in solution are formed in the gas phase. Specifically, positive ions in solution are pushed by the electric field to the tip of the capillary and ultimately emitted as a fine mist of positively charged droplets. These droplets shrink in size through solvent evaporation and Rayleigh fission. This latter process occurs when the electric field at the droplet surface overcomes surface tension causing smaller droplets to form spontaneously. Eventually, desolvated ions are created which drift under the influence of the electric field towards the sampling orifice of the mass spectrometer. A stream of dry nitrogen (or 'curtain' gas) flows across the sampling orifice to further assist droplet drying. The ions then proceed from the sampling orifice towards a skimmer orifice of the mass analyzer, beyond which differential pumping is applied to attain the vacuum required for mass analysis. An electric field is also applied between the sampler and skimmer to push ions towards the skimmer, as well as accelerate ions through the curtain gas. This helps to decluster ions and can even be used to fragment them. This electric field, which can be adjusted in real time while collecting data, is particularly useful for probing non-covalent interactions between a ligand and a protein. Three types of mass analyzers are typically used for ESI-MS (quadrupole, time-of-flight and ion cyclotron resonance), the specifics of which are reviewed extensively<sup>89</sup> and will not be discussed here.

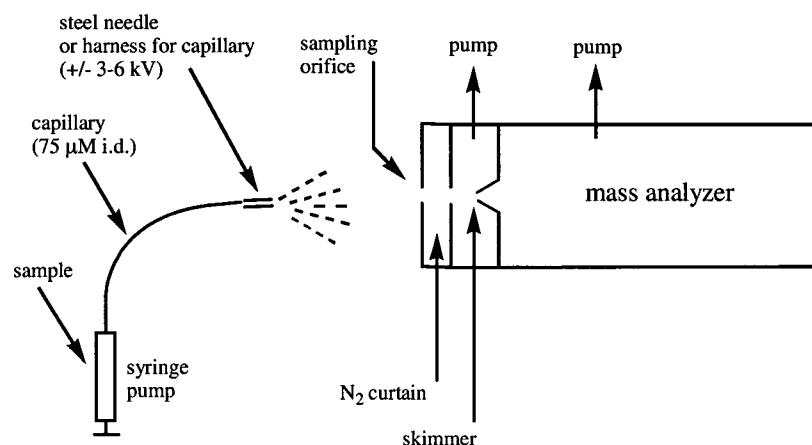


**Figure 2-1:** Simplified scheme of ESI-MS.

In the commonly used positive-ion mode of operation of ESI-MS, three classes of positive ions may be observed. These are atoms or molecules that carry an inherent positive charge (such as a quaternary amine or  $\text{Na}^+$ ), adduct ions (a neutral molecule combined with a cation, typically  $\text{Na}^+$ ,  $\text{K}^+$ , or  $\text{NH}_4^+$ ) or protonated ions. Adduct ions, which can complicate a mass spectrum, can be minimized by desalting the sample prior to analysis. In the case of large structures, such as proteins, the ion is multiply charged from the attachment of several protons. Thus in the corresponding mass spectrum one observes several ion forms of differing  $m/z$  values and intensities, each corresponding to a different charge state. The entire series of ions is commonly known as a charge envelope. It should be noted that the charge states in an envelope do not correlate with the number of basic sites on a protein. Instead, the distribution of the charge envelope is exquisitely sensitive to the conformation of the protein ion in the gas phase, which is in turn a snapshot of the corresponding solution fold (Figure 2-2).<sup>90</sup> Thus depending on the initial solution conditions, a gas phase protein ion with a native, denatured or intermediate gas phase fold may be generated. In general, a native conformation yields an envelope with lower charge states than a denatured conformation, stemming from the fact that the latter has a greater surface area on which protons may attach. Due to the remarkably mild nature of the ESI process, as well as the sensitivity of the resulting charge envelope to protein conformation, ESI-MS not only serves an important role in investigations on the primary structure of proteins (and other biomolecules),<sup>91,92</sup> but also in the study of non-covalent protein interactions,<sup>93</sup> protein folding,<sup>94-96</sup> and the structures of gas phase proteins.<sup>97-99</sup>

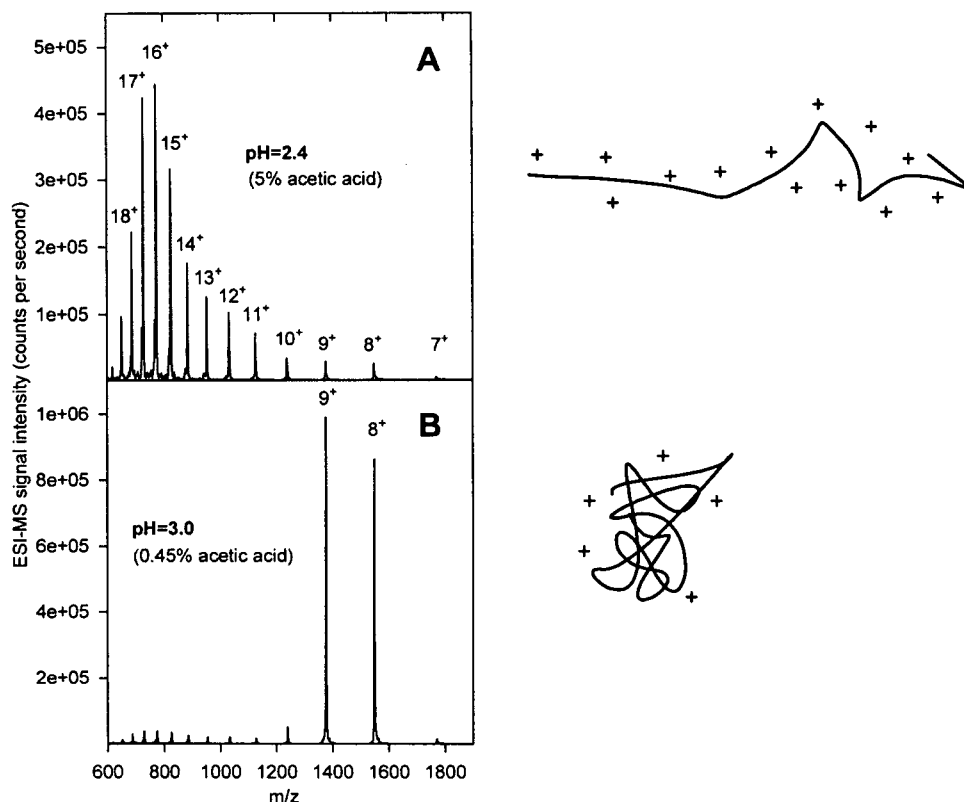


**Figure 2-2:** ESI-MS of cytochrome *c* denatured at pH 2.4 (a) and in the native fold at pH 3.0 (b). Reproduced with permission.<sup>100</sup>

The new method of “time-resolved” ESI-MS, which couples a continuous-flow mixing capillary directly to an ESI source (Figure 2-3), allows the rates of chemical reactions to be monitored with a mass spectrometer. At the current state of development it can be used to measure reaction kinetics on a time-scale of tens of milliseconds.<sup>101</sup> The first successful application of time-resolved ESI-MS on a sub-second time scale involved the study of protein folding kinetics.<sup>100,101</sup> Different protein conformations in solution were identified by the different charge state distributions they generate during ESI. It was demonstrated that this technique is especially useful in studying the kinetics of folding reactions that are coupled to the loss or binding of a ligand. Protein states with and without ligand can be easily separated by their different masses if the ligand-protein interactions are not disrupted during ESI.

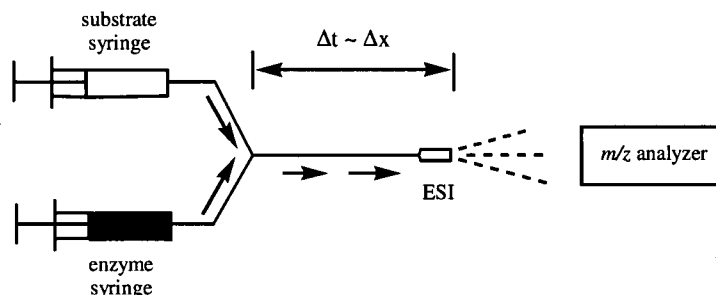


**Figure 2-3:** Experimental apparatus for time-resolved ESI-MS. Arrows indicate solution flow. The flow time  $\Delta t$  in the reaction capillary is proportional to the capillary length  $\Delta x$ .

Recently it was proposed that time-resolved ESI-MS could become a powerful tool to monitor the kinetics of enzymatic reactions.<sup>102</sup> Potentially, ESI-MS will allow the simultaneous detection of substrates, intermediates, and products of enzymatic reactions, as well as the detection of covalent or non-covalent enzyme-substrate complexes. The use of ESI-MS could obviate the need for chromophoric substrates and coupled assays that are currently required to monitor the kinetics of most enzymatic reactions. Indeed, the detection of enzyme-inhibitor complexes<sup>103</sup> and steady-state enzyme-substrate or product complexes by ESI-MS<sup>104</sup> has been demonstrated previously. Likewise, covalent enzyme intermediates have been detected in serine proteases,<sup>105</sup> elastase,<sup>106</sup>  $\beta$ -lactamase,<sup>107-109</sup> and numerous glycosidases.<sup>82</sup> Lee et al.<sup>110</sup> used a continuous sample introduction system to monitor the steady-state kinetics of lactase. More recently, a pulsed-flow device coupled to ESI-MS, operating on a 30 ms time-scale, was used successfully to detect a highly unstable tetrahedral-intermediate in the reaction catalyzed by 5-enolpyruvoyl-shikimate-3-phosphate synthase,<sup>111</sup> but no kinetic parameters were determined. However, a stopped-flow device coupled to ESI-MS, capable of a 25 ms time scale, was used to monitor the Britton reverse transport kinetics of carbonic anhydrase.<sup>112</sup>

Pre-steady state analysis has been applied widely to the study of transient intermediates in enzymic reactions<sup>113-116</sup> including the covalent intermediates formed by retaining glycosidases. Stopped-flow UV-Vis spectroscopy was used to determine the glycosylation and deglycosylation rate constants for *Cellulomonas fimi*  $\beta$ -1,4-glycanase<sup>62,117</sup> and *Agrobacterium* sp.  $\beta$ -glucosidase<sup>34,64,118</sup> using substrates that were hydrolyzed with rate-limiting deglycosylation. Likewise, the pre-steady state 'bursts' of phenolate observed for the hydrolysis of reactive aryl- $\beta$ -galactosides by *Escherichia coli* (lac Z)  $\beta$ -galactosidase provided early evidence for a glycosyl-enzyme intermediate.<sup>119-121</sup> The remainder of this chapter describes the

first use of time-resolved ESI-MS to monitor the pre-steady state kinetics of enzymatic reactions by direct observation of transient enzyme intermediates.

### Application of Time-resolved ESI-MS to *Agrobacterium* sp. $\beta$ -glucosidase

To apply time-resolved ESI-MS to enzyme kinetics, we initially chose the reaction of *Agrobacterium* sp.  $\beta$ -glucosidase (Abg) with D-glucal as a model system. This reaction involves attack of the enzyme nucleophile (Glu 358) on the reactive enol-ether of D-glucal, forming a 2-deoxy glucosyl-enzyme intermediate (Figure 2-4). The low  $k_{cat}$  and  $K_M$  values previously determined with *p*-nitrophenyl 2-deoxy  $\beta$ -D-glucoside ( $k_{cat} = 0.025 \text{ s}^{-1}$ ,  $K_M = 15 \text{ }\mu\text{M}$ ,  $37^\circ\text{C}$ ), which forms the same 2-deoxy-glucosyl enzyme as D-glucal, suggested accumulation of this intermediate, and indeed pre-steady state kinetic analysis was possible with this substrate.<sup>34</sup> The dramatic reduction in the deglycosylation rate was attributed to substantial contributions of the 2-hydroxyl to catalysis in Abg, which are absent in this particular glycosyl-enzyme.<sup>34</sup>

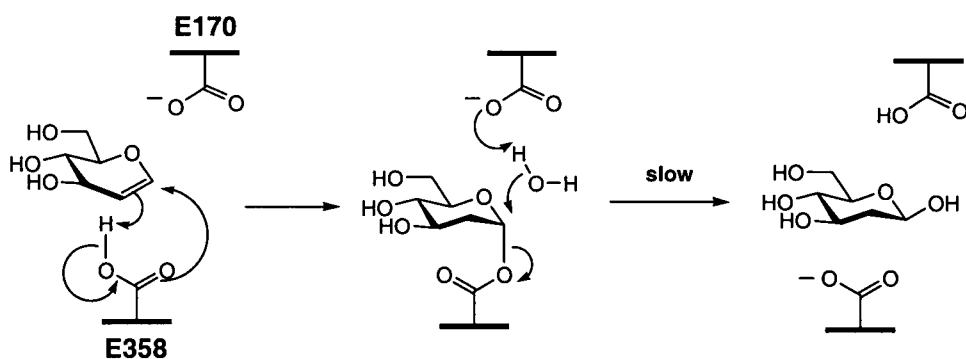


**Figure 2-4:** Mechanism for the reaction of Abg with D-glucal.

Initially, the ESI mass spectrum of Abg was obtained under 'native' conditions (5 mM ammonium acetate, pH 6.86) in the absence of substrate (Figure 2-5). Low charge states were observed for monomeric Abg ( $M 6^+$  to  $M 14^+$ ), consistent with a structure of a folded enzyme in the gas phase. Under denaturing conditions (5% acetonitrile, 0.1% TFA), the charge states observed in the ESI mass spectrum of Abg typically range from  $30^+$  to  $60^+$  (data not shown). Intriguingly, charge states that could only be assigned to dimeric and tetrameric forms of Abg were also observed. The relative abundance of the multimeric ion peaks could be increased by decreasing the declustering voltage (data not shown). Although multimers could also form non-specifically, this result is consistent with previous gel filtration studies that indicated Abg was

predominantly dimeric in solution. Likewise, the recent X-ray crystal structure of a *Bacillus circulans* sp.  $\beta$ -glucosidase, which has 46% sequence identity to Abg, revealed an octameric form for that enzyme, also consistent with prior biochemical studies.<sup>122</sup> That multimeric forms of Abg are observed by ESI-MS suggests that the forces involved in forming these complexes must be reasonably strong, and may have an impact on catalysis itself. Indeed, in the structure of the *Bacillus* enzyme the active sites in each dimer appear to face one another and limit access of substrate. This suggests that the monomer is the more active form of the enzyme.

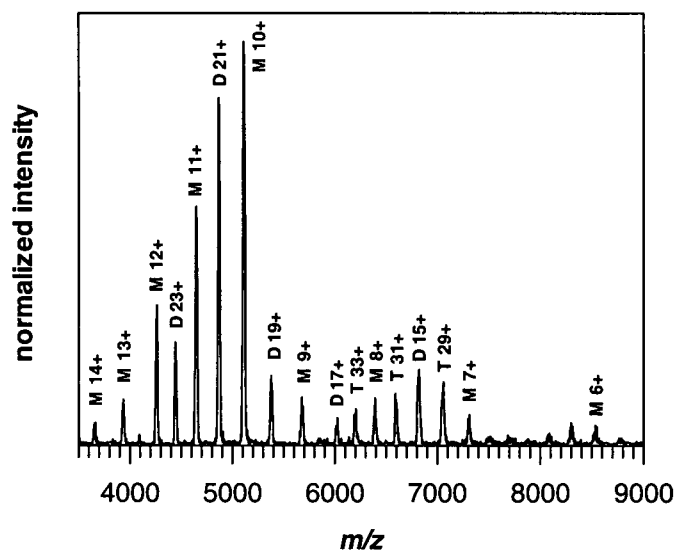


**Figure 2-5:** ESI mass spectrum of Abg (MW = 51 200 Da) under 'native' conditions (29  $\mu$ M Abg, 5 mM ammonium acetate, pH 6.86, 23°C). Charge states attributed to monomeric (M), dimeric (D) and tetrameric (T) forms of Abg are indicated. Note that monomeric peaks may also include dimeric and tetrameric forms of Abg (e.g.: M 10<sup>+</sup> = D 20<sup>+</sup> = T 40<sup>+</sup>).

Having established appropriate ESI conditions, the reaction of Abg with D-glucal was investigated. Two separate syringes mounted on a syringe pump (Figure 2-3) were charged with solutions of Abg and D-glucal, each buffered with 5 mM ammonium acetate (pH 7). The syringes were simultaneously advanced at 4  $\mu$ L min<sup>-1</sup> to give a total flow rate of 8  $\mu$ L min<sup>-1</sup> downstream of the reaction tee (75  $\mu$ m internal diameter). Reaction capillary lengths ranging from 1 to 187 cm afforded reaction times of 0.5 s to 81 s at this flow rate. After 81 s reaction with 10 mM D-glucal a shift in the mass spectrum was observed, corresponding to complete accumulation of Abg as the 2-deoxy glucosyl intermediate. Upon closer examination of the 10<sup>+</sup> charge state it became apparent that complete resolution of the free and covalent intermediate forms of Abg ( $\Delta$  +147 amu) would not be possible (Figure 2-6). This was due to the

heterogeneity of the enzyme, in which a proportion of the enzyme population is missing an *N*-terminal methionine ( $\Delta -132$  amu). The spectrum was further complicated by an intermediate species, which could not be assigned, corresponding to Abg less 50 amu. Nevertheless, the mass shift was unambiguous. Moreover, after some time the mass spectrum was observed to shift back to its original position, corresponding to complete turnover of D-glucal and recovery of the free enzyme (data not shown).

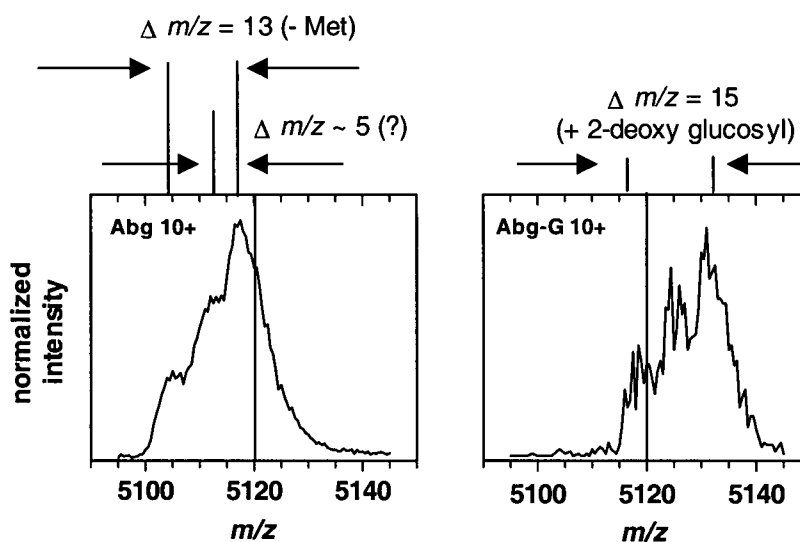


**Figure 2-6:** Analysis of the  $10^+$  charge state in the Abg ESI mass spectrum before ( $\text{Abg } 10^+$ ) and after reaction with D-glucal (10 mM, 81 s) to form the 2-deoxy glucosyl enzyme intermediate ( $\text{Abg-G } 10^+$ ). The small shoulder at  $m/z$  5105 in the  $\text{Abg } 10^+$  spectrum corresponds to Abg missing the *N*-terminal methionine (MW = 132 amu). The origin of the 'middle' shoulder at  $m/z$  = 5113 is unknown. The MW of the 2-deoxy glucosyl adduct is 147 amu.

A time course for this reaction at various concentrations of D-glucal was obtained by varying the reaction capillary length while maintaining constant total flow rate ( $8 \mu\text{L min}^{-1}$ ). Data collection was limited to the most abundant ion, in this case the  $10^+$  charge state (Figure 2-7). Over a period of approximately 80 s the position of the  $10^+$  charge state was observed to shift to that of the covalent intermediate form of Abg, indicating that this time regime corresponded to the pre-steady state of the reaction. Moreover, as the concentration of D-glucal increased (0.5 to 10 mM) the rate at which Abg accumulated as the covalent intermediate increased, as expected. Despite being unable to quantify free and covalent intermediate forms of the enzyme as a function of time, the reaction constant ( $k_{+2}$ ) for this reaction can be estimated to be  $1\text{-}10 \text{ s}^{-1}$  ( $23^\circ\text{C}$ ). In comparing these results with those obtained with the substrate *p*-nitrophenyl 2-deoxy- $\beta$ -D-glucoside ( $k_{+2} = 19 \text{ s}^{-1}$ ,  $K_d = 4.4 \text{ mM}$ ,  $37^\circ\text{C}$ ),<sup>34</sup> which forms the same 2-deoxy glucosyl

intermediate, it is evident that the reaction with the enol ether moiety of D-glucal is comparable to the reaction with the anomeric carbon bearing a *p*-nitrophenol leaving group.

The results with Abg and D-glucal illustrate one shortfall of kinetic analysis by time-resolved ESI-MS. Specifically, the mass spectra of reactants and products must be clearly resolved to allow accurate measurement of the progress of the reaction. If one is monitoring changes in the mass of the enzyme directly, the enzyme population must be homogeneous. An alternative is to monitor substrate and product mass spectra, rather than the enzyme. However, what was encouraging from these results was our ability to monitor a reaction, if only at a qualitative level, with a substrate that did not offer a simple assay on the timescale considered here. The only alternative would be to synthesize radiolabelled D-glucal and use rapid quench-flow methods. Of perhaps even greater interest would be to examine the response of dimeric and tetrameric forms of Abg to glycosylation with D-glucal. Is catalysis reduced or enhanced relative to monomeric forms of the enzyme? Complete isolation of the covalent intermediate as the 2-fluoro-glucosyl-enzyme is also possible, allowing one to make 'static' comparisons of free and intermediate forms of Abg.

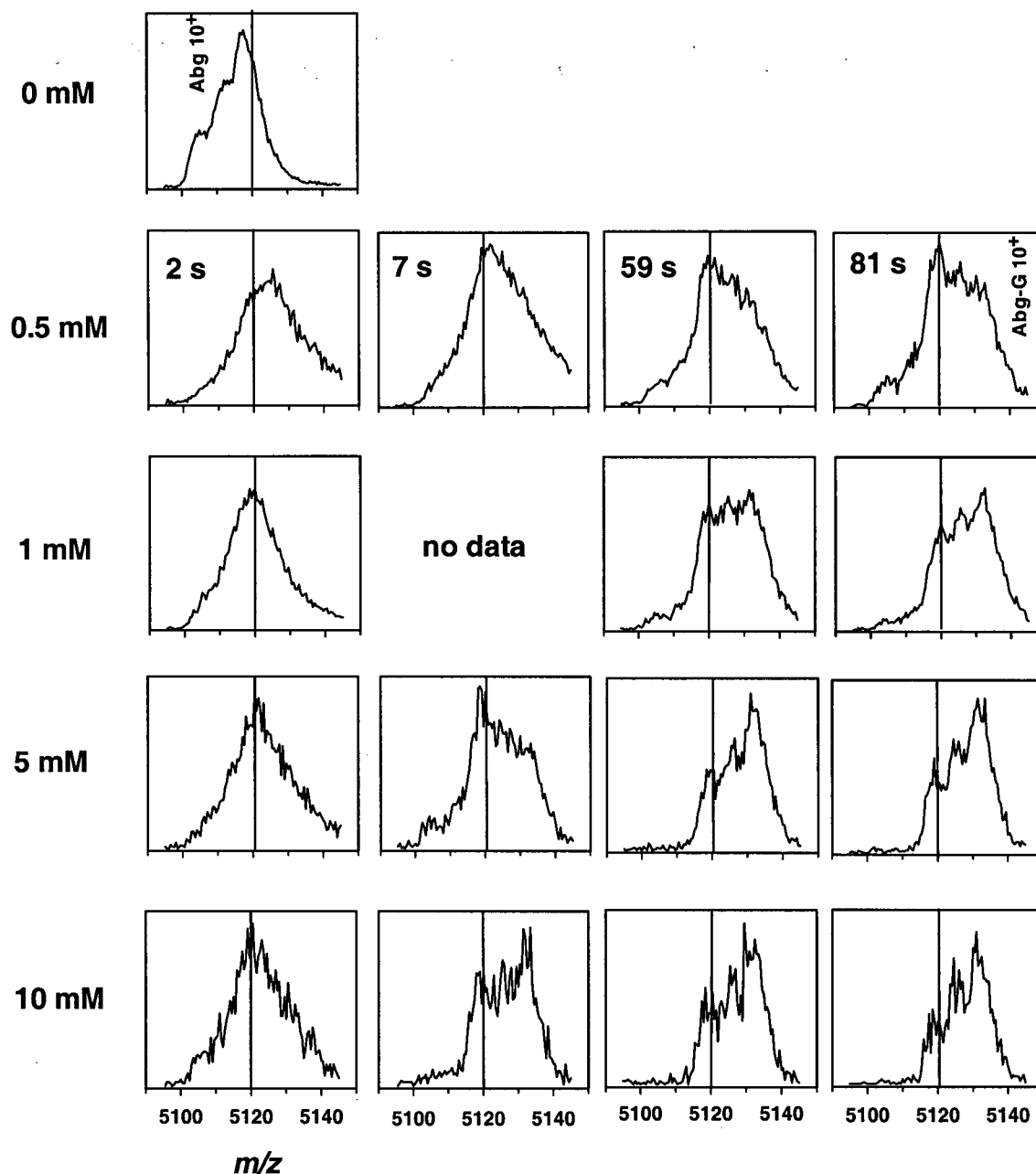


**Figure 2-7:** Monitoring the reaction of Abg (24 μM) with D-glucal in the pre-steady state with time-resolved ESI-MS (5 mM ammonium acetate, pH 7, 23°C). Only the 10<sup>+</sup> charge state is shown, with the vertical line indicating  $m/z = 5120$ . Final, mixed concentrations of D-glucal and reaction times are indicated. Abg-G = glycosyl-enzyme

### Application of Time-resolved ESI-MS to *Bacillus circulans* Xylanase

An extensively characterized xylanase from *Bacillus circulans* (Bcx) was chosen as a second model enzyme system for time-resolved ESI-MS. This is a small Family 11 glycosidase that cleaves the β-1,4 glycosidic bonds of xylan to release xylobiose. Hydrolysis occurs with retention of anomeric configuration,<sup>28</sup> necessarily implying the involvement of a covalent

xylobiosyl-enzyme intermediate ( $E-X_2$ ) as part of the classical double-displacement mechanism (Figure 2-8). Glu 78 was identified as the catalytic nucleophile by trapping the covalent intermediate with 2,4-dinitrophenyl 2-deoxy-2-fluoro  $\beta$ -xylobioside and subsequent analysis of the proteolytically digested enzyme by ESI-MS/MS techniques.<sup>123</sup> Moreover, the free and glycosyl-enzyme intermediate forms of Bcx have been characterized by X-ray crystallography<sup>87,124</sup> and NMR spectroscopy.<sup>69,125,126</sup> Wild type Bcx has not been amenable to pre-steady state kinetic analysis by stopped-flow UV-Vis spectroscopy due to the fact that the glycosylation step is rate-limiting with all known synthetic substrates.<sup>63</sup> However, as shown in this study, the deglycosylation step is rate-limiting for the mutant Bcx Y80F with the substrate 2,5-dinitrophenyl  $\beta$ -D-xylobioside (2,5-DNPX<sub>2</sub>), leading to accumulation of  $E-X_2$  at a rate that can be monitored in the pre-steady state phase by time-resolved ESI-MS.

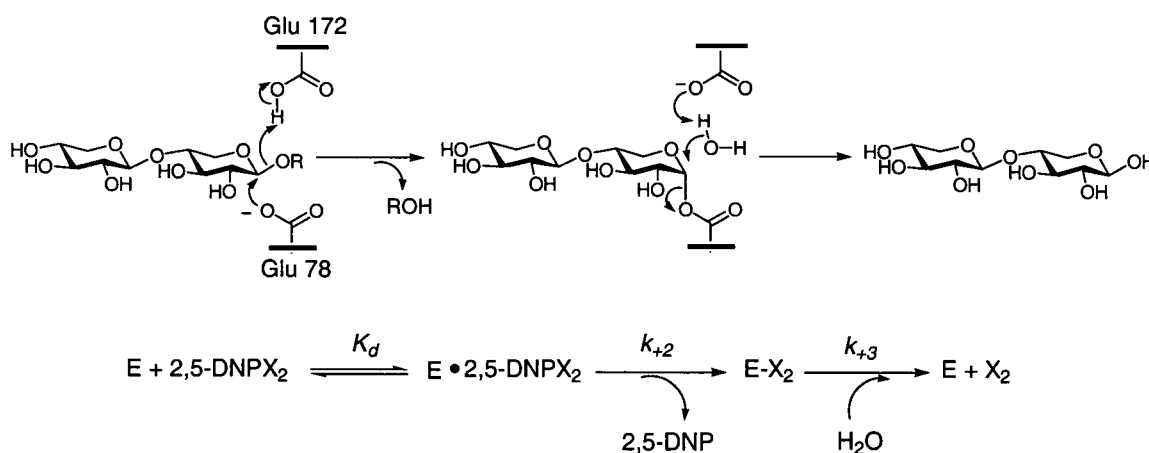


**Figure 2-8:** Mechanism and kinetic scheme for the hydrolysis of 2,5-dinitrophenyl  $\beta$ -D-xylobioside (2,5-DNPX<sub>2</sub>) by *Bacillus circulans* xylanase (Bcx).

### Steady-state kinetics and stopped-flow spectroscopy

The kinetic behaviour of a retaining glycosidase such as Bcx may be analyzed according to the three step mechanism illustrated in Figure 2-8. In order to monitor meaningful pre-steady state kinetics for the formation of the covalent intermediate  $E-X_2$  or the corresponding release of 2,5-DNP the deglycosylation step must be rate limiting ( $k_{+2} > k_{+3}$ ). In the case of the wild type Bcx, glycosylation ( $k_{+2}$ ) is rate limiting, even with the most reactive of aryl- $\beta$ -xylobiosides.<sup>63</sup> The corresponding Y80F mutant hydrolyzes 2,5-DNPX<sub>2</sub> 480 fold slower ( $k_{cat} = 0.042 \text{ s}^{-1}$ ) than the wild type enzyme ( $k_{cat} = 20 \text{ s}^{-1}$ ), while a substantially lower  $K_M$  (60  $\mu\text{M}$  for the mutant, 1.8 mM for the wild type) suggests the accumulation of  $E-X_2$ . That deglycosylation is now rate limiting

is verified by the pre-steady state bursts of 2,5-DNP observed by stopped-flow UV-Vis spectroscopy (Figure 2-9). This change in rate determining step supports the role of Tyr 80 in positioning the attacking water, as well as perturbing the pKa of Glu 172 through a hydrogen bond.<sup>63,87</sup> The loss of this interaction in the Y80F mutant has been observed to increase the pKa's of Glu 172 (from 6.8 to 7.8) and Glu 78 (from 4.6 to 4.8), resulting in a shift in pH optimum from 5.7 to 6.3 (M.D. Joshi, L.P. McIntosh, personal communication). This substantial increase in pKa for the general acid-base catalyst can be expected to reduce both glycosylation and deglycosylation rates. However, the reactive aglycone of 2,5-DNPX<sub>2</sub> (pKa = 5.1) does not require general acid catalytic assistance for departure, therefore hydrolysis rates will be limited only by the deglycosylation step, resulting in accumulation of E-X<sub>2</sub>. It is interesting to note that the Y80F mutation has a greater deleterious effect on the hydrolysis rate of 2,5-DNPX<sub>2</sub> than mutations that eliminate general acid-base catalysis altogether (E172N, E172S)<sup>63</sup> underscoring the importance of this residue to catalysis.

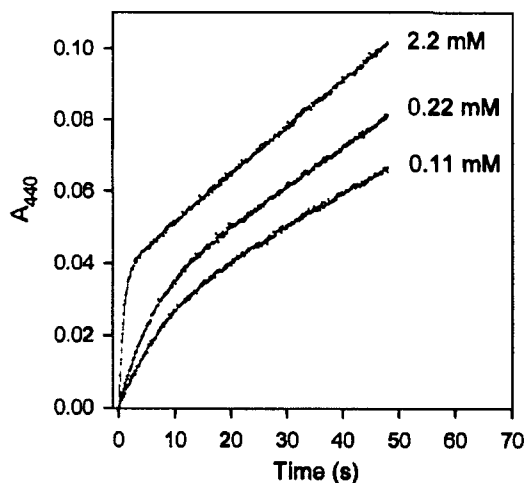


**Figure 2-9:** Hydrolysis of 2,5-DNPX<sub>2</sub> by Bcx Y80F (10 μM), monitoring the release of 2,5-DNP in the pre-steady state by stopped-flow UV-Vis spectroscopy. The substrate concentrations for the individual curves are as indicated.

#### *Observation of the covalent intermediate by time-resolved ESI-MS*

As noted above, the rate-limiting step for wild type Bcx is glycosylation, even with the reactive substrate 2,5-DNPX<sub>2</sub>. However, the glycosylation and deglycosylation rates must be of the same order of magnitude because a low steady-state concentration (~ 5%) of E-X<sub>2</sub> was detected in the time-resolved ESI mass spectrum when Bcx was mixed with 2.2 mM 2,5-DNPX<sub>2</sub>, a concentration which afforded approximately half-saturation of the enzyme ( $K_M = 1.8$  mM)

(Figure 2-10). If glycosylation had been very much slower than deglycosylation ( $k_{+2} \ll k_{+3}$ ), E-X<sub>2</sub> would not have accumulated to a detectable level. It is noteworthy that indirect detection of E-X<sub>2</sub> had been impossible using stopped-flow UV-Vis spectroscopy.<sup>63</sup> Indeed, this intermediate had only been accessible through trapping with a mechanism-based inactivator.<sup>123</sup>

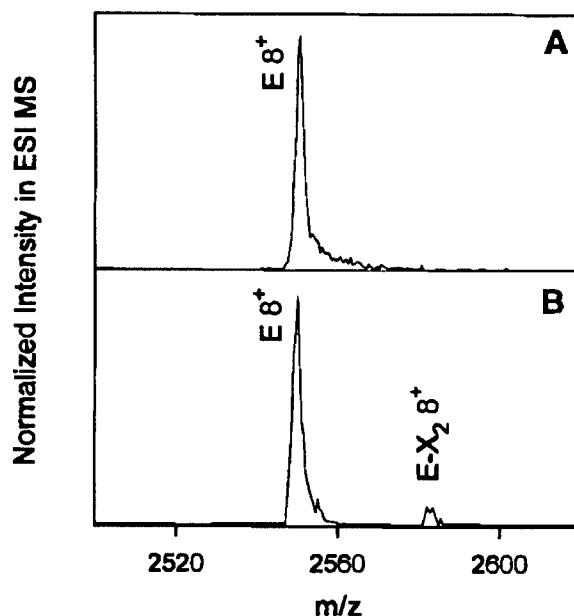


**Figure 2-10:** Detection of a transient enzyme intermediate with time-resolved ESI-MS. ESI mass spectra of wild type Bcx (4  $\mu$ M) recorded before (A) and after mixing with 2,5-DNPX<sub>2</sub> (2.2 mM) for 130 ms (B). Only the 8<sup>+</sup> peaks are shown. The small peak at  $m/z = 2583$  (B) corresponds to the covalent xylobiosyl-enzyme intermediate (E-X<sub>2</sub>).

The ESI mass spectrum of the mutant Bcx Y80F in 5 mM ammonium acetate buffer (pH 6.3, no substrate) displays a charge state distribution that is virtually identical to that of the wild type enzyme, with a characteristic maximum at 8<sup>+</sup> (data not shown). The  $m/z$  values of the peaks in the spectrum agree with the calculated mass of the mutant (MW = 20 384 Da). A very similar spectrum was recorded 0.5 s after mixing the enzyme with 0.11 mM 2,5-DNPX<sub>2</sub> (Figure 2-11, A). However, after 4.2 s (Figure 2-11, B) each of the peaks in the spectrum displayed a pronounced satellite peak. Based on the  $m/z$  values, these satellite peaks can be assigned to the covalent xylobiosyl-enzyme intermediate E-X<sub>2</sub> (MW = 20 649 Da). The spectrum recorded after 48 s (Figure 2-11, C) displayed an even higher intensity for the E-X<sub>2</sub> peaks. Similar intensity ratios between E and E-X<sub>2</sub> peaks were observed for the different charge states for all reaction times and substrate concentrations.

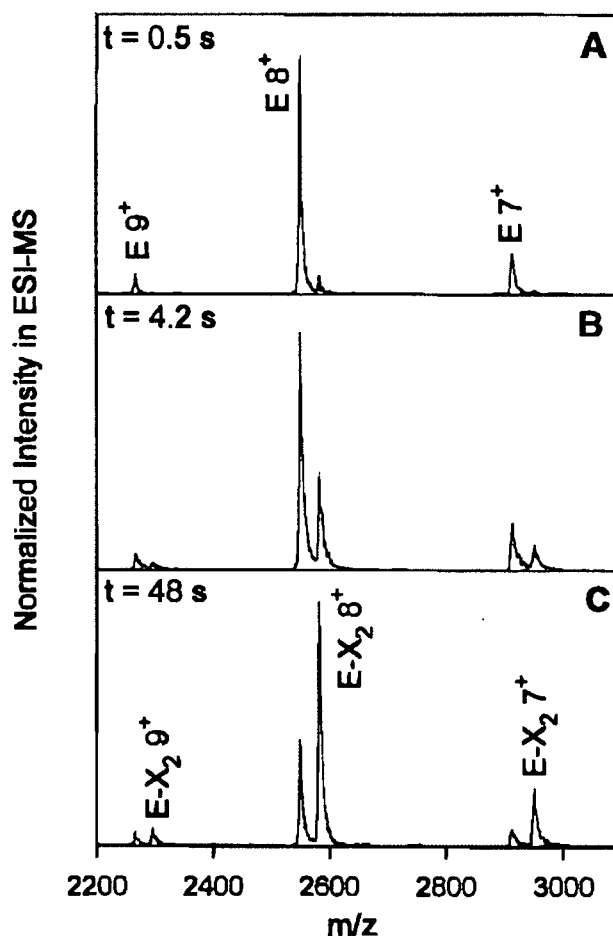


**Figure 2-11:** ESI mass spectra recorded at 0.5 s (A), 4.2 s (B) and 48 s (C) after mixing a solution of Bcx Y80F (0.08 mg/mL, 4  $\mu$ M) with the substrate 2,5-DNPX<sub>2</sub> (110  $\mu$ M). Peaks in the spectrum correspond to free enzyme (E) and the covalent xylobiosyl-enzyme intermediate (E-X<sub>2</sub>).

### *Pre-steady state kinetic analysis by time-resolved ESI-MS*

From Figure 2-11 (A-C) it is evident that the ESI charge state distributions for the free enzyme E and the intermediate E-X<sub>2</sub> are very similar; both have most of their overall intensity in the respective 8<sup>+</sup> peak. The average of several spectra afforded reproducible intensity ratios for the two 8<sup>+</sup> peaks, which can be used as a measure of the relative concentration of E-X<sub>2</sub> in solution as a function of time. Measurement of peak areas gave identical values for the fraction of E-X<sub>2</sub>. The results of some representative pre-steady state kinetic measurements are shown in Figure 2-12. Consistent with the kinetic scenario in which  $k_{+2} > k_{+3}$  (Figure 2-8), the steady state concentration of the covalent complex E-X<sub>2</sub> with saturating substrate comprised 95% of the total enzyme. As observed for the rate of phenolate release (Figure 2-9), the pre-steady state

accumulation of E-X<sub>2</sub> follows first order kinetics. The dependence of  $k_{obs}$  on substrate concentration is shown in Figure 2-13. The absence of any saturation behaviour would indicate that the  $K_d$  value for binding of 2,5-DNPX<sub>2</sub> to Bcx Y80F is in the high millimolar range, consistent with  $K_M$  values measured previously for the hydrolysis of less reactive substrates by wild type Bcx.<sup>127</sup>

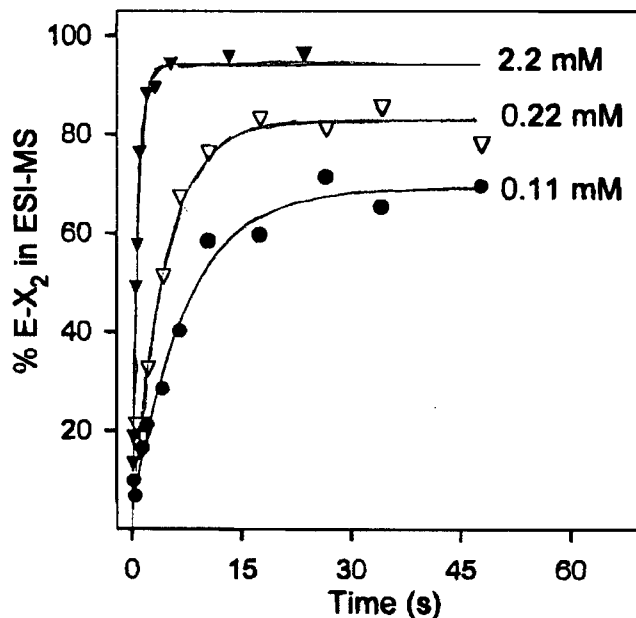


**Figure 2-12:** Relative contribution of the 8<sup>+</sup> ion generated from the covalent xylobiosyl-enzyme intermediate (E-X<sub>2</sub>) in the ESI mass spectrum as a function of time. The substrate concentrations for the individual curves are as indicated. Circular and triangular symbols represent experimental data, solid lines are single exponential fits to the data.

### *Non-covalent enzyme-substrate complexes*

The spectra in Figure 2-11 do not show any peaks that could be assigned to non-covalent enzyme-substrate or enzyme-product complexes. Recently it was observed that non-covalent inhibitor complexes formed by trypsin could only be detected by ESI-MS operating at low declustering voltages.<sup>128</sup> Similar attempts were made to detect non-covalent complexes formed by Bcx Y80F under very “mild” ion sampling conditions (declustering voltage 30 V). Under these conditions a whole series of peaks was observed for each charge state which could be assigned to gas phase ions having the composition E-(DNPX<sub>2</sub>)<sub>n</sub> with values of  $n$  ranging from 0 to about 5. This series is most likely due to the formation of non-specific gas phase adducts rather than specific enzyme-substrate or product complexes. This notion is supported by the

observation of similar clusters for the covalent intermediate E-X<sub>2</sub> [i.e. E-X<sub>2</sub>(DNPX<sub>2</sub>)<sub>n</sub>] under saturating steady-state conditions. That specific enzyme-substrate complexes are not observed in this system is not surprising; Ganem has shown previously with hen egg white lysozyme that specific non-covalent complexes are only observed when the dissociation constant is in the micro-molar range or lower.<sup>104</sup> As noted above, the  $K_d$  values in this case are much higher.

### ***Stopped-flow UV-Vis spectroscopy vs time-resolved ESI-MS***

As dictated by the kinetic mechanism shown in Figure 2-8, the first order rate of release of 2,5-DNP in the pre-steady state must be equal to the rate of accumulation of E-X<sub>2</sub>. On this basis traditional stopped-flow UV-Vis spectroscopy can be used to verify the accuracy of time-resolved ESI-MS. The linear fits of the data in Figure 2-13 (solid and dashed lines) show that the correlations of  $k_{obs}$  with substrate concentration determined by each method agree very well, within experimental error. According to the kinetic scheme in Figure 2-8, the first order rate constant for the release of phenolate, or the accumulation of E-X<sub>2</sub>, is given by equation 2-1<sup>34,113</sup>:

$$k_{obs} = k_{+3} + \frac{k_{+2}[S]}{K_d + [S]} \quad (2-1)$$

The low solubility of 2,5-DNPX<sub>2</sub> precluded saturation of Bcx Y80F in the pre-steady state, therefore equation 2-1 could not be used to determine the individual values for  $k_2$  and  $K_d$ . However, in the absence of saturation kinetics ( $[S] < K_d$ ) equation 2-1 simplifies to:

$$k_{obs} = k_{+3} + \frac{k_{+2}[S]}{K_d} \quad (2-2)$$

Therefore, the slope of the plots in Figure 5 yield the second order rate constant of  $k_2/K_d = 0.65 \text{ mM}^{-1}\cdot\text{s}^{-1}$ . This is in excellent agreement with the corresponding second order rate constant,  $k_{cat}/K_M = 0.70 \text{ mM}^{-1}\cdot\text{s}^{-1}$ , obtained from steady state kinetic analysis.

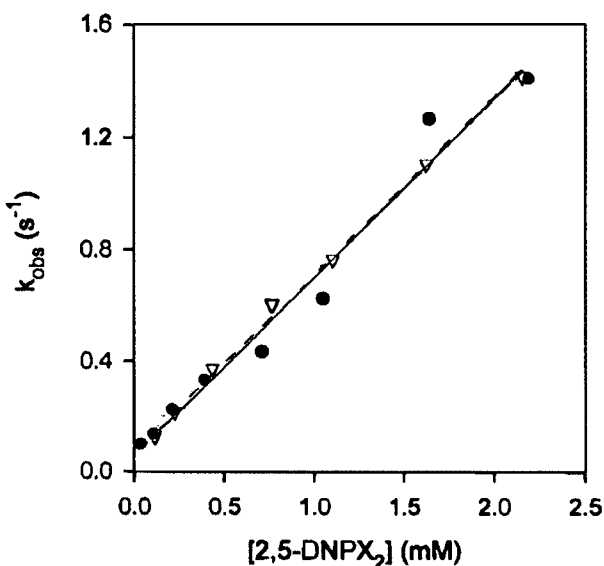


**Figure 2-13:** Validation of time-resolved ESI-MS by stopped-flow UV-Vis spectroscopy. The first order rate constant ( $k_{obs}$ ) for the pre-steady state accumulation of E-X<sub>2</sub> (filled circles), monitored by time-resolved ESI-MS, and the corresponding release of 2,5-DNP (open triangles), monitored by stopped-flow UV-Vis spectroscopy, plotted as a function of 2,5-DNPX<sub>2</sub> concentration. Linear fits of the data derived from each method are shown as solid and dashed lines.

## Conclusions and Epilogue

This study demonstrates that the pre-steady state kinetic parameters for an enzymatic reaction can be determined by time-resolved ESI-MS. In the case of Bcx, identical kinetic parameters are obtained using traditional stopped-flow UV-Vis spectroscopy, thereby verifying the accuracy of this new technique. The time resolution of the apparatus used in this work is currently limited to tens of milliseconds<sup>101</sup> this being determined by the length of the reaction capillary, and is therefore limited to enzymes with  $k_2$  values less than  $\sim 10$  s<sup>-1</sup>. Rapid chemical quench methods for monitoring enzyme intermediates currently can provide better time resolution. However, these methods require the use of radiolabelled substrates and are prone to artifacts arising from non-specific entrapment of the radioactive label. The time-resolved ESI-MS technique avoids this problem. As well, considerable improvements in flow rate are possible. Indeed, the pulsed-flow apparatus used by Paiva *et al*<sup>111</sup> for time-resolved ESI-MS generated flow rates approximately 100 fold faster than those used in this study. As noted by Northrop<sup>102</sup> the advantage of time-resolved ESI-MS over traditional pre-steady state techniques is the unambiguous identification of mechanistically important intermediates by direct observation of their mass. This advantage was aptly demonstrated by ESI-MS studies on the inhibition of

TEM-2  $\beta$ -lactamase by clavulanic acid, in which the observed mass of the acyl-enzyme intermediate formed was 44 Da less than predicted, the result of decarboxylation of the inhibitor following acylation of the enzyme.<sup>108,109</sup> As well, time-resolved ESI-MS does not require chromophoric substrates, thereby providing an opportunity to conduct enzyme kinetics with more 'native' substrates without the need for coupled assays.<sup>102</sup> Moreover, in principle, it is possible to simultaneously observe product formation and substrate depletion in addition to monitoring the formation and depletion of enzyme intermediates. Therefore a host of kinetic data may be generated in a single experiment.

Since publication of the results with Bcx the potential of time-resolved ESI-MS in the study of enzyme kinetics and mechanism has received greater consideration.<sup>114</sup> Following the pioneering work of Covey et al<sup>110</sup> the steady-state kinetics of ricin<sup>129</sup> and an  $\alpha$ -glucosidase<sup>130</sup> have been determined by ESI-MS and MALDI, respectively. Enzyme activity has even been monitored in cells using ESI-MS to quantify biotin-linked substrates and products recovered from cell lysates.<sup>131</sup> On a more demanding time-scale, the pre-steady state kinetics of a penicillin-binding protein were determined with a quench-flow apparatus and subsequent analysis of the covalently modified enzyme by HPLC ESI-MS.<sup>132</sup> Similarly, rapid quench techniques have been coupled with ESI and MALDI-MS to determine the pre-steady state kinetics of a fucosyltransferase,<sup>133</sup> a phosphatase<sup>134</sup> and dTDP-glucose-4,6-dehydratase.<sup>135</sup> In the phosphatase study, as in the case of Bcx, covalent modification of the enzyme was monitored directly and the rates obtained were verified spectrophotometrically. Moreover, in the fucosyltransferase and dehydratase studies, it was possible to simultaneously observe substrates, intermediate species and the final products and thereby obtain the corresponding pre-steady state rate constants. Conventional stopped-flow spectrophotometry and radioactivity based assays also verified these results. It is a tribute to Dexter Northrop's foresight that the general outcomes of all of these studies are predicted in his influential 1997 review.<sup>102</sup>

**Chapter 3 Mechanistic Investigations into the Retaining  $\beta$ -  
Mannosidase *Cellulomonas fimi* Man2A**

### *Cellulomonas fimi* $\beta$ -mannosidase Man2A

*Cellulomonas fimi* is a gram-positive bacterium that has the capability of degrading and subsisting on a number of plant polysaccharides, including cellulose, xylan and galactomannan. Cex is one enzyme involved in the hydrolytic breakdown of cellulose and xylan, but the catabolic pathway for galactomannan, consisting of  $\beta(1,4)$  linked mannose residues with  $\alpha(1,6)$  galactose substitution, was unknown. This became the topic of the Ph.D. work of Dominik Stoll in Professor R.A.J. Warren's lab at the University of British Columbia,<sup>136</sup> who was successful in cloning three genes expressing enzymes involved in the hydrolytic breakdown of galactomannan.<sup>137</sup> These were determined to be an  $\alpha$ -galactosidase, a  $\beta$ -mannanase and a  $\beta$ -mannosidase (Figure 3-1).

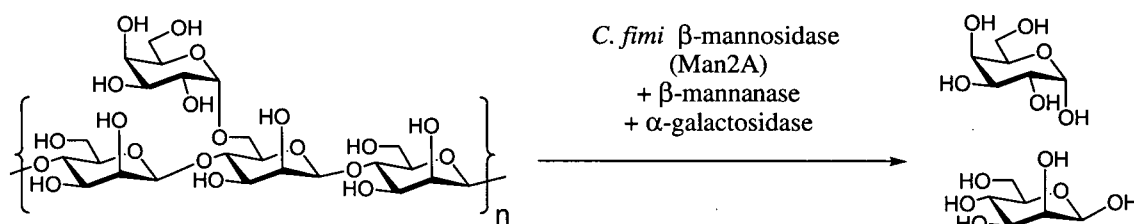


**Figure 3-1:** Enzymes involved in the degradation of galactomannan by *Cellulomonas fimi*.

The predicted peptide sequence of the 95 kDa  $\beta$ -mannosidase, named Man2A, marked this enzyme as a member of the Family 2 retaining  $\beta$ -glycosidases. A retaining mechanism was further established by labeling the active site nucleophile with the mechanism based inactivator 2-deoxy-2-fluoro  $\beta$ -D-mannosyl fluoride (Figure 3-2).<sup>138</sup> Following proteolysis and sequencing of the labeled peptide by ESI-MS/MS methods the labeled nucleophile was identified as Glu 519. Sequence alignment with other Family 2 glycosidases suggested Glu 429 was the general acid-base.

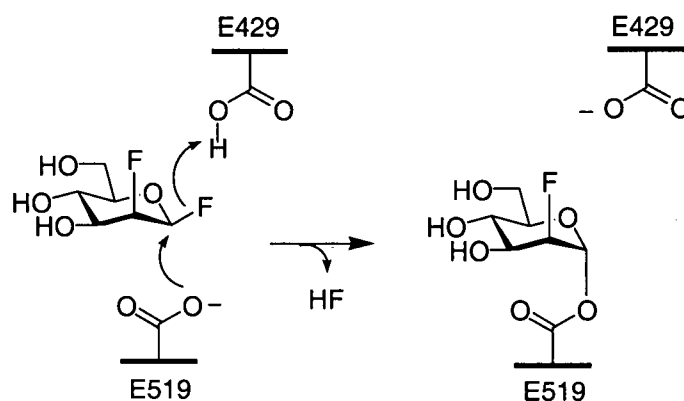


**Figure 3-2:** Labeling of the nucleophile E519 of Man2A with 2-deoxy-2-fluoro  $\beta$ -D-mannosyl fluoride. The acid-base catalyst E429 was predicted from sequence alignments.

Dominik Stoll generously provided the Man2A clone for mechanistic investigations in our lab. This was indeed an excellent opportunity from a mechanistic perspective. A retaining  $\beta$ -mannosidase had not been studied in great detail, owing to the difficulty in synthesizing the prerequisite  $\beta$ -mannoside substrates. A particular interest in this case was the contribution of the 2-hydroxyl to catalysis. As noted in Chapter 1, interactions at the 2-position appear to be universally strong in  $\beta$ -glycosidase catalysis. This was hypothesized to arise primarily from a hydrogen bond between the 2-hydroxyl and the nucleophile in the glycosylation and deglycosylation transition states. Indeed, in the case of *E. coli*  $\beta$ -galactosidase, also a member of Family 2, this interaction is worth a remarkable  $10 \text{ kcal mol}^{-1}$ .<sup>35,139</sup> However, a similar interaction in the Man2A transition state is impossible due to the axial orientation of the 2-hydroxyl in  $\beta$ -mannosides. Therefore the question arises whether interactions at the 2-position in  $\beta$ -mannosidase catalysis are as important as in other glycosidases.

### Synthesis of Substrates for Man2A

The initial challenge prior to studying Man2A was the synthesis of a series of  $\beta$ -mannoside substrates with varying reactivity.  $\beta$ -Mannosides are recognized as the most difficult of glycosidic linkages to form owing to the cis relationship of the glycosidic bond and the 2-position, as well as an anomeric configuration that is contrary to the influence of the anomeric effect. Only two chromophoric  $\beta$ -mannosides are commercially available, *p*-nitrophenyl  $\beta$ -mannoside (PNPMan) and methylumbelliferyl  $\beta$ -mannoside (MuMan), both of which have

leaving groups with very similar  $pK_a^{lg}$  values (7.18 and 7.6, respectively). Fortunately, a convenient and  $\beta$ -stereoselective synthesis of PNPMan had been published by Garegg<sup>140</sup> involving a Mitsunobu glycosylation (Figure 3-3).

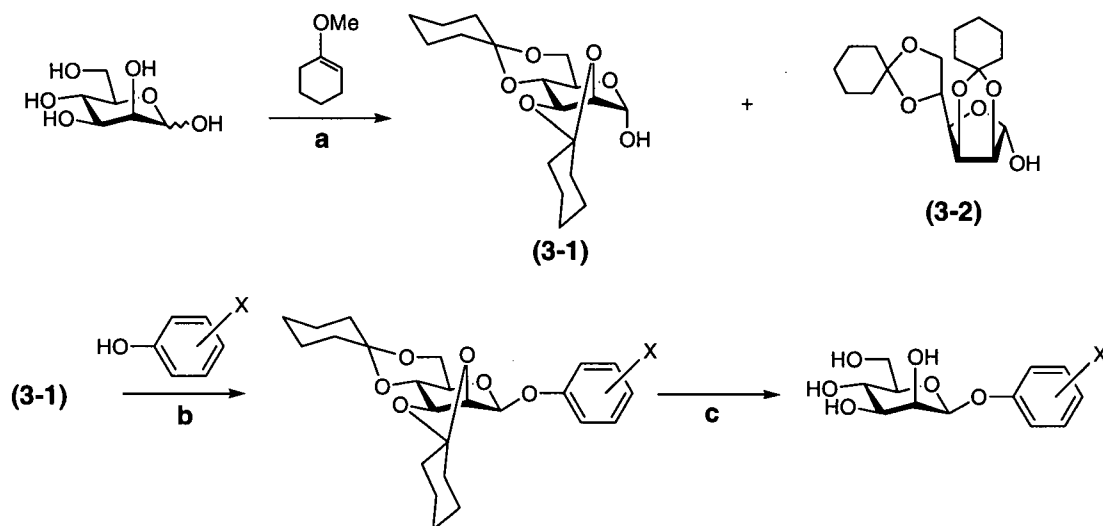


**Figure 3-3:** Synthesis of aryl  $\beta$ -D-mannopyranosides. (a) 4 eq. 1-methoxy-1-cyclohexene, 2.5 mol.% TsOH, DMF, 40°C, 30 mm Hg, 30 min., 30% (**3-1**), 20% (**3-2**); (b) 1.4 eq. phenol, 1.4 eq. DEAD, 1.4 eq. Ph<sub>3</sub>P, toluene, RT, 2-3 hrs., 50-85%; (c) 4% HCl in MeOH, 4°C, overnight.

Reaction of D-mannose with 1-methoxy-1-cyclohexene produced the di-*O*-cyclohexylidene mannopyranose **3-1** which was readily crystallized free of the thermodynamic mannofuranose product (**3-2**) in modest yield. Subsequent Mitsunobu mannosylation of a number of substituted phenols, with  $pK_a$ 's ranging from 4 to 10, afforded  $\beta$ -mannosides as the major products and total glycosylation yields of 50-85% (Table 3-1). The  $\alpha$ - and  $\beta$ -anomers were readily separated by silica gel chromatography and deprotection of the purified  $\beta$ -glycosides was achieved in acidic methanol.

**Table 3-1:** Yields and anomeric selectivity of Mitsunobu mannosylation of substituted phenols.

Phenol Substituent	Phenol pK <sub>a</sub>	Yield (%) <sup>a</sup>			β/α <sup>b</sup>
		β	α	Total	
H	9.99	48	8	56	6:1
4-chloro	9.38	75	10	85	7.5:1
4-cyano	8.49	76	8	84	9.1:1
3-nitro	8.39	77	6	83	13:1
4-nitro	7.18	50	-	50	-
4-chloro,2-nitro	6.45	50	-	50	-
2,5-dinitro	5.15	52	22	74	2.4:1
2,4-dinitro	3.96	38	15	53	2.6:1

a) Isolated yields. b) Ratios based on isolated yields.

A valuable probe of oxocarbenium ion transition state character in glycosidase reactions involves the measurement of alpha deuterium kinetic isotope effects ( $\alpha$ D-KIE's). Such measurements require a glycoside substrate with a deuterium installed at the anomeric carbon. Synthesis of an aryl  $\beta$ -[1-<sup>2</sup>H]-mannoside (Figure 3-4) was readily achieved by Swern oxidation of the anomeric hydroxyl of **3-1** to produce the mannosylactone **3-3**. Reduction of **3-3** with sodium borodeuteride afforded 1-deuterio labelled **3-4** which was used to glycosylate 2,5-dinitrophenol under Mitsunobu conditions. Deprotection in acidic methanol afforded the required deuterium labelled substrate 2,5-dinitrophenyl  $\beta$ -D-[1-<sup>2</sup>H]-mannopyranoside.

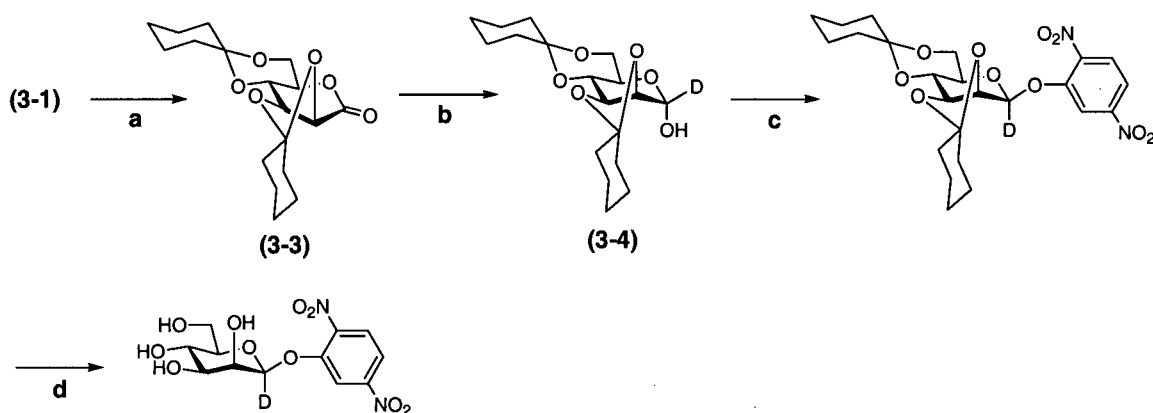


**Figure 3-4:** Synthesis of 2,5-dinitrophenyl  $\beta$ -D-[1-<sup>2</sup>H]-mannopyranoside: (a) (i) (COCl)<sub>2</sub>, DMSO, DCM, -78°C, 25 min., (ii) Et<sub>3</sub>N, RT, 73% (recryst.); (b) NaBD<sub>4</sub>, D<sub>2</sub>O, THF, 0°C, 3 hrs., 90%; (c) 2,5-dinitrophenol, Ph<sub>3</sub>P, DEAD, toluene, RT, 2 hrs., 65% ( $\beta/\alpha = 4.9:1$ ); (d) 4% HCl / MeOH, 0°C, 9 hrs., 42% (recryst.).

Synthesis of 2-deoxy  $\beta$ -glycosides, like the  $\beta$ -mannosides, is also difficult owing to the absence of a participating group at C-2 to direct  $\beta$ -selectivity.<sup>141</sup> Fortunately, in the case of aryl 2-deoxy- $\beta$ -glycosides, novel  $\beta$ -stereoselective glycosylation chemistry has been developed based

on 2-deoxy- $\alpha$ -glycosyl phosphorodithioate donors (Figure 3-5).<sup>142-144</sup> The phosphorodithioc acid **3-5**, prepared by condensation of 2,2-dimethylpropane-1,3-diol with phosphorus pentasulfide,<sup>145</sup> cleanly added to 3,4,6-tri-*O*-acetyl-D-glucal to give the 2-deoxy- $\alpha$ -glycosyl phosphorodithioate donor (**3-6**) as the major product.<sup>146</sup> This is a notable reaction because the usual result of acid catalysed additions to glycols is allylic or Ferrier rearrangement to 1-substituted 2,3-unsaturated sugars.<sup>147</sup> Uncatalyzed glycosylation of 4-nitrophenoxide (resin bound) with **3-6** was slow, but afforded the per-*O*-acetylated 4-nitrophenyl 2-deoxy- $\beta$ -glycoside (**3-7**) in good yield and  $\beta$ -stereoselectivity ( $\beta/\alpha \sim 10:1$ ). Interestingly, the electrophilic promoters for this type of glycosylation do not appear to accelerate the reaction, but instead lead to poor stereoselectivity.<sup>142</sup> Removal of the acetates was achieved with sodium methoxide in methanol to give 4-nitrophenyl 2-deoxy- $\beta$ -D-*arabino*-hexopyranoside (**3-8**).

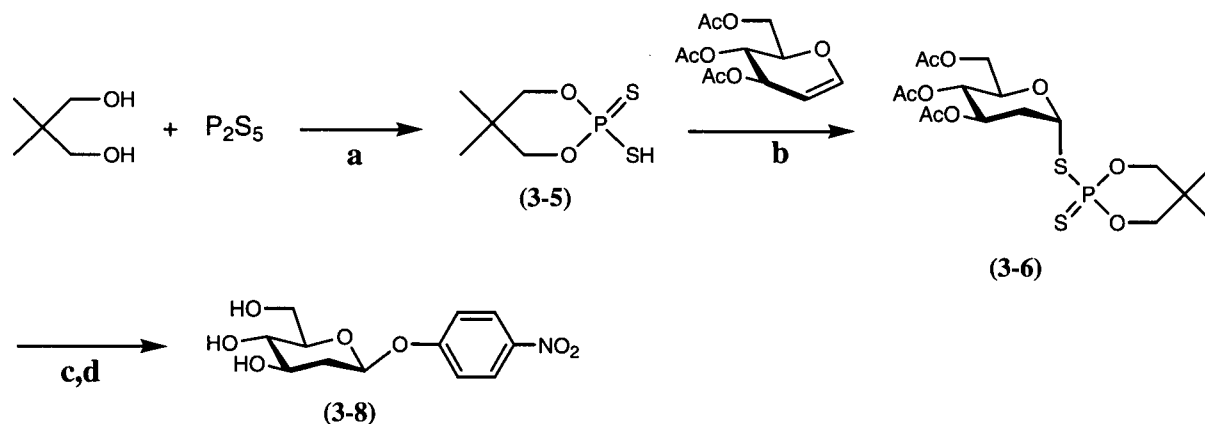


**Figure 3-5:** Synthesis of 4-nitrophenyl 2-deoxy- $\beta$ -D-*arabino*-hexopyranoside (**3-8**): a) toluene, reflux, 2.5 hrs., 65%; b) benzene, RT, 24 hrs., 60%; c) 10:1 isopropanol / benzene, Amberlyst A-26 (4-nitrophenoxide form), RT, 13 days, 63%,  $\beta/\alpha \sim 10:1$ ; d) NaOMe / MeOH, RT, 35 min. then Amberlite IR-120 ( $H^+$ ), 70%.

### Brønsted Analysis of Man2A

As noted previously in the Ph.D. work of Dominik Stoll,<sup>136</sup> the kinetic behaviour of Man2A towards aryl  $\beta$ -mannosides proved to be complex (Figure 3-6). The plots of reaction velocity versus substrate concentration for all aryl  $\beta$ -mannosides ( $pK_a^{lg} = 3.96-9.4$ ) all have the appearance of substrate inhibition. An exception was observed for the least reactive of the series, phenyl  $\beta$ -mannoside ( $pK_a^{lg} = 9.99$ ), which followed normal saturation behaviour within the same concentration range as the other substrates, although at higher concentrations ( $> 6$  mM) modest inhibition was observed.

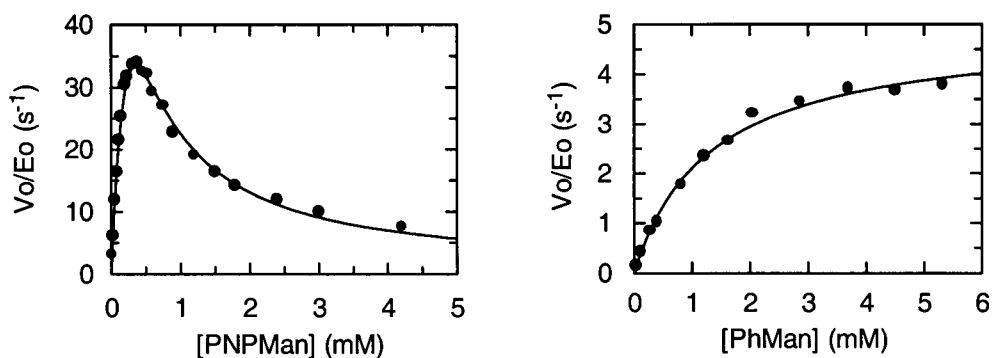


**Figure 3-6:** Plots of reaction velocity ( $V_o/E_o$ ) versus substrate concentration for Man2A catalyzed hydrolyses of 4-nitrophenyl  $\beta$ -mannoside (PNPMan) and phenyl  $\beta$ -mannoside (PhMan).

Substrate inhibition occurs when a second molecule of substrate binds to the Michaelis complex of the enzyme, resulting in a ternary complex that has reduced activity (Figure 3-7a).<sup>148</sup> This is not an unknown behaviour for glycosidases,<sup>149,150</sup> which frequently have long active site clefts to accommodate multiple monosaccharide units of a polysaccharide chain, and thus have the potential to bind two aryl glycosides simultaneously in an unproductive fashion. In the case of a retaining glycosidase a second type of ternary complex may arise from a substrate-inhibited covalent intermediate (Figure 3-7b). In order for this to occur, at a kinetically significant level, the deglycosylation step would need to be rate determining so that the covalent intermediate may accumulate and receive a second substrate molecule. The resulting ternary complex may be a true dead-end species, or possibly a transglycosylation complex in which the subsequent transglycosylation step ( $k_{trans}$ ) is slower than the hydrolysis pathway ( $k_{hydro}$ ). If the intermediate enzyme species are combined (Michaelis and covalent intermediate) as well as the corresponding inhibition pathways, the standard equation for substrate inhibition may be used (equation 3-1).<sup>148</sup> Table 3-2 lists the kinetic parameters determined for the reaction of Man2A with aryl  $\beta$ -mannosides using equation 3-1.

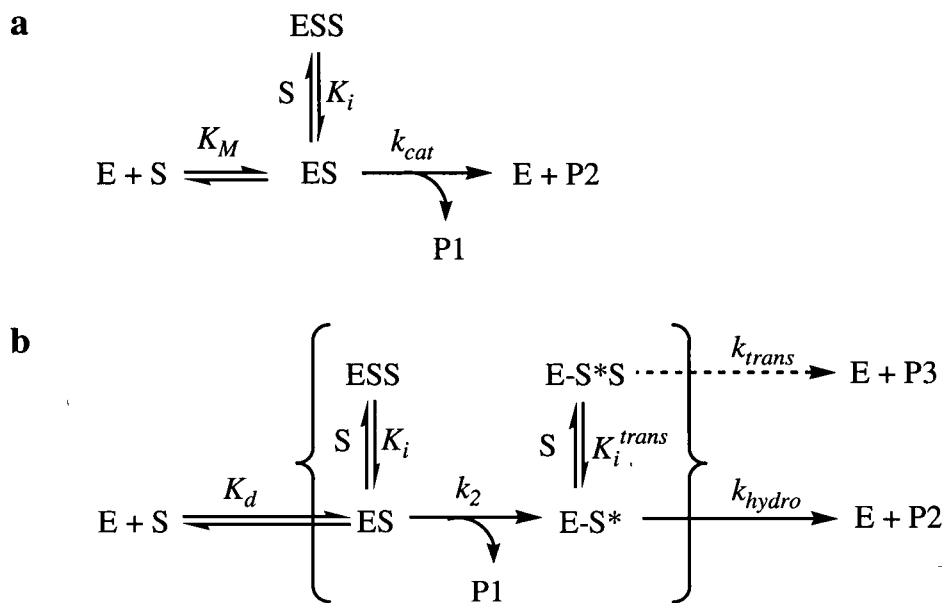


**Figure 3-7:** (a) Simplified kinetic scheme for substrate inhibition. (b) Proposed kinetic scheme for substrate inhibition of Man2A (E) during the hydrolysis of an aryl  $\beta$ -mannoside (S). ES = Michaelis complex; E-S\* = covalent intermediate; ESS = substrate inhibited Michaelis complex; E-S\*S = substrate inhibited covalent intermediate or transglycosylation complex;  $K_i$  and  $K_i^{trans}$  are inhibition (dissociation) constants for the second substrate molecule; P1 = phenol; P2 = mannose; P3 = disaccharide transglycosylation product.

$$\frac{V_o}{E_o} = \frac{k_{cat}[S]}{K_M + [S] + \frac{[S]^2}{K_i}} \quad (3-1)$$

**Table 3-2:** Kinetic parameters for the reaction of Man2A with substituted aryl  $\beta$ -mannosides (pH 7, 25°C) determined with equation 3-1.

aglycone	pKa <sup>lg</sup>	$k_{cat}$ (s <sup>-1</sup> )	$K_M$ (mM)	$K_i$ (mM)	$\frac{k_{cat}}{K_M}$ (s <sup>-1</sup> ·mM <sup>-1</sup> )
2,4-Dinitro	3.96	119 (6)	0.27 (0.02)	1.02 (0.09)	440
2,5-Dinitro	5.15	150 (20)	0.42 (0.08)	0.24 (0.04)	364
4-Chloro, 2-nitro	6.45	230 (50)	0.8 (0.2)	0.19 (0.05)	290
4-Nitro	7.18	179 (9)	0.78 (0.05)	0.16 (0.01)	230
Mu	7.6	61 (4)	0.19 (0.02)	0.47 (0.05)	320
3-Nitro	8.39	33 (5)	0.5 (0.1)	0.15 (0.04)	66
4-Chloro	9.4	7 (1)	0.36 (0.08)	1.3 (0.3)	19
Phenyl	9.99	7.9 (0.4)	2.7 (0.2)	8.8 (0.8)	3

A Brønsted plot of  $\log k_{cat}$  versus the pKa of the leaving group reveals an apparent downward break in the correlation occurring at approximately pKa 7.2 (Figure 3-8a). This break can be ascribed to a change in the rate determining step, from deglycosylation with the reactive

substrates ( $\text{pK}_a^{\text{lg}} \leq 7$ ) to glycosylation with the less reactive substrates ( $\text{pK}_a^{\text{lg}} > 7$ ). The  $\beta_{\text{lg}}$  value ( $-0.54 \pm 0.05$ ) obtained from the slope of the leaving group dependent section of the Brønsted plot reflects a glycosylation transition state with approximately 50% negative charge development on the departing glycosidic oxygen. This can arise from either partial glycosidic bond cleavage with no proton donation from the acid-base catalyst, or complete glycosidic bond cleavage with partial proton donation. The corresponding Brønsted plot for  $k_{\text{cat}}/K_M$  also shows a non-linear, downward breaking correlation (Figure 3-8b). A similar concave-down correlation was observed for Abg.<sup>33</sup> Since this parameter represents the second order rate constant for capture of substrate by free enzyme, a break in the correlation is not expected because there can be no change in rate determining step unless substrate binding reaches diffusion control ( $10^8 \text{ s}^{-1} \cdot \text{M}^{-1}$ ). However, the  $k_{\text{cat}}/K_M$  values determined here are well below the diffusion limit.

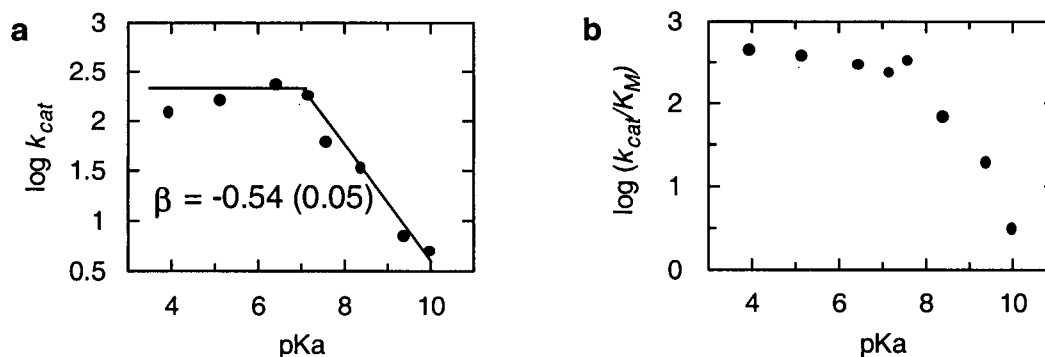


**Figure 3-8:** Dependence of  $\log k_{\text{cat}}$  (a) and  $\log (k_{\text{cat}}/K_M)$  (b) on  $\text{pK}_a^{\text{lg}}$  for wild type Man2A catalysed hydrolyses of aryl  $\beta$ -mannosides.

A complementary experiment to the Brønsted analysis above is partitioning of the covalent intermediate between water and an added acceptor.<sup>148</sup> Because the covalent intermediate will react faster with a more nucleophilic acceptor, an increase in rate can be expected for substrates for which deglycosylation is rate limiting. Accordingly, the rate of reaction of Man2A with a substrate for which deglycosylation is rate limiting, 2,5-dinitrophenyl  $\beta$ -mannoside, is increased by added ethylene glycol (Figure 3-9a), but not the rate of disappearance of a glycosylation rate limiting substrate, phenyl  $\beta$ -mannoside (Figure 3-9b). This is in agreement with the Brønsted plot for  $\log k_{\text{cat}}$  (Figure 3-8a).

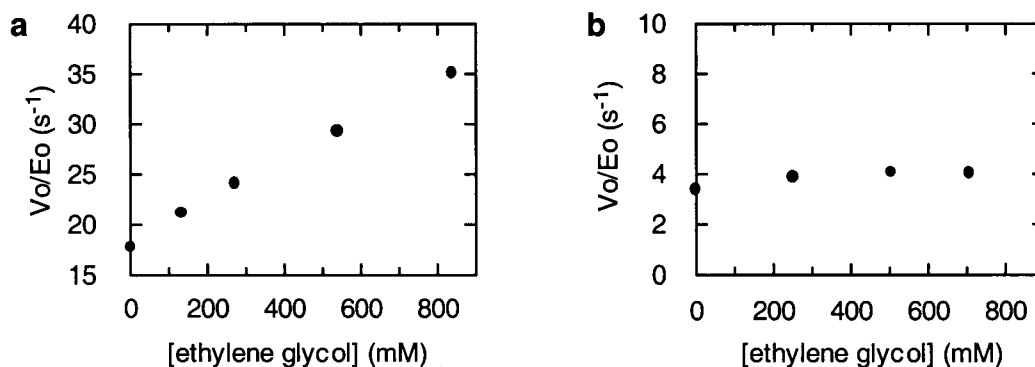


**Figure 3-9:** Dependence of the reaction rate of Man2A wt with saturating substrate and added ethylene glycol: (a) 2,5-dinitrophenyl  $\beta$ -mannoside (3.8 mM); (b) phenyl  $\beta$ -mannoside (10.6 mM).

### pH-Rate Dependence of Man2A

The pH dependence of  $k_{cat}/K_M$  for the reaction of Man2A with two different substrates was examined (Figure 3-10). In each case  $k_{cat}/K_M$  shows a dependence on a single ionisation event in the active site. Essentially identical pKa's were observed with 4-nitrophenyl  $\beta$ -mannoside (pKa =  $7.6 \pm 0.1$ ) and phenyl  $\beta$ -mannoside (pKa =  $7.7 \pm 0.1$ ), as one would expect because  $k_{cat}/K_M$  presumably reflects ionisations on the free enzyme (or substrate). The ionisations of the general acid-base catalyst and the nucleophile may be anticipated to dominate the pH-rate profile of a retaining glycosidase, and indeed such ionisations have been assigned in the case of *Bacillus circulans* xylanase<sup>69</sup> and *Cellulomonas fimi* exoglycanase.<sup>60,62</sup> The relatively high pKa observed here might be attributed to the acid-base catalyst, which requires an elevated pKa to perform acid catalysis in the glycosylation step.<sup>69</sup> A corresponding low pKa ionisation (< 5) that would be expected from the nucleophile could not be observed for Man2A due to the instability of the enzyme below pH 5.5.

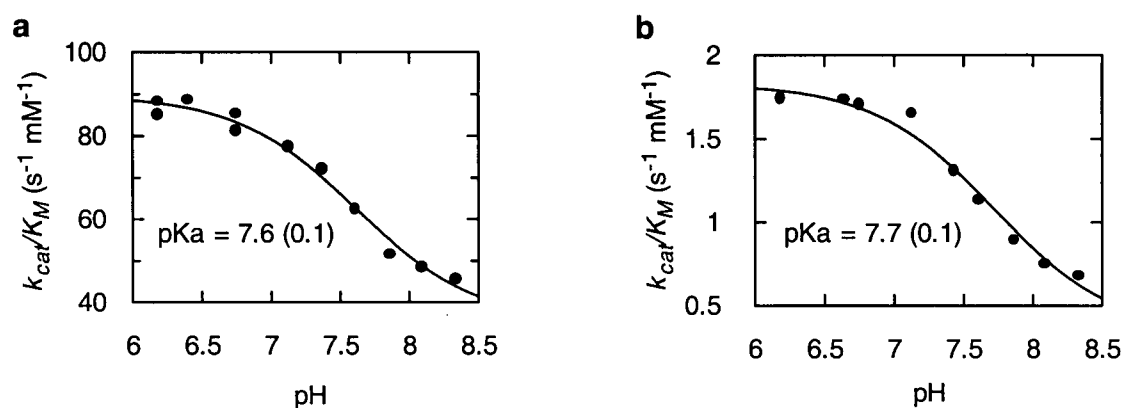


**Figure 3-10:** Dependence of  $k_{cat}/K_M$  on pH for the reaction of 4-nitrophenyl  $\beta$ -mannoside (a) and phenyl  $\beta$ -mannoside (b) with Man2A (25°C).

### Identification of the General Acid-Base Catalyst in Man2A

A rigorous approach towards the identification of the general acid-base catalyst of a retaining glycosidase in the absence of a 3-dimensional structure requires deletion of the predicted residue by site directed mutagenesis followed by assessment of the resulting mutant by kinetic analysis and chemical rescue.<sup>59</sup> Alignment of the amino acid sequence of Man2A with other Family 2 glycosidases indicated that E429A was strictly conserved and matched the predicted acid-base catalyst in *E. coli*  $\beta$ -galactosidase (Figure 3-11).

<i>C. fimi</i> $\beta$ -mannosidase Man2A (AF126472)	↓	<b>H</b> ASLVLVWNGG <b>N</b> EN 430
Human $\beta$ -mannosidase (U60337)		<b>H</b> PSIIIWSG <b>N</b> EN 457
<i>E. coli</i> , lac Z $\beta$ -galactosidase (J01636)		<b>H</b> PSVIIW <b>S</b> LG <b>N</b> ES 462
Human $\beta$ -glucuronidase (M15182)		<b>H</b> PAVVMW <b>S</b> VA <b>N</b> EP 452

**Figure 3-11:** Alignment of the amino acid sequence of Man2A with selected Family 2 glycosidases. Conserved residues are in bold. The acid-base catalyst is indicated with an arrow. GenBank codes are in parentheses.

The Man2A mutant E429A was kindly provided by Dominik Stoll and tested with aryl  $\beta$ -mannoside substrates. As expected for an acid-base mutant, Man2A E429A reacted only with substrates with good leaving groups that do not require acid catalysis in the glycosylation step. Only 2,4-dinitrophenyl and 2,5-dinitrophenyl  $\beta$ -mannoside reacted with Man2A, whereas no hydrolysis was observed with 4-nitrophenyl or 3-nitrophenyl  $\beta$ -mannoside. Because base catalysis in the deglycosylation step is not possible for a mutant missing the acid-base catalyst, the deglycosylation step will be very slow. If the glycosylation step is accelerated sufficiently

with a reactive leaving group, then deglycosylation will be rate limiting and the glycosyl-enzyme will accumulate. This was indeed evident from the low  $k_{cat}$  ( $12 \text{ min}^{-1}$ ) and  $K_M$  ( $< 1 \text{ }\mu\text{M}$ ) values observed for the reaction of Man2A E429A with 2,5-dinitrophenyl  $\beta$ -mannoside (2,5DNPMan). Interestingly, substrate inhibition is nearly absent in the reaction of 2,5DNPMan with Man2A E429A (Figure 3-12), unlike the severe inhibition observed with the wild type enzyme (Figure 3-6).

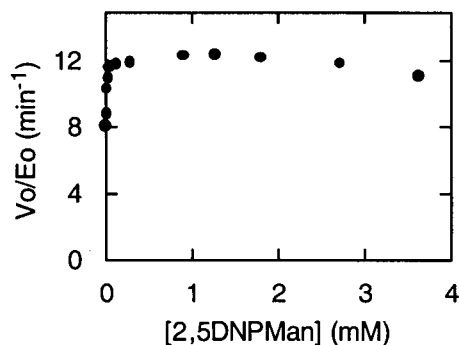


**Figure 3-12:** Reaction rate versus substrate concentration for the reaction of Man2A E429A with 2,5-dinitrophenyl  $\beta$ -mannoside (pH 7,  $25^\circ\text{C}$ ).

The dependence of  $k_{cat}$  as a function of pH for the reaction of 2,5DNPMan with Man2A E429A was described by two ionisations corresponding to pKa's of 6.1 and 8.4 (Figure 3-13). As  $k_{cat}$  reports on the deglycosylation step for this mutant, and because the mutant is supposedly missing the acid-base catalyst, these ionisations cannot readily be assigned. Direct ionisation of the nucleophile is impossible during deglycosylation, and chemical rescue studies (described below) confirm that the acid-base catalyst is absent in the E429A mutant. Therefore the ionisations must arise from other groups in the active site. Intriguingly, citric acid activates the mutant in a pH dependent manner (Figure 3-13, open circles), an effect that was not observed with the wild type enzyme. The activation by citric acid was also concentration dependent, which suggests this is a form of chemical rescue of the acid-base mutant. It is possible that citric acid could function as a general-base catalyst or as a nucleophile in the deglycosylation step. However, the increase in rate as a function of decreasing pH is inconsistent with both possibilities, as protonation of citric acid is deleterious to both roles. Alternatively, protonation of one of the other carboxyl groups of citric acid may allow it to bind in the Man2A E429A active site and perform chemical rescue.

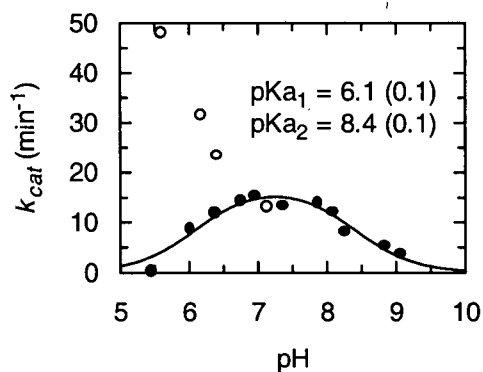


**Figure 3-13:** Dependence of  $k_{cat}$  on pH for the reaction of 2,5DNPMan with Man2A E429A (25°C). Open circles represent rates obtained in citric acid buffer. The curve is a fit of the data (filled circles) by a double ionisation function. The calculated pKa's are indicated.

A characteristic of acid-base mutants of retaining glycosidases is the enhancement of catalytic activity observed with activated substrates when the mutant is provided a small anionic nucleophile such as azide or formate (Figure 3-14). Unlike water, a small anion does not require general-base catalysis to function as a nucleophile in the deglycosylation step and thus can react with the glycosyl-enzyme in mutants missing the acid-base catalyst, thereby increasing the turnover rate. Such enhancement of activity is observed for the reaction of 2,5DNPMan with Man2A E429A in the presence of azide. Saturation-like kinetic behaviour is observed as a function of azide concentration (Figure 3-15), and remarkably little azide is required to attain maximum acceleration of rate ( $K_M^{app} = 0.56$  mM). By analogy to rescue studies on *Cellulomonas fimi* exoglycanase<sup>60</sup> and *E. coli* (lac Z)  $\beta$ -galactosidase acid-base mutants,<sup>61</sup> the saturation kinetic behaviour observed with azide does not represent true binding of the anion in the active site. Instead, this reflects the change in rate-determining step as azide concentration is raised, such that eventually glycosylation becomes rate-limiting. Kinetic parameters were determined for Man2A E429A with 2,5DNPMan in the presence of "saturating" azide (100 mM). Consistent with an 18 fold increase in turnover number ( $k_{cat} = 221 \pm 8$   $\text{min}^{-1}$ ) is a corresponding increase in  $K_M$  value ( $25 \pm 3$   $\mu\text{M}$ ). Furthermore, the mechanism for azide rescue shown in Figure 3-14 was confirmed by performing the reaction on a preparative scale and isolating  $\beta$ -D-mannopyranosyl azide as the major product (as indicated by  $^1\text{H}$  NMR).

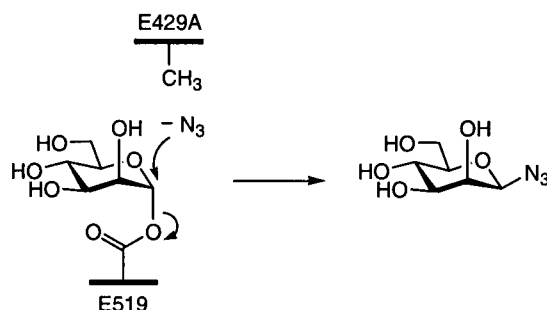


**Figure 3-14:** Mechanism for azide rescue of Man2A E429A

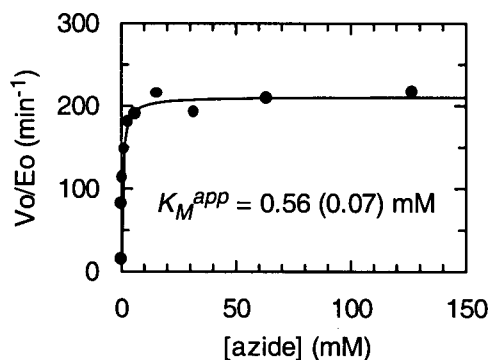


**Figure 3-15:** Reaction rate of Man2A E429A with 2,5DNPMAN (1.88 mM) as a function of azide concentration (pH 7, 25°C). The curve is a fit of the data to the Michaelis Menten equation.

The energetic cost of removing the acid-base catalyst on glycosylation and deglycosylation steps can be determined by application of equation 3-2 (where  $k$  is the appropriate kinetic parameter).<sup>148</sup> The measurable  $K_M$  value observed for Man2A E429A in the presence of 100 mM azide allows  $k_{cat}/K_M$  to be determined ( $8840 \text{ min}^{-1} \cdot \text{mM}^{-1}$ ) and compared with the wild type enzyme ( $k_{cat}/K_M = 21\,840 \text{ min}^{-1} \cdot \text{mM}^{-1}$ ), indicating a 2.5 fold reduction in rate. Because this parameter reports on the glycosylation step in each case, the minimal reduction in rate as a result of eliminating acid catalysis is consistent with the good leaving group ability of 2,5-dinitrophenol, which requires minimal, if any, protonic assistance to depart. However, the deglycosylation rate, reflected by the corresponding  $k_{cat}$  values ( $12 \text{ min}^{-1}$  for E429A in the absence of azide,  $9000 \text{ min}^{-1}$  for wild type) is reduced 750 fold ( $\Delta\Delta G^\ddagger = 3.9 \text{ kcal mol}^{-1}$ ), reflecting the considerably greater need of base catalyzed attack of water on the glycosyl-enzyme intermediate. This energetic cost is similar to that observed for the E461G acid-base

mutant of *E. coli* (lac Z)  $\beta$ -galactosidase ( $Mg^{2+}$  form) using deglycosylation rate limiting substrates (1300-1700 fold reduction in  $k_{cat}$ ,  $\Delta\Delta G^\ddagger = 4.2$ - $4.4$  kcal mol $^{-1}$ ).<sup>61,151</sup>

$$\Delta\Delta G^\ddagger = RT \ln \left( \frac{k_{WT}}{k_{mut}} \right) \quad (3-2)$$

### Kinetic Isotope Effects

In contrast to the situation with wild-type Man2A, the standard saturation kinetic behaviour observed for the E429A mutant with the substrate 2,5-DNP  $\beta$ -mannoside allows facile and accurate measurements of  $\alpha$ -DKIE's on  $k_{cat}$ . Using the substrate 2,5-DNP  $\beta$ -[1- $^2$ H]-mannoside and the protio analogue under saturating conditions (2 mM), a significant  $k_H/k_D$  value of  $1.12 \pm 0.01$  was observed (average of 7 measurements). Doubling the concentration of deuterio and protio substrates afforded the same  $k_H/k_D$  value, indicating that this effect is not the result of a contaminant in either substrate. Surprisingly,  $k_H/k_D$  increased substantially to  $1.166 \pm 0.009$  (6 determinations) in the presence of 100 mM azide. This is an effect that is specific to the nucleophilicity of azide, and not a non-specific salt effect, because the same measurement in 100 mM NaCl afforded a  $k_H/k_D$  value of  $1.111 \pm 0.007$  (3 determinations). The increase in  $\alpha$ -DKIE is also suspiciously similar to increases observed for the reaction of  $\alpha$ -glucosyl fluoride<sup>152</sup> and *N,N*-dimethyl-*N*-(methoxymethyl)anilinium ions<sup>9</sup> with nucleophiles that are 'softer' than water (e.g. azide), as well as for the reaction of *Botryodiplodia theobromae* Pat  $\beta$ -glucosidase with glycerol when deglycosylation is rate determining.<sup>153</sup> However, as noted in the previous section, the presence of 100 mM azide changes the rate determining step from deglycosylation to glycosylation. Therefore, the  $\alpha$ DKIE value of 1.166 reports on the glycosylation transition state (which does not involve azide) and the smaller  $\alpha$ DKIE of 1.12 reports on the deglycosylation transition state. This is directly opposite to what has been observed in wild type glycosidases (see Chapter 1), where the glycosylation transition state has less  $S_N1$  character (i.e. has a smaller  $\alpha$ DKIE on  $k_{cat}$ ) than the deglycosylation transition state.<sup>33,117,154</sup> The absence of the acid-base catalyst in Man2A E429A may cause this difference of oxocarbenium ion character in each step. In the deglycosylation step the absence of base catalysis will demand greater pre-association of the attacking water, thus producing the smaller  $\alpha$ DKIE value. However, the 2,5-dinitrophenol leaving group in the glycosylation step can sustain negative charge development on the phenol

oxygen in the absence of acid catalysis, and thus can tolerate substantial bond cleavage to the anomeric carbon of the substrate. This would produce the larger  $\alpha$ DKIE value observed.

### Evaluating the Role of the 2-Hydroxyl in Catalysis

The substrate 4-nitrophenyl 2-deoxy- $\beta$ -mannoside (PNP-2D-Man) proved to be a slow substrate with wild type Man2A. Unlike the parent substrate PNPMan, saturation of Man2A could not be achieved with PNP-2D-Man. The absence of a measurable  $K_M$  value also implies that glycosylation is the rate limiting step for this substrate. A comparison of  $k_{cat}/K_M$  values for PNPMan ( $289 \text{ s}^{-1} \text{ mM}^{-1}$ ) and PNP-2D-Man ( $0.039 \text{ s}^{-1} \text{ mM}^{-1}$ ), which presumably reports on the glycosylation step in both cases, indicates a 7400 fold reduction in this parameter as a result of the removal of the 2-hydroxyl. From equation 3-2 the corresponding activation energy difference in the glycosylation transition state ( $\Delta\Delta G^\ddagger$ ) is calculated to be  $5.3 \text{ kcal mol}^{-1}$ . The energetic contribution of the 2-hydroxyl in Man2A is comparable to that observed for *Agrobacterium* sp.  $\beta$ -glucosidase ( $4.5 \text{ kcal mol}^{-1}$ )<sup>34</sup> but is substantially lower than the value obtained for *E. coli*  $\beta$ -galactosidase ( $10 \text{ kcal mol}^{-1}$ ).<sup>35</sup> This is likely a minimum estimate for this effect, given the electron withdrawing properties of the hydroxyl group which tend to make glucosides inherently less reactive than their 2-deoxy counterparts. Thus, despite not having the necessary geometry to form a strong hydrogen bond between the 2-hydroxyl and the nucleophile (Figure 3-16a), Man2A has apparently developed substantial interactions between the 2-hydroxyl and other residues in the active site at the transition state (Figure 3-16b). This also points to a universal role of the 2-hydroxyl in catalysis by  $\beta$ -glycosidases.

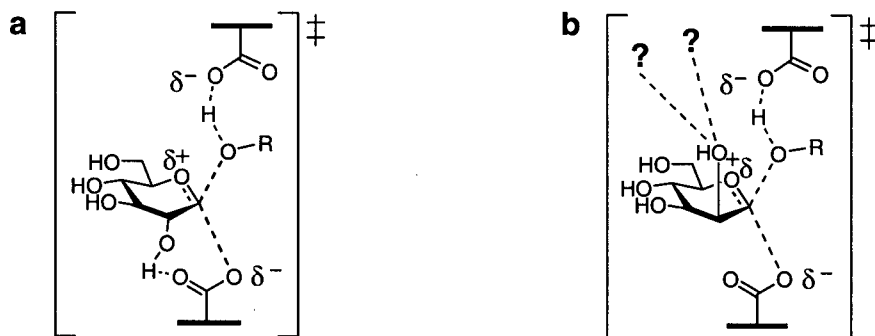


**Figure 3-16:** A comparison of the role of the 2-hydroxyl in the transition states of a  $\beta$ -glucosidase (a) and a  $\beta$ -mannosidase (b).

## Conclusions

This study describes the first detailed kinetic analysis of a retaining  $\beta$ -mannosidase, Man2A. Synthesis of a series of aryl  $\beta$ -mannosides of vastly different reactivities was essential for this work (in order to allow isolation of the glycosylation and deglycosylation steps) and was readily achieved by Mitsunobu mannosylation of substituted phenols. The contribution of the axial 2-hydroxyl of  $\beta$ -mannoside substrates to Man2A catalysis ( $\Delta\Delta G^\ddagger = 5.3 \text{ kcal mol}^{-1}$ ) is comparable to that observed for retaining enzymes that act on substrates with equatorial configured 2-hydroxyls. This suggests that the 2-hydroxyl is universally important to retaining  $\beta$ -glycosidase catalysis, regardless of its position relative to the glycosidase nucleophile. The acid-base catalyst of Man2A was unequivocally identified as E429A by a combination of sequence alignment with other enzymes, mutagenesis and azide rescue. Alpha-deuterium kinetic isotope effects measured for the reaction of 2,5-dinitrophenyl  $\beta$ -mannoside with the Man2A E429A revealed greater oxocarbenium ion character was present in the glycosylation step than in the deglycosylation step. This is opposite to what is normally observed in wild type glycosidases and may be attributed to the absence of the acid-base catalyst.

## **Chapter 4 Introduction to Glycosyl Transfer Reactions and Glycosynthases**

## **Glycosides in Biology**

The occurrence of glycosides in biology is extensive, ranging from oligosaccharides and polysaccharides through glycoproteins, proteoglycans, and peptidoglycans to saponins and antibiotics (Figure 4-1). No other biopolymer rivals the potential complexity of the primary structure of oligosaccharides. Whereas DNA, RNA, and polypeptides consist of monomers linked by one specific type of linkage, the glycosidic linkages that comprise oligosaccharides can be formed to any one of several hydroxyl groups on a sugar monomer, and additionally have one of two stereochemical (anomeric) configurations. Add to this complexity the conformational repertoire of glycosidic bonds and the monomer rings as well as secondary and tertiary interactions between rings (such as hydrogen bonds), the range of structures that can be formed is essentially infinite. Not surprisingly then, oligosaccharides mediate many of the precise receptor-ligand communication phenomena found on cell surfaces as well as within. Likewise, microorganisms manufacture multitudes of glycoside-containing secondary metabolites for the primary purpose of waging chemical warfare on competitors and predators. Yet very benign and stable structures are also found, which are well suited to structural roles, such as that provided by cellulose in plants and the peptidoglycan layer in bacterial cell walls, as well as energy storage in the form of starch or glycogen. For these reasons, oligosaccharides are irresistible targets for synthesis.

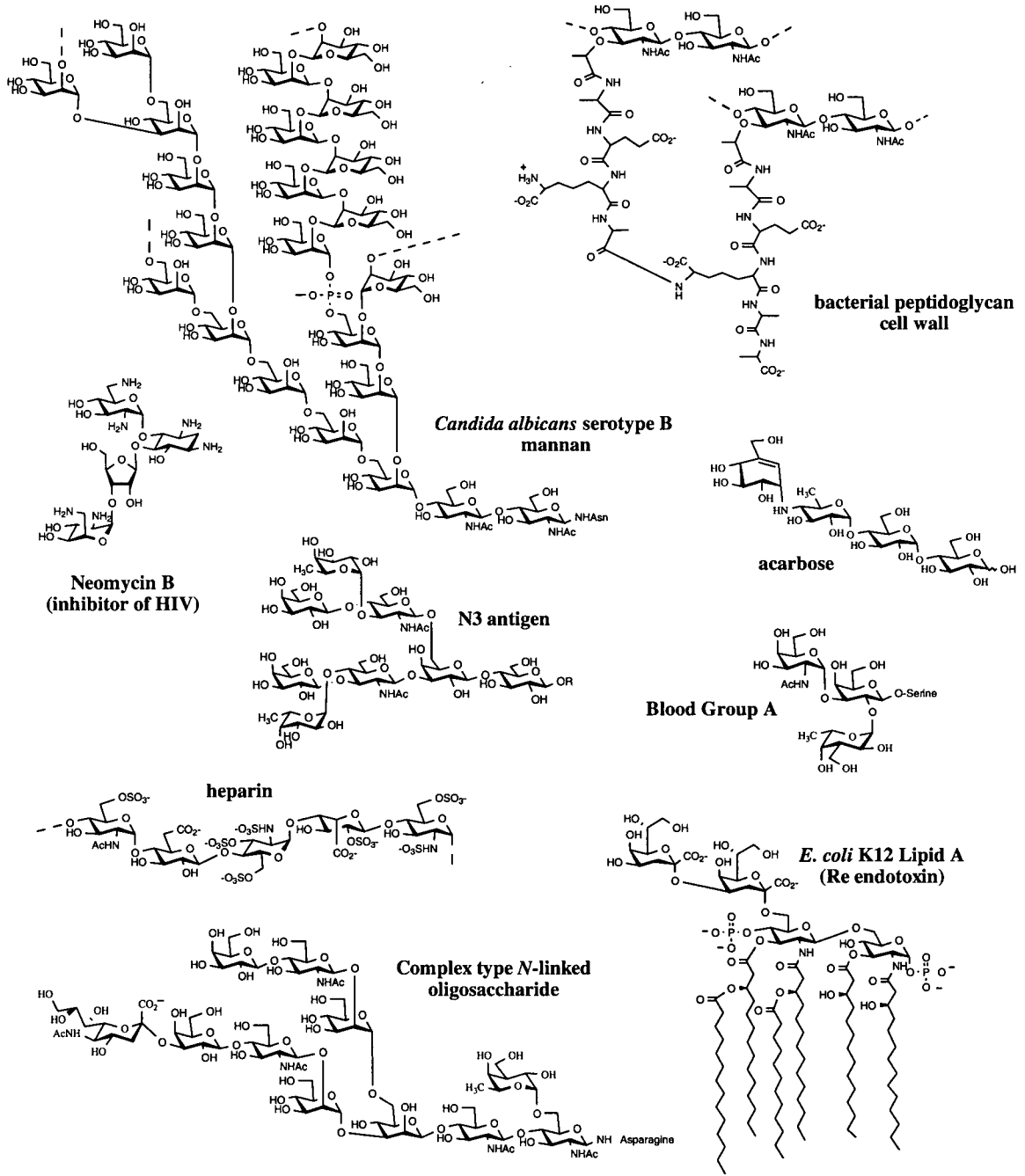
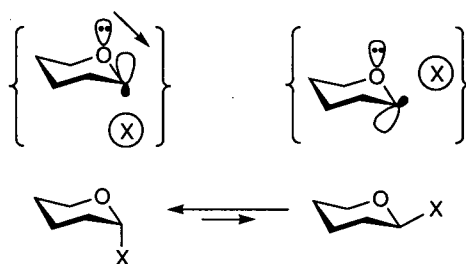


Figure 4-1: Examples of oligosaccharides of biological significance.

### 'Chemical' Synthesis of Glycosidic Bonds

To study the roles of glycosides in biology as well as develop therapeutics based on glycoside structures, one needs facile, high yielding chemistry to form glycosidic bonds. The challenge of glycosidic bond synthesis is twofold: controlling regioselectivity and stereochemistry. The issue of regioselectivity is met through creative use of protecting groups. Because a typical monosaccharide bears five hydroxyl groups that may act as acceptors for a glycosylation reaction, oligosaccharide synthesis is arguably the most demanding genre of chemistry in terms of protecting group chemistry and is the inspiration for a large body of literature.<sup>147</sup> Beyond normal steric considerations, the stereochemistry of the desired linkage is influenced by two factors: the anomeric effect and neighbouring group participation. In the absence of the latter, the anomeric effect favours the anomer of a glycosidic bond that allows a stabilizing interaction between the lone pair on the endocyclic oxygen of the monosaccharide ring and the antibonding orbital of the glycosidic bond (Figure 4-2).



**Figure 4-2:** Molecular orbital representation of the anomeric effect.

This is the dominant effect in glycosylation reactions that are reversible. Neighbouring group participation, generally manifested from a hydroxyl adjacent to the anomeric carbon, can be exploited to enforce the formation of a desired anomeric configuration depending on whether the linkage desired is *cis* or *trans* to the neighbouring hydroxyl group (Figure 4-3). Only *trans* glycosidic bonds can be enforced in this way (Figure 4-3, i and ii).



**Figure 4-3:** Trans (i, ii) and cis (iii, iv) glycosidic linkages.

Classic neighbouring group participation involves a carbonyl group in the form of an ester (acetate, benzoyl) or amide (*N*-acetyl, *N*-phthalimide) at the 2-position (Figure 4-4a). Others include 2-deoxy-2-iodo glycosides (for the synthesis of 2-deoxy glycosides, Figure 4-4b) and the 2-hydroxyl itself (glycosyl epoxides, Figure 4-4c).

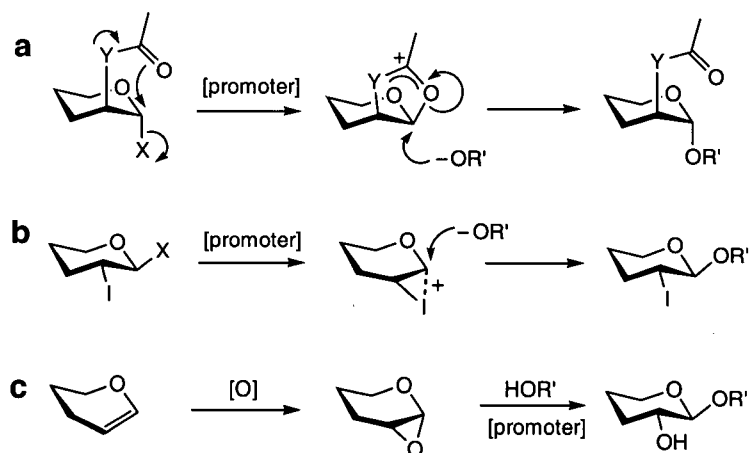


**Figure 4-4:** Neighbouring group effects: (a) acetate or amide, (b) 2-deoxy-2-iodo glycoside, (c) glycosyl epoxide.

Lacking the favour of neighbouring group participation, and often working against the dictates of the anomeric effect, *cis* glycosidic bonds are more difficult to synthesize. Consequently, glycosylations designed to achieve such linkages typically suffer from a lack of stereoselectivity. This is particularly true for  $\beta$ -mannosides, and as will be described in Chapter 6, very few chemical methods exist that can synthesize these bonds with complete stereoselectivity. On average, seven chemical steps are required to synthesize a single glycosidic bond.<sup>155</sup> Even with excellent yields with each step, the overall yield for each glycosidic bond formed is modest in the best cases. Therefore, as the number of glycosidic bonds required to assemble a desired oligosaccharide increases, the final yield of the product diminishes rapidly, while the time and cost of production likewise increase.

## Glycosyltransferases

Enzymatic synthesis of glycosidic bonds has the potential to eliminate problems with regioselectivity and anomeric stereoselectivity. The glycosyltransferases offer numerous opportunities in this regard. One class of these enzymes is that of the sugar nucleotide dependent transferases. These are enzymes involved strictly in biosynthetic processes which use an activated glycosyl species as the glycosyl donor in order to ensure that the reaction proceeds in the direction of glycosyl transfer. As with glycosidases, these transferases catalyze either inverting or retaining reactions, although the precise mechanistic details, particularly with the retaining transferases, are not well understood.<sup>156,157</sup> In most cases the donor is a nucleoside diphosphate sugar such as uridine diphospho- $\alpha$ -D-glucose (4-1), thus the leaving group will be a nucleoside diphosphate. In one case, however, CMP-*N*-acetyl neuraminic acid (4-2), the donor is a nucleoside monophosphate. Different nucleotides (uridine, guanidine, and cytidine) are used for the transfer of different sugars. Another type of donor employed for syntheses catalyzed by many membrane bound glycosyl transferases is that of the dolichol phosphate sugars (4-3), themselves synthesized from a nucleoside phosphate sugar.

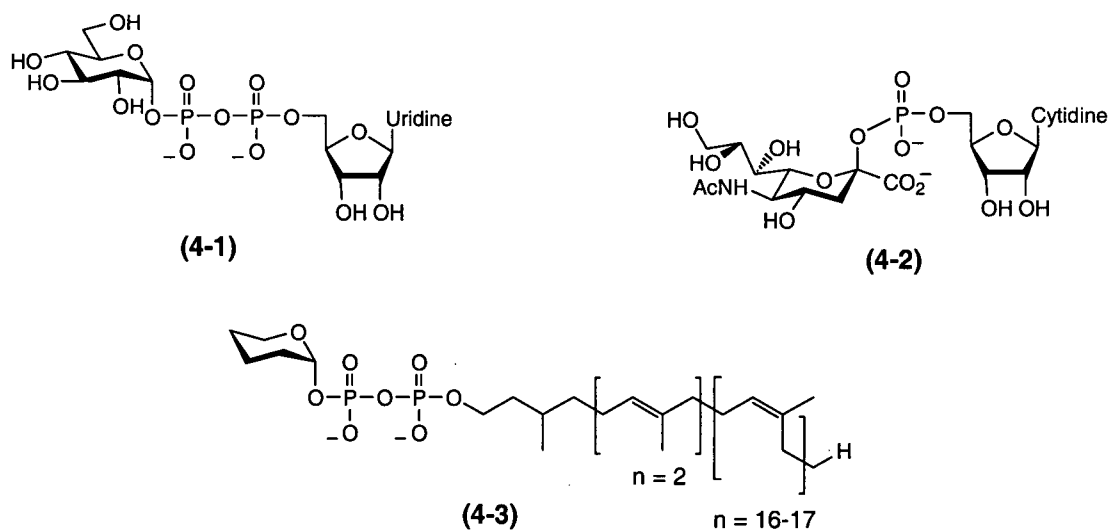


**Figure 4-5:** Representative structures of glycosyltransferase donor sugars.

Most glycosyltransferases are membrane bound, rendering their direct isolation difficult and their aqueous stability poor in free form. Also, the sugar nucleotide donors they require have, until recently, been difficult to isolate or synthesize in quantity. However, these two problems are rapidly receding due to advances in molecular biology. In the last decade the

cloning and overexpression of the soluble catalytic domains of glycosyltransferases has expanded exponentially, leading to advances in mechanistic<sup>157-160</sup> and structural<sup>157,161,162</sup> understanding of these enzymes, as well as their increased availability for synthesis. Indeed, the cloning of enzymes required for the *in situ* regeneration of sugar nucleotide donors has allowed effective, although complex, 'one pot' syntheses of complex oligosaccharides,<sup>163</sup> including sialyl Lewis X (Figure 4-6),<sup>164</sup> the sialyl T antigen<sup>165</sup> and hyaluronic acid.<sup>166</sup> Likewise, metabolic engineering has allowed glycosyltransferases and appropriate coupling enzymes to be expressed *in vivo* for large scale bacterial production of oligosaccharides.<sup>167,168</sup> On a simpler scale, *in situ* generation of a sugar nucleotide donor by a retaining glycosyltransferase using a glycosyl fluoride and the corresponding nucleotide has been demonstrated recently (Figure 4-7),<sup>169</sup> and may prove to be a general strategy with other retainers. Accordingly, glycosyltransferases are enjoying increasingly widespread use for the synthesis of complex oligosaccharides.<sup>170-176</sup>

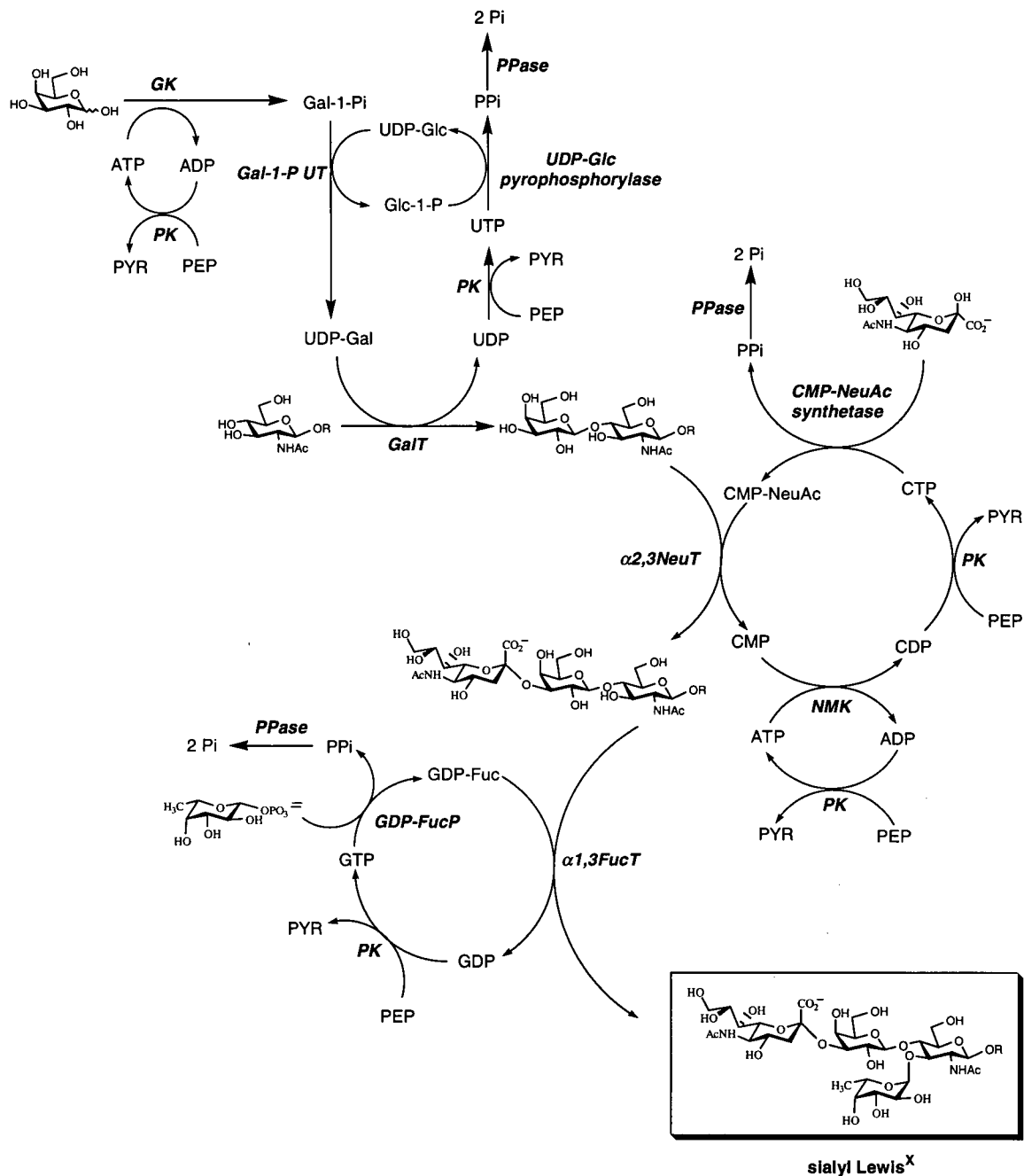


**Figure 4-6:** Synthesis of sialyl Lewis X using glycosyltransferases and in-situ generation of sugar nucleotide donors with coupling enzymes.<sup>164</sup> PK, pyruvate kinase; PPase, pyrophosphatase; UDP-GlcP, UDP-glucose pyrophosphorylase; GDP-FucP, GDP-fucose pyrophosphorylase; GK, galactokinase; NMK, nucleoside monophosphate kinase; Gal-1-P UT, galactose-1-phosphate uridylyltransferase; GalT, galactosyltransferase; α<sub>2,3</sub>NeuAcT, α-2,3-sialyltransferase; α<sub>1,3</sub>FucT, α-1,3 fucosyltransferase.

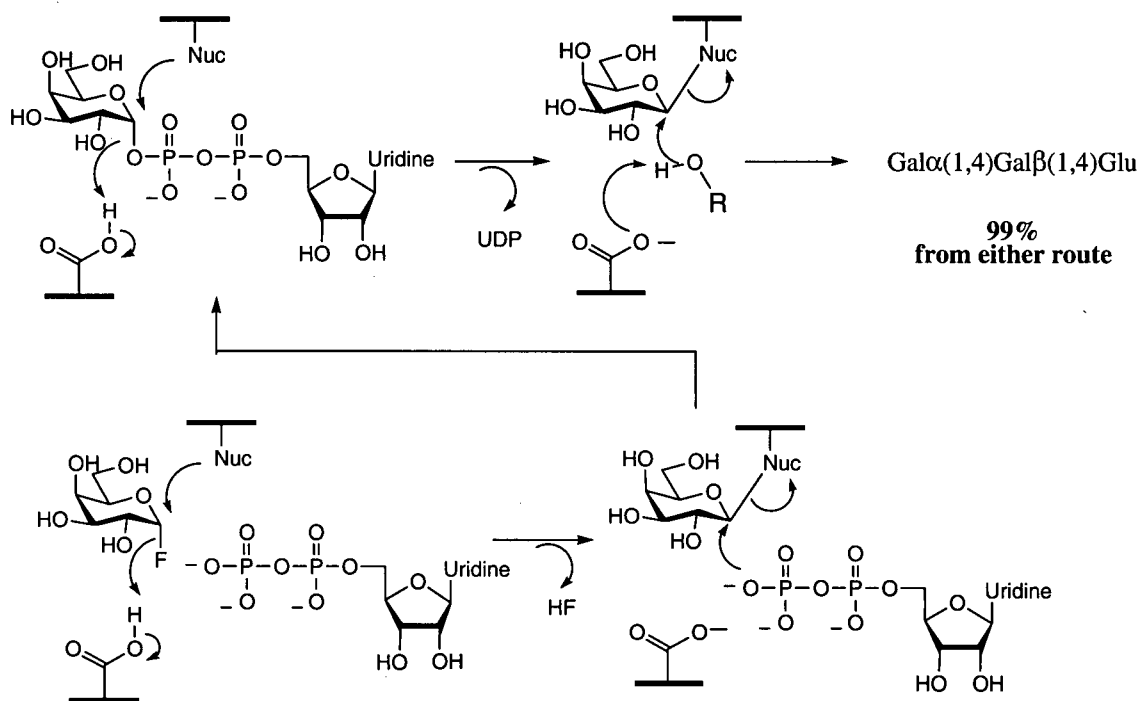


**Figure 4-7:** Postulated mechanism for the retaining  $\alpha$ -galactosyltransferase from *Neisseria meningitidis* (upper pathway) and mechanism for in situ generation of UDP-galactose from  $\alpha$ -galactosyl fluoride and UDP (lower pathway).<sup>169</sup>

A second, broad class of glycosyl transferases exists in which transfer occurs from a species other than a sugar nucleotide. The most commonly occurring of these are those in which the donor is an oligosaccharide or polysaccharide and transfer occurs to another sugar or to a phosphate moiety. The best studied examples are those of enzymes involved in  $\alpha$ -glucan conversion. These are cyclodextrin glucanotransferase<sup>50,177</sup> which carries out an intramolecular glycosyl transfer, thereby making cyclic oligosaccharides, and glycogen phosphorylase<sup>178</sup> which carries out transfer of glucosyl units from glycogen to phosphate as an acceptor. The former is of considerable interest for the large scale synthesis of cyclodextrins (alpha, beta, gamma), which are valuable as solubilizing agents.

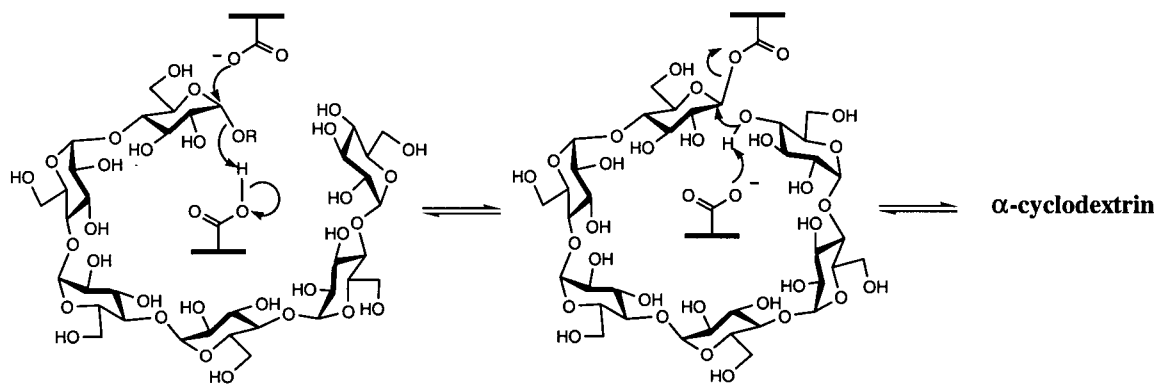


**Figure 4-8:** Synthesis of  $\alpha$ -cyclodextrin by cyclodextrin glucanotransferase.

## Glycosidases

Numerous strategies for oligosaccharide synthesis are possible with glycosidases. Owing to their ease of expression, isolation, stability, as well as the availability and low cost of their substrates, this class of enzyme has enjoyed a long history in synthetic applications.<sup>179</sup> As noted previously, glycosidases divide into retaining and inverting classes, and both can be used to synthesize glycosidic bonds.

### *Inverting glycosidases*

Inverting glycosidases normally hydrolyse glycosidic bonds with inversion of configuration, but when provided with a glycosyl fluoride of opposite anomeric configuration to that of the usual substrate, the enzyme will catalyze transglycosylation (Figure 4-9a). This is historically known as the Hehre mechanism for inverting glycosidases (reviewed in <sup>180</sup>). However, because the products formed are also substrates for the normal inverting hydrolysis mechanism, oligosaccharide yields are inherently low. However, an analogous reaction has been reported for *Cellulomonas uda* cellobiose phosphorylase, which normally catalyzes the phosphorolysis of cellobiose into  $\alpha$ -glucose-1-phosphate and glucose.<sup>181</sup> When given  $\alpha$ -glucosyl fluoride as a donor and glucose as an acceptor in the absence of phosphate, cellobiose is synthesized rapidly ( $k_{cat} = 7 \text{ s}^{-1}$ ,  $k_{cat}/K_M = 2250 \text{ M}^{-1} \cdot \text{s}^{-1}$ ) and quantitatively (B. Nidetzky, personal communication).

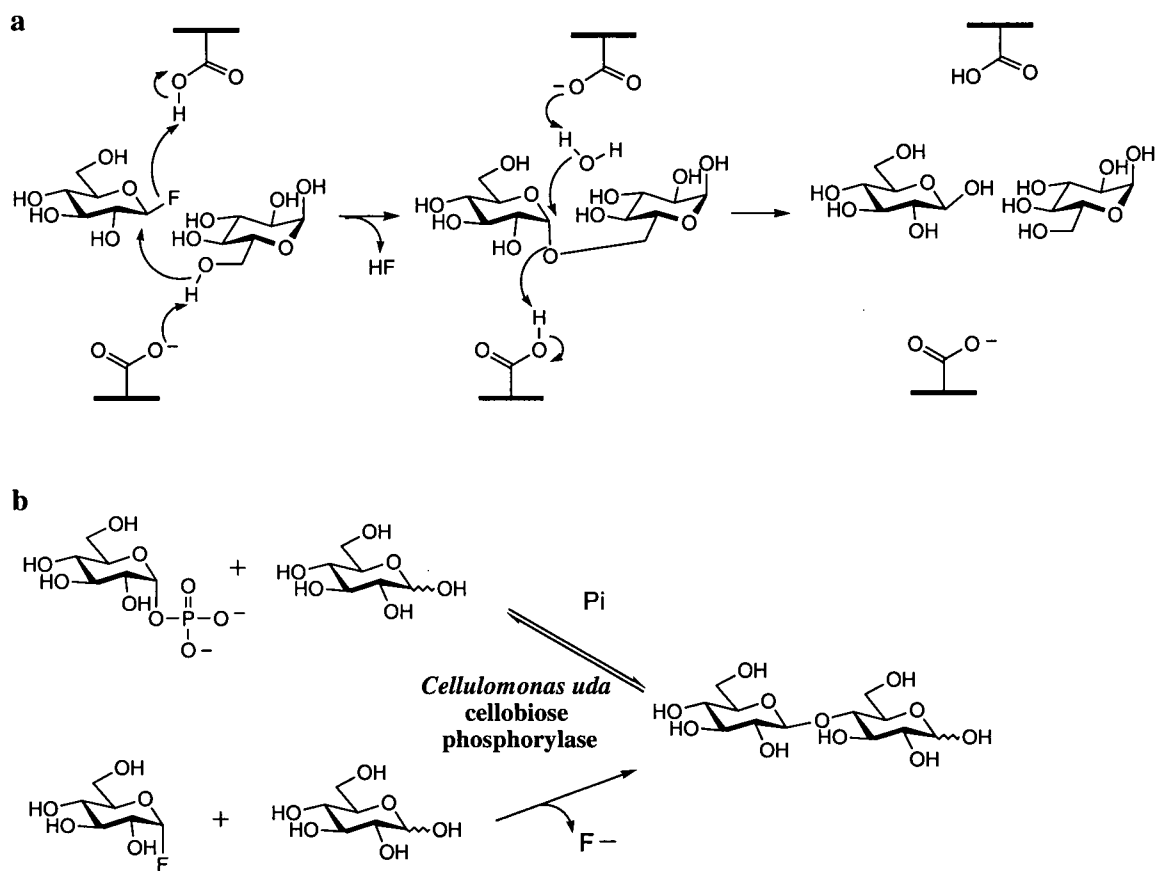


**Figure 4-9:** Hehre mechanism for inverting glycosidases: (a)  $\beta$ -glucosyl fluoride with trehalase,<sup>182</sup> (b)  $\alpha$ -glucosyl fluoride with cellobiose phosphorylase.<sup>181</sup>

### Retaining glycosidases

Retaining glycosidases are more commonly used for synthesis (reviewed in <sup>155,179</sup>). This primarily stems from the opportunity to partition the discrete covalent intermediate formed by these enzymes between hydrolysis and transglycosylation pathways (Figure 4-10).

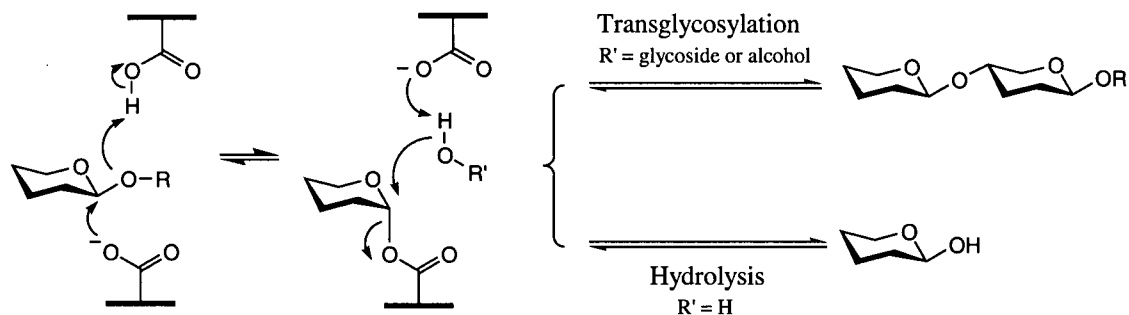


**Figure 4-10:** Transglycosylation and hydrolysis pathways for partitioning of a covalent intermediate.

There are two approaches in which the covalent intermediate may be partitioned. In the 'reverse hydrolysis' or 'thermodynamic' approach a high concentration of monosaccharide is incubated with the enzyme to drive the equilibrium away from hydrolysis and towards synthesis (Figure 4-11a). To further reduce competition by hydrolysis an organic solvent is often included, such as acetonitrile, or the acceptor alcohol itself may serve this purpose if it is a solvent (Figure 4-11b). However, a minimum fraction of water is usually essential to maintain enzyme activity (10-20%), and this ultimately diminishes yields through hydrolysis of products. This problem has been partly circumvented by coating glycosidases in lipids, thereby allowing synthesis to be performed in neat organic solvents (e.g. benzene)<sup>183</sup> or in aqueous-organic phase transfer systems.<sup>184</sup> However, the use of organic solvents is ultimately limited by the solubilities of the sugar donors and acceptors.

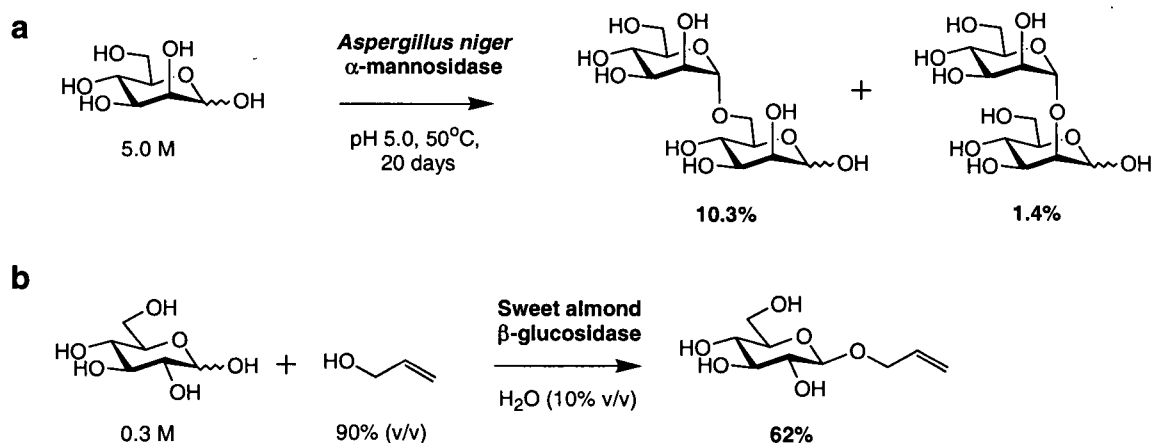


**Figure 4-11:** Examples of the thermodynamic approach to glycoside synthesis with retaining glycosidases: (a) self glycosylation of donor,<sup>185</sup> (b) alcohol acceptor acts as co-solvent.<sup>186</sup>

In the 'kinetic' approach an activated donor substrate is required, having a  $k_{cat}/K_M$  value much greater than that of the product oligosaccharide. These are typically *p*-nitrophenyl glycosides, glycosyl fluorides (reviewed in<sup>180</sup>) or oligosaccharides (Figure 4-12). With chitinases it has proven possible to introduce the donor directly as the reactive intermediate formed during catalysis, in this case an oxazoline (Figure 4-12c).<sup>187</sup> The kinetic method has the benefit of requiring only low concentrations of substrates (typically 10-100 mM donor) and greater versatility as more variation in donor structure is tolerated (due to the reactivity of the leaving group) and stoichiometric introduction of a variety of glycoside acceptors becomes possible (due to reduced competitive inhibition with the donor for the acceptor binding site). As with the thermodynamic approach, competing hydrolysis of the covalent intermediate in the

kinetic method is often reduced with organic co-solvents. Nevertheless, overall product yields rarely exceed 50%.

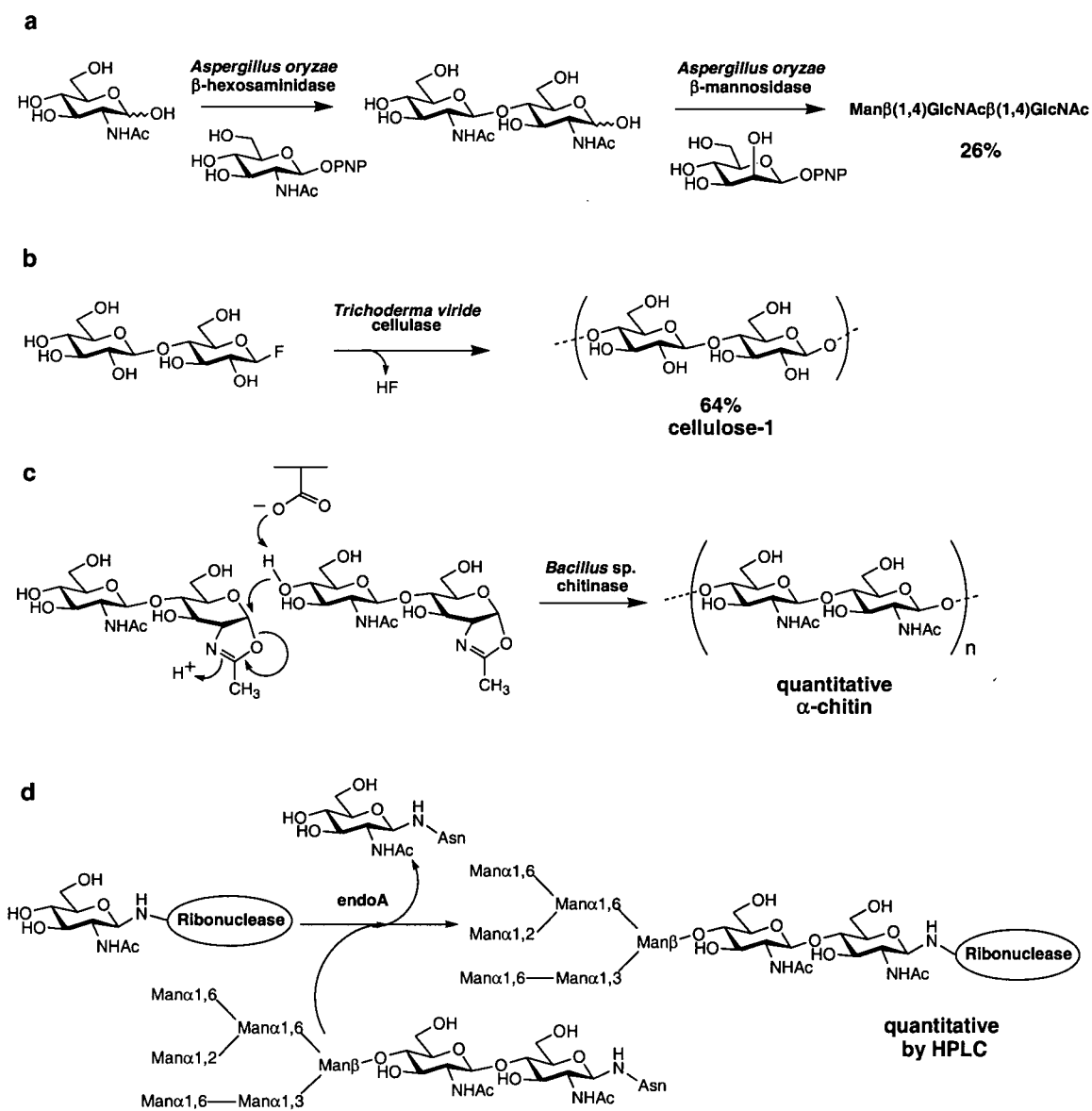


**Figure 4-12:** Examples of the kinetic approach to oligosaccharide synthesis using retaining glycosidases with activated donor substrates: (a) *p*-nitrophenyl  $\beta$ -glycosides,<sup>188</sup> (b)  $\beta$ -glycosyl fluoride,<sup>189</sup> (c) oxazoline of chitobiose,<sup>187</sup> (d) an oligosaccharide.<sup>190</sup>

As shown in Figure 4-12, both *exo* and *endo* retaining glycosidases can be used for glycosyl transfer reactions. The *endo* glycosidases offer the advantage of transferring oligosaccharide blocks rather than simple monosaccharide units (Figure 4-12b,c). Quite large block transfers are possible, as illustrated by the transfer of a heptasaccharide to ribonuclease by endo H (Figure 4-12d). Some *endo* retaining glycosidases can transfer single oligosaccharide

blocks, capped with a terminal galactose residue, which prevents further polymerization due to the absence of a suitably placed (equatorial) 4-hydroxyl. The galactose residue can be subsequently removed by the application of  $\beta$ -galactosidase and thus make the oligosaccharide product available for further glycosylations (Figure 4-13). Of course, it is the implicit goal of enzyme catalyzed oligosaccharide synthesis to avoid any protection or deprotection steps.

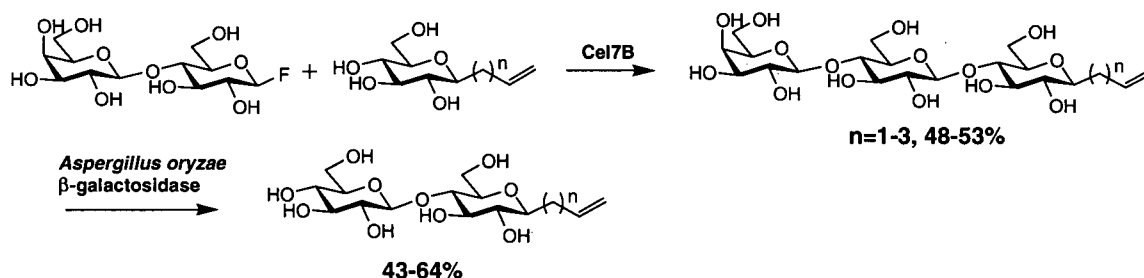


**Figure 4-13:** Kinetic transfer of a single glucose unit with an *endo*-glycosidase, *Humicola insolens* Cel7B, using  $\beta$ -lactosyl fluoride as a donor and subsequent cleavage with  $\beta$ -galactosidase.<sup>191</sup>

In a related, but remarkable example, the inverting *endo*-glycosidase T4 phage lysozyme was converted into a retaining transglycosidase by substituting T26, a residue near the  $\beta$ -face of a substrate, for histidine (T26H).<sup>192</sup> The resulting imidazole side chain occupied the position normally reserved for the attacking water and presumably attacked the anomeric carbon of the substrate to form a reactive glycosyl-imidazolium covalent intermediate (Figure 4-14). This intermediate had a high preference for glycosyl transfer to oligosaccharide acceptors ( $k_{trans}/k_{hydro} = 10:1$ ), resulting in the synthesis of oligosaccharide products.

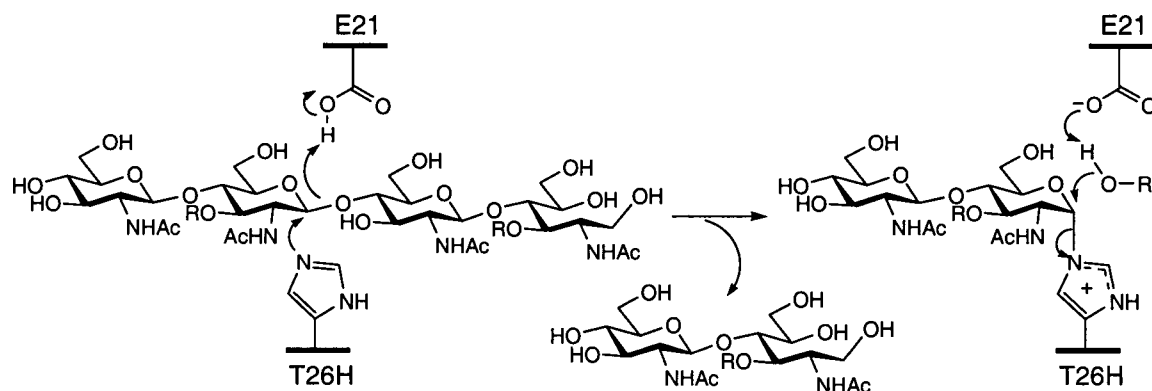


**Figure 4-14:** Mechanism for transglycosylation by the T4 phage lysozyme mutant T26H. R = DAla-DGlu-DAPA, R' = second equivalent of substrate.<sup>192</sup>

*Agrobacterium* sp.  $\beta$ -glucosidase (Abg) has also been used successfully for kinetic transglycosylation reactions. *p*-Nitrophenyl  $\beta$ -D-galactopyranoside and  $\beta$ -D-mannopyranosyl fluoride were used as donors to a variety of thiosugar acceptors, with yields exceeding 60% for the best donor-acceptor combination.<sup>193</sup> Interestingly,  $\beta$ (1,3) linked products were favoured over  $\beta$ (1,4). Abg could also synthesise 2-deoxy  $\beta$ -glycosides using D-glucal as the kinetic donor (Figure 4-15). As demonstrated in Chapter 2, D-glucal rapidly forms a covalent 2-deoxy glycosyl enzyme which is subsequently slow to turn over in the absence of an acceptor. Along with  $\beta$ -mannosides, the 2-deoxy  $\beta$ -glycosidic bonds are the most challenging linkages to form due to the absence of neighbouring group effects to direct the stereochemistry of this linkage.

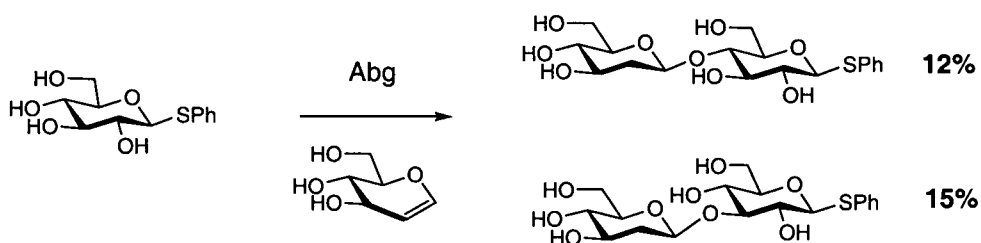


**Figure 4-15:** Synthesis of 2-deoxy glycosides using Abg and D-glucal as donor.

### Glycosynthases

A more recent synthetic approach with retaining glycosidases, and the progenitor of this thesis, eliminates the hydrolysis pathway by site directed mutagenesis of the retaining glycosidase. The study leading to the development of these mutant glycosidases, called 'glycosynthases', is noteworthy because the initial intent was not focused on generating synthetically useful catalysts. The intent was, in fact, to engineer the *Agrobacterium* sp. retaining  $\beta$ -glucosidase to be an inverting glycosidase. This was readily achieved by deleting the catalytic nucleophile with the mutation E358A, producing a mutant virtually devoid of glycosidic bond cleaving activity, even with the reactive substrate 2,4-dinitrophenyl  $\beta$ -glucoside (2,4DNPGlu).<sup>30</sup> However, when provided with an external anionic nucleophile, such as formate or azide, a  $10^5$  fold increase in the rate of 2,4DNPGlu cleavage was observed. This was the result of the anion taking the place of the missing nucleophile, attacking the anomeric carbon of the substrate, and effecting glycosidic bond cleavage (Figure 4-16a). The product formed in this case was not glucose, but the corresponding  $\alpha$ -glucosyl azide (or  $\alpha$ -glucosyl formate). Not only did the inverted stereochemistry of the cleavage product mark this mutant as an inverting glycosidase, but also its

ability to cleave  $\alpha$ -glucosyl fluoride through a Hehre mechanism (Figure 4-16b), albeit slowly ( $k_{cat} = 5.5 \text{ min}^{-1}$ ,  $K_M = 53 \text{ mM}$ ) due to the poor ability of  $\alpha$ -glucosyl fluoride to act as an acceptor. Nevertheless, due to the absence of a catalytic nucleophile, and thus the inability of the mutant to cleave glycosidic bonds without chemical rescue, the resulting  $\alpha$ -cellobiosyl fluoride product accumulated.

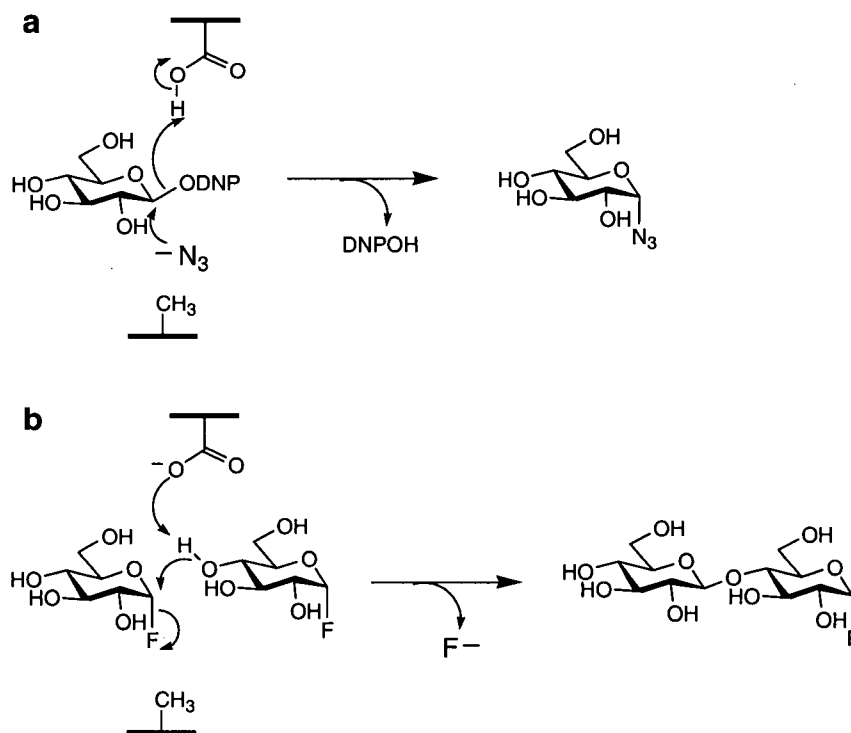


**Figure 4-16:** Mechanism for *Agrobacterium* sp.  $\beta$ -glucosidase mutant E358A acting as an inverting glucosidase in the presence of azide (a) and as a 'glycosynthase' with  $\alpha$ -glucosyl fluoride (b). DNP = 2,4-dinitrophenyl.

The synthetic utility of the Abg E358A mutant was explored further using aryl monosaccharides and disaccharides as acceptors.<sup>194</sup> These drastically improved rates of transglycosylation, presumably through additional binding interactions achieved with the aryl aglycons, resulted in markedly improved yields of oligosaccharide products. Yields with disaccharide acceptors such as *p*-nitrophenyl  $\beta$ -cellobioside exceeded 90% and yields with aryl  $\beta$ -glycosides typically exceeded 80%. Using  $\alpha$ -glucosyl fluoride as a donor a range of di-, tri-, and tetrasaccharides were obtained (Figure 4-17a). However, using  $\alpha$ -galactosyl fluoride only a single glycosylation of the acceptor was catalysed due to absence of a suitably positioned 4-hydroxyl in the product to receive a second transfer (Figure 4-17b). High yields were also

obtained with this donor, exceeding 90% with disaccharide acceptors. Also noteworthy was the regioselectivity obtained with Abg E358A. Unlike the wild type enzyme, which generally made a mixture of products favouring the  $\beta(1,3)$  linkage,<sup>193</sup> the Abg E358A mutant was purely  $\beta(1,4)$  regioselective. The one exception was obtained with PNP  $\beta$ -xylopyranoside as an acceptor, in which  $\beta(1,3)$  regioselectivity was observed.

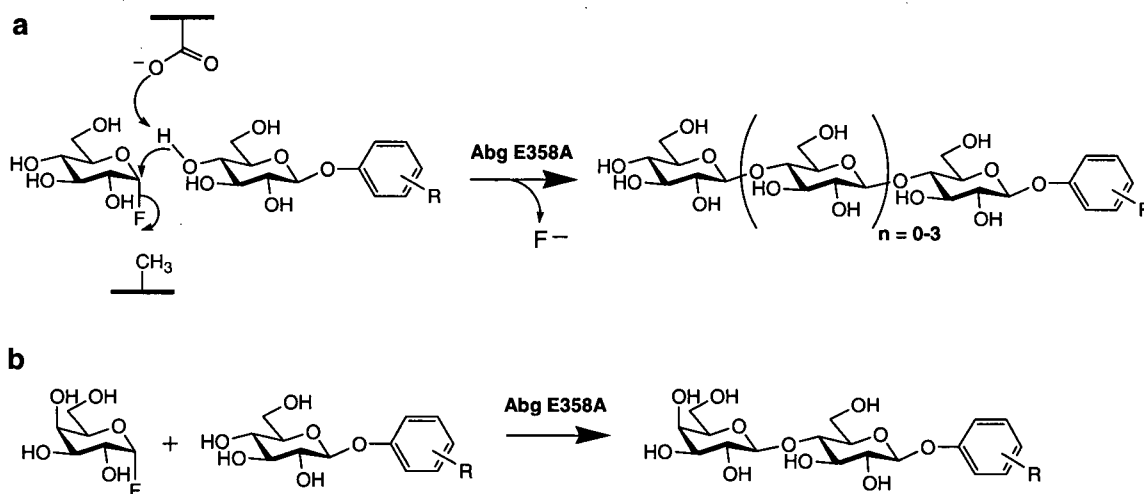


**Figure 4-17:** Reaction schemes for Abg E358A using  $\alpha$ -glucosyl fluoride (a) and  $\alpha$ -galactosyl fluoride (b) as donors.

An impressive number of glycosides acted as viable acceptors, including aryl  $\beta$ -mannosides, xylosides and 2,4-dinitrophenyl 2-deoxy-2-halo- $\beta$ -glucosides. These latter acceptors allowed the synthesis of di- and trisaccharide inactivators for retaining cellulases (Figure 4-18), and were successfully applied to the identification of active site nucleophiles in these enzymes,<sup>195,196</sup> as well as revealing active site interactions in X-ray crystallographic studies.<sup>71,83,197</sup> Such compounds would be impossible to prepare by transglycosylation with the wild type enzyme because rapid inactivation would occur with the acceptor. Likewise, glycosylation of a nitroxide-labelled glucoside to yield nitroxide-labelled cellotriose and cellotetraose derivatives provided ligands for NMR studies of the binding modes of cellooligosaccharides to cellulose binding domains (Fig 4-19a).<sup>198</sup> Other labels, such as carbon-13, deuterium, or tritium could also be incorporated at any position in an oligosaccharide chain to provide specific probes of protein-ligand interactions or to serve as radiolabelled substrates (Figure 4-19b).



including branched oligosaccharides (Figure 4-19c). This example also raises the intriguing possibility of tuning the reactivity of the donor to control the regioselectivity of glycosylation.

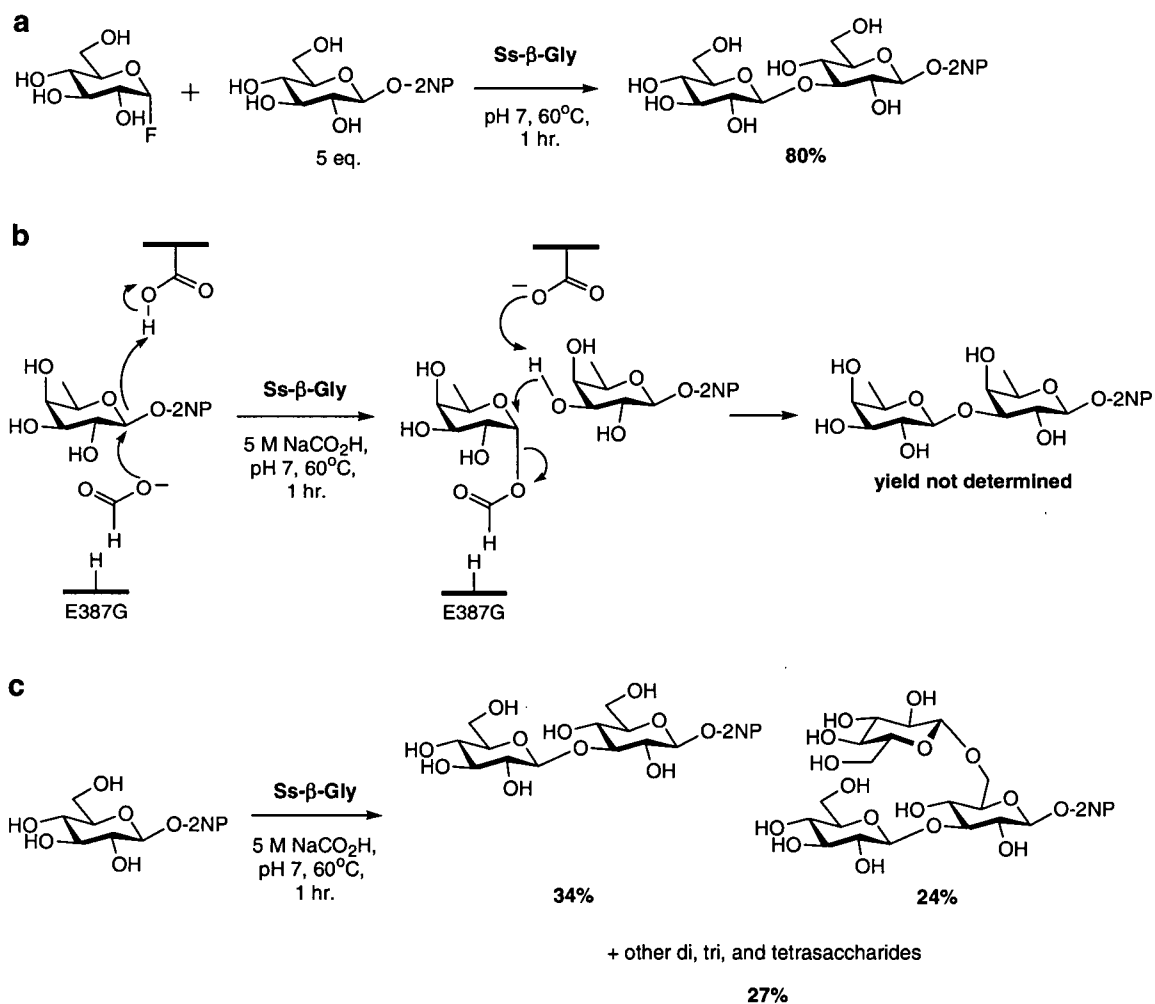


**Figure 4-20:** *Sulfolobus solfataricus* E387G glycosynthase (Ss- $\beta$ -Gly): (a)  $\alpha$ -Glucosyl fluoride donor, (b) *in situ* generation of  $\alpha$ -D-fucopyranosyl formate donor (c) *in situ* generation of  $\alpha$ -glucosyl formate donor.<sup>199</sup> 2NP = 2-nitrophenyl.

Glycosynthases can also be derived from *endo*-glycosidases. The first of these was the E134A mutant of *Bacillus licheniformis* 1,3-1,4- $\beta$ -glucanase (Family 16) which transferred  $\alpha$ -laminaribiosyl fluoride to  $\beta$ -glucosides,  $\beta$ -cellobiosides and  $\beta$ -laminaribiosides with  $\beta$ -(1,4) specificity, but not to  $\beta$ -galactosides or *N*-acetyl  $\beta$ -glucosaminide acceptors (Figure 4-21).<sup>200</sup>

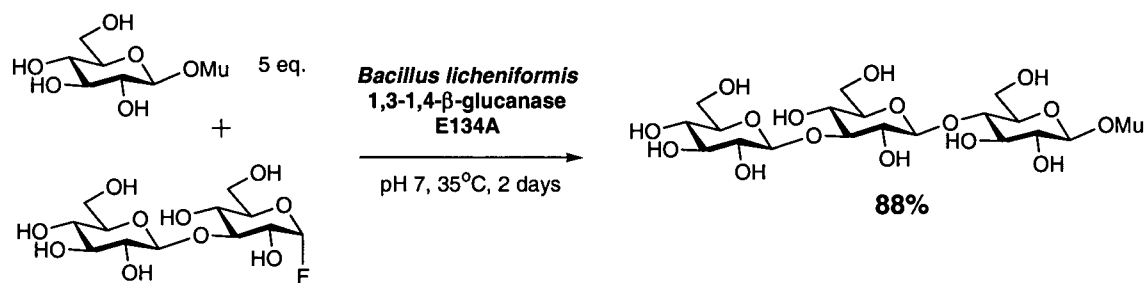


**Figure 4-21:** *Bacillus licheniformis* E134A glycosynthase.<sup>200</sup>

A second *endo*-glycosynthase, the E197A mutant of *Humicola insolens* endocellulase Cel7B (formerly called endoglucanase I), readily condensed substituted  $\alpha$ -cellobiosyl fluorides to yield a variety of derivatized cellulose oligomers, including branched cellulose chains (Figure 4-22 a).<sup>201</sup> However, analogous to the transglycosylation behaviour of the wild type enzyme,<sup>191</sup> single glycosyl transfers could be achieved with  $\alpha$ -lactosyl fluoride (Figure 4-22b).

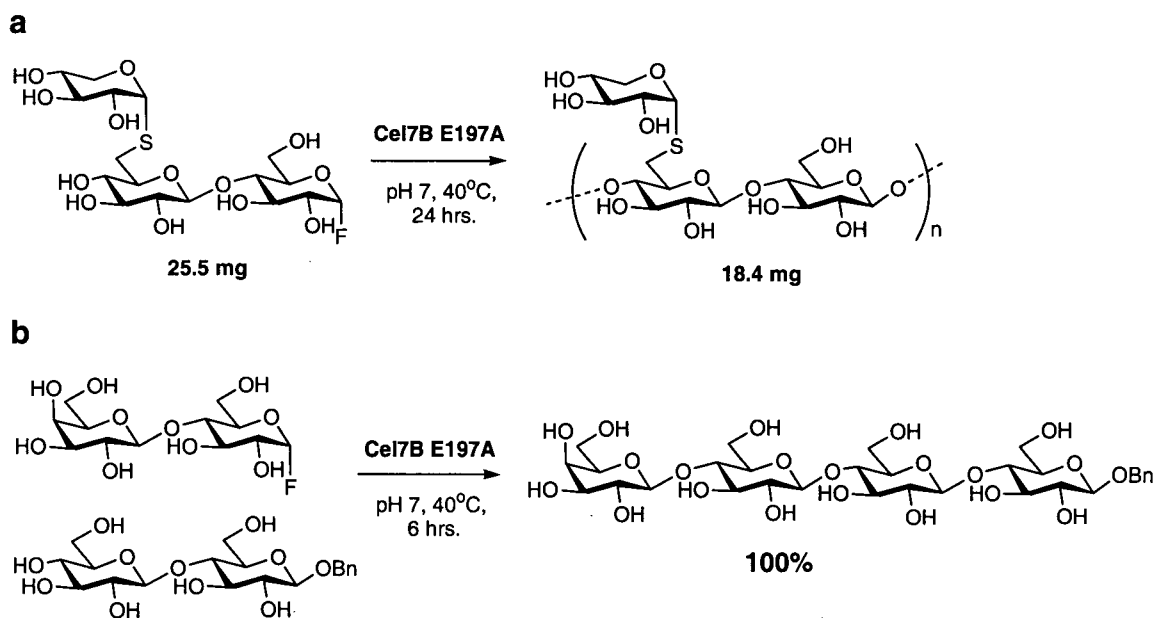


**Figure 4-22:** *Humicola insolens* Cel7B E197A 'cellulosynthase'. (a) Substituted  $\alpha$ -cellobiosyl fluoride donor, (b)  $\alpha$ -Lactosyl fluoride donor.<sup>201</sup>

## Objectives of This Thesis: Glycosynthases

The glycosynthase component of this thesis has two broad aims:

1. To improve glycosynthase activity through site directed mutagenesis.
2. To study glycosynthase behaviour through reaction kinetics and product analysis. Two classes of reactions are considered:
  - i. chemical rescue of glycosidic bond cleaving activity
  - ii. transglycosylation using  $\alpha$ -glycosyl fluoride donors

As will be seen, chemical rescue and transglycosylation are complementary approaches by which to probe glycosynthase mechanism because one is approximately the microscopic reverse of the other (Figure 4-23). Furthermore, chemical rescue allows the *in situ* generation of labile  $\alpha$ -glycosyl donors, which normally could not be prepared through standard synthetic methods.

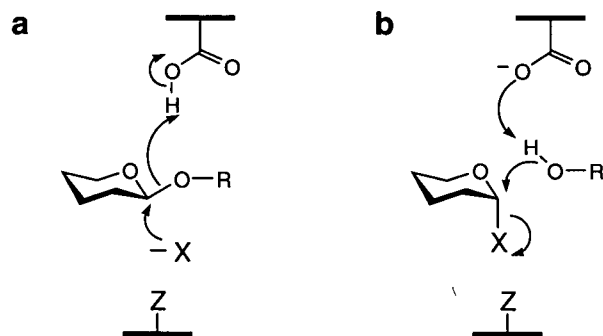


Figure 4-23: Chemical rescue (a) and transglycosylation (b) as complementary glycosynthase probes.

**Chapter 5 Engineering Enhanced Glycosynthase Activity  
in *Agrobacterium* sp.  $\beta$ -glucosidase**

### Improving Glycosynthase Activity

There are a number of reasons for wanting to improve the rates of a glycosynthase reaction. Obviously, a more potent glycosynthase should provide higher oligosaccharide yields in a shorter length of time and require less enzyme to do so. Likewise, improved catalysis may enable glycosylation of poor acceptors, thereby broadening the synthetic utility of a given glycosynthase. Most importantly, once key catalytic features of a glycosynthase are optimized, these features may serve as a template for the creation of glycosynthases from other glycosidases. This latter goal was inspired by the troubling observation that the simple mutation of a catalytic nucleophile to alanine in a retaining glycosidase did not universally produce a glycosynthase. More confounding was the finding that this was true even for retaining glycosidases that had impressive transglycosylation activity as wild type enzymes, such as *Thermoanaerobacterium saccharolyticum*  $\beta$ -xylosidase<sup>202</sup> and *Bacillus circulans*  $\beta$ -galactosidases.<sup>203</sup>

Initially the problem may be one of finding the best reaction for a given glycosynthase. This is not a trivial task, as it has become apparent that the best acceptor for a glycosynthase often defies prediction. Graduate work by Jan Blanchard approached this problem by examining the reactivation rates of retaining glycosidases trapped as 2-fluoro glycosyl enzymes.<sup>204</sup> As noted in Chapter 1, an acceptor glycoside can accelerate reactivation through transglycosylation. Accordingly, the best acceptors for transglycosylation can be identified by relative reactivation rates. This method was readily adapted to a 96 well plate format in which each well contains a sample of trapped enzyme plus a different acceptor. After incubation for a period of time a chromophoric substrate for the free glycosidase is added to each well. A spectrophotometric plate reader is then used to measure relative rates in each well, thus yielding relative reactivation rates. Most importantly, the best acceptors identified by this screen have proved to be the best acceptors for the corresponding glycosynthase.

Just as there are numerous reasons for wanting to improve a glycosynthase, there are also a number of ways to do so, which broadly can be divided into irrational and rational design strategies. Irrational design involves random mutation of a glycosynthase gene, either globally or within defined regions of the enzyme, thereby creating a library of mutants. Error prone PCR or DNA shuffling between homologous genes have both been used to create glycosynthase libraries. A given library can be expressed in *E. coli* or on the surface of phage and subsequently be screened for improved transglycosylation activity. The screen itself is the key problem here

since, unlike reactions that break a bond, the convenient release of a chromophore or fluorophore cannot be directly coupled to a transglycosylation reaction.

Screening assays involving radiolabelled substrates are a potential solution. One approach under development involves linking a potential acceptor to a membrane. An *E. coli* based glycosynthase library, plated on a Petri dish and provided with a radiolabelled  $\alpha$ -glycosyl fluoride donor, is placed in physical contact with the membrane and the cells lysed. Following an appropriate reaction time, excess donor is washed from the membrane. Radioactive spots are then traced back to active glycosynthase colonies saved on a replica plate. This method has the potential to assay any donor-acceptor combination. However, apart from the inherent difficulties in preparing and working with radioactive donors, one has no control over the concentration of the acceptor, or how the covalent attachment of an acceptor to a membrane will affect reaction with a glycosynthase.<sup>205</sup>

Phage display is also a possible screening methodology. Analogous to the acceptor screen developed by Jan Blanchard, phage that display active retaining glycosidase mutants are initially trapped using a biotin linked 2-fluoro glycoside inactivator and isolated from the rest of the phage library on a streptavidin column. A solution of acceptor is then applied to the column. Glycosidase mutants that are effective in catalyzing transglycosylation to the acceptor release the phage. Subsequent transfection of *E. coli* with these phage can then be used to express the mutants of interest. The underlying premise in all of this is that a glycosidase mutant that is readily trapped and subsequently reactivated by an acceptor will catalyze the corresponding glycosynthase reaction upon mutation of the catalytic nucleophile.

A clever *in vivo* coupled assay was developed by Dr. Christoph Mayer in this lab, which takes advantage of the convenience of fluorescent substrates, to screen for improved Abg glycosynthase activity.<sup>206</sup> This particular screen used *Cellulomonas fimi* exocellulase CenD as a coupling enzyme, since this enzyme has excellent activity towards 4-methylumbelliferyl  $\beta$ -cellotrioside, but not 4-methylumbelliferyl  $\beta$ -glucoside. The latter is a good acceptor for an Abg glycosynthase. Therefore, by co-expressing CenD in *E. coli* with a library of Abg nucleophile mutants in the presence of  $\alpha$ -glucosyl fluoride and 4-methylumbelliferyl  $\beta$ -glucoside, colonies containing active glycosynthases fluoresce as a result of synthesis and subsequent hydrolysis of 4-methylumbelliferyl  $\beta$ -cellotrioside. The shortfall of this approach is the need for a coupling glycosidase that is highly specific for the oligosaccharide product formed, which is often not

possible to find. Nevertheless, this strategy was successful in 'rediscovering' a more active Abg glycosynthase, E358G,<sup>194</sup> which will be described below.

In parallel with the 'irrational' methods described above, a rational approach to engineering enhanced glycosynthase activity was undertaken. The glycosynthase transition state can be expected to involve development of negative charge on the departing fluoride of the donor as the acceptor hydroxyl attacks from the opposite face of the anomeric carbon. What Abg E358A appears to lack are interactions that would stabilize the development of negative charge on fluoride. Chemical rescue studies with E358A, as well as other mutants (see below) indicate that very little room is available on the  $\alpha$ -face of a substrate in the position normally occupied by the nucleophile E358. With this in mind the conservative mutation E358S was conceived as a way to introduce a potential hydrogen bond to fluoride in the transition state without undue steric interference. This chapter examines the catalytic properties of E358S, as well as other mutants derived at this position.

### **Transglycosylation Kinetics with Abg E358 mutants**

As described in Chapter 4 (see Figure 4-17), a glycosynthase reaction with an  $\alpha$ -glycosyl fluoride donor involves the release of fluoride. The concentration of this anion is readily measured as a function of time with a fluoride electrode, thereby providing a convenient assay of glycosynthase activity. Transglycosylation rates for Abg E358 mutants were examined by using a fluoride electrode and Table 5-1 lists apparent kinetic parameters obtained with  $\alpha$ -galactosyl or  $\alpha$ -glucosyl fluoride as donors and PNP  $\beta$ -glucoside or  $\beta$ -cellobioside as acceptors. With either  $\alpha$ -glucosyl fluoride or  $\alpha$ -galactosyl fluoride as donors (at a fixed concentration of acceptor), E358S exhibits the highest  $k_{cat}/K_M$  values of all mutants. Relative to E358A, the  $k_{cat}/K_M$  value for E358S is 24 fold greater with  $\alpha$ -galactosyl fluoride and, interestingly, only 7 fold greater with  $\alpha$ -glucosyl fluoride. Surprisingly, E358G was also an effective catalyst, with  $k_{cat}/K_M$  values for either donor only 1.5 times lower than with E358S. Considering the data for  $\alpha$ -glucosyl fluoride, the advantage of the E358S mutation over E358A and E358G appears to manifest primarily in a reduced  $K_M$  value (0.8 mM), since the  $k_{cat}$  values for E358A and E358G are equivalent or greater. If one can treat  $K_M$  in this case as a true binding constant, this suggests that the serine side chain improves binding of the donor in the ground state. This may arise from a hydrogen bond to fluorine, but the fact that fluorine (bonded to carbon) is a poor hydrogen bond acceptor renders this interaction unlikely.<sup>207</sup> The E358C mutant displayed the poorest

glycosynthase activities. Although the cysteine side chain can engage in hydrogen bonds, the considerably greater size of sulphur relative to oxygen (i.e. as in E358S) most likely has negative steric effects. Indeed, chemical rescue studies described below indicate that very little space is available near the position of E358.

Substrate inhibition behaviour was observed for both PNP  $\beta$ -glucoside and PNP  $\beta$ -cellobioside ( $K_i = 2$  to  $7$  mM) when  $\alpha$ -galactosyl fluoride was used as donor (at a fixed concentration), suggesting that each competes with the donor for the  $-1$  binding site. This is not surprising because both PNP  $\beta$ -glucoside<sup>33,34</sup> and cellobiose<sup>77</sup> are excellent substrates for wild type Abg, and therefore can be expected to bind reasonably well to the  $-1$  subsite of the mutant. What is remarkable, however, are the very high apparent  $K_M$  values observed for both acceptors. This is contrary to any expectation that good glycoside acceptors will bind strongly to the aglycone subsites ( $+1$ ,  $+2$ , etc.). Notably, the  $K_M$  value for PNP  $\beta$ -cellobioside ( $K_M = 70$  mM), the best acceptor known for Abg glycosynthases, is nearly 2 fold greater than the weaker acceptor, PNP  $\beta$ -glucoside ( $K_M = 45$  mM).

The pH dependence of the transglycosylation rate was also examined for E358S and E358A (Figure 5-1). No significant effect on  $(k_{cat}/K_M)_{app}$  was observed for either mutant over a range of pH 9 to 5. Although one might have expected a titration corresponding to the acid-base catalyst E170, this profile is analogous to the very broad pH-rate profile observed for wild type Abg.<sup>33</sup>

**Table 5-1:** Apparent kinetic parameters for transglycosylation reactions of Abg E358 mutants (25°C, pH 7).

	DONOR			ACCEPTOR	
	$k_{cat}$ ( $\text{min}^{-1}$ )	$K_M$ (mM)	$k_{cat}/K_M$ ( $\text{min}^{-1} \text{mM}^{-1}$ )	$K_M$ (mM)	$K_i^a$ (mM)
	$\alpha$ -galactosyl fluoride <sup>b</sup>			PNP $\beta$ -glucoside <sup>c</sup>	
E358A	-	>1000	0.034	-	-
E358C	-	>1000	0.018	-	-
E358S	177	220	0.800	45	7
	$\pm 4$	$\pm 12$		$\pm 9$	$\pm 2$
E358G	-	-	0.56	-	-
	$\alpha$ -galactosyl fluoride <sup>d</sup>			PNP $\beta$ -cellobioside <sup>e</sup>	
E358S	396	181	2.2	70	2
	$\pm 15$	$\pm 18$		$\pm 12$	$\pm 0.4$
	$\alpha$ -glucosyl fluoride <sup>f</sup>			PNP $\beta$ -cellobioside	
E358A	63	5.9	11	-	-
	$\pm 2$	$\pm 0.4$			
E358S	65	0.79	82	-	-
	$\pm 1$	$\pm 0.04$			
E358G	332	6.6	50	-	-
	$\pm 3$	$\pm 0.2$			

a) Substrate inhibition observed. b) Parameters obtained with [PNP  $\beta$ -glucoside] fixed at 22 mM. c) [ $\alpha$ -GalF] = 57 mM. d) [PNPC] = 11 mM. e) [ $\alpha$ -GalF] = 66 mM. f) [PNPC] = 11 mM.

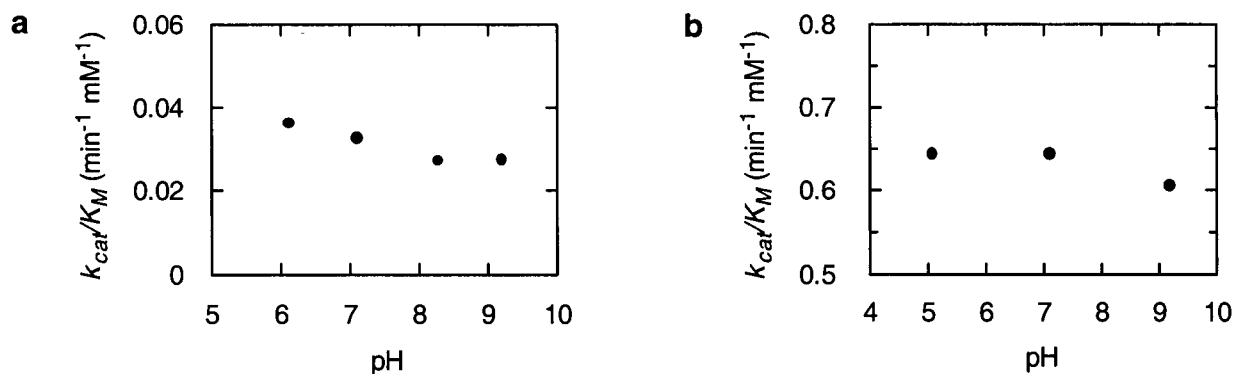


**Figure 5-1:** pH dependence of  $k_{cat}/K_M$  for the reaction of  $\alpha$ -galactosyl fluoride with Abg E358A (a) and Abg E358S (b) using PNP  $\beta$ -glucoside (20 mM) as acceptor (25°C).

### Synthesis of Oligosaccharides With Abg E358S

The synthetic utility of Abg E358S was investigated using  $\alpha$ -glucosyl fluoride or  $\alpha$ -galactosyl fluoride as donors to various acceptors (Tables 5-2 and 5-3). The yields of oligosaccharides (determined by HPLC, with masses confirmed by ESI-MS) were generally better than or comparable to those reported previously for E358A.<sup>194</sup> An increased rate of glycosylation is expected to improve yields as a result of less loss of the donor glycosyl fluoride to spontaneous

hydrolysis. It is also significant that PNP or benzyl *N*-acetyl  $\beta$ -glucosaminide, which are weak acceptors for E358A, were glycosylated by E358S to form *N*-acetyl lactosaminides in reasonable yield (63-64%) (Table 5-2). *N*-Acetyl lactosamine is a valuable precursor to various cell surface oligosaccharides, such as the N3 antigen (Chapter 4, Figure 4-1). Such syntheses could easily be done on a large scale since the E358S mutant can be produced in gram quantities. Other glycoside acceptors that were quantitatively galactosylated by E358S (by TLC analysis) include octyl  $\beta$ -glucoside and PNP  $\beta$ -gentiobioside. NMR spectroscopic analysis of the per-*O*-acetylated products listed in Tables 5-2 and 5-3 indicated exclusive formation of  $\beta$ (1,4) glycosidic bonds by E358S, as was previously observed with E358A.<sup>194</sup> Thus the enhancement in glycosylation activity afforded by the E358S mutation does not change regioselectivity.

**Table 5-2:** Yields of transglycosylation reactions with Abg E358S using  $\alpha$ -galactosyl fluoride as a donor. All linkages formed are  $\beta$ (1,4). Product numbers are indicated in parentheses.

Acceptor	Oligosaccharide Yield (%) <sup>a</sup>	
	di-	tri-
PNP $\beta$ -glucoside <sup>b</sup>	98 (5-1)	-
PNP $\beta$ -cellobioside	-	98 (5-2)
PNP $\beta$ -mannoside	80 (5-3)	-
PNP <i>N</i> -acetyl- $\beta$ -glucosaminide	63 (5-4)	-
Benzyl <i>N</i> -acetyl- $\beta$ -glucosaminide	64 <sup>c</sup> (5-5)	-

a) Determined by HPLC. b) PNP = *para*-nitrophenyl. c) Isolated yield.

**Table 5-3:** Yields of transglycosylation reactions with Abg E358S using  $\alpha$ -glucosyl fluoride as a donor. All linkages formed are  $\beta$ (1,4). Product numbers are indicated in parentheses.

Acceptor	Oligosaccharide Yield (%) <sup>a</sup>			Total
	di-	tri-	tetra-	
PNP $\beta$ -glucoside	-	83 (5-6a)	13 (5-6b)	96
PNP $\beta$ -cellobioside	-	88 (5-6a)	7 (5-6b)	95
PNP $\beta$ -mannoside	17 (5-7a)	25 (5-7b)	17 (5-7c)	59

a) Determined by HPLC

### Chemical Rescue of Abg E358 Mutants

As expected, Abg E358S and E358G mutants are virtually devoid of  $\beta$ -glycosidic bond cleaving activity, even with the reactive substrate 2,4-dinitrophenyl  $\beta$ -glucoside. However, as was observed previously with Abg E358A (see Chapter 4, Figure 4-16)<sup>30</sup> and other retaining

glycosidase nucleophile mutants,<sup>208,209</sup> substantial glycosidic bond cleaving activity could be restored to Abg E358S and E358G upon the addition of azide or formate (Figure 5-2). Hyperbolic, saturation behaviour was not observed for formate or azide at a fixed concentration of 2,4-dinitrophenyl  $\beta$ -glucoside, indicating that strong, specific binding of the anion in the Abg active site does not occur (Figure 5-2). Any levelling or reduction of activity observed at high (molar) concentrations of anion likely reflects enzyme death or ionic strength effects.

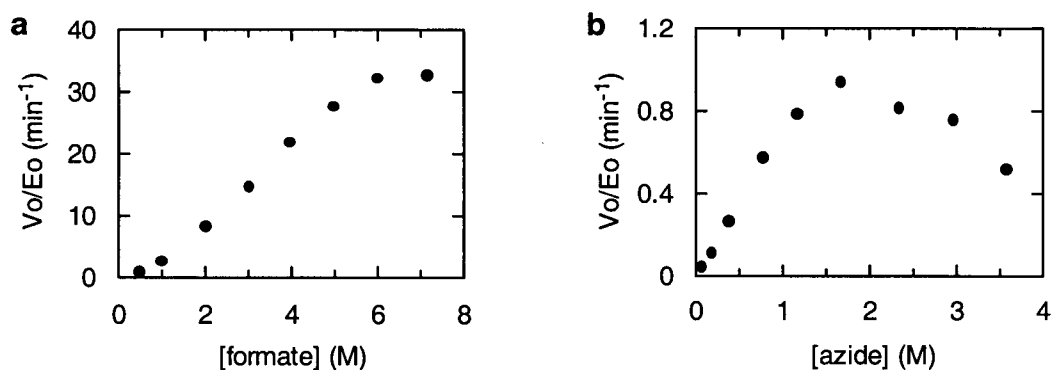


**Figure 5-2:** Plots of reaction rate vs anion concentration for the reaction of Abg E358S with 2,4-dinitrophenyl  $\beta$ -glucoside (2.8 mM) and (a) formate or (b) azide (pH 7, 37°C).

A remarkable dependence on pH was observed for chemical rescue of all E358 mutants, with the greatest rate observed at pH 5. Figure 5-3 illustrates this dependence for E358G and azide. Rates could not be obtained beyond pH 5 due to the instability of Abg. Such a pH dependence has not been reported for nucleophile mutants of other retaining glycosidases, although a similar effect was observed for azide rescue of an acid-base mutant.<sup>208</sup> The titration in Figure 5-3 seems unlikely to arise from azide ( $pK_a = 4.77$ ) because protonation of the nucleophile at low pH would be expected to reduce activity (although deletion of negative charge by protonation may assist entry of azide into the active site). A more likely candidate would be the acid-base catalyst E170. In the wild type enzyme this residue would be expected to have a relatively high  $pK_a$  (7-8) to function as an acid catalyst in the glycosylation step.<sup>69</sup> However, the absence of the negative charge from E358 in the nucleophile mutant can be expected to effect a drop in the  $pK_a$  of E170 (by as much as 2-3  $pK_a$  units). Indeed, in the crystal structure of a very similar Family 1 enzyme the acid-base catalyst actually appears to interact directly with the nucleophile through a hydrogen bond (see Figure 5-9 below). Therefore, in the case of E358 nucleophile mutants, the capacity of E170 to function as an acid catalyst in protonating the 2,4-dinitrophenolate leaving group would improve at lower pH values.

Although 2,4-dinitrophenol does not rigorously require protonic assistance to depart ( $\text{pK}_a^{\text{lg}} = 3.96$ ), an effect might be expected due to hydrogen bonding.

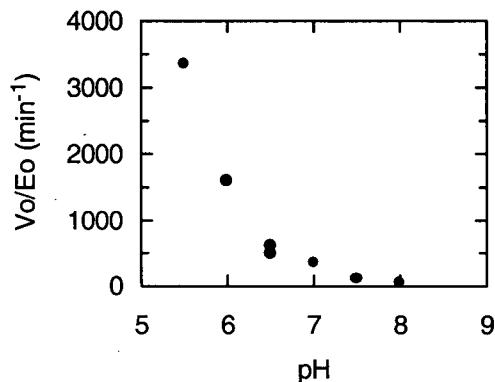


**Figure 5-3:** pH dependence for the reaction of Abg E358G with 2 M azide and 2,4-dinitrophenyl  $\beta$ -glucoside (1.1 mM) at 25°C.

Kinetic parameters for chemical rescue of Abg E358 nucleophile mutants at pH 7 and 6 are given in Tables 5-4 and 5-5, respectively. In the case of azide rescue of E358A and E358S,  $k_{cat}$  increases with decreasing pH, whereas only minor changes are observed for the corresponding  $K_M$  values. Thus the dramatic pH effect shown in Figure 5-3 is primarily a  $k_{cat}$  effect. Also noteworthy from Tables 5-4 and 5-5 is the relative order of  $k_{cat}/K_M$  values for chemical rescue. In the case of azide rescue at pH 6 (Table 5-3), this order correlates with the size of the E358X side chain (E358G  $\gg$  E358A  $>$  E358S), and thus is most likely steric in origin. Indeed, the fact that acetate does not rescue activity with any of the E358 mutants, whereas formate is a potent rescue nucleophile, suggests that very little space is available for an anion in all cases. The chemical rescue order is in direct contrast to the relative glycosynthase activities of these mutants, in which E358S is comparable to E358G and significantly more active than E358A. Possible reasons for this are discussed below.

The markedly greater activity of E358G with anions is also of special note, particularly with formate, which approaches wild type kinetic parameter values. Such a marked response to formate has been observed previously for a glycine nucleophile mutant, SS- $\beta$ -Gly, also a Family 1  $\beta$ -glucosidase.<sup>209</sup> It has been suggested that this is due to formate acting as an accurate mimic of the missing glutamate carboxyl.<sup>208,209</sup> Brønsted analysis and measurement of the contribution of the substrate 2-hydroxyl to catalysis in the Abg E358G - formate system, described below, attempt to assess this proposal.

**Table 5-4:** Kinetic parameters for the reaction of Abg E358 mutants with 2,4-dinitrophenyl  $\beta$ -glucoside and anions at pH 7, 37°C.

	$k_{cat}$ ( $\text{min}^{-1}$ )	$K_M$ (mM)	$k_{cat}/K_M$ ( $\text{min}^{-1} \cdot \text{mM}^{-1}$ )	Behaviour at high [S]
Abg wt <sup>a</sup>	5270	0.031	170 000	sat.
Abg E358A	0.0006 <sup>b</sup>	-	-	-
+ 5 M formate	92 $\pm$ 1	0.057 $\pm$ 0.003	1600	trans.
+ 2 M formate	44.3	0.20	220	trans.
+ 2 M azide	18.3	0.54	34	trans.
Abg E358S	-	-	-	-
+ 5 M formate	19.9	0.033	603	trans.
+ 2 M formate	8.27	0.063	131	trans.
+ 2 M azide	0.933	0.097	9.62	trans.

a) Data from<sup>33</sup> b) Data from<sup>30</sup>**Table 5-5:** Kinetic parameters for the reaction of Abg E358 mutants with 2,4-dinitrophenyl  $\beta$ -glucoside and anions at pH 6, 25°C.

	$k_{cat}$ ( $\text{min}^{-1}$ )	$K_M$ (mM)	$k_{cat}/K_M$ ( $\text{min}^{-1} \cdot \text{mM}^{-1}$ )	Behaviour at high [S]
Abg wt	5040	0.0214	235 500	sat.
Abg E358A	<0.001	-	-	-
+ 2 M azide	86 $\pm$ 1	0.34 $\pm$ 0.01	250	trans.
Abg E358G	0.08	-	-	-
+ 2 M formate	2570 $\pm$ 20	0.081 $\pm$ 0.002	31 700	sat.
+ 2 M azide	1360 $\pm$ 10	0.171 $\pm$ 0.004	7950	trans.
Abg E358S	<0.001	-	-	-
+ 2 M azide	2.95 $\pm$ 0.04	0.126 $\pm$ 0.005	23.4	trans.

The initial product formed by chemical rescue of retaining glycosidase nucleophile mutants with azide or formate is the corresponding  $\alpha$ -glycosyl azide<sup>30</sup> or  $\alpha$ -glycosyl formate.<sup>208</sup> Interestingly, the dependence of reaction rate upon substrate concentration during azide rescue of Abg nucleophile mutants suggests that  $\alpha$ -glucosyl azide acts as a glycosyl donor (Figure 5-4). A linear, non-saturating rate dependence is observed at high substrate concentrations (> 0.5 mM), which is a characteristic feature of retaining glycosidases that catalyze transglycosylation. This includes wild type Abg, in which reaction of the enzyme with PNP  $\beta$ -xyloside produces a similar rate curve, as well as a disaccharide product at high substrate concentrations.<sup>33</sup> Although  $\alpha$ -glycosyl azides are stable compounds (as are  $\alpha$ -glycosyl fluorides), a  $\text{pK}_a^{\text{lg}}$  of 4.77 for azide implies that this anion, although a strong nucleophile, is a reasonable leaving group. Indeed, glycosyl azides are known to function as substrates for wild type and mutant glycosidases.<sup>151</sup>

A similar rate dependence on substrate concentration is observed for formate rescue of Abg E358A and E358S mutants (Figure 5-5).  $\alpha$ -Glucosyl formate is a highly reactive species that is known to act as an effective glycosyl donor with SS- $\beta$ -Gly, the Family 1 glycosynthase

(see Chapter 4).<sup>199,209</sup> This is also true for Abg E358G, in which reaction with formate (2 M) and 2,4-dinitrophenyl  $\beta$ -glucoside (29 mM, pH 6, RT) afforded a 2,4-dinitrophenyl disaccharide as a major product, as observed by TLC and ESI-MS. Interestingly, unlike rescue with azide (Figure 5-4c), formate rescue of the E358G mutant displays normal saturation kinetics (Figure 5-5c). Wild type Abg also displays saturation kinetics with 2,4-dinitrophenyl  $\beta$ -glucoside, perhaps supporting the notion that formate acts as an accurate mimic of the missing glutamate in E358G. However, the observation of saturation kinetics with formate rescue of E358G, despite catalysis of transglycosylation, suggests that the relative rates of formation and breakdown of the  $\alpha$ -glycosyl donor will dictate the shapes of the velocity curves shown in Figures 5-4 and 5-5. A kinetic model of chemical rescue is presented in this chapter which attempts to rationalize this rate behaviour.

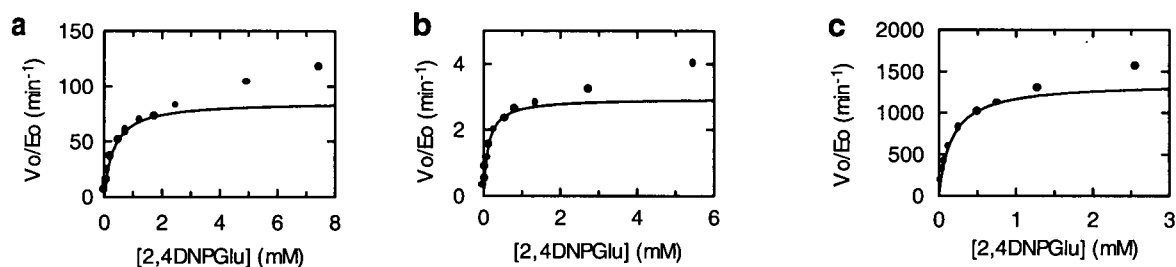


**Figure 5-4:** Plots of rate versus substrate concentration for the reaction of Abg E358 nucleophile mutants with 2,4-dinitrophenyl  $\beta$ -glucoside and 2 M azide (pH 6, 25°C). Curves are fits of the appropriate range of data to the Michaelis Menten equation. (a) E358A; (b) E358S; (c) E358G.

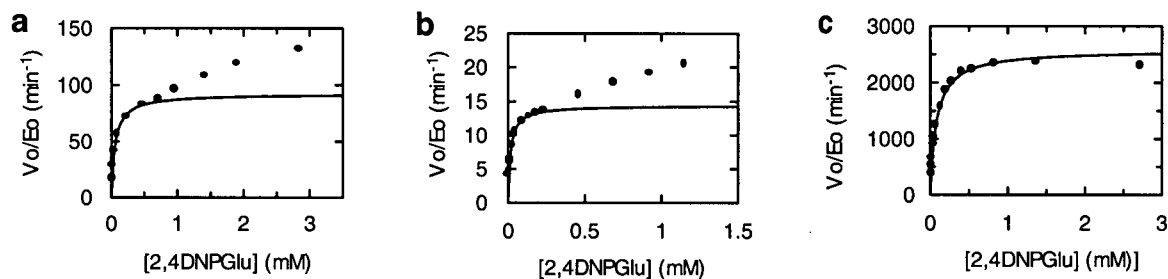


**Figure 5-5:** Plots of rate versus substrate concentration for the reaction of Abg E358 nucleophile mutants with 2,4-dinitrophenyl  $\beta$ -glucoside and formate. Curves are fits of the appropriate range of data to the Michaelis Menten equation. (a) E358A, 5 M formate, pH 7, 37°C; (b) E358S, 5 M formate, pH 7, 37°C; (c) E358G, 2 M formate, pH 6, 25°C.

### Brønsted Analysis of Abg E358G

The potent activity restored to Abg E358G by formate allows reaction with relatively unreactive aryl  $\beta$ -glucosides (Table 5-6), as was observed with the SS- $\beta$ -Gly glycosynthase.<sup>199</sup> In this way the transition state for formate rescue of E358G may be examined in a Brønsted relationship by varying the pKa of the phenol leaving group. Remarkably, a potential break is observed in the Brønsted plot, just as was observed for the wild type enzyme (Figure 5-6).<sup>33</sup> Because a downward break calls for a change in the rate determining step, this suggests that for the more reactive substrates (phenol pKa < 7) the reaction (or release) of the  $\alpha$ -glucosyl formate product is rate limiting. The low  $K_M$  value obtained with 2,4-DNP  $\beta$ -glucoside (80  $\mu$ M) suggests that this non-covalent intermediate may well accumulate in the mutant active site, much like the covalent intermediate accumulates in wild type Abg with this substrate.<sup>33</sup> Therefore, these data strongly agree with the proposal<sup>209</sup> that formate is an accurate 'biomimic' of the wild-type E358 carboxylate side chain in the E358G active site.

**Table 5-6:** Kinetic parameters for the reaction of Abg E358G with aryl  $\beta$ -glucosides and 2 M formate (pH 6, 25°C).

phenol substituent	pKa	$k_{cat}$ ( $\text{min}^{-1}$ )	$K_M$ (mM)	$k_{cat}/K_M$ ( $\text{min}^{-1} \text{mM}^{-1}$ )
2,4-dinitro	3.96	2570 $\pm$ 20	0.081 $\pm$ 0.002	31 700
2,5-dinitro	5.15	1910 $\pm$ 20	0.210 $\pm$ 0.005	9 100
4-chloro, 2-nitro	6.45	2800 $\pm$ 40	0.180 $\pm$ 0.009	15 500
4-nitro	7.18	24.7 $\pm$ 0.2	0.860 $\pm$ 0.015	29

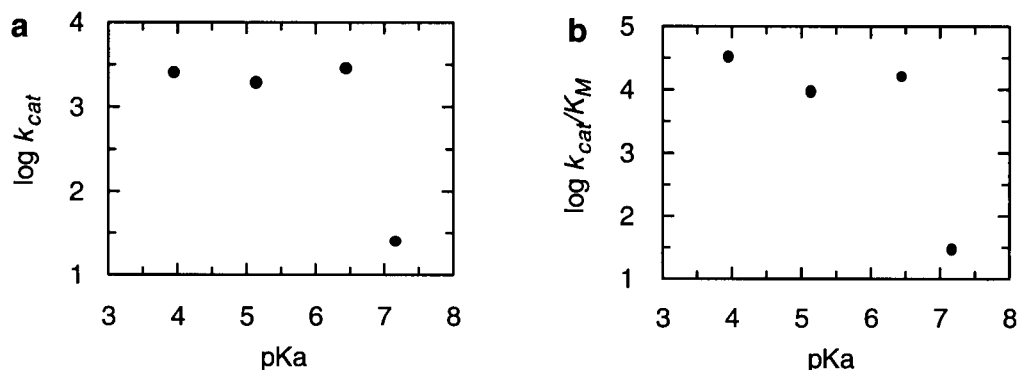


**Figure 5-6:** Brønsted relationships for the reaction of Abg E358G with formate and aryl  $\beta$ -glucosides. (a) Plot of  $\log k_{cat}$  vs pKa of the aglycone phenol; (b) plot of  $\log k_{cat}/K_M$  vs pKa of the aglycone phenol.

### Contribution of the Substrate 2-Hydroxyl to Chemical Rescue and Transglycosylation

Wild type Abg relies heavily on interactions with the 2-hydroxyl of a glucoside substrate to perform catalysis, interactions at this position being worth some  $4.5 \text{ kcal mol}^{-1}$  of activation energy.<sup>34</sup> Saturation kinetics were obtained for the reaction of E358G with the substrate analogue PNP 2-deoxy- $\beta$ -glucoside and 2 M formate (pH 6, 25°C), yielding  $k_{cat}$  and  $K_M$  values of  $1.59 \pm 0.05 \text{ min}^{-1}$  and  $2.1 \pm 0.2 \text{ mM}$ , respectively. A comparison of the  $k_{cat}/K_M$  value for this substrate ( $0.76 \text{ min}^{-1} \text{ mM}^{-1}$ ) to that obtained for formate rescue with PNP  $\beta$ -glucoside (Table 5-7) indicates a 38 fold decrease in this parameter as a result of removing the 2-hydroxyl. This corresponds to a  $2.1 \text{ kcal mol}^{-1}$  difference in activation energies (see Chapter 3, equation 3-2), a typical energy value for a normal hydrogen bond. In wild type Abg the large contribution of the 2-hydroxyl towards transition state stabilization is believed to arise primarily from a strong hydrogen bond between this position and the carbonyl oxygen of the nucleophile (E358). A strong hydrogen bond is not likely to occur with a loosely bound formate in the E358G active site. Nevertheless, the contribution of the 2-hydroxyl is significant to formate rescue of E358G. Indeed, this is likely a minimum estimate of the magnitude of this interaction since 2-deoxy glycosides are typically 1000 fold more reactive than the parent compounds.

It is also noteworthy that 2-deoxy-2-fluoro- $\alpha$ -glucosyl fluoride does not function as a donor with Abg E358S and the acceptor PNP  $\beta$ -cellobioside. The corresponding reaction with  $\alpha$ -glucosyl fluoride is rapid and high yielding (see above). By analogy to the trapping of retaining glycosidases by 2-fluoro sugars, this result illustrates two features of the glycosynthase transition state: that interactions with the donor 2-hydroxyl are important, and that substantial oxocarbenium ion character is present. The relative importance of each, however, remains an open question.

### Donor Interactions in the Glycosynthase Transition State

By analogy to a wild type retaining glycosidase in which the bulk of transition state stabilization is applied to the -1 sugar during glycosidic bond cleavage, we believed that interactions with the  $\alpha$ -glucosyl fluoride donor in the glycosynthase transition state, obtained by mutation of the nucleophile position, would likewise result in the greatest enhancement in activity. The 24 fold greater glycosynthase activity of E358S relative to E358A supports the idea that the serine hydroxyl can stabilize the glycosylation transition state. Gas phase and solution studies lend insight into how this may occur. Although fluorine is, at best, a poor hydrogen bond

acceptor,<sup>207,210</sup> desolvated fluoride can form some of the strongest hydrogen bonds known, with hydrogen bond energies of 30 kcal mol<sup>-1</sup> realized with methanol or ethanol as partners in the gas phase.<sup>211</sup> Likewise, the departure of fluoride during the solvolysis of  $\alpha$ - or  $\beta$ -glucosyl fluoride is acid catalyzed.<sup>8,152,212</sup> Favourable interactions between fluoride and alcohols in solution are also known. For example, the solvolysis of  $\alpha$ -glucosyl fluoride in mixtures of trifluoroethanol (pKa = 12.4) or phenol (pKa = 9.99) is essentially S<sub>N</sub>i; nearly 90% of the trifluoroethyl or phenyl glycoside product recovered is of *retained* anomeric configuration.<sup>213</sup> In the case of trifluoroethanol, this could be attributed to an unfavourable dipole effect that prevents attack from the  $\beta$ -face.<sup>7</sup> However, a hydrogen bond between the departing fluoride and relatively acidic trifluoroethanol (or phenol) in an internal return mechanism could also account for the observed  $\alpha$ -selectivity (Figure 5-7a).<sup>213</sup> The serine hydroxyl in Abg E358S may interact similarly with departing fluoride (Figure 5-8a)

The E358S mutation also introduces a potential hydrogen bond to the 2-hydroxyl of the glycosyl fluoride donor (Figure 5-8a). As noted above, this is an important contribution to catalysis in wild type Abg (Figure 5-8b). Likewise, the inability of 2-deoxy-2-fluoro  $\alpha$ -glucosyl fluoride to function as a donor with E358S suggests that the 2-position is, at least in part, involved in catalysis of glycosylation. This proposal also receives support from solution studies. The solvolysis of  $\beta$ -glucosyl fluoride in ethanol / trifluoroethanol mixtures gives predominantly inverted products. This has been attributed to a hydrogen bond between the 2-hydroxyl of the substrate and the incoming alcohol on the  $\alpha$ -face of the substrate (Figure 5-7b).<sup>213</sup>

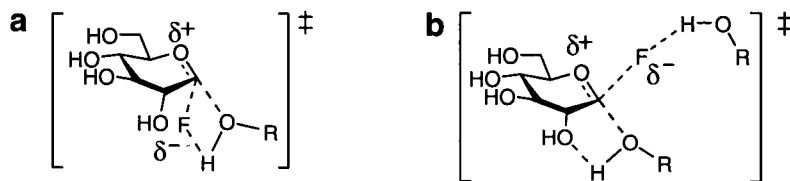


**Figure 5-7:** Proposed transition states for the solvolysis of (a)  $\alpha$ -glucosyl fluoride (R = Ph, CF<sub>3</sub>CH<sub>2</sub>) and (b)  $\beta$ -glucosyl fluoride (R = CF<sub>3</sub>CH<sub>2</sub>, Et) in alcohol mixtures.

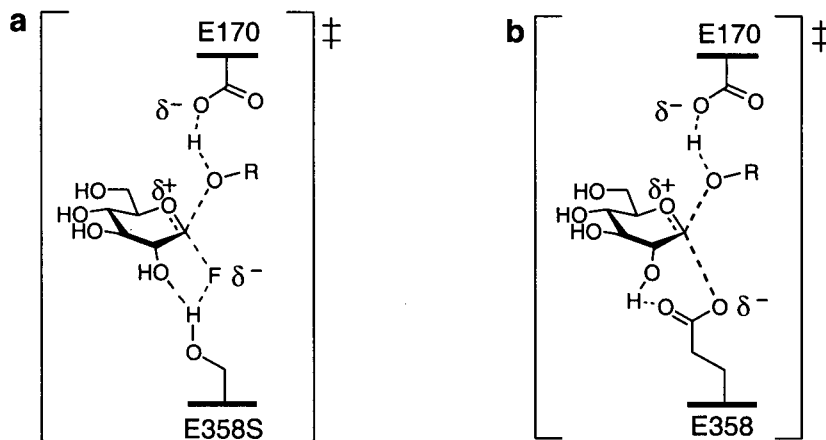


**Figure 5-8:** A comparison of the hypothetical glycosylation transition state for Abg E358S (a) and the transition state for the wild type enzyme (b).

All of the arguments in favour of Abg E358S forming a hydrogen bond to fluoride are at odds with the comparable glycosynthase activity observed for the E358G mutant. However, the glycosylation transition state for Abg E358G may also benefit from a hydrogen bond. Although a structure is not yet available for Abg, an X-ray crystal structure has been solved for a very similar enzyme, *Bacillus circulans* sp.  $\beta$ -glucosidase (46% sequence identity).<sup>122</sup> In the active site of this enzyme, Tyr 296 forms a strong hydrogen bond (2.72 Å) to the carboxyl oxygen of the nucleophile, Glu 355 (Figure 5-9). This residue is conserved with Tyr 298 of Abg. It has been shown in the E358D mutant of Abg that Tyr 298 will infrequently attack the anomeric carbon of 2,4-dinitrophenyl  $\beta$ -glucoside, resulting in labelling of this residue.<sup>118</sup> Thus for Abg E358G, it is possible that Tyr 298 can form a hydrogen bond to departing fluoride, which presumably would occupy a similar position to that of the missing E358 carboxyl oxygen.

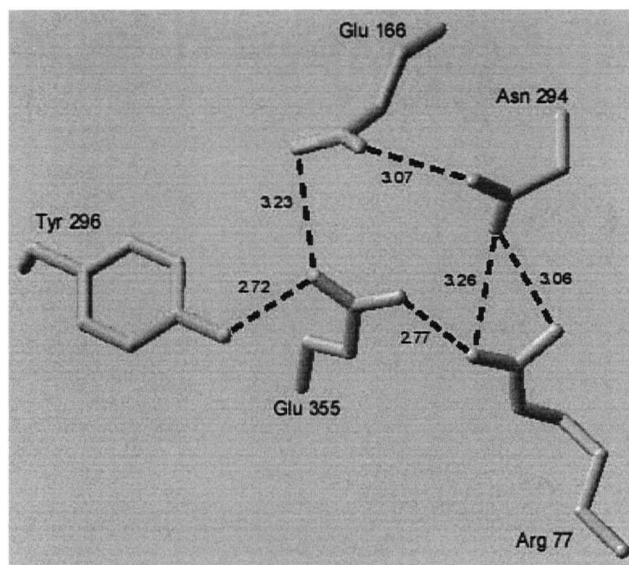


**Figure 5-9:** Active site residues in *Bacillus circulans* sp.  $\beta$ -glucosidase<sup>122</sup> that are conserved in Abg. Glu 355 is the nucleophile, Glu 166 the acid-base catalyst. Lengths ( $\text{\AA}$ ) of predicted hydrogen bonds are indicated.

### Acceptor Interactions with Glycosynthases

The fact that good acceptors for Abg glycosynthases have poor apparent  $K_M$  values is seemingly a paradox (Table 5-1). Poor acceptor binding is not unique to Abg; high  $K_d$  values ( $> 50$  mM) have been measured for acceptors used to reactivate a number of retaining glycosidases trapped as 2-fluoro glycosyl-enzymes, as will be discussed below (Table 5-7). This may, however, reflect the original purpose of a glycosidase active site, that being to hydrolyse glycosidic bonds. Strong aglycone binding would result in product inhibition for a glycosidase. Moreover, as discussed in Chapter 1, structural examination of a number of Michaelis complexes has shown that significant distortion is applied to the  $-1$  sugar. This is most likely achieved by maintaining strong binding to the  $-1$  sugar while applying destabilizing forces to the leaving group (in the  $+1$  site), with these interactions reaching maximum effect at the transition state. The effect of such aglycone interactions is illustrated by the similar  $k_{cat}$  values for *Agrobacterium* sp.  $\beta$ -glucosidase catalyzed hydrolyses of 2,4-dinitrophenyl  $\beta$ -glucoside ( $10\ 100\ \text{min}^{-1}$ ) and cellobiose ( $9\ 900\ \text{min}^{-1}$ ). Likewise, Abg is trapped as readily by 2'-deoxy-2'-fluorocellobiose as with 2,4-dinitrophenyl 2-deoxy-2-fluoro- $\beta$ -glucoside.<sup>77</sup> Thus aglycon binding by Abg effectively renders a glucose moiety ( $\text{pK}_a^{\text{lg}} \sim 14$ ) as good a leaving group as 2,4-dinitrophenol ( $\text{pK}_a^{\text{lg}} = 3.96$ ). Therefore, one can argue in the context of microscopic reversibility that the same transition state



Steady-state analysis of the scheme in Figure 5-10 yields the velocity equation 5-1, which is merely an extension of the velocity equation derived for the double-displacement mechanism of a retaining glycosidase (5-2):

$$\frac{V}{Et} = \frac{\left( \frac{k_2(k_3 + k_4[S])}{k_2 + k_3 + k_4[S]} \right) [S]}{Kd \left( \frac{(k_3 + k_4[S])}{k_2 + k_3 + k_4[S]} \right) + [S]} \quad (5-1)$$

$$\frac{V}{Et} = \frac{\left( \frac{k_2 k_3}{k_2 + k_3} \right) [S]}{Kd \left( \frac{k_3}{k_2 + k_3} \right) + [S]} \quad (5-2)$$

A direct fit of equation 5-1 to the plots in Figures 5-4 and 5-5 above is not helpful due to the grouping of individual kinetic constants. A more useful exercise is to assign reasonable values to these constants to generate a plot similar to those in Figures 5-4 and 5-4. Then the value of each constant can be changed while holding all others fixed to determine the effect on the resulting plot. The danger in this exercise, of course, is that there may well be more than one solution for a given curve, particularly with a multi-parameter equation.

A typical transglycosylation curve generated from equation 5-1 is shown in Figure 5-11. For this plot an 'unbiased'  $K_d$  of 1 was chosen and the glycosylation rate constant was set to ensure accumulation of the  $\alpha$ -glycosyl donor intermediate ( $k_2 = 100 \text{ min}^{-1}$ ). The hydrolysis ( $k_3 = 10 \text{ min}^{-1}$ ) and transglycosylation ( $k_4 = 5 \text{ min}^{-1}$ ) steps chosen in this case represent a partitioning ratio ( $k_4/k_3$ ) of 0.5 towards the second equivalent of substrate.

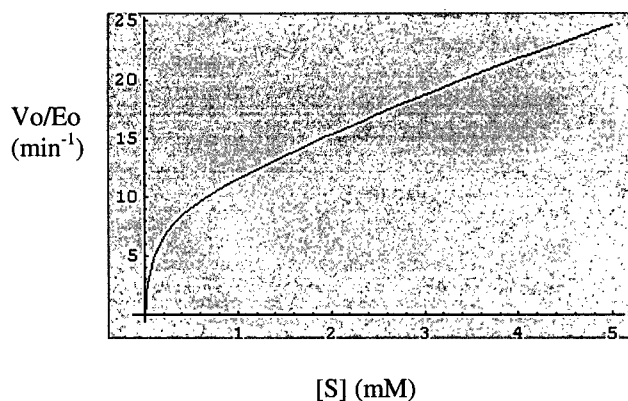


**Figure 5-11:** Simulated plot of substrate concentration versus reaction rate for chemical rescue of a glycosynthase using equation 5-1. Values of kinetic constants used:  $K_d = 1$ ,  $k_2 = 100 \text{ min}^{-1}$ ,  $k_3 = 10 \text{ min}^{-1}$ ,  $k_4 = 5 \text{ min}^{-1}$ .

Figure 5-12 illustrates the response of the curve shown in Figure 5-11 as a result of changing the rate constants in isolation. Variation in the dissociation constant of the substrate ( $K_d$ ) from unfavourable to favourable binding, as well as increasing the rate of  $\alpha$ -glycosyl donor synthesis ( $k_2$ ), both decrease the apparent  $K_M$  value of the curve, as expected (Figure 5-12a,b). Accumulation of the  $\alpha$ -glycosyl donor intermediate (enzyme bound) may well explain the unusually low  $K_M$  values measured for formate and azide rescue of Abg mutants (Tables 5-6 and 5-5). Increasing the rate of hydrolysis (or release) of the  $\alpha$ -glycosyl donor ( $k_3$ ), or the rate of transglycosylation ( $k_4$ ), to exceed the rate of donor synthesis produces standard saturation kinetics as a result of faster turnover of enzyme (Figure 5-12c,d). Either scenario might apply to the case of formate rescue of Abg E358G, which displays saturation kinetics (Figure 5-5c). However, if the rate of donor synthesis and transglycosylation are increased in tandem, a low apparent  $K_M$  is maintained while the slope of the linear portion of the curve increases (Figure 12e). Changes in slope are not evident in Figures 5-4 and 5-5, but are observed for chemical rescue of *Cellulomonas fimi*  $\beta$ -mannosidase Man2A nucleophile mutants (see Chapter 6 and Chapter 8).

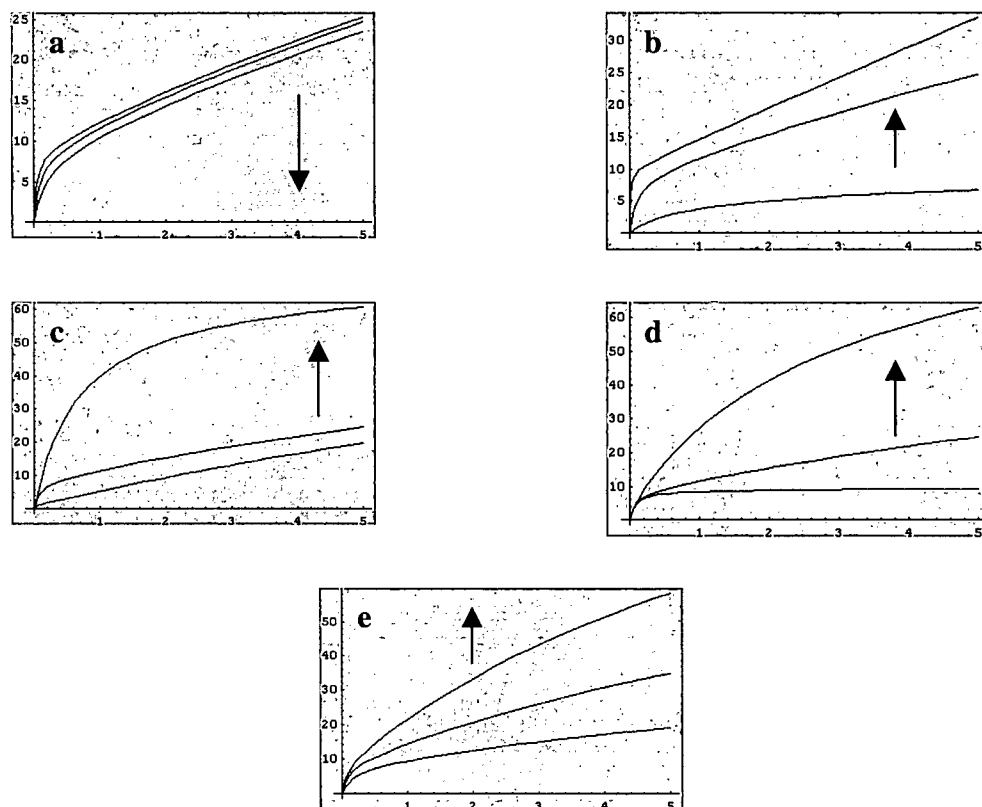


**Figure 5-12:** Simulations of chemical rescue using equation 5-1. Arrows indicate sequence of plots for each value of constant. Starting values are given in Figure 5-11. (a) Change in substrate dissociation constant:  $K_d = 0.5, 1, 2$ . (b) Increasing rate of donor synthesis:  $k_2 = 10, 100, 1000 \text{ min}^{-1}$ . (c) Increasing rate of hydrolysis (or donor release):  $k_3 = 1, 10, 200 \text{ min}^{-1}$ . (d) Increasing rate of transglycosylation:  $k_4 = 0.1, 5, 50 \text{ min}^{-1}$ . (e) Concurrent increase in donor synthesis and transglycosylation:  $k_2 = 50, 100, 150 \text{ min}^{-1}$ ;  $k_4 = 5, 10, 20 \text{ min}^{-1}$ .

### Prediction of Glycosynthase Activity

As noted above, simple deletion of the catalytic nucleophile of a retaining glycosidase, particularly if the mutation is merely to alanine, does not always produce a glycosynthase. Insight into the glycosynthase potential of a retaining glycosidase might be gained by examination of the kinetic parameters for turnover of the 2-fluoro glycosyl enzyme derived from the scheme shown in Figure 5-13. This scheme is essentially the same as that for chemical rescue (Figure 5-11), but includes a binding step for the acceptor ( $K_{trans}$ ). Reactivation of the trapped covalent intermediate, which may be regarded as a model of the glycosynthase bound  $\alpha$ -glycosyl fluoride, can occur by transfer of the 2-fluoro glycosyl moiety to water or to a competing acceptor glycoside (Figure 5-13). Table 5-7 lists reactivation parameters for a number of retaining glycosidases and the results of glycosynthase conversions attempted thus far. Although this is only a partial survey, glycosidases that yield active glycosynthases appear to have 2 reactivation characteristics:



these acceptors often greatly accelerate turnover of the 2-fluoro-glycosyl enzyme intermediates. Indeed, the turnover of the Abg intermediate increases nearly 3000 fold with PNP  $\beta$ -glucoside as acceptor. As discussed above, the qualities of a good acceptor appear to stem from kinetic (or reactivity) effects, that are manifested primarily in the transition state, rather than ground state binding.

**Table 5-7:** Kinetic parameters for reactivation of 2-fluoro glycosyl enzyme intermediates.

Enzyme	inactivator	$k_{H_2O}$ ( $\text{min}^{-1}$ )	acceptor	$k_{trans}$ ( $\text{min}^{-1}$ )	$K_{trans}$ (mM)	$k_{trans}/k_{H_2O}$	Glycosynthase <sup>a</sup>	Ref.
Abg	2FDNPGlc	$1 \times 10^{-5}$	$\beta$ -glucosyl benzene	$5 \times 10^{-3}$	59	<b>500</b>	E358A ++	206
							E358S ++++	215
							E358G +++++	244
"	"	"	PNPGlu (20 mM)	$2.7 \times 10^{-2}$	-	<b>2700</b>	"	
"	2F $\beta$ -ManF	$1 \times 10^{-3}$	$\beta$ -glucosyl benzene	$6 \times 10^{-3}$	64	<b>6</b>	"	
"	2FDNPGal	$5 \times 10^{-3}$	$\beta$ -glucosyl benzene	<b>0.355</b>	69	<b>71</b>	"	
<i>E. coli</i> , lacZ $\beta$ -galactosidase	2FDNPGal	$2.7 \times 10^{-4}$ (25C)	glucose	$4.8 \times 10^{-3}$	460	<b>18</b>	E537S +	35, 216
<i>Streptomyces lividans</i> CelB	2FDNPC	$2.2 \times 10^{-3}$	cellobiose	$2.5 \times 10^{-2}$	54	<b>11</b>	E120A + E120S +	150
<i>Cellulomonas fimi</i> Man2A	2F $\beta$ -ManF	$2 \times 10^{-3}$	gentiobiose	$4 \times 10^{-2}$	78	<b>20</b>	E519A + E519S ++	138
<i>Humicola insolens</i> Cel7B	2FDNPC	$3 \times 10^{-4}$	cellobiose (20 mM)	$1.5 \times 10^{-2}$	-	<b>50</b>	E197A ++	197
Cex	2FDNPC	$8.5 \times 10^{-6}$	cellobiose (55 mM)	$1.9 \times 10^{-5}$	-	<b>2.2</b>	Ala inactive	117
Bcx	2FDNPX <sub>2</sub>	$2.1 \times 10^{-3}$	benzyl thio $\beta$ -xylobioside	$3 \times 10^{-2}$	46	<b>14</b>	Ala inactive	123
<i>Thermoanaerobacterium saccharolyticum</i> $\beta$ -xylosidase	2FDNXPyl	$1 \times 10^{-5}$	xylose (45 mM)	$5 \times 10^{-5}$	-	<b>5</b>	Ala inactive Ser inactive	217
"			xylobiose (45 mM)	$8 \times 10^{-4}$	-	<b>80</b>		
<i>Candida albicans</i> endoglucanase	2FDNPGlc	$1.9 \times 10^{-3}$	benzyl thio $\beta$ -glucoside	<b>0.024</b>	56	<b>13</b>	No data	196
<i>Fusarium oxysporum</i> endoglucanase I	2FDNPC	$1.1 \times 10^{-4}$	cellobiose (19.5 mM)	$4.8 \times 10^{-3}$	-	<b>44</b>	No data	195

a) Plus signs (+) are a qualitative measure of glycosynthase activity and not directly proportional.

## Conclusions

This study demonstrates that placement of a hydroxyl group in a glycosynthase active site near the position of the fluoride leaving group of a glycosyl fluoride donor can substantially enhance catalysis of transglycosylation. This hydroxyl group can be provided by serine (as in Abg E358S) or possibly tyrosine (as may be the case in Abg E358G). The origin of this rate

enhancement is an open question, but by analogy to solvolysis studies on glycosyl fluorides the most likely source is a hydrogen bond between fluoride and the hydroxyl group in the transglycosylation transition state. Chemical rescue studies with azide and formate indicate that  $\alpha$ -glucosyl azide and  $\alpha$ -glucosyl formate, generated *in situ*, can also act as donors for transglycosylation. A kinetic model suggests that accumulation of the  $\alpha$ -glucosyl azide or formate donor in the glycosynthase -1 subsite (generated *in situ*), as well as negligible binding of an acceptor substrate in the +1, +2 subsites, is required to produce the non-saturating kinetic plots observed. The possibility of accumulation of a non-covalent intermediate during chemical rescue is further strengthened by the apparent break in the Brønsted plot for formate rescue of Abg E358G. Likewise, poor binding of glycoside acceptors is not only observed for the Abg glycosynthase reactions, but also for the reactivation of 2-fluoro-glycosyl-enzyme intermediates. This strongly argues that the reactivity of glycoside acceptors is manifested by binding interactions in the transglycosylation transition state, not by binding in the ground state.

**Chapter 6 Development of a Mannosynthase From  
*Cellulomonas fimi*  $\beta$ -Mannosidase Man2A**

## Chemical and Enzymatic Synthesis of $\beta$ -Mannosides

The  $\beta$ -D-mannopyranoside linkage is found in a number of biological structures (see Figure 4-1), most notably in the core trisaccharide of *N*-linked glycoproteins,<sup>218</sup> as well as within the antigenic polysaccharides of yeasts,<sup>219-221</sup> *Salmonella*<sup>222</sup> and glycolipids.<sup>223,224</sup> Due to the *cis* relationship with the 2-position (see Chapter 4, Figure 4-3) this is arguably the most difficult glycosidic bond to synthesize chemically and has inspired numerous approaches (reviewed in 225,226). Some of the more popular glycosylation methods include the use of insoluble silver silicate as a catalyst with  $\alpha$ -mannosyl halides<sup>227</sup> or 2-oxo-glycosyl halides,<sup>228</sup> oxidation and reduction of the 2-position,<sup>228,229</sup> inter-<sup>230</sup> or intramolecular<sup>231</sup> displacement at C-2, intramolecular aglycone delivery<sup>232,233</sup> and the generation of  $\alpha$ -mannosyl triflate donors from mannosyl sulfoxides<sup>234</sup> (Figure 6-1). Despite these successes, each method requires a number of protection and activation steps prior to glycosylation, and few methods can achieve complete anomeric stereoselectivity.<sup>232,234</sup>

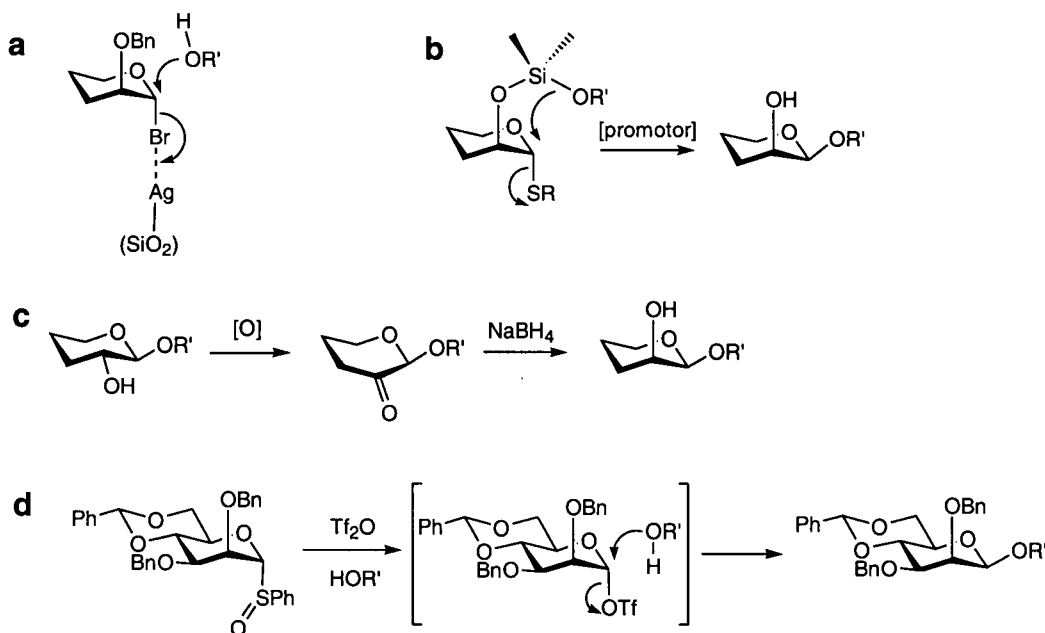


**Figure 6-1:** Examples of 'chemical'  $\beta$ -mannosylation methods: (a) insoluble silver silicate catalyst; (b) intramolecular aglycone delivery; (c) oxidation-reduction of the 2-position; (d) *in situ* generation of  $\alpha$ -mannosyl triflate from mannosyl sulphoxide.

Enzymatic synthesis of  $\beta$ -mannosides avoids the problem of anomeric stereoselectivity and often eliminates problems with regioselectivity as well.<sup>155</sup> Successful transfer of  $\beta$ -mannosyl residues to a variety of acceptor sugars has been achieved using retaining  $\beta$ -glycosidases under

kinetic conditions (see Chapter 4).<sup>193,235-238</sup> However, as discussed in Chapter 4, the yields of these transglycosylation reactions are inherently modest as the product formed is a substrate for the glycosidase used, resulting in hydrolysis. Further, this approach requires the preparation of a  $\beta$ -mannoside as a glycosyl donor, thereby minimising advantages. Substantially better yields have been obtained with recombinant yeast and *Salmonella*  $\beta$ -mannosyltransferases (60-90%),<sup>239-243</sup> but these enzymes are limited by their requirement for a complex acceptor. With the challenges of chemical and enzymatic syntheses in mind, efforts were undertaken to develop a glycosynthase approach to  $\beta$ -mannoside synthesis.

### Engineering a $\beta$ -Mannosynthase

The retaining  $\beta$ -mannosidase *Cellulomonas fimi* Man2A described in Chapter 3 was chosen as a template for a  $\beta$ -mannosynthase. As noted previously, the active site nucleophile was identified as Glu519 by labelling the enzyme with the mechanism based inactivator 2-deoxy-2-fluoro  $\beta$ -D-mannosyl fluoride.<sup>138</sup> In an initial effort by Dominik Stoll, mutation of the nucleophile to alanine (E519A) produced a poor mannosynthase, from which only an 8% yield of di- and trisaccharides was obtained upon the reaction of  $\alpha$ -D-mannosyl fluoride ( $\alpha$ -ManF) with *para*-nitrophenyl  $\beta$ -D-mannopyranoside (PNP  $\beta$ -mannoside). Based upon the success with *Agrobacterium* sp.  $\beta$ -glucosidase (Abg) in which a much more effective glycosynthase was obtained by replacing the catalytic nucleophile with serine (see Chapter 5),<sup>244</sup> Dr. Oyekanmi Nashiru made the analogous E519S mutation in Man2A and generously provided ample quantities of this mutant for analysis. Gratifyingly, Man2A E519S also proved to be a much more effective glycosynthase, affording a 99% overall yield (determined by HPLC) of oligosaccharides from the reaction of  $\alpha$ -ManF with PNP  $\beta$ -D-cellobioside (Table 6-1). A number of other sugars also acted as viable acceptors, with oligosaccharide yields typically in excess of 70% (Table 6-1). Reaction times varied from 24 hours for disaccharide acceptors to several days for the poorer monosaccharide acceptors. Unfortunately, benzyl  $\beta$ -D-glucosaminide, PNP  $\beta$ -D-glucosaminide or chitobiose would not function as acceptors, which would have afforded precursors to the core trisaccharide of *N*-linked glycoproteins. However, more active mannosynthase mutants may prove successful in mannosylating derivatives of GlcNAc. Indeed, as noted in Chapter 5, it proved possible to synthesize *N*-acetyl lactosamine in good yield from  $\alpha$ -galactosyl fluoride and benzyl  $\beta$ -GlcNAc using the more active *Agrobacterium* sp. E358S glycosynthase. Nevertheless, Table 6-1 illustrates a diverse range of

structures that are mannosylated by Man2A E519S, including maltol, which has little resemblance to a sugar. Interestingly, maltol was singly mannosylated by Man2A E519S to afford **6-7** as the primary product in modest yield (47% for the isolated per-*O*-acetylated product).

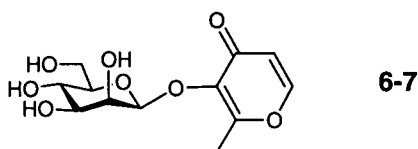


**Table 6-1:** Products synthesized with Man2A E519S using  $\alpha$ -mannosyl fluoride as donor. Product numbers are given in bold.

Acceptor	Oligosaccharide Yield (%) <sup>[a]</sup>					
	di	tri	tetra	penta	hexa	TOTAL
PNP $\beta$ -mannoside <sup>[b]</sup>	21	32	19	2	-	74
	<b>6-1a</b> $\beta(1,4)$	<b>6-1b (5)</b> $\beta(1,4)\beta(1,4)$ <b>6-1c (2)</b> $\beta(1,4)\beta(1,3)$	<b>6-1d (5)</b> all $\beta(1,4)$ <b>6-1e (1)</b> $\beta(1,4)\beta(1,4)\beta(1,3)$			
2,4-DNP 2-deoxy-2-fluoro- $\beta$ -mannoside <sup>[c]</sup>	7	39	15	8	1	70
		<b>6-2a (1)</b> $\beta(1,4)\beta(1,4)$ <b>6-2b (1)</b> $\beta(1,4)\beta(1,3)$				
PNP $\beta$ -glucoside	22	36	13	-	-	71
	<b>6-3a</b> $\beta(1,3)$	<b>6-3b (1)</b> $\beta(1,4)\beta(1,4)$ <b>6-3c (15)</b> $\beta(1,4)\beta(1,3)$	<b>6-3d</b> $\beta(1,4)\beta(1,4)\beta(1,3)$			
PNP $\beta$ -xylobioside	8	64	19	3	-	94
	<b>6-4a (1)</b> $\beta(1,4)$ <b>6-4b (1)</b> $\beta(1,3)$	<b>6-4c (1)</b> $\beta(1,4)\beta(1,4)$ <b>6-4d (2)</b> $\beta(1,4)\beta(1,3)$	<b>6-4e (1)</b> all $\beta(1,4)$ <b>6-4f (1)</b> $\beta(1,4)\beta(1,4)\beta(1,3)$			
PNP $\beta$ -cellobioside	-	27	56	5	1	99
		<b>6-5a (8)</b> $\beta(1,3)$ <b>6-5b (5)</b> $\beta(1,4)$	<b>6-5c (4)</b> $\beta(1,4)\beta(1,4)$ <b>6-5d (1)</b> $\beta(1,4)\beta(1,3)$	<b>6-5e</b> all $\beta(1,4)$		
PNP $\beta$ -gentiobioside	-	34	49	8	0.5	91
		<b>6-6a</b> $\beta(1,3)$	<b>6-6b</b> $\beta(1,4)\beta(1,3)$			
maltol	-	-	-	-	-	47 <sup>[d]</sup> <b>6-7</b>

(a) Yields determined by HPLC and based on remaining acceptor. Relative ratios of products indicated in parentheses. Sequence of linkages formed in each product is indicated. (b) PNP = *para*-nitrophenyl. (c) 2,4-DNP = 2,4-dinitrophenyl. (d) Yield of isolated, per-*O*-acetylated product.

The H-1, H-2 coupling constant of the mannosyl glycosidic bond is an unreliable indicator of anomeric configuration because the value is virtually the same in each case. This is not so for the C-1, H-1 coupling constant measured for the anomeric carbon of the mannose residue, where typically  $J = 150$  Hz is observed for alpha linkages and  $J = 160$  Hz for  $\beta$ -linkages.<sup>245</sup> Although the mannosynthase mechanism demands that a  $\beta$ -mannoside linkage is formed, the mannoside linkage formed was confirmed to be  $\beta$  by the 160 Hz  $J(C-1, H-1)$  coupling constant measured for C-1 of the mannose residue in the disaccharide products **6-1a** and **6-3a**. NMR analyses of the per-*O*-acetylated products also indicated that a mixture of  $\beta(1,3)$  and  $\beta(1,4)$  linkages was synthesized by Man2A E519S (Table 6-1). A notable example was the mixture derived from PNP  $\beta$ -gentiobioside, which afforded branched tri- and tetrasaccharide products **6-6a** and **6-6b** in which a mannose residue is  $\beta(1,3)$  linked to the PNP bearing glucose residue (Figure 6-2). Branched oligosaccharide products synthesized by glycosynthases have been reported previously (see Chapter 4).<sup>199,201</sup>

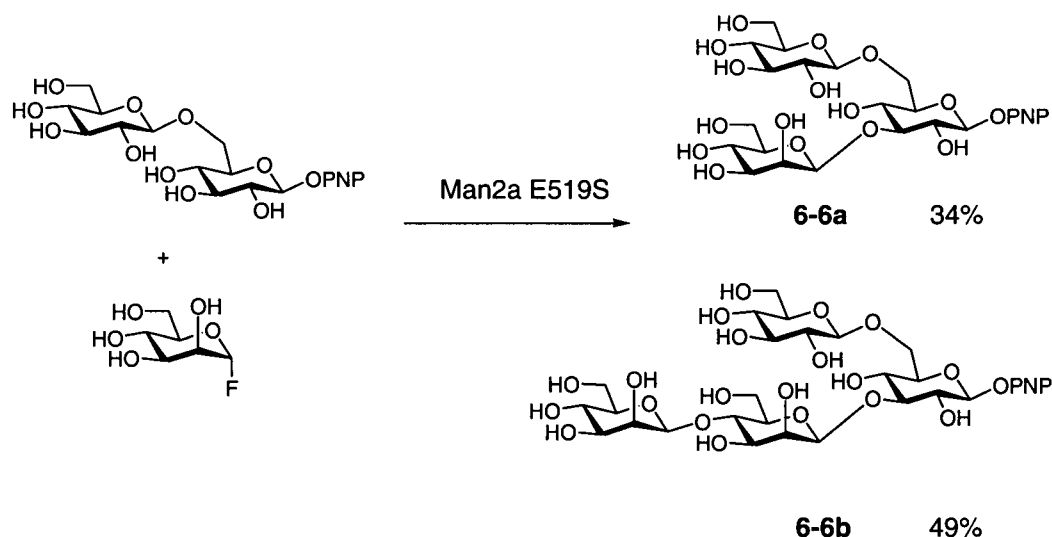


**Figure 6-2:** Synthesis of branched oligosaccharide products with Man2A E519S from PNP  $\beta$ -gentiobioside and  $\alpha$ -mannosyl fluoride.

### Transglycosylation Kinetics with Man2A E519A and E519S

Kinetic parameters for transglycosylation by the Man2A E519A and E519S mutants were determined by use of a fluoride electrode to monitor fluoride release during the coupling of  $\alpha$ -ManF with PNP  $\beta$ -cellobioside (Table 6-2). In the presence of a fixed concentration of PNPC (20-30 mM), typical saturation kinetics were observed for  $\alpha$ -ManF with both mutants.

Interestingly, saturation could not be achieved with PNPC (up to 35 mM PNPC) in the presence of a saturating concentration of  $\alpha$ -ManF (50 mM), despite this being the best acceptor for the mannosynthase. As noted in Chapter 5, good binding is not a prerequisite for a good acceptor. Indeed, acceptor  $K_M$  values of 45 and 70 mM were measured for PNP  $\beta$ -glucoside and PNP  $\beta$ -cellobioside, respectively, as acceptors for Abg E358S (Chapter 5). Likewise,  $K_d$  values measured for acceptors of trapped 2-fluoro-glycosyl enzyme intermediates are typically greater than 50 mM (Chapter 5).

**Table 6-2:** Apparent transglycosylation kinetic parameters for Man2A E519S and E519A.

	$\alpha$ -ManF		PNP $\beta$ -cellobioside	
	$k_{cat}$ ( $\text{min}^{-1}$ )	$K_M$ (mM)	$k_{cat}/K_M$ ( $\text{min}^{-1} \text{mM}^{-1}$ )	$k_{cat}/K_M$ ( $\text{min}^{-1} \text{mM}^{-1}$ ) <sup>c</sup>
<b>E519A</b>	0.334 $\pm 0.005^a$	0.57 $\pm 0.02$	0.58	0.0133 $\pm 0.0005^d$
<b>E519S</b>	11.8 $\pm 0.2^b$	0.70 $\pm 0.03$	17	0.353 $\pm 0.008^e$

a) [PNPC] fixed at 20 mM. b) [PNPC] = 30 mM. c) No saturation with PNPC observed. d) [ $\alpha$ -ManF] = 24 mM. e) [ $\alpha$ -ManF] = 52 mM.

The apparent  $k_{cat}/K_M$  values of  $0.35 \text{ min}^{-1} \cdot \text{mM}^{-1}$  and  $0.013 \text{ min}^{-1} \cdot \text{mM}^{-1}$  for Man2A E519S and E519A, respectively, were determined from the slope of the plot of rate versus PNPC concentration. This corresponds to a 27 fold transglycosylation rate enhancement for E519S relative to the E519A mutant and is remarkably similar to the 24 fold increase observed for Abg E358S (using  $\alpha$ -galactosyl fluoride as a donor). As in the case of Abg E358S, this enhancement may arise from a hydrogen bond between the serine hydroxyl and the departing fluoride in the transglycosylation transition state. Transglycosylation rates were also studied as a function of pH. Man2A E519S was found to be most active between pH 5 and 6 (Figure 6-3), which is remarkably fortunate because  $\alpha$ -ManF undergoes rapid spontaneous hydrolysis above pH 7, presumably through the base catalyzed formation of a 1,2 epoxide.<sup>246</sup> The increased activity of this mutant at low pH is also somewhat contradictory because decreasing the pH might be expected to protonate the acid-base catalyst, E429, and consequently inhibit the capacity of this residue to function as a base catalyst in the transglycosylation reaction.

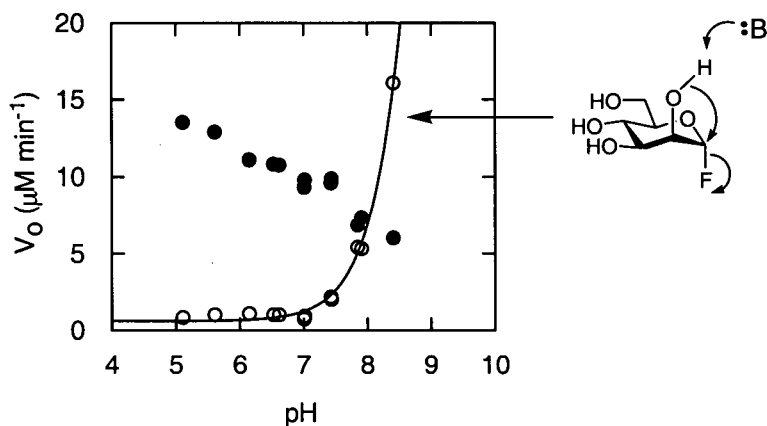


**Figure 6-3:** Reaction of Man2A E519S (5.5  $\mu\text{M}$ ) with  $\alpha\text{-ManF}$  (5.8 mM) and PNPC (5 mM) as a function of pH (filled circles).  $V_o$  refers to the rate of fluoride release. Spontaneous hydrolysis rates of  $\alpha\text{-ManF}$  are indicated by open circles. The curve is included for clarity. Mechanism of base catalyzed hydrolysis of  $\alpha\text{-ManF}$  is indicated.

### Azide rescue of Man2A E519A and E519S

As observed for Abg nucleophile mutants, substantial glycosidic bond cleaving activity could be restored to Man2A nucleophile mutants in the presence of azide (Table 6-3). Even with the reactive substrate 2,4-dinitrophenyl  $\beta$ -mannoside, virtually no activity could be detected with Man2A E519A or E519S in the absence of azide. The addition of azide (1 M, pH 6, 25°C), however, increased  $k_{cat}$  values 17 000 to 22 000 fold. This is likely a minimum value for the increase, given that trace wild type activity, as well as contamination by halides (described in Chapter 8), can mask the true activity of the mutant.

A notable difference is the significantly lower azide rescue activity of the E519S mutant relative to that of E519A. Although a hydrogen bond between azide and the serine hydroxyl is a possibility, steric effects between azide, which is approximately 2.5 Å in length, and the serine side chain are most likely greater than for alanine. Contrasting behaviour is also observed for the rate dependencies of azide rescue at high substrate concentrations (Figure 6-4). This difference appears to correlate with the corresponding glycosynthase activities of the two mutants. With E519S a linear, non-saturating increase in rate is observed with increasing substrate concentration (above 1 mM), consistent with a transglycosylation reaction utilizing  $\alpha$ -mannosyl azide as a donor that is faster than release (or hydrolysis) of the donor itself (Figure 6-4a). The E519A mutant seemingly reverts to wild type behaviour (see Chapter 3) and exhibits weak substrate inhibition at high concentrations of substrate (Figure 6-4b). This is consistent with the weak glycosynthase activity of E519A, which is further challenged by the relatively

unreactive donor,  $\alpha$ -mannosyl azide (i.e. release of  $\alpha$ -mannosyl azide is faster than transglycosylation).

**Table 6-3:** Kinetic parameters for the reaction of Man2A nucleophile mutants with 2,4-dinitrophenyl  $\beta$ -mannoside and azide (pH 6, 25°C)

	$k_{cat}$ ( $\text{min}^{-1}$ )	$K_M$ (mM)	$k_{cat}/K_M$ ( $\text{min}^{-1} \cdot \text{mM}^{-1}$ )	Behaviour at high [S]
<b>Man2A wt</b>	27 000 $\pm$ 4000	0.6 $\pm$ 0.1	45 000	sub. inhib. $K_i = 0.31$ $\pm$ 0.06 mM
<b>Man2A E519A</b> + 1 M azide	< 0.008 174 $\pm$ 3	- 0.193 $\pm$ 0.009	- 901	- sub. inhib. $K_i = 42$ $\pm$ 4 mM
<b>Man2A E519S</b> + 1 M azide	0.0015 25.2 $\pm$ 0.2	- 0.044 $\pm$ 0.002	- 573	- trans.

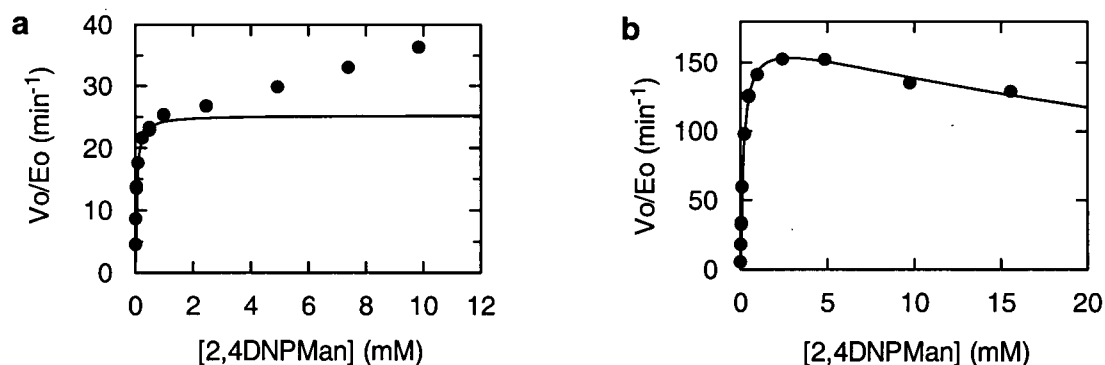


**Figure 6-4:** Reaction rate versus 2,4-dinitrophenyl  $\beta$ -mannoside (2,4DNPMan) concentration for the reaction with Man2A E519S (a) and E519A (b) in the presence of 1 M azide (pH 6, 25°C). The curves in (a) and (b) are fits of the data to the Michaelis Menten and substrate inhibition equations, respectively.

The pH dependence of azide rescue with Man2A E519S was also examined (Figure 6-5). A marked increase in rate is observed at low pH values, which continued beyond the range of stability of the mutant. The conspicuous similarity of this dependence to that observed for azide rescue with Abg E358G (see Figure 5-3) suggests that a similar residue is being titrated in both cases. For the same reasons discussed in Chapter 5, the most likely candidate is the acid-base catalyst, E429.

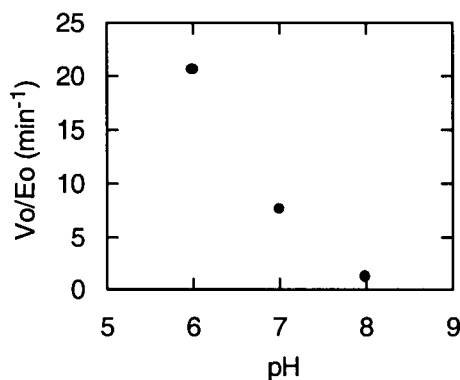


**Figure 6-5:** pH dependence of the reaction of 2,4-dinitrophenyl  $\beta$ -mannoside (1 mM) with Man2A E519S and azide (2 M, 25°C).

### Conclusions

This study extends the glycosynthase methodology to the synthesis of  $\beta$ -mannosides, one of the most difficult glycosidic bonds to synthesize by standard chemical methods. This was made possible by improving the transglycosylation rates of a poor glycosynthase (Man2A E519A) with the introduction of a serine side chain in the active site (Man2A E519S). As was observed with Abg glycosynthases (particularly with  $\alpha$ -galactosyl fluoride donors), the serine mutation enhanced  $k_{cat}/K_M$  values for transglycosylation  $\sim 25$  fold over the alanine mutant. Achieving this result in a completely different enzyme system strengthens the hypothesis that a hydroxyl group positioned near a fluoride leaving group will accelerate the reaction catalysed. Azide rescue of Man2A E519A and E519S produced completely different reaction velocity behaviours at high substrate concentrations, which can be explained by  $\alpha$ -mannosyl azide acting as a glycosyl donor and the very different glycosynthase activities of these mutants. This strengthens the view that chemical rescue is an essential part of the characterization of glycosynthase reactivity.

**Chapter 7 Development of a 'Cellulosynthase' from  
*Streptomyces lividans* endoglucanase CelB**

## Introduction

The degradation of cellulose into cellooligosaccharides by bacterial and fungal microbes is achieved by the secretion of cellulases into the extracellular medium. Cellulases may cleave the  $\beta$ -(1,4) glycosidic bonds of cellulose with either retention or inversion of anomeric configuration. The lab of Professor Claude Dupont (Centre de recherche en microbiologie appliquée, Université du Québec) has cloned the gene for the bacterial cellulase, *Streptomyces lividans* CelB, a 36 kDa endoglucanase that has been assigned on the basis of sequence to Family 12 (formerly known as family H).<sup>247</sup> Typical of many cellulases, the tertiary structure of CelB consists of an *N*-terminal signal peptide and a catalytic domain connected to a *C*-terminal cellulose binding domain by a flexible linker.<sup>26</sup> The structure of the catalytic domain was recently solved to 1.75 Å resolution,<sup>248</sup> revealing a jelly-roll fold that is remarkably similar to that found in the Family 11 xylanases, thereby confirming the prediction from hydrophobic cluster analysis that these two glycosidase families comprise a structurally related 'clan' (GH-C).<sup>249</sup>

Although the stereochemical course of substrate hydrolysis has not been determined for CelB, another member of family 12, *Humicola insolens* endoglucanase III, is known to hydrolyze cellooligosaccharides with retention of anomeric configuration. Therefore, the catalytic nucleophile of CelB may be identified by trapping the covalent intermediate with a 2-fluoro sugar inactivator, proteolysis of the labelled enzyme and analysis by ESI-MS/MS. This labelling strategy was used to identify the nucleophile in the family 11 *Bacillus circulans* xylanase (Bcx) as Glu 78<sup>123</sup> allowing the sole other Glu residue in this enzyme (Glu 172) to be assigned as the acid-base catalyst. Because Bcx and CelB belong to the same structurally related clan (GH-C), a direct comparison of the Bcx structure<sup>124</sup> with the structure of CelB permitted the preliminary assignment of Glu 120 and Glu 203 as the nucleophile and acid-base catalysts, respectively.<sup>248</sup> The structure also revealed that the carboxyl moieties of these residues are located 7 Å apart on opposite sides of a long, active site cleft which can accommodate five glucopyranoside moieties (-3 to +2). The first part of this chapter describes the steady state kinetic behaviour of CelB (provided by Professor Dupont) with 2,4-dinitrophenyl  $\beta$ -cellobioside (DNPC), as well as trapping of the covalent intermediate with the corresponding inactivator, 2,4-dinitrophenyl 2-deoxy-2-fluoro- $\beta$ -cellobioside (2FDNPC). The nucleophile was verified to be E120.

Once the catalytic nucleophile of CelB is known with certainty, this residue may be mutated accordingly to produce a potential glycosynthase. Because CelB is an *endo* glycosidase, the efficient transfer of oligosaccharide blocks may be possible with the corresponding glycosynthase, as has been possible with other *endo* enzymes (see Chapter 4). The second component of this chapter examines the glycosynthase activity of CelB E120A, E120S, and E120G mutants, prepared by Professor Dupont's lab.

### Steady-State and Inactivation Kinetics of CelB

CelB readily hydrolyzed DNPC to produce a biphasic velocity profile (Figure 7-1) that is characteristic of substrate inhibition, as was previously described for *Cellulomonas fimi* Man2A (see Chapter 3). A direct fit of this plot with the substrate inhibition equation 3-1 gave kinetic parameters of  $k_{cat} = 40 \pm 1 \text{ s}^{-1}$ ,  $K_M = 0.35 \pm 0.03 \text{ mM}$ , and  $K_i = 24 \pm 4 \text{ mM}$ . The long, open binding cleft observed by X-ray crystallography suggested that CelB could accommodate five to six glucopyranosyl units (-3 to +2 or +3), therefore the simultaneous binding of two molecules of DNPC to form an unproductive ternary complex is certainly possible. It is noteworthy that the structure of CelB includes a surface loop (see Figure 7-8) that closes over the active site cleft upon substrate binding, and that a reduction in the distance separating the putative nucleophile and acid-base residues (7 Å) to the typical retaining glycosidase span of 5.5 Å appears to be necessary for catalysis.<sup>29,248</sup> Such conformational adjustments may inadvertently stabilize a non-productive ternary complex.

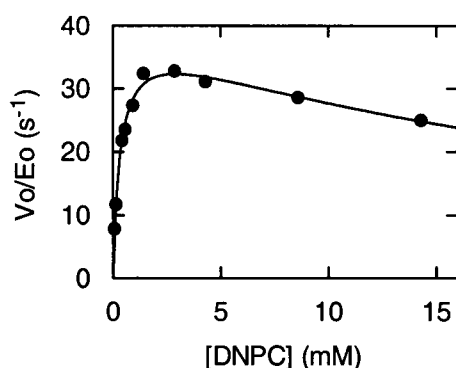


**Figure 7-1:** Plot of reaction velocity vs substrate concentration for the reaction of DNPC with *Streptomyces lividans* CelB. The curve is a fit of the data to the substrate inhibition equation.

Substrate inhibition is also observed with the mechanism based inactivator 2FDNPC. The initial time dependence of inactivation of CelB through the accumulation of a covalent 2-

fluoro cellobiosyl-enzyme intermediate followed first order kinetics (Figure 7-2a). Complete inactivation of the enzyme was not possible (~90% inactivation, Figure 7-2a), suggesting relatively fast turnover of the covalent intermediate. The corresponding dependence of  $k_{obs(inact)}$  on [2FDNPC] (Figure 7-2b) parallels the velocity curve observed for the hydrolysis of DNPC. Fitting this curve directly with an equation analogous to 3-1 gave inactivation parameters of  $k_{inact} = 0.29 \pm 0.02 \text{ min}^{-1}$ ,  $K_{inact} = 0.72 \pm 0.08 \text{ mM}$ , and  $K_i = 8 \pm 1 \text{ mM}$ . This inactivation is active site specific, as shown by the reduction in  $k_{obs(inact)}$  with 2.84 mM 2FDNPC from  $0.18 \pm 0.02 \text{ min}^{-1}$  to  $0.048 \pm 0.007 \text{ min}^{-1}$  in the presence of 47.4 mM cellobiose (Figure 7-3), a competitive inhibitor of CelB (approximate  $K_i = 5 \text{ mM}$ ). The ratio of these rate constants (0.27) is in reasonable agreement with the predicted protection ratio (0.34, see Experimental). The catalytic competence of the trapped 2-fluorocellobiosyl-enzyme intermediate is demonstrated by the spontaneous reactivation observed when the trapped enzyme is freed of excess inactivator ( $k_{H2O} = 0.0022 \text{ min}^{-1}$ ,  $t_{1/2} = 314 \text{ min}$ ). Furthermore, reactivation is accelerated in a saturable fashion (Figure 7-4) through a transglycosylation mechanism (see Chapter 5, Figure 5-13) when cellobiose is added as an acceptor ligand, yielding the kinetic parameters  $k_{react} = 0.025 \pm 0.003 \text{ min}^{-1}$  and  $K_{react} = 68 \pm 17 \text{ mM}$ .

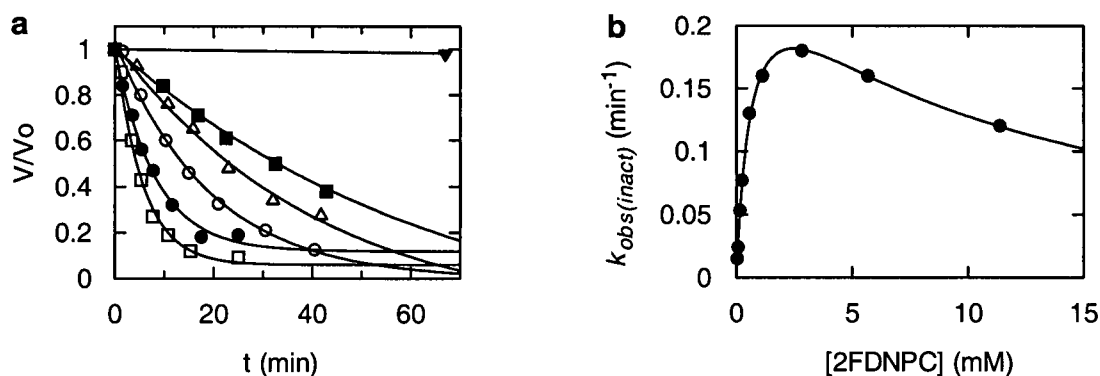


**Figure 7-2:** Inactivation of CelB by 2FDNPC. (a) Representative data for the loss of activity ( $V/V_0$ ) over time in the presence of various concentrations of 2FDNPC:  $\square$ , 2.84 mM;  $\bullet$ , 11.38 mM;  $\circ$ , 0.17 mM;  $\Delta$ , 0.087 mM;  $\blacksquare$ , 0.057 mM. (b) Plot of  $k_{obs(inact)}$  vs [2FDNPC]. The curve is a fit of the data to the substrate inhibition equation ( $k_{inact} = 0.29 \pm 0.02 \text{ min}^{-1}$ ,  $K_{inact} = 0.72 \pm 0.08 \text{ mM}$ ,  $K_i = 8 \pm 1 \text{ mM}$ ).

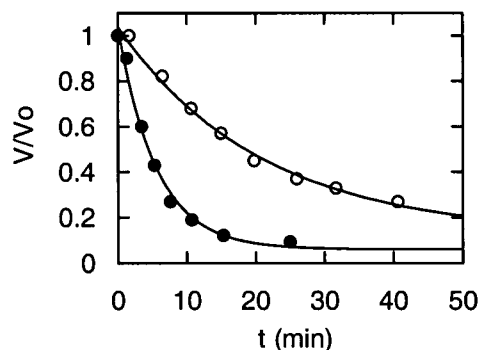


**Figure 7-3:** Protection against inactivation with cellobiose. Inactivation of CelB in the presence of 2.84 mM 2FDNPC (●) or 2.84 mM 2FDNPC with 47 mM cellobiose (○).

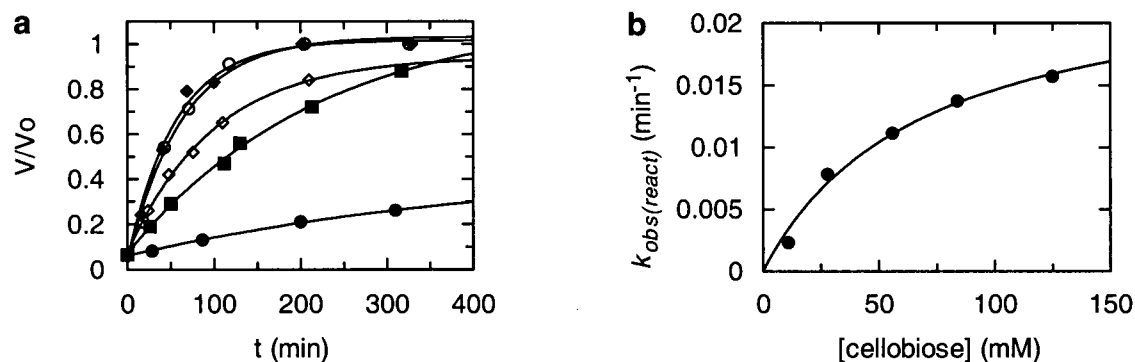


**Figure 7-4:** Turnover of the 2-deoxy-2-fluorocellobiosyl CelB intermediate via hydrolysis or transglycosylation. (a) Reactivation of CelB over time in the presence of various concentrations of cellobiose: ●, 0 mM; ■, 11 mM; ◇, 28 mM; ○, 84 mM; ◆, 125 mM. (b) Plot of  $k_{obs(react)}$  vs [cellobiose]. The curve corresponds to  $k_{react} = 0.025 \pm 0.003 \text{ min}^{-1}$  and  $K_{react} = 68 \pm 17 \text{ mM}$ .

A comparison of the inactivation and reactivation kinetics with the steady state kinetics of DNPC can provide an estimate of the kinetic consequences of the 2-fluorine substitution. The deglycosylation rate, reflected by  $k_{cat}$  and  $k_{H_2O}$ , is reduced  $1.1 \times 10^6$  fold, a value that is comparable to those observed for *Agrobacterium* sp.  $\beta$ -glucosidase,<sup>34</sup> *E. coli*, *lac Z*  $\beta$ -galactosidase,<sup>216</sup> *Fusarium oxysporum* endoglucanase I,<sup>195</sup> and *Clostridium thermocellum* endoglucanase CelC.<sup>250</sup> The glycosylation rate, reflected by  $k_{cat}/K_M$  and  $k_{inact}/K_{inact}$ , is reduced to a lesser degree,  $1.7 \times 10^4$  fold. This difference may reflect the finding that the deglycosylation transition state typically has greater oxocarbenium ion character than the glycosylation step and thus is more seriously affected by the fluorine substitution.<sup>33,251</sup> In contrast to these large

transition state effects, the similarity of  $K_{inact}$  and  $K_i$  to the corresponding  $K_M$  and  $K_i$  values for DNPC suggests that the 2-fluorine substitution has a minimal impact on substrate binding.

### Identification of the Catalytic Nucleophile of CelB

The ESI mass spectrum of intact CelB (data not shown) provided a mass of 24 567 Da for the catalytic domain, which is identical to the average  $[M + H]^+$  mass predicted for the sequence. The corresponding ESI mass spectrum of labeled CelB (data not shown) indicated that 50% of the enzyme had increased in mass by 326 Da  $\pm$  6 Da, consistent with incorporation of a single 2-fluorocellobiosyl moiety (327 Da). However, according to an assay of activity with DNPC prior to ESI-MS, the labeled enzyme was estimated to be >90% inactivated. The origin of the discrepancy between the ESI-MS analysis and the activity assay is not clear, but it is most likely due to loss of label on the HPLC column prior to MS analysis. Nevertheless, this degree of labeling was sufficient to identify the nucleophile as described below.

The labeled CelB was markedly resistant to digestion with pepsin relative to the unlabeled enzyme as judged by HPLC profiles of the digests over time. This resistance to proteolysis has been observed with other trapped glycosidases and is attributed to a stabilization of the glycosidase structure upon formation of the covalent intermediate.<sup>215</sup> Fortunately, it was possible to denature the labeled CelB (by boiling) prior to proteolysis without significant loss of the label. Figure 7-5a shows the peptic digest of the labeled enzyme resolved by reverse phase HPLC using ESI-MS as a detector. Labeled peptide(s) were detected in a second HPLC run with the spectrometer operating in neutral loss mode. This involved scanning the HPLC eluent with the first and third quadrupoles (Q1 and Q3), while subjecting the gas phase peptide ions to mild fragmentation with a neutral gas in the collision cell (Q2). The  $\alpha$ -acylal bond of the label is significantly more labile than any other bond in the peptide and readily cleaves in a homolytic fashion, leaving the peptide with its original charge, but with a decreased mass. With Q3 offset from Q1 by the mass of the label that is lost in the collision cell, peptides originally bearing this label can be detected. As shown in Figure 7-5b, scanning for the loss of the 2-fluorocellobiosyl label (327 Da) from a singly charged peptide produced a fragment of mass  $m/z$  947.5 Da that was not present in the unlabeled digest (Figure 7-5c). Subtraction of the mass of the label ( $947.5 - 327 + 1 H^+$ ) yields an unlabeled peptide of  $m/z$  621.5. A computer aided search<sup>252</sup> of the CelB sequence for a peptide with an average mass of  $621.5 \pm 1$  Da produced only eight sequences, including QTEIM, which corresponds to the region of the putative nucleophile Glu 120.

Examination of the total ion chromatogram for the unlabeled digest confirmed the presence of a peptide of  $m/z$  621.5 with a retention time essentially identical to that of the labeled peptide.

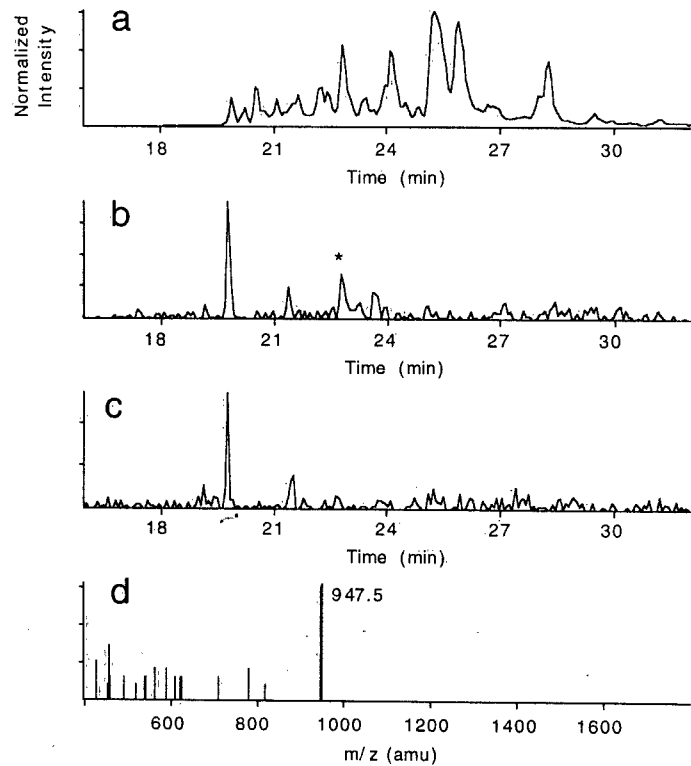


**Figure 7-5:** Detection of the 2-deoxy-2-fluorocellobiosyl labeled peptide by ESI-MS/MS. (a) Total ion chromatogram (TIC) for the peptic digest of CelB labeled with 2FDNPC. (b) TIC for the labeled CelB digest, with ESI-MS/MS operating in neutral loss mode. Only those peptides that lose a neutral fragment of  $m/z = 327$  (the mass of the label) are detected. The labeled peptide of interest is indicated with an asterisk (\*). (c) TIC for the peptic digest of the unlabeled enzyme in neutral loss mode. (d) Mass spectrum for the labeled peptide (\*) eluted at 23 min. in (b).

The sequence QTEIM was confirmed by ESI-MS-MS analysis of the labeled peptide isolated by HPLC. Q1 was set to  $m/z$  947.5 to selectively introduce the peptide to the collision chamber (Q2), with the resulting daughter ion spectrum detected by Q3. As shown in Figure 7-6, the spectrum contains a series of 'b' ions (*N*-terminal fragments produced by cleavage between CO-NH bonds) corresponding to the fragments QT ( $m/z$  229.5), QTE ( $m/z$  358.5), QTEI ( $m/z$  472.5), and QTEIM ( $m/z$  603.5). A series of 'y' ions (*C*-terminal fragments produced by cleavage between CO-NH bonds) are also observed, corresponding to M ( $m/z$  149), IM ( $m/z$  262), and EIM ( $m/z$  392.5) fragments. Unequivocal evidence for the position of the label at E120 is provided by fragmentation of the label itself (Figure 7-6). Cleavage of the internal

glycosidic bond to release the terminal glucosyl moiety gives rise to a series of 'b' ions bearing a 2-fluoro glucopyranosyl residue (164 Da) corresponding to QTE ( $m/z$  523.5), QTEI ( $m/z$  636.5), and QTEIM ( $m/z$  767.5). Full 2-fluoro-cellobiosyl labeled 'b' ions are also observed: QTE ( $m/z$  685), QTEI ( $m/z$  798.5), and QTEIM ( $m/z$  930). However, a labeled 'b' or 'y' ion corresponding to QT is not observed, thereby eliminating the unlikely possibility of threonine acting as the nucleophile.

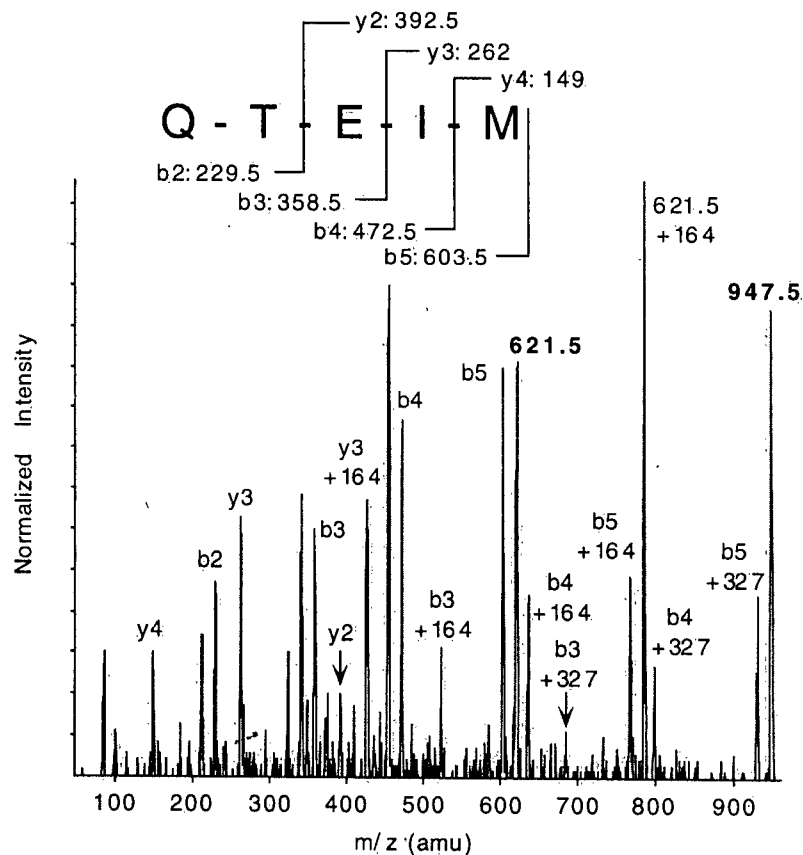


**Figure 7-6:** Daughter ion mass spectrum for the 2-deoxy-2-fluorocellobiosyl labeled peptide ( $m/z$  947.5) produced by ESI-MS/MS. The 'b' and 'y' ions corresponding to the sequence QTEIM are indicated, as well as the corresponding 2-fluoroglucopyranosyl (164 Da) and 2-fluorocellobiosyl (327 Da) labeled forms.

### Structural Features of Family 12 Glycosidases

Having firmly established the identity of the catalytic nucleophile of CelB as E120, the amino acid sequence of CelB was compared to those of other Family 12 glycosidases. As expected, the sequence surrounding the nucleophile of Family 12 enzymes (E(I/L)M(I/V)W) is highly conserved, consistent with the critical role of the nucleophile in catalysis (Figure 7-7). The

sequence surrounding the putative acid-base catalyst, E203, is considerably less conserved. This implies that the structure of the acid-base region is subject to a reduced evolutionary pressure, which may reflect the lesser contribution of the acid-base residue to catalysis relative to that of the nucleophile, as observed in other retaining glycosidases.<sup>59</sup> This is also consistent with the greater tolerance for changes in the position of the acid-base catalyst, as shown for the Family 11 Bcx.<sup>63</sup>

		↓			↓
<i>S. lividans</i> CelB	118	Q <b>TE</b> IMIWFNRVGP <b>IQPIG</b>	135	194	YLTSVQAG <b>FEP</b> WQNG 208
<i>S. rochei</i> A2	155	R <b>TE</b> IMIWFNRVQ <b>IQPIG</b>	172	231	YLTSIQAG <b>FEP</b> WQNG 245
<i>S. halstedii</i>	155	R <b>TE</b> IMIWLNKVGP <b>IQPIG</b>	172	231	YLTSVQAG <b>FEP</b> WQNG 245
<i>M. tuberculosis</i>	48	QQ <b>E</b> IMIWFNHQGS <b>IQPVG</b>	65	124	YLTSIRAG <b>LEP</b> WSDG 138
<i>R. marinus</i>	157	GA <b>EL</b> MIWLNWNGGV <b>MPGG</b>	174	233	YLHAVET <b>GFEL</b> WEGG 247
<i>A. aculeatus</i>	132	DY <b>EL</b> MIWLARYGGV <b>QPIG</b>	149	209	YLITLQ <b>FGTE</b> PFTGG 223
<i>T. reesei</i> EGIII	130	DY <b>EL</b> MIWLGKYGD <b>IGPIG</b>	147	207	YVLSYQ <b>FGTE</b> PFTGS 221
<i>A. awamorii</i>	130	DY <b>EL</b> MIWLARYGSV <b>QPIG</b>	147	211	HLITLQ <b>CGTE</b> PFTGG 225
<i>A. oryzae</i>	130	DY <b>EL</b> MIWLARYGT <b>IQPIG</b>	147	211	YLINMQ <b>FGTE</b> PFTGG 225
<i>E. carotovora</i> CelS	156	T <b>DEL</b> MIWLNNTNAG- <b>PAG</b>	172	237	YISSVE <b>FGTE</b> IF-GG 250
<i>E. carotovora</i> CelB	156	T <b>DEL</b> MIWLNNTNAG- <b>PAG</b>	172	237	YISSVEL <b>GT</b> EIF-GG 250
<i>T. neapolitana</i> endoA	132	D <b>VE</b> IMVWFYFN <b>ELT-PGG</b>	148	222	YFTV <b>WEIGTE</b> -FGSP 235
<i>T. neapolitana</i> endoB	150	D <b>VE</b> IMVWFYNN <b>ILM-PGG</b>	166	241	YFCV <b>WEIGTE</b> -FGDP 254
<i>T. maritima</i> CelA	132	D <b>VE</b> IMVWFYFN <b>VLTPGG</b>	148	222	YFTV <b>WEIGTE</b> -FGSP 235
<i>T. maritima</i> CelB	150	DA <b>E</b> IMVWFYNN <b>VLM-PGG</b>	166	241	YFCV <b>WEIGTE</b> -FGDP 254

**Figure 7-7:** Alignment of the sequence regions containing the labeled nucleophile and the putative general acid-base catalyst of CelB with other Family 12 endoglucanases. Accession numbers from the National Center for Biotechnology Information (NCBI) are indicated in brackets. The sequences shown are: *S. lividans* CelB (2462718); *Streptomyces rochei* (strain A2) endoglucanase (1076114); *Streptomyces halstedii* endoglucanase (2209260); *Mycobacterium tuberculosis* 'hypothetical' endoglucanase (2896727); *Rhodothermus marinus* endoglucanase (2304961); *Aspergillus aculeatus* endoglucanase I (FI-CMCASE) (121835); *Hypocrea jecorina* (*Trichoderma reesei*) endoglucanase III (2116583); *Aspergillus awamori* (var. *kawachi*) endoglucanase A (CMCASE-I) (2494338); *Aspergillus oryzae* endoglucanase (2467373); *Erwinia carotovora* endoglucanase S (121830); *Erwinia carotovora* endoglucanase B (2570837); *Thermotoga neapolitana* endoglucanase A (1934673); *Thermotoga neapolitana* endoglucanase B (1934674); *Thermotoga maritima* endoglucanase A (1297061); *Thermotoga maritima* endoglucanase B (1297062). The sequence numbering includes the signal peptide sequences, with the exception of CelB, which begins at D41 of the NCBI entry. Absolutely conserved residues are shown in bold. The proposed nucleophiles and acid-base catalysts are indicated by arrows (↓ and ↓, respectively).

Shortly following publication of these results<sup>150</sup> the 3-dimensional structure of CelB trapped as a 2-fluoro-cellootriosyl intermediate was solved by X-ray crystallography.<sup>83</sup> Electron density corresponding to the E120-labeled intermediate as well as the hydrolyzed 2-fluoro cellootriose product was observed. This is consistent with the relatively fast turnover of 2FDNPC described above, which would certainly be significant on the timescale of X-ray crystallography. When compared to the structure of the free enzyme<sup>248</sup> a loop that was previously disordered was

observed to be well-defined in the labeled enzyme (Figure 7-8). This loop carries Asn 155 and Asn 158, two residues that are in close contact with the fluorine at the 2-position and the nucleophile E120, respectively. The movement of this loop also reduced the distance separating E120 and the acid-base catalyst E203 to 5.8 Å, a value more typical of a retaining glycosidase. Moreover, E203 is also positioned to interact with the 6-hydroxyl of the -1 sugar, suggesting that substrate binding may help set the pKa of this residue. This structure also predicts that the portion of the substrate binding to the aglycone subsites would need to be distorted slightly to avoid steric clashes with the enzyme, particularly M122. Distortion of the aglycone appears to be consistent with the high dissociation constant observed for cellobiose (68 mM) as an acceptor of the 2-fluorocellobiosyl enzyme.

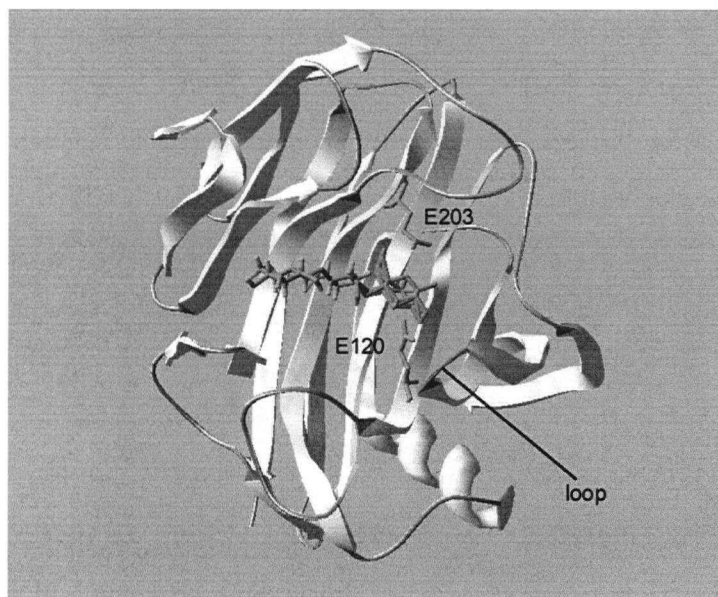


**Figure 7-8:** Structure of 2-fluorocellobiosyl labeled CelB<sup>83</sup>. The nucleophile (E120), acid-base catalyst (E203) and the loop that becomes ordered in the complex are indicated.

### Glycosynthase Activity of CelB Nucleophile Mutants

Relatively high reactivation parameter values are obtained for the turnover of the 2-fluorocellobiosyl intermediate of CelB ( $k_{react} = 0.025 \text{ min}^{-1}$ ,  $k_{react}/k_{H_2O} = 11$ ). As discussed in Chapter 5, the potential for glycosyl transfer to acceptors reflected by these parameters suggest that CelB is a good candidate for a glycosynthase. Three nucleophile mutants of CelB (E120A, E120S, and E120G) were prepared by the lab of Professor Claude Dupont (Centre de Recherche

en Microbiologie Appliquée, Institut Armand-Frappier, Université du Québec) for testing as glycosynthases.

Reactions with these mutants using  $\alpha$ -cellobiosyl fluoride as a donor and PNP  $\beta$ -cellobioside as an acceptor (pH 7, RT) proceeded slowly and failed to consume more than 50% of the acceptor (as judged by TLC). However, a significant amount of white precipitate formed over time. With  $\alpha$ -lactosyl fluoride as the donor, only one tetrasaccharide product was observed, consistent with a single glycosyl transfer, but once again this reaction proceeded slowly and failed to go to completion (< 50%). Variation of pH (5-9) had no noticeable effect on reaction rate or conversion (as judged by TLC). Moreover, reaction solutions turned yellow, suggesting that some wild type contaminant was present. This was confirmed by the low activity observed with these mutants on the substrate DNPC, which could be reduced substantially by treatment of the enzyme with the inactivator 2FDNPC. This is not surprising considering that these mutants were over-expressed in *Streptomyces lividans*, which naturally produces the wild type enzyme.

Interestingly, reaction of these mutants with only  $\alpha$ -cellobiosyl fluoride proved to be more successful. Using CelB E120S (0.7 mg/mL), 49 mg of  $\alpha$ -cellobiosyl fluoride was converted to 40.5 mg of a water insoluble, white precipitate in less than 18 hrs. (pH 7.9, RT). This corresponds to an oligosaccharide yield of 85%. Acetylation of this product by the Miles' method<sup>253</sup> produced a new polymeric product that was soluble in chloroform. The <sup>1</sup>H NMR spectrum of the per-*O*-acetylated product was consistent with cellulose tri-*O*-acetate<sup>189</sup> and the <sup>13</sup>C NMR spectrum matched data previously reported for cellopentaose per-*O*-acetate as well as cellulose tri-*O*-acetate.<sup>254</sup> Moreover, the ESI mass spectrum revealed a significant ion peak ( $m/z = 2349 [M - CH_3CO + H]^+$ ) corresponding to a per-*O*-acetylated octasaccharide product (M.W. = 2408 Da). Because this peak was observed at the detection limit of the ESI instrument ( $m/z = 2400$ ), it is quite possible that CelB E120S is capable of more than 4 sequential transfers of a cellobiosyl unit. Thus CelB E120S functions as an effective cellosynthase (Figure 7-9), despite trace amounts of wild type enzyme in the mutant preparation. The failure of PNP  $\beta$ -cellobioside or PNP  $\beta$ -glucoside to act as effective acceptors is surprising, but most likely results from the acceptors competing with the  $\alpha$ -glycosyl fluoride donor for glycone binding subsites (-1, -2). It is also noteworthy that the acceptor screen developed by Jan Blanchard indicated that methyl  $\alpha$ -cellobioside, a structural analogue of  $\alpha$ -cellobiosyl fluoride, was the best acceptor for 2-fluorocellobiosyl labeled CelB.<sup>204</sup> This agrees with the high yield observed for the polymerization of  $\alpha$ -cellobiosyl fluoride by CelB E120S.

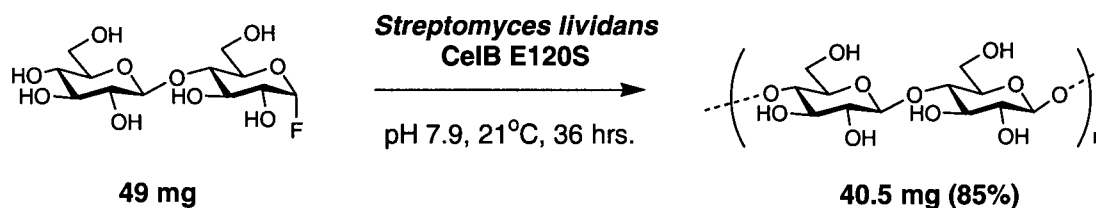


**Figure 7-9:** CelB E120S acting as a ‘cellulosynthase’.

Kinetic parameters for the polymerization of  $\alpha$ -cellobiosyl fluoride by CelB E120 mutants were determined by use of a fluoride electrode (Table 7-1). Standard saturation kinetics were observed with all mutants, and all  $k_{cat}$  values ( $1\text{-}2\text{ min}^{-1}$ ) were significantly lower than those previously observed with the Abg and Man2A glycosynthases (Chapters 5 and 6). Indeed, unlike the significant increase in transglycosylation rates observed with Abg and Man2A serine nucleophile mutants, the E120S mutant is merely 1.7 fold faster than the E120A mutant (comparing  $k_{cat}/K_M$  values). The sluggish performance of these catalysts may be inherent to the structure of CelB. As noted above, formation of the wild type glycosyl enzyme (and most likely substrate binding) involves substantial reorganization of a loop which serves to deliver residues to interact with the substrate and nucleophile. With a key interaction to this loop missing in the E120 mutants, the structure of the active site provided by this loop may be compromised. Likewise, because the acid-base catalyst hydrogen bonds to the 6-hydroxyl of the  $-1$  sugar, a pKa change in this residue as a result of deleting the negative charge of the nucleophile may be expected to effect substrate binding. A poorly assembled active site structure also appears to be reflected by the weak enhancement in glycosidic bond cleaving activity observed for these mutants with azide and DNPC (data not shown). Examination of the structures of CelB E120 mutants complexed with cellobiose could address these issues.

**Table 7-1:** Kinetic parameters for the reaction of CelB nucleophile mutants with  $\alpha$ -cellobiosyl fluoride (pH 7, 25°C).

Mutant	$k_{cat}$ ( $\text{min}^{-1}$ )	$K_M$ (mM)	$k_{cat}/K_M$ ( $\text{min}^{-1} \cdot \text{mM}^{-1}$ )
E120S	$1.72 \pm 0.06$	$2.8 \pm 0.3$	0.61
E120A	$0.96 \pm 0.05$	$2.7 \pm 0.4$	0.35
E120G	$0.127 \pm 0.006$	$4.7 \pm 0.5$	0.027

## Conclusions

Identification of the catalytic nucleophile in *Streptomyces lividans* endoglucanase CelB as E120 using the 2-fluoro glycoside inactivator methodology opened the possibility of engineering a new glycosynthase. Reactivation parameters for the trapped 2-fluorocellobiosyl intermediate indicated that CelB had fair glycosynthase potential. Indeed, the mutations E120A, E120G, and E120S all produced weakly active glycosynthases, with E120S being the most active. The relatively poor glycosynthase activity of these mutants may stem from a poorly structured active site produced by deletion of the nucleophile. The best reaction catalyzed by these mutants was, by far, the polymerization of  $\alpha$ -cellobiosyl fluoride to yield cellulose. This opens the possibility of using this catalyst to form novel polymeric structures based on a cellulose backbone.

## **Chapter 8    Enzymatic    Synthesis    of    Carbon-Fluorine Bonds**

## Mechanisms of Enzymatic Halogenation

Halogenated secondary metabolites are ubiquitous in Nature. Over 3000 natural products containing chlorine, bromine, or iodine have been characterized to date, and scores are added to the list each year.<sup>255,256</sup> There is, however, a notable scarcity of fluorinated natural products, of which only 13 are known (Figure 8-1).<sup>257</sup> This may in part stem from the limited bioavailability of fluoride, which exists primarily in insoluble mineral forms.<sup>258,259</sup> Equally elusive is an enzymatic mechanism for fluorination, as no enzyme with fluorinating activity has yet been isolated.<sup>257</sup>

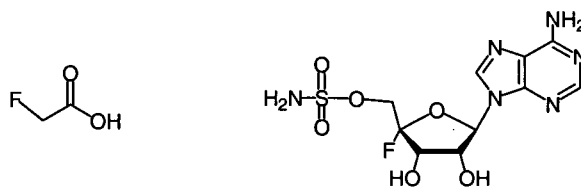


**Figure 8-1:** Examples of fluorinated natural products: fluoroacetate and nucleocidin.

A key aspect of the fluorination mechanism will be the nature of the fluorinating species: electrophilic, radical, or nucleophilic. An electrophilic halogenation mechanism is well known for the haloperoxidases (vanadium, heme, and cofactor free classes).<sup>260-263</sup> This mechanism involves oxidation of  $\text{Cl}^-$ ,  $\text{Br}^-$ , or  $\text{I}^-$  by a peroxide to form a hypohalous acid that in turn halogenates the substrate (Figure 8-2). A radical chlorination mechanism is thought to be involved in the biosynthesis of barbamide,<sup>264</sup> presumably initiated by a chlorate species (e.g.  $\text{HOCl}$ ).<sup>265</sup> However, genetic analysis of biosynthetic pathways suggest that haloperoxidases may not be involved in the biosynthesis of many halometabolites.<sup>266</sup> Likewise, the apparent lack of substrate specificity and regioselectivity displayed by haloperoxidases, presumably arising from the high reactivity and diffusable nature of the hypohalous acid that is generated, also suggests that halometabolite biosynthesis is not their primary function.<sup>263</sup> In the case of enzymatic fluorination, the chemical oxidation of fluoride to “ $\text{F}^+$ ” ( $E^\circ = 2.87 \text{ V}$ ),<sup>267</sup> the strongest oxidizing agent known, is impossible and therefore electrophilic or radical fluorination mechanisms are untenable.<sup>259</sup>

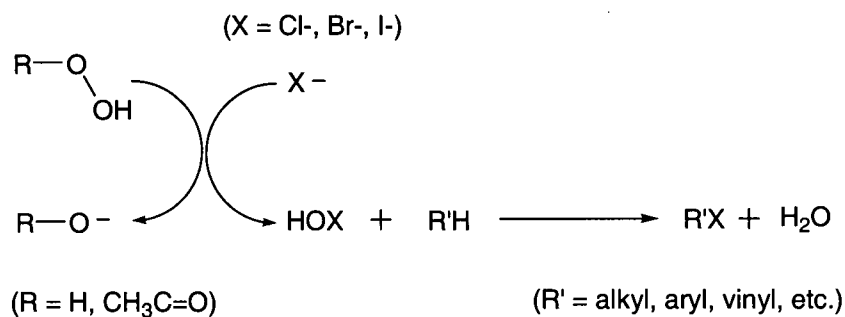


**Figure 8-2:** Simplified scheme for a haloperoxidase reaction.

In light of the problems associated with electrophilic halogenation, a nucleophilic mechanism may be a more general route towards halometabolite biosynthesis. However, this mechanism is thus far poorly defined. Nucleophilic halogenation has only been demonstrated for the methylation of  $\text{Br}^-$ ,  $\text{Cl}^-$ , and  $\text{I}^-$  by *S*-adenosylmethionine methyl transferases (Figure 8-3a).<sup>268</sup> Nevertheless, it appears that this example is merely the first of many enzymes employing halides as nucleophiles. A newly discovered class of enzymes, the FAD-NADH dependent halogenases, are believed to use a halide to attack epoxide substrates (Figure 8-3b).<sup>266,269</sup> Likewise, extensive work on *Streptomyces cattleya* will most likely produce the first wild type fluorinating enzyme,<sup>270,271</sup> which is thought to use a fluoride nucleophile to synthesize fluoroacetate.<sup>259</sup>

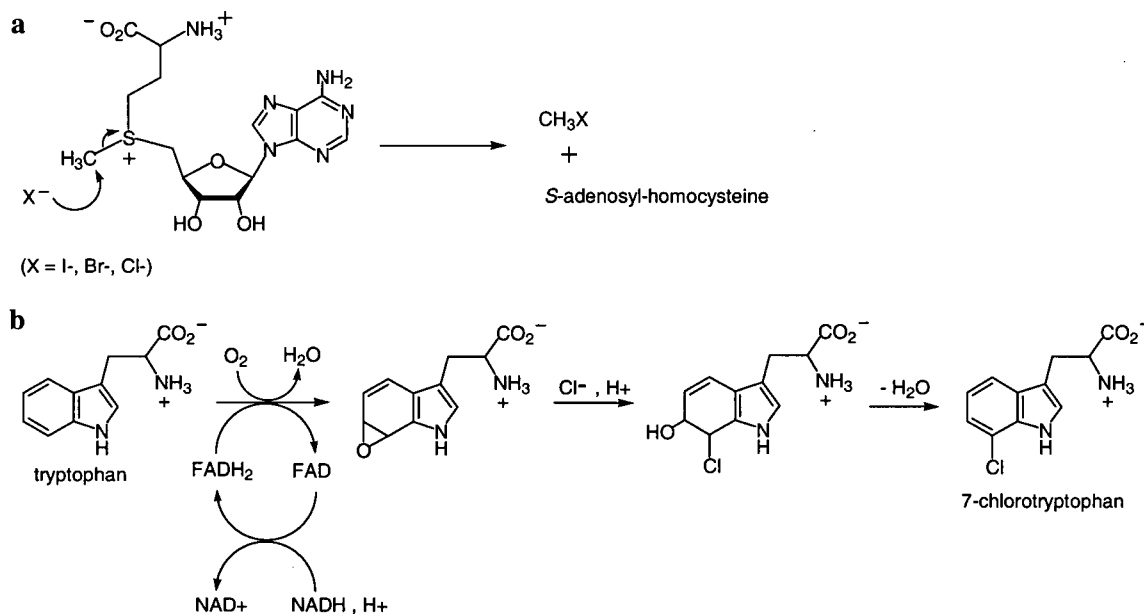


**Figure 8-3:** Nucleophilic halogenation mechanisms. (a) Synthesis of methyl halides by *S*-adenosylmethionine methyltransferase.<sup>268</sup> (b) Proposed mechanism for synthesis of 7-chlorotryptophan (a precursor to pyrrolnitrin) by NADH-FAD dependent halogenases.<sup>266</sup>

### Nucleophilic Fluorination by Glycosynthases

Given the scarcity of data on nucleophilic halogenation by enzymes, particularly with fluoride, it is significant that the glycosynthases derived from *Agrobacterium* sp.  $\beta$ -glucosidase (Abg) and *Cellulomonas fimi*  $\beta$ -mannosidase (Man2A) catalyze the formation of carbon-fluorine bonds using nucleophilic fluoride. As noted previously, replacement of the catalytic glutamate nucleophile in Abg (E358) or Man2A (E519) with alanine, glycine or serine renders the usual double displacement mechanism inoperable and virtually no glycosidic bond cleaving activity is detectable. However, when assayed with the appropriate 2,4-dinitrophenyl  $\beta$ -glycoside substrate in the presence of fluoride, substantial glycosidic bond activity is restored (Figure 8-4, Table 8-1). As with azide rescue (see Chapters 5 and 6), the reaction with fluoride was also pH dependent, with the highest rates observed at pH 6 and lower (data not shown).

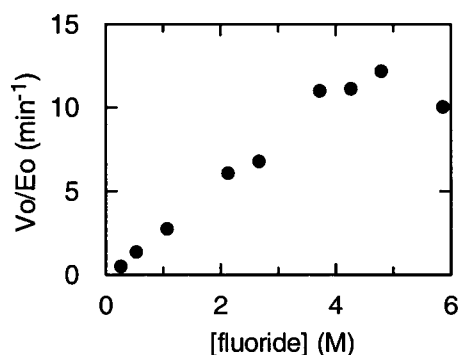


**Figure 8-4:** Plot of reaction rate versus fluoride (KF) concentration for the reaction of Abg E358S with 2,4-dinitrophenyl  $\beta$ -glucoside (2.75 mM) at pH  $\sim$  7, 37°C.

Chemical rescue by fluoride has been observed previously with a mutant glutamate dehydrogenase, but this was the result of fluoride fulfilling an electrostatic role.<sup>272</sup> With Abg and Man2A nucleophile mutants, fluoride acts as a nucleophile and the product of the glycosidic bond cleaving reaction is the corresponding  $\alpha$ -glycosyl fluoride (Figure 8-5a, first step) as confirmed by TLC,  $^1\text{H}$  and  $^{19}\text{F}$  NMR. In the case of Abg E358G, the apparent  $k_{cat}$  value for carbon-fluorine bond formation exceeds  $2\text{ s}^{-1}$  (Table 8-1). As one would expect from the glycosynthase activity of these mutants, the  $\alpha$ -glycosyl fluoride product in turn acts as a glycosyl donor in a subsequent transglycosylation reaction with a second molecule of 2,4-dinitrophenyl  $\beta$ -glucoside, thus forming new glycosidic bonds (Figure 8-5a, second step).

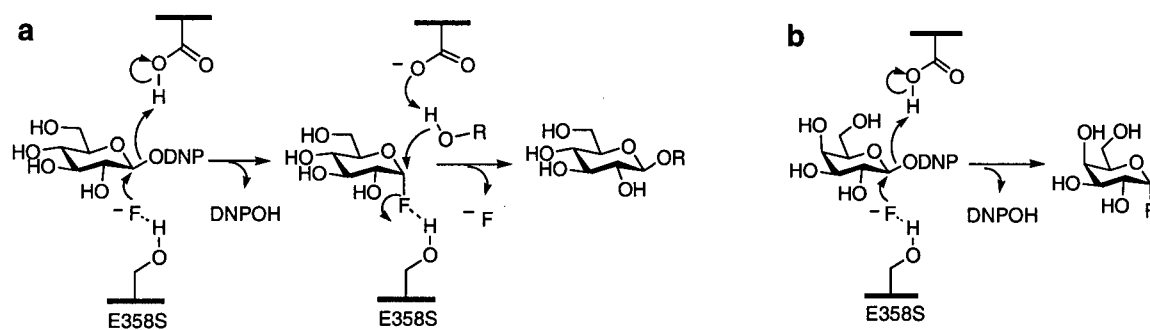


**Figure 8-5:** (a) Abg E358S catalyzing nucleophilic fluorination of 2,4-dinitrophenyl  $\beta$ -glucoside and subsequent transfer of  $\alpha$ -glycosyl fluoride to a second equivalent of substrate (R). (b) Abg E358S synthesizing  $\alpha$ -galactosyl fluoride.

**Table 8-1:** Kinetic parameters for Abg and Man2A nucleophile mutants catalyzing glycosidic bond cleavage of 2,4-dinitrophenyl  $\beta$ -glucoside and 2,4-dinitrophenyl  $\beta$ -mannoside, respectively, using halides as nucleophiles (pH 6, 25°C).

	$k_{cat}$ ( $\text{min}^{-1}$ )	$K_M$ (mM)	$k_{cat}/K_M$ ( $\text{min}^{-1} \cdot \text{mM}^{-1}$ )
<b>Abg wt</b>	5040	0.0214	235 000
+ 2 M KF	3600	0.024	150 000
<b>Abg E358A</b>	<0.001	-	-
+ 2 M KF	21.5	0.131	164
+ 2 M NaCl	1.00	0.112	8.93
<b>Abg E358G</b>	0.08	-	-
+ 2 M KF	131	0.157	834
+ 2 M NaCl	44.8	0.086	521
+ 2 M NaBr	11.2	0.144	77.8
+ 2 M KI	n/a <sup>a</sup>	-	-
<b>Abg E358S</b>	<0.001	-	-
+ 2 M KF	28.9	0.044	657
<b>Man2A wt</b>	27 000	0.6	45 000
+ 2 M KF	7 900	0.22	36 000
<b>Man2A E519A</b>	<0.008	-	-
+ 2 M KF	20.7	0.131	158
<b>Man2A E519S</b>	0.0015	-	-
+ 2 M KF	14.0	0.036	389

a) No activity.

The relatively modest glycosynthase (transglycosylation) activity of Man2A E519S allowed isolation of  $\alpha$ -mannosyl fluoride as the major product, which was characterized by  $^1\text{H}$  and  $^{19}\text{F}$  NMR. However, the much greater glycosynthase activity of the Abg mutants resulted in rapid synthesis of oligosaccharide products, as observed by TLC and ESI-MS. Indeed, the rate constant for turnover of  $\alpha$ -glucosyl fluoride with Abg E358S exceeds  $1 \text{ s}^{-1}$ . Nevertheless, a low concentration of  $\alpha$ -glucosyl fluoride could be observed by  $^{19}\text{F}$  NMR during the reaction of 2,4-DNP  $\beta$ -glucoside with Abg E358G and fluoride ( $\delta$  -74.3, dd,  $J = 55.4, 24.9$  Hz, referenced to  $\text{CF}_3\text{CO}_2\text{H}$ ). Moreover, the analogous reaction with 2,4-dinitrophenyl  $\beta$ -D-galactoside and Abg E358G resulted in the formation of  $\alpha$ -D-galactosyl fluoride as the major product, which was isolated and characterized. As noted previously,  $\alpha$ -galactosyl fluoride cannot glycosylate a second 2,4-dinitrophenyl  $\beta$ -galactoside substrate due to the absence of a suitably positioned (equatorial) 4-hydroxyl (Figure 8-5b).<sup>244</sup> The wild type enzymes did not catalyze the formation of  $\alpha$ - or  $\beta$ -glycosyl fluorides, as indicated by  $^{19}\text{F}$  NMR, presumably due to electrostatic or steric effects preventing access to fluoride. This is not surprising considering the precision of chemical rescue demonstrated thus far with glycosidase mutants.<sup>59</sup>

The transglycosylation reaction is also reflected in the steady state kinetic behaviour of the nucleophile mutants at high concentrations of 2,4-dinitrophenyl glycoside (Figure 8-6). A non-saturating, linear relationship of reaction velocity versus substrate concentration is observed above 0.5 mM in all cases. As predicted by the kinetic model presented in Chapter 5, the slope of the linear region appears to correlate with the glycosynthase activity of the mutant. In the case of Abg E358S and E358A, the  $k_{cat}$  values for the turnover of  $\alpha$ -glucosyl fluoride are similar ( $\sim 65 \text{ min}^{-1}$ ), although the corresponding  $K_M$  values are considerably different (see Chapter 5, Table 5-1). Likewise, the slopes of the corresponding fluoride rescue plots are similar (Figure 8-6a). In contrast, the  $k_{cat}$  value for Man2A E519S for the turnover of  $\alpha$ -mannosyl fluoride ( $12 \text{ min}^{-1}$ ) is considerably greater than that for E519A ( $0.33 \text{ min}^{-1}$ ) and this too is reflected in the relative slopes of the fluoride rescue plots (Figure 8-6b).

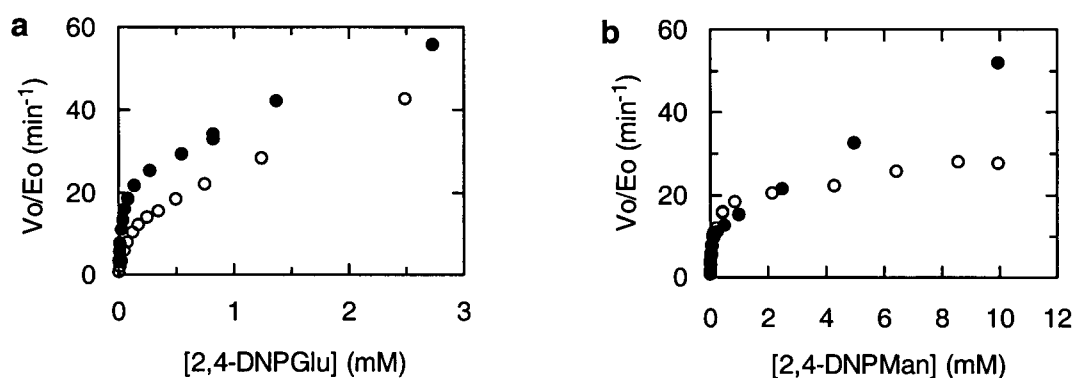


**Figure 8-6:** Plots of reaction velocity vs substrate concentration for the reaction of Abg and Man2A nucleophile mutants with 2,4-dinitrophenyl glycosides and fluoride (2 M, pH 6, 25°C). (a) Plots for Abg E358A (O) and E358S (●). (b) Plots for Man2A E519A (O) and E519S (●).

### Hydrogen Bonding to Fluoride

Also noteworthy from the  $k_{cat}/K_M$  values is the fluorination activity of the Man2A E519S, Abg E358S and Abg E358G mutants (Table 8-1). This activity is considerably greater than that for the corresponding alanine mutants. It is probable that this difference arises from hydrogen bonding to fluoride. In the case of the serine mutants, this hydrogen bond would arise from the serine hydroxyl group. As proposed previously, a hydrogen bond formed with the departing fluoride ion in the glycosynthase transition state (Figure 8-5a, second step), may also explain the  $\sim 25$  fold greater glycosynthase activity of Man2A and Abg serine mutants relative to the alanine mutants.<sup>244,273</sup> More surprising is the high fluorination activity of Abg E358G, which would

appear to offers no such side chain. However, as discussed in Chapter 5, structural evidence suggests that Tyr 298 in this mutant may provide an equally good, if not better, hydrogen bond in the fluorination or transglycosylation transition states.

### Kinetic Isotope Effects

The transition state character of the fluorination transition state for the Abg nucleophile mutants was examined through  $\alpha$ -DKIE's. Using the substrate 2,4-dinitrophenyl  $\beta$ -[1- $^2$ H]-glucoside  $\alpha$ -DKIE's of  $1.055 \pm 0.017$  for E358S,  $1.057 \pm 0.022$  for E358A and  $1.076 \pm 0.026$  for E358G were obtained for  $k_{cat}/K_M$ . These values are all similar and suggest that the corresponding oxocarbenium ion transition state for each mutant is only partly developed. This may be the result of significant nucleophilic participation of fluoride in the transition state, much like Glu 358 is proposed to interact in the glycosylation transition state of wild type Abg. Indeed, these  $\alpha$ -KIE's are quite similar to that observed for the wild type enzyme in the glycosylation step.<sup>33</sup>

### Glycosynthases as Halogenases

The Abg E358G and E358A mutants can also catalyze nucleophilic halogenation of 2,4-dinitrophenyl  $\beta$ -glucoside using chloride and bromide (2 M). Although the corresponding  $\alpha$ -glucosyl halides are too unstable to isolate directly, transglycosylation products resulting from transfer to a second equivalent of substrate were observed by TLC and ESI-MS. Nevertheless, an attempt was made using  $^1$ H NMR to observe the synthesis of  $\alpha$ -galactosyl chloride during the reaction of Abg E358G with 2,4-dinitrophenyl  $\beta$ -galactoside and 2 M NaCl (pD 5.6, 300K). As with  $\alpha$ -galactosyl fluoride, a transglycosylation reaction is not possible and the accumulation of  $\alpha$ -galactosyl chloride is expected (Figure 8-5b). Indeed, a small resonance was observed by  $^1$ H NMR (Figure 8-7) which may correspond to the anomeric proton of  $\alpha$ -D-galactosyl chloride ( $\delta$  5.45, d,  $J = 3.1$  Hz, referenced to HDO). However, the instability of this compound precludes synthesis of a standard that could confirm this result.

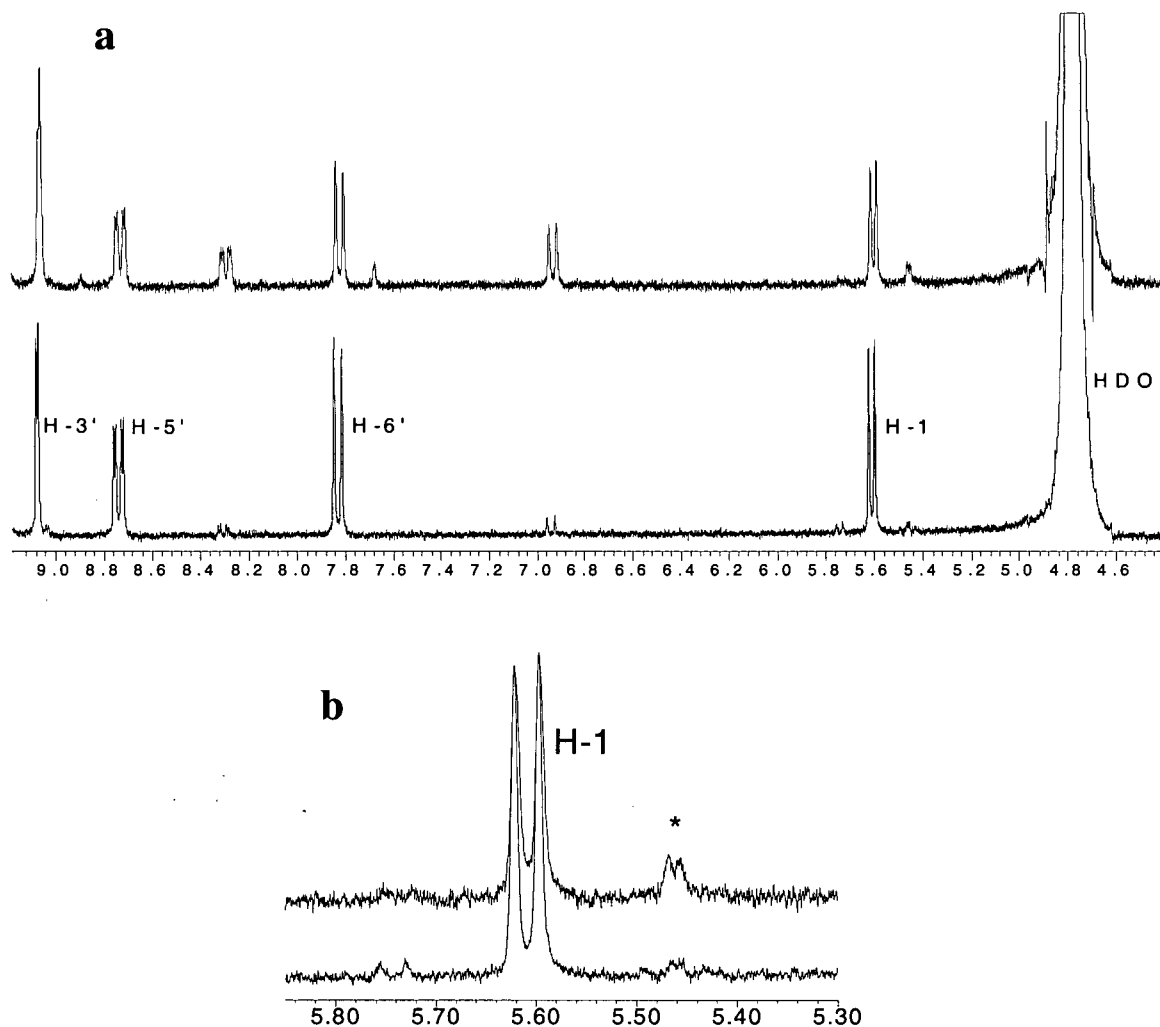


**Figure 8-7:**  $^1\text{H}$  NMR spectra (300 MHz) of the reaction of Abg E358G (19  $\mu\text{M}$ ) with 2,4-dinitrophenyl  $\beta$ -galactoside (7 mM) in the presence of 2 M NaCl (100 mM citrate, pD 5.65). (a) Region of aromatic and anomeric proton resonances. Upper spectrum obtained during the reaction with E358G after 145 min. at 300K. Lower spectrum obtained under the same conditions in absence of E358G after 145 min.. (b) Expansion of the anomeric region. The resonance at 5.45 ppm (\*) is proposed to arise from H-1 of  $\alpha$ -galactosyl chloride.

Unusual kinetic behaviour is observed at high 2,4-DNPGlu concentrations when chloride or bromide ions are used as nucleophiles with Abg E358G. Although E358A displays a linear, non-saturating rate dependence on glycoside substrate concentration with chloride (Figure 8-8a), E358G displays substrate inhibition with the same anion (Figure 8-8b). With bromide, E358G displays typical saturating kinetics (data not shown). Despite these differences, transglycosylation does occur with chloride or bromide with either mutant at high substrate concentrations, as noted above. However, it is possible that the transglycosylation pathway with  $\alpha$ -glucosyl chloride or bromide donors may be slow or inhibitory with E358G.

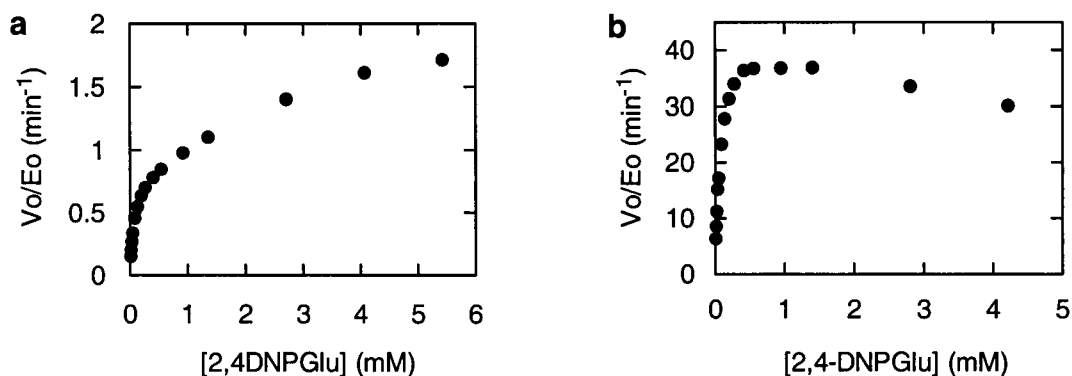


**Figure 8-8:** Reaction rates versus 2,4-dinitrophenyl  $\beta$ -glucoside concentration for Abg E358A (a) and E358G (b) in the presence of chloride (2 M, pH 6, 25°C).

The high hydration energy of fluoride ( $117 \text{ kcal} \cdot \text{mol}^{-1}$ ) might be expected to severely limit its participation as a nucleophile in biochemical processes.<sup>259</sup> Intriguingly, a comparison of  $k_{cat}/K_M$  values for E358G and E358A (Table 8-1) indicates an order of halide reactivity ( $\text{F}^- > \text{Cl}^- > \text{Br}^-$ ) opposite to that expected in aqueous solution. Although this may be the result of steric constraints in the Abg active site, this order of halide nucleophilicity has also been observed in organic solvents and in the gas phase.<sup>274,275</sup> This suggests that desolvation of the halide occurs in the active site of Abg, and indeed this is highly probable given the limited size of the reaction cavity. The reactivity order may also reflect a stabilizing 'synergism'<sup>276</sup> in the halogenation transition state between hard, weakly polarizable attacking and leaving groups (i.e. fluoride and phenolate oxygen). Synergism may also cause a similar reversal in reactivity observed for the reaction of methyl glycosides<sup>277</sup> and  $\alpha$ -glucosyl fluoride<sup>7</sup> with halides in aqueous solution. Synergism is also consistent with the halide reactivity order observed for the *S*-adenosylmethionine methyltransferase reaction ( $\text{I}^- \gg \text{Br}^- > \text{Cl}^-$ ), which involves a 'soft' leaving group, sulphur (Figure 8-3).<sup>268</sup> Fluoride, notably, is not a substrate for *S*-adenosylmethionine methyl transferases. However, one must also consider that halide specificity may have evolved in these enzymes.

### Fluorination Activity of a General Acid-Base Mutant

The generality of enzymatic nucleophilic fluorination is further demonstrated by the ability of the E429A acid-base mutant of Man2A to synthesize  $\beta$ -mannosyl fluoride. This mutant readily forms the covalent intermediate with the reactive substrate 2,5-dinitrophenyl  $\beta$ -mannoside

(Figure 8-9). Due to the absence of base catalysis in the second step, deglycosylation is slowed and the covalent intermediate accumulates, as evidenced by very low  $k_{cat}$  and  $K_M$  values ( $k_{cat} = 12 \text{ min}^{-1}$ ,  $K_M < 1 \text{ }\mu\text{M}$ ). However, fluoride (1 M KF) can attack the anomeric carbon of the covalent intermediate, resulting in faster turnover of the enzyme ( $k_{cat} = 87 \text{ min}^{-1}$ ) and a corresponding rise in  $K_M$  (7.7  $\mu\text{M}$ ), as well as the formation of  $\beta$ -mannosyl fluoride. The  $\beta$ -mannosyl fluoride product could not be isolated and is not expected to accumulate as it is also a good substrate for Man2A.<sup>138</sup> Nevertheless, while monitoring the reaction directly by  $^{19}\text{F}$  NMR spectroscopy (Figure 8-10) a resonance corresponding to a low steady-state concentration of  $\beta$ -mannosyl fluoride was observed ( $\delta$  -146.7, d,  $J = 49 \text{ Hz}$ , referenced to  $\text{CFCl}_3$ ).

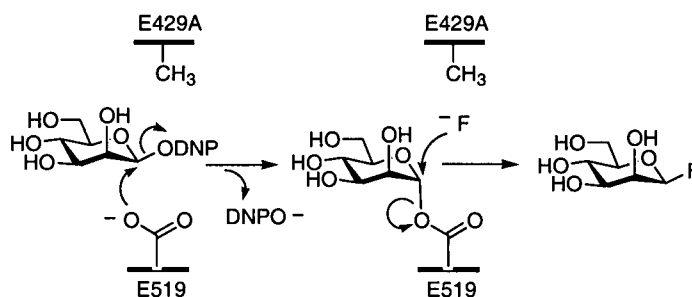


**Figure 8-9:** Man2a E429A catalysing nucleophilic fluorination of the mannosyl-enzyme covalent intermediate, forming  $\beta$ -D-mannosyl fluoride. DNP = 2,5-dinitrophenyl.

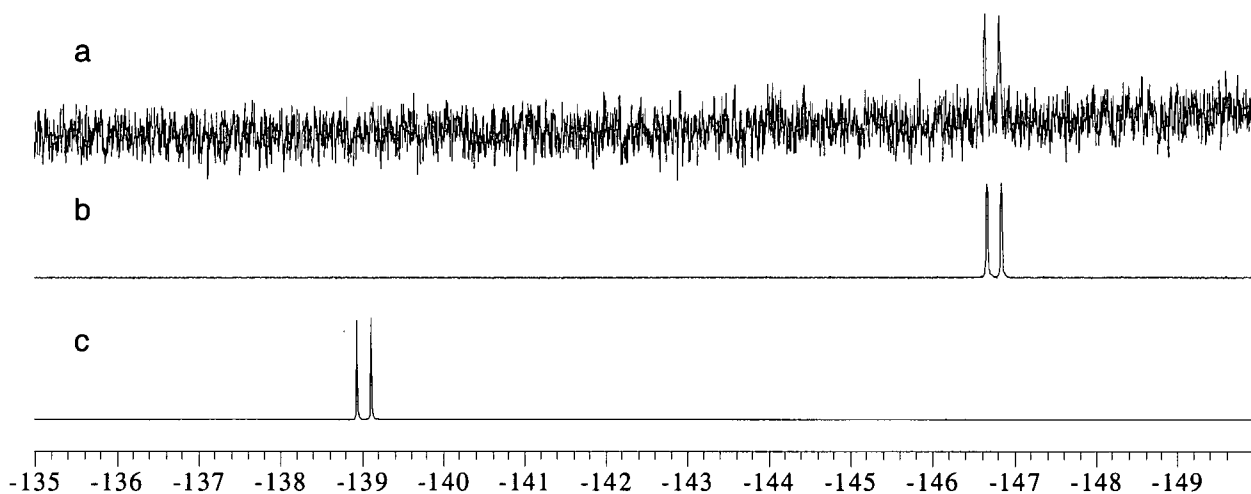


**Figure 8-10:** (a)  $^{19}\text{F}$  NMR spectrum (282 MHz, referenced to  $\text{CFCl}_3$ ) of the reaction of Man2A E429A with 2,5-dinitrophenyl  $\beta$ -mannoside in the presence of 1 M KF (pH 7, 300 K) after 30 min.. (b) Spectrum of  $\beta$ -D-mannosyl fluoride. (c) Spectrum of  $\alpha$ -D-mannosyl fluoride.

A notable enhancement in the activity of Man2A E429A is also observed with chloride and bromide (Figure 8-11). Although the enhancement in rate is modest (~10 % increase with 1 M bromide, 55% with 1 M chloride), the example set by fluoride implies that chloride and bromide also effect this rate increase by serving as external nucleophiles. Likewise, the relative order of halide reactivity with the E429A mutant ( $F^- \gg Cl^- > Br^-$ ) suggests that desolvation and synergy in the halogenation transition state may be at play, barring any steric effects, as observed for the nucleophile mutants of Abg.

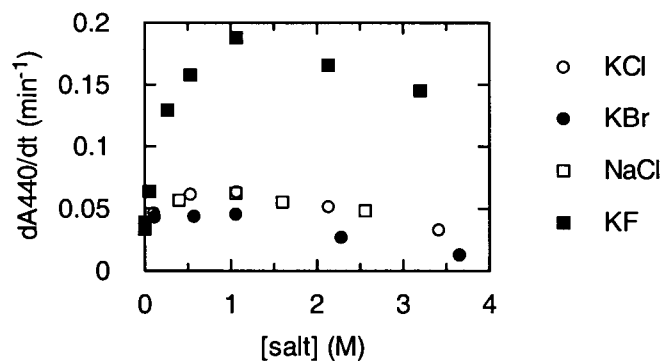


**Figure 8-11:** Plots of initial rates versus salt concentration for the reaction of Man2A E429A (0.575  $\mu$ M) with 2,5-dinitrophenyl  $\beta$ -mannoside (1.88 mM, pH 7, 25°C).

## Conclusions

The catalysis of carbon-fluorine bond formation by mutants of two unrelated glycosidases, each using a nucleophilic fluorination mechanism, demonstrates the feasibility of such a mechanism occurring in Nature. Indeed, it is particularly interesting that one of the known fluorinated natural products, nucleocidin (Figure 8-1), is itself a glycosyl fluoride and may well be formed by an analogous mechanism. As suggested by this work, catalytic features of nucleophilic fluorination may involve hydrogen bonding and desolvation of the anion. This work also raises the possibility of engineering other enzymes to catalyze nucleophilic fluorination of medically significant compounds.

## Catalytic Promiscuity

It is standard practice to name an enzyme according to the substrate (or class of substrates) that yields the highest  $k_{cat}/K_M$  values. In some cases enzymes are perfectly evolved towards their particular substrate, with  $k_{cat}/K_M$  values approaching the diffusion limit ( $10^8 \text{ M}^{-1} \cdot \text{s}^{-1}$ ). During the course of evolution, beneficial catalytic features in one enzyme may be appropriated by gene recombination, or merely by chance through spontaneous mutation. Often an existing structural platform is modified, giving rise to common folds and binding sites, termed 'superfamilies'<sup>278</sup> that catalyze numerous reactions. The  $\alpha/\beta$  barrel (TIM barrel), to which Abg and Man2A belong, is one such platform. The consequence of this evolutionary history, in addition to simple chance, is the ability of many enzymes to catalyse multiple chemical transformations, albeit at  $k_{cat}/K_M$  values that are often far below that of the choice substrates (reviewed in <sup>279</sup>). Some examples of catalytic promiscuity include the oxidase activity of hemoglobin,<sup>280</sup> the phosphotriesterase activity of chymotrypsin, and the nitrilase activity of L-asparaginase.<sup>279</sup> This is frequently to the advantage of the enzymologist, who can use such reactions to conduct facile assays of enzyme activity, as well as tune the reactivity of a substrate. For example, glycosidases are routinely assayed with aryl glycosides or glycosyl fluorides. However, not only does catalytic promiscuity allow interrogation of an enzyme mechanism with a wide range of chemistries, but it also provides the opportunity to engineer new catalytic activity. This activity may be latent; the rough catalytic features and structure may be present for catalysis, but remodeling of the active site is required for catalysis of a new reaction to occur. Such engineering of new activity may be done through rational design or, more often, through directed evolution where large libraries of mutants are created by random mutagenesis or DNA shuffling, and then screened for the desired activity. There are many successful examples of rationally designed or evolved enzyme functions,<sup>281-284</sup> but three of the most dramatic examples are the transformation of *E. coli* cyclophilin, an isomerase of X-Pro bonds, into an X-Pro specific protease,<sup>285</sup> the conversion of *E. coli* indoleglycerol-phosphate synthase into phosphoribosylanthranilate isomerase<sup>286</sup> and conversion of dimeric chorismate mutase into an active monomer.<sup>287</sup> In each case the new activity was completely absent in the wild type enzyme, and the resulting mutants catalyzed their new reactions with 'wild-type' enzyme activities ( $k_{cat}$  values of  $1-10 \text{ s}^{-1}$ ).

Glycosidases are also catalytically promiscuous. The wild type enzymes are capable of cleaving carbon-oxygen, carbon-nitrogen, carbon-sulphur and carbon-halide bonds. Likewise,

the Hehre mechanism for inverting glycosidases has long been cited as evidence of the catalytic 'plasticity' in these enzymes (see Chapter 4).<sup>288</sup> The catalytic features of inverting and retaining glycosidases are remarkably similar, and from a crude perspective only differ in the distance spanning the two catalytic carboxyl groups. Thus it has been possible to transform one into the other with single mutations of these residues, as is the case for T4 lysozyme and Abg nucleophile mutants.<sup>30,289-291</sup>

Indeed, a striking feature of glycosidases is their amenability to functional group replacement, particularly at the position of the acid-base catalyst or the nucleophile (for retainers). This has not been overlooked in Nature, as illustrated by the bizarre acid-base chemistry performed by *Sinapis alba* myrosinase (see Chapter 1).<sup>67</sup> The rate accelerations achieved by functional group replacement are outstanding, particularly with the retaining nucleophile mutants of Abg described in this thesis. Measurement of 'true'  $k_{cat}$  values for glycosidic bond cleavage by these mutants is a distinct challenge due to contamination by wild type enzyme or exogenous nucleophiles, but approach  $10^{-5} \text{ s}^{-1}$  in the case of Abg E358A.<sup>30</sup> Thus the  $k_{cat}$  values of  $1\text{-}45 \text{ s}^{-1}$  observed for Abg nucleophile mutants in the presence of azide, formate or halides represent accelerations in excess of  $10^5$  fold. Likewise, these nucleophile mutants (particularly Abg) use  $\alpha$ -glycosyl fluoride substrates to catalyse glycosylation reactions with  $k_{cat}$  values exceeding  $5 \text{ s}^{-1}$ . A rate acceleration in this case cannot even be calculated because the wild type retaining glycosidases presented in this thesis do not accept  $\alpha$ -glycosyl fluorides as substrates.

By describing the transformation of catalytic function from that of a glycosidase to a glycosynthase and then to a halogenase, this thesis demonstrates how a diverse set of chemistries can arise from one active site. Although these new reactions can be exploited for purely synthetic purposes, it is more intriguing to use these new chemistries as a lens through which to understand catalysis of the corresponding wild type enzyme, as well as understand how similar reactions might arise in Nature.

## **Experimental Methods**

## Chapter 2: Application of Mass Spectrometry to Enzyme Kinetics

### General

The substrate 2,5-dinitrophenyl  $\beta$ -xylobioside (2,5-DNPX<sub>2</sub>) was synthesized according to published procedures.<sup>127</sup> The mutation of Bcx, yielding the Y80F substitution, has also been described previously.<sup>124</sup> This mutant was generously provided by Dr. Manish Joshi and Prof. Lawrence McIntosh (Department of Biochemistry, University of British Columbia). Prior to kinetic studies, solutions of wild type Bcx (MW 20,400) and mutant Bcx Y80F (MW 20,384) were exhaustively desalted with freshly prepared 10 mM ammonium acetate (pH 6 for wild type, pH 6.30 for the mutant) using a centrifugal concentrator (Amicon) with a nominal molecular weight cut-off of 10 kDa. The concentrations of wild type and mutant Bcx were determined from the extinction coefficient  $A_{280}^{0.1\%} = 2.50$ . This extinction coefficient was derived from active site titration of Bcx Y80F with 2,5-DNPX<sub>2</sub> (see below).

### Steady-state kinetics

Steady-state kinetic studies were performed on a Unicam 8700 UV-Vis spectrometer equipped with a circulating water bath. Assay solutions, prepared in black quartz cuvettes (1 cm path length), consisted of an appropriate concentration of substrate in 5 mM ammonium acetate (pH 6.0 for wild type Bcx, pH 6.3 for Bcx Y80F), pre-equilibrated at 23°C. Substrate hydrolysis was initiated with the addition of an aliquot of enzyme (0.629  $\mu\text{g/mL}$  wild type Bcx, 220  $\mu\text{g/mL}$  Bcx Y80F, final concentrations) and the initial rate of phenolate release was monitored at 440 nm ( $\Delta\epsilon = 3.57 \text{ mM}^{-1}\cdot\text{cm}^{-1}$ ).<sup>127</sup> Hydrolysis rates were determined at 10 substrate concentrations ranging from 0.2 to 5 times the  $K_M$  value, where possible. The resulting velocity curve was fitted with the standard Michaelis-Menten equation using the program GraFit.<sup>292</sup>

### Stopped-flow spectroscopy

Pre-steady state kinetics were performed on a stopped-flow UV-Vis spectrometer (Applied Photophysics, Model SF.17MV) equipped with a circulating water bath. Aliquots (100  $\mu\text{L}$  each) of an appropriate concentration of 2,5-DNPX<sub>2</sub> (in de-ionized water) and Bcx Y80F (0.41 mg/mL, 20  $\mu\text{M}$ , in 10 mM ammonium acetate, pH 6.3), were pneumatically driven from 2.5 mL Hamilton syringes (equilibrated at 23°C) into a mixing cell. The release of phenolate was monitored at 440 nm for a total of 50 seconds, and the resulting time course fitted to the equation

$A_{440}(t) = A(1 - \exp(-k_{obs}t)) + Bt + C$  using the program GraFit. The observed first-order rate constant ( $k_{obs}$ ) for the pre-steady state release of phenolate was determined at 7 substrate concentrations (ranging from 0.1 mM to 2.2 mM).

The published extinction coefficient for Bcx ( $A_{280}^{0.1\%} = 4.08$ )<sup>124</sup> is an estimate based on the number of tyrosine and tryptophan residues in the protein, rather than an exact value determined from a complete amino acid quantification. A more accurate measure of enzyme concentration can be derived from the stopped-flow experiments because 2,5-DNPX<sub>2</sub> acts as an active site titrant with Bcx Y80F due to rate-limiting deglycosylation ( $k_{+2} \gg k_{+3}$ ).<sup>114</sup> Using a sample of Bcx Y80F diluted 133 fold from the stock solution, a burst of 10.1  $\mu$ M 2,5-DNP (0.036 absorbance units) was observed (Figure 1) when mixed with excess 2,5-DNPX<sub>2</sub> (2.2 mM). This corresponds to 0.206 mg/mL enzyme or 27.4 mg/mL in the stock solution. Time resolved ESI-MS measurements indicated that >95% of the enzyme is converted to E-X<sub>2</sub> under these conditions (see below), therefore it is unlikely that this burst underestimates the concentration of enzyme<sup>114</sup>. A 561 fold dilution of the stock solution yielded an absorbance of 0.122 at 280 nm, which corresponds to an extinction coefficient of  $A_{280}^{0.1\%} = 2.50$ . The concentrations of wild type Bcx and Bcx Y80F quoted in this study are derived from this corrected extinction coefficient.

### **Time-resolved ESI-MS**

Time-resolved ESI-MS measurements were carried out as described previously.<sup>100,101</sup> Briefly, two syringes (1 mL volume each) were advanced simultaneously by a syringe pump. One syringe contained enzyme (0.165 mg/mL wild type or Y80F Bcx) in 10 mM ammonium acetate buffer (pH 6.0 for wild type Bcx, pH 6.3 for Bcx Y80F). The other syringe contained 2,5-DNPX<sub>2</sub> in deionized water. The enzymatic reaction was initiated by mixing the solutions from both syringes in a reaction tee. This tee was connected to an ESI source by a reaction capillary with an inner diameter of 75  $\mu$ m. Lengths of the reaction capillaries varied between 1 cm and 186 cm. The total flow rates used for the experiments were 10  $\mu$ L/min and 20  $\mu$ L/min, corresponding to minimum and maximum reaction times of 0.13 s and 47.8 s, respectively. Slightly different charge state distributions were observed at different flow rates. Therefore, for a given substrate concentration the flow rate was kept constant and the reaction time was varied only by changing the length of the reaction capillary. Apparently the velocity distribution in the reaction capillary translates into a narrow distribution of solution “age”, even though simple

models indicate that the flow rates used here are too low to induce turbulent flow and adequate mixing.<sup>115</sup> Under laminar flow conditions used here the solution next to the capillary wall is retarded relative to solution in the middle of the capillary due to friction, resulting in a distribution of solution age. However, computer simulations show that the distortion of the measured kinetics under laminar flow conditions is remarkably small.<sup>293</sup> This is because the age distribution is narrowed by the effect of molecular diffusion between outer and inner solutions. Accordingly, there is excellent agreement between the stopped-flow data (that achieves turbulent flow) and time-resolved ESI-MS data in this and previous studies.<sup>100,101</sup> The enzyme and substrate concentrations given in Chapter 2-4 correspond to the final concentrations (i.e. after the mixing step). Multiply charged gas phase protein ions were generated at the exit of the reaction capillary by pneumatically assisted ESI and were analyzed in a quadrupole mass spectrometer constructed 'in house'.<sup>100</sup> The voltage difference between the orifice and the RF-only quadrupole ("declustering voltage") was 130 V unless stated otherwise. All experiments were carried out at room temperature ( $23 \pm 1^\circ\text{C}$ ). The relative ratio of E-X<sub>2</sub> to free enzyme at a given time point was determined from the relative intensities (peak heights) of the 8<sup>+</sup> ions, averaged from 30 scans. The time courses for the accumulation of E-X<sub>2</sub> were fit to the equation  $C(t) = C_{SS}(1 - \exp(-k_{obs}t))$  where  $C(t)$  is the concentration of E-X<sub>2</sub> as a function of time  $t$ , and  $C_{SS}$  is the steady state concentration of E-X<sub>2</sub>. The first order rate constant,  $k_{obs}$ , was determined at 8 concentrations of 2,5-DNPX<sub>2</sub> ranging from 0.035 to 2.2 mM.

### Chapter 3: Mechanistic Investigations into the Retaining $\beta$ -Mannosidase *Cellulomonas fimi* Man2A

#### General

The expression and purification of wild type Man2A is described elsewhere.<sup>137</sup> The wild type plasmid was provided by Dr. Dominik Stoll. The acid-base mutant Man2A E429A was also prepared by Dr. Stoll. <sup>1</sup>H NMR (400 MHz, Bruker) and <sup>13</sup>C NMR (100 MHz, Varian) data for the aryl 2,3:4,6-di-*O*-cyclohexylidene- $\beta$ -D-mannopyranosides can be found in Tables 3-3 and 3-4 (see below). <sup>1</sup>H NMR (400 MHz, Bruker) data for the deprotected aryl  $\beta$ -mannosides can be found in Table 3-5 (see below).

#### Mitsunobu Glycosylation of Phenols<sup>140</sup>

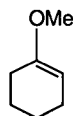
Phenols were dried by repeated evaporation (3  $\times$ ) from acetonitrile on a rotovap. 4-Chlorophenol and phenol were vacuum distilled from 4 Å molecular sieves prior to use. 2,3:4,6-Di-*O*-cyclohexylidene  $\alpha$ -D-mannopyranose (**2-1**) (1-3 g), triphenylphosphine (1.4 eq.) and substituted phenol (1.4 eq.) were dissolved in dry toluene (50 mL) and the vessel purged with dry nitrogen. DEAD (1.4 eq.) was added dropwise via syringe and the reaction stirred at room temperature in the dark. Within 20 minutes crystalline triphenylphosphine oxide was observed to form. The reaction was typically complete (by TLC) in 1.5 to 2 hrs.. The reaction mixture was concentrated *in vacuo* and the bulk of the triphenylphosphine oxide removed by recrystallization (1-2  $\times$ ) from PE/EtOAc. After concentration *in vacuo*, the reaction mixture was dissolved in DCM and washed with saturated sodium bicarbonate (for phenols with pKa's  $\leq$  7) or 0.1 M NaOH (for phenols with pKa's  $>$  7) followed by brine. After drying over MgSO<sub>4</sub> and concentration *in vacuo* the crude mixture of  $\beta$ - and  $\alpha$ -anomers were purified by silica gel chromatography. <sup>1</sup>H and <sup>13</sup>C NMR data for the aryl 2,3:4,6-di-*O*-cyclohexylidene- $\beta$ -D-mannopyranosides can be found in Tables 3-3 and 3-4.

#### Deprotection of Aryl 2,3:4,6-Di-*O*-Cyclohexylidene- $\beta$ -D-Mannopyranosides

Each aryl di-*O*-cyclohexylidene- $\beta$ -mannopyranoside (1-2 g) was suspended in dry methanol (100 mL), chilled to 0°C and the vessel purged with dry nitrogen. Acetyl chloride (4 mL) was added dropwise with stirring via syringe. The reaction was maintained at 4°C overnight whereupon TLC indicated complete deprotection. The solvent was evaporated *in vacuo* followed by several evaporations of dry diethyl ether to remove the bulk of the HCl. Acid stable

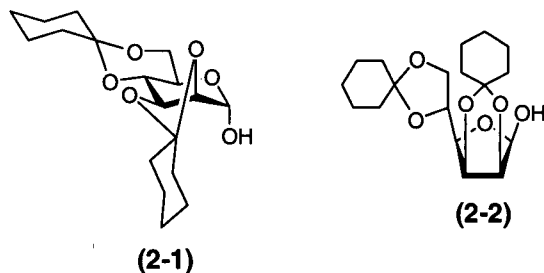
aryl  $\beta$ -mannosides ( $\text{pK}_a^{\text{lg}} \leq 7$ ) typically crystallized spontaneously during this process and could be isolated accordingly. Acid sensitive aryl  $\beta$ -mannosides ( $\text{pK}_a^{\text{lg}} > 7$ ) required immediate passage through a silica gel column to remove trace HCl or rapid hydrolysis would ensue.  $^1\text{H}$  NMR data for aryl  $\beta$ -D-mannopyranosides can be found in Table 3-5.

**1-Methoxy-1-cyclohexene**<sup>294,295</sup>



Trimethyl orthoformate (554 mL, 5.06 mol, 1.05 eq.) was added slowly to a  $0^\circ\text{C}$  solution of cyclohexanone (500 mL, 4.82 mol) and tosic acid (5 g) then allowed to stand at room temperature for 20 hrs.. 1-Methoxy-1-cyclohexene was obtained by fractional distillation (337 g, 62% yield, 95% pure by GC). b.p. =  $137\text{-}140^\circ\text{C}$  (lit.  $137\text{-}138^\circ\text{C}$ ).<sup>295</sup>  $^1\text{H}$  NMR (200 MHz,  $\text{CDCl}_3$ ):  $\delta$  4.58 (t,  $J = 3.5, 3.5$  Hz, 1 H, allylic H), 3.50 (s, 3 H, -OMe), 2.00 (m, 4 H, allylic  $\text{CH}_2$ ), 1.60 (m, 4 H, homoallylic  $\text{CH}_2$ ).

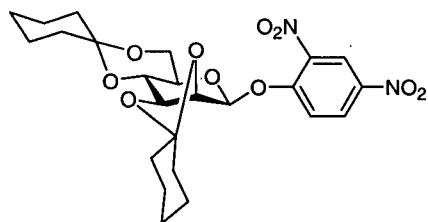
**2,3:4,6-Di-O-cyclohexylidene  $\alpha$ -D-mannopyranose (2-1) and 2,3:5:6-di-O-cyclohexylidene D-mannofuranose (2-2)**<sup>140,296</sup>



D-Mannose (94.3 g, 0.523 mol) and tosic acid (2.5 g) were dissolved in dry DMF (500 mL). 1-Methoxy-1-cyclohexene (238 g, 2.12 mol, 4 eq.) was added dropwise and the reaction subsequently maintained at  $40^\circ\text{C}$  on a rotovap (30 mm Hg) for 30 min.. TLC indicated completion of reaction. Sodium bicarbonate (6 g) was added and the reaction mixture concentrated under high vacuum. The crude was diluted in diethyl ether (1.2 L), washed with water and brine, dried over  $\text{MgSO}_4$ , then concentrated *in vacuo*. Recrystallization of the crude material from petroleum ether provided 2,3:4,6-di-O-isopropylidene  $\alpha$ -D-mannopyranose (2-1) (54 g, 30%). Subsequent recrystallizations of the crude material furnished 2,3:5:6-di-O-

cyclohexylidene D-mannofuranose (**2-2**) (40 g, 20%). The pyranoside derivative proved to be highly acid sensitive and readily rearranged in acidic  $\text{CDCl}_3$  to the thermodynamically stable furanoside. **Data for 2-1:** Rf (4:1 petroleum ether/EtOAc) = 0.33; m.p.: 171-173°C (lit. 174-175°C);<sup>140</sup>  $^1\text{H}$  NMR (400 MHz,  $\text{CDCl}_3$ ):  $\delta$  5.43 (d, 1 H,  $J$  = 3.2 Hz, H-1), 4.17 (m, 2 H, H-2,3), 3.83 (m, 1 H, H-5), 3.75 (m, 2 H, 2  $\times$  H-6), 2.60 (d, 1 H,  $J$  = 3.2 Hz, -OH, disappears upon addition of  $\text{D}_2\text{O}$ ), 1.9 and 1.7-1.3 (m, 20 H, 2  $\times$  cyclohexylidene), Anal. calcd. for  $\text{C}_{18}\text{H}_{28}\text{O}_6$  (340.41): C, 63.51; H, 8.29. Found: C, 63.51; H, 8.18. **Data for 2-2:** Rf (4:1 petroleum ether/EtOAc) = 0.38;  $^1\text{H}$  NMR (200 MHz,  $\text{CDCl}_3$ ):  $\delta$  5.37 (d, 1 H,  $J$  = 2.2 Hz, H-1), 4.76 (dd, 1 H,  $J$  = 3.5, 5.8 Hz, H-3), 4.57 (d, 1 H,  $J$  = 5.9 Hz, H-2), 4.40 (ddd, 1 H,  $J$  = 5.9, 5.9, 5.9 Hz, H-5), 4.23 (dd, 1 H,  $J$  = 3.6, 5.9 Hz, H-4), 4.02 (m, 2 H,  $J$  = 5.9 Hz, 2  $\times$  H-6), 2.72 (d, 1 H,  $J$  = 2.3 Hz, -OH), 1.7-1.2 (m, 20 H, 2  $\times$  cyclohexylidene).

**2,4-Dinitrophenyl 2,3:4,6-di-O-cyclohexylidene- $\beta$ -D-mannopyranoside (and  $\alpha$ -anomer)**



Protected **2-1** (1.0 g, 2.94 mmol) was reacted with 2,4-dinitrophenol according to the Mitsunobu protocol above. After work-up the crude mixture was loaded onto a silica gel column as a concentrated DCM solution and eluted with a gradient of 15:10:1 to 5:4:1 DCM/PE/EtOAc to obtain brittle foams for both anomers (0.57 g  $\beta$ -anomer, 0.22 g  $\alpha$ -anomer,  $\beta/\alpha$  = 2.6:1, 0.79 g total, 1.56 mmol, 53%). Rf  $\beta$ -anomer (5:4:1 DCM/PE/EtOAc) = 0.48; Rf  $\alpha$ -anomer (5:4:1 DCM/PE/EtOAc) = 0.82.  $^1\text{H}$  and  $^{13}\text{C}$  NMR data for the  $\beta$ -anomer can be found in Tables 3-3 and 3-4. Anal. calcd. for  $\text{C}_{24}\text{H}_{30}\text{N}_2\text{O}_{10}$  (506.5): C, 56.91; H, 5.97; N, 5.53. Found: C, 57.21; H, 6.07; N, 5.32; ESI-MS:  $m/z$  = 507.5 [ $\text{M} + \text{H}$ ]<sup>+</sup>.  $^1\text{H}$  NMR data for  $\alpha$ -anomer (200 MHz,  $\text{CDCl}_3$ ):  $\delta$  8.73 (d, 1 H,  $J$  = 2.8 Hz, H-3 Ph), 8.40 (dd, 1 H,  $J$  = 2.7, 9.3 Hz, H-5 Ph), 7.45 (d, 1 H,  $J$  = 9.3 Hz, H-6 Ph), 5.98 (d, 1 H,  $J$  < 1 Hz, H-1), 4.42 (dd, 1 H,  $J$  = 5.6, < 1 Hz, H-2), 4.32 (dd, 1 H,  $J$  = 5.6, 7.8 Hz, H-3), 3.82 (dd, 1 H,  $J$  = 7.8, 9.5 Hz, H-4), 3.77-3.54 (m, 3 H, H-5, 2  $\times$  H-6).

***2,5-Dinitrophenyl 2,3:4,6-di-O-cyclohexylidene- $\beta$ -D-mannopyranoside***

Protected **2-1** (2.55 g, 7.50 mmol) was reacted with 2,5-dinitrophenol according to the Mitsunobu protocol above. After work-up the crude mixture was loaded onto a silica gel column as a concentrated DCM solution and eluted with 10:1 PE/EtOAc to obtain  $\beta$ - and  $\alpha$ -anomers as brittle foams (1.98 g  $\beta$ -anomer, 0.85 g  $\alpha$ -anomer, 2.83 g total, 5.59 mmol, 74%,  $\beta/\alpha = 2.3:1$ ). Rf  $\beta$ -anomer (4:1 PE/EtOAc) = 0.50; Rf  $\alpha$ -anomer (4:1 PE/EtOAc) = 0.62. Anal. calcd. for  $C_{24}H_{30}N_2O_{10}$  (506.5): C, 56.91; H, 5.97; N, 5.53. Found for the  $\beta$ -anomer: C, 57.01; H, 5.95; N, 5.35.

***4-Chloro-2-nitrophenyl 2,3:4,6-di-O-cyclohexylidene- $\beta$ -D-mannopyranoside***

Protected **2-1** (2.0 g, 5.88 mmol) was reacted with 4-chloro-2-nitrophenol according to the Mitsunobu protocol above. After the usual work-up the crude material was absorbed onto silica gel, applied to a silica gel column and eluted with 10:1 PE/EtOAc. Both anomers were obtained as brittle foams following evaporation of solvent (1.46 g  $\beta$ -anomer, 2.94 mmol, 50%). Rf  $\beta$ -anomer (10:1 PE/EtOAc) = 0.11; Rf  $\alpha$ -anomer (10:1 PE/EtOAc) = 0.38. Anal. calcd. for  $C_{24}H_{30}ClNO_8$  (495.9): C, 58.12; H, 6.10; N, 2.82. Found for the  $\beta$ -anomer: C, 57.87; H, 6.17; N, 2.70.

***4-Nitrophenyl 2,3:4,6-di-O-cyclohexylidene- $\beta$ -D-mannopyranoside***

Protected **2-1** (2.8 g, 8.23 mmol) was reacted with 4-nitrophenol according to the Mitsunobu protocol above. Following work-up the crude material was loaded onto a silica gel column as a concentrated DCM solution and eluted with a gradient of 10:1 to 4:1 PE/EtOAc. Evaporation of the solvent afforded  $\beta$ - and  $\alpha$ -anomers as brittle foams (1.90 g  $\beta$ -anomer, 4.12 mmol, 50%). Rf  $\beta$ -anomer (4:1 PE/EtOAc) = 0.51; Rf  $\alpha$ -anomer (4:1 PE/EtOAc) = 0.65. Anal. calcd. for  $C_{24}H_{31}NO_8$  (461.5): C, 62.46; H, 6.77; N, 3.03. Found for the  $\beta$ -anomer: C, 62.28; H, 6.77; N, 2.98.

***3-Nitrophenyl 2,3:4,6-di-O-cyclohexylidene- $\beta$ -D-mannopyranoside***

Protected **2-1** (3.0 g, 8.81 mmol) was reacted with 3-nitrophenol according to the Mitsunobu protocol above. Following work-up the crude material was absorbed onto a silica gel, applied to a silica gel column and eluted with 6:1 PE/EtOAc. Evaporation of the solvent afforded brittle foams for both anomers (3.14 g  $\beta$ -anomer, 0.24 g  $\alpha$ -anomer, 3.38 g total, 7.32 mmol, 83%,  $\beta/\alpha =$

13:1). Rf  $\beta$ -anomer (6:1 PE/EtOAc) = 0.24; Rf  $\alpha$ -anomer (6:1 PE/EtOAc) = 0.36. Anal. calcd. for  $C_{24}H_{31}NO_8$  (461.5): C, 62.46; H, 6.77. Found for the  $\beta$ -anomer: C, 62.25; H, 6.90.

***4-Bromophenyl 2,3:4,6-di-O-cyclohexylidene- $\beta$ -D-mannopyranoside***

Protected **2-1** (2.0 g, 5.96 mmol) was reacted with 4-bromophenol according to the Mitsunobu protocol above. After work-up, the crude material was repetitively (3  $\times$ ) purified by silica gel chromatography (10:1 PE/EtOAc). Evaporation of the solvent afforded both anomers as pale yellow solids (0.72 g  $\beta$ -anomer, 0.15 g  $\alpha$ -anomer, 0.87 g total, 1.76 mmol, 29%,  $\beta/\alpha$  = 4.8:1). Anal. calcd. for  $C_{24}H_{31}BrO_6$  (495.4): C, 58.19; H, 6.31. Found for the  $\beta$ -anomer: C, 58.37; H, 6.30.

***4-Chlorophenyl 2,3:4,6-di-O-cyclohexylidene- $\beta$ -D-mannopyranoside***

Protected **2-1** (3.0 g, 8.81 mmol) was reacted with freshly distilled 4-chlorophenol according to the Mitsunobu protocol above. Following the usual work-up the crude material was absorbed onto silica gel, applied to a silica gel column and eluted with a gradient of 40:3 to 10:1 PE/EtOAc. Evaporation of solvent afforded both anomers as solids that would not recrystallize (2.98 g  $\beta$ -anomer, 0.40 g  $\alpha$ -anomer, 3.38 g total, 7.51 mmol, 85%,  $\beta/\alpha$  = 7.5:1). Rf  $\beta$ -anomer (10:1 PE/EtOAc) = 0.31; Rf  $\alpha$ -anomer (10:1 PE/EtOAc) = 0.55. Anal. calcd. for  $C_{24}H_{31}ClO_6$  (450.9): C, 63.92; H, 6.93. Found for the  $\beta$ -anomer: C, 64.10; H, 7.11.

***4-Cyanophenyl 2,3:4,6-di-O-cyclohexylidene- $\beta$ -D-mannopyranoside***

Protected **2-1** (2.0 g, 5.96 mmol) was reacted with 4-cyanophenol according to the Mitsunobu protocol above. After the usual work-up the crude material was purified by silica gel chromatography (10:1 PE/EtOAc). Evaporation of the solvent afforded both anomers as solids that would not recrystallize (2.01 g  $\beta$ -anomer, 0.22 g  $\alpha$ -anomer, 2.23 g total, 5.05 mmol, 85%,  $\beta/\alpha$  = 9.1:1). Anal. calcd. for  $C_{25}H_{31}NO_6$  (441.5): C, 68.01; H, 7.08; N, 3.17. Found for the  $\beta$ -anomer: C, 67.75; H, 7.21; N, 3.38.  $^1H$  NMR data for the  $\alpha$ -anomer (400 MHz,  $CDCl_3$ ):  $\delta$  7.58 (d, 2 H,  $J$  = 8.9 Hz, H-3,5 Ph), 7.07 (d, 2 H,  $J$  = 8.9 Hz, H-2,6 Ph), 5.83 (d, 1 H,  $J$  < 1 Hz, H-1), 4.36 (dd, 1 H,  $J$  = 5.5, < 1 Hz, H-2), 4.28 (dd, 1 H,  $J$  = 5.6, 7.9 Hz, H-3), 3.81 (dd, 1 H,  $J$  = 8.0, 10.1 Hz, H-4), 3.71 (m, 2 H, 2  $\times$  H-6), 3.60 (ddd, 1 H,  $J$  = 6.1, 9.8, 9.8 Hz, H-5), 1.90 and 1.8-1.3 (m, 20 H, 2  $\times$  cyclohexylidene).

***Phenyl 2,3:4,6-di-O-cyclohexylidene- $\beta$ -D-mannopyranoside***

Protected **2-1** (3.0 g, 8.81 mmol) was reacted with freshly distilled phenol according to the Mitsunobu protocol above. Following work-up the crude material was absorbed onto silica gel, applied to a silica gel column and eluted with a gradient of 40:3 to 10:1 PE/EtOAc. Evaporation of the solvent afforded  $\beta$ - and  $\alpha$ -anomers as brittle foams (1.75 g  $\beta$ -anomer, 0.29 g  $\alpha$ -anomer, 2.04 g total, 4.90 mmol, 56%,  $\beta/\alpha = 6:1$ ). Rf  $\beta$ -anomer (4:1 PE/EtOAc) = 0.60; Rf  $\alpha$ -anomer (4:1 PE/EtOAc) = 0.67. Anal. calc. for C<sub>24</sub>H<sub>32</sub>O<sub>6</sub> (416.5): C, 69.21; H, 7.74. Found for the  $\beta$ -anomer: C, 69.03; H, 7.83.

***2,4-Dinitrophenyl  $\beta$ -D-mannopyranoside***

Deprotection of 1.90 g (3.75 mmol) of the protected mannoside was complete in 4 hrs. at 4°C in 4% HCl/MeOH. Rf (7:2:1 EtOAc/MeOH/H<sub>2</sub>O) = 0.65. White crystals formed spontaneously upon evaporation of HCl/MeOH (0.71 g, 2.05 mmol, 55%). Small, white needles were obtained by recrystallization from Et<sub>2</sub>O/MeOH (0.47 g, 1.35 mmol, 36%). Anal. calcd. for C<sub>12</sub>H<sub>14</sub>N<sub>2</sub>O<sub>10</sub> · H<sub>2</sub>O (346.25 + 18.02): C, 39.57; H, 4.43; N, 7.69. Found: C, 39.73; H, 4.29; N, 7.51. This product was remarkably base sensitive, rapidly rearranging to a UV active compound in alkaline solutions (Rf (7:2:1 EtOAc/MeOH/H<sub>2</sub>O) = 0.74). This is most likely the result of the base catalyzed migration of the 2,4-dinitrophenyl aglycone to the 2-hydroxyl.<sup>297</sup> For this reason solutions of 2,4-dinitrophenyl  $\beta$ -D-mannopyranoside were freshly prepared and buffered at pH 5-6.

***2,5-Dinitrophenyl  $\beta$ -D-mannopyranoside***

Deprotection of 1.90 g (3.75 mmol) of the protected mannoside was complete overnight at 4°C in 4% HCl/MeOH. A yellow solid was obtained upon evaporation of HCl/MeOH. Recrystallization 2 × from EtOH afforded small white crystals (0.280 g, 0.81 mmol, 21%). M.p. = 149-151°C. Rf (7:2:1 EtOAc/MeOH/H<sub>2</sub>O) = 0.60. Anal. calcd. for C<sub>12</sub>H<sub>14</sub>N<sub>2</sub>O<sub>10</sub> (346.25): C, 41.63; H, 4.08; N, 8.09. Found: C, 41.51; H, 4.09; N, 7.90.

***4-Chloro-2-nitrophenyl  $\beta$ -D-mannopyranoside***

Deprotection of 1.45 g (2.92 mmol) of the protected mannoside was complete overnight at 4°C in 4% HCl/MeOH. Small, pale yellow needles were obtained by recrystallization (2 ×) of the crude

solid from EtOH (0.329 g, 0.98 mmol, 34%). Rf (7:2:1 EtOAc/MeOH/H<sub>2</sub>O) = 0.60. Anal. calcd. for C<sub>12</sub>H<sub>14</sub>ClNO<sub>8</sub> (335.7): C, 42.94; H, 4.20; N, 4.17. Found: C, 43.00; H, 4.24; N, 4.14.

#### ***4-Nitrophenyl β-D-mannopyranoside***

Deprotection of 1.84 g (3.99 mmol) of the protected mannoside was complete overnight at 4°C in 4% HCl/MeOH. Evaporation of the solvent afforded a crude pale yellow solid that was recrystallized from EtOH to yield white needles (0.71 g, 2.36 mmol, 59%). Rf (7:2:1 EtOAc/MeOH/H<sub>2</sub>O) = 0.49. Anal. calcd. for C<sub>12</sub>H<sub>15</sub>NO<sub>8</sub> (301.25): C, 47.84; H, 5.02; N, 4.65. Found: C, 47.70; H, 5.09; N, 4.46.

#### ***3-Nitrophenyl β-D-mannopyranoside***

Deprotection of 2.98 g (6.62 mmol) of the protected mannoside was complete overnight at 4°C in 4% HCl/MeOH. A syrup was obtained upon evaporation of the solvent. Chromatography of the crude on silica gel (27:2:1 EtOAc/MeOH/H<sub>2</sub>O) and evaporation of the solvent afforded a white solid, which was recrystallized from EtOH to obtain hygroscopic white needles (0.843 g, 2.80 mmol, 42%). M.p. = 158-160°C. Rf (7:2:1 EtOAc/MeOH/H<sub>2</sub>O) = 0.49. Anal. calcd. for C<sub>12</sub>H<sub>15</sub>NO<sub>8</sub> (301.25): C, 47.84; H, 5.02; N, 4.65. Found: C, 47.93; H, 4.94; N, 4.44.

#### ***4-Chlorophenyl β-D-mannopyranoside***

Deprotection of 2.98 g (6.62 mmol) protected mannoside in 4% HCl/MeOH was complete overnight at 4°C. Evaporation of the solvent afforded a syrup that was subsequently purified by silica gel chromatography (27:2:1 EtOAc/MeOH/H<sub>2</sub>O). A white solid (0.97 g, 3.34 mmol, 50%) was obtained upon evaporation of the solvent, which was subsequently recrystallized from EtOH (0.748 g, 2.57 mmol, 39%). M.p. = 164-165°C. Rf (7:2:1 EtOAc/MeOH/H<sub>2</sub>O) = 0.55. Anal. calcd. for C<sub>12</sub>H<sub>15</sub>ClO<sub>6</sub> · 1/2 H<sub>2</sub>O (290.7 + 9.01): C, 48.09; H, 5.39. Found: C, 48.21; H, 5.59.

#### ***Phenyl β-D-mannopyranoside***

Deprotection of 1.75 g (4.20 mmol) of the protected mannoside was complete overnight at 4°C in 4% HCl/MeOH. Evaporation of the solvent afforded a syrup that was purified by silica gel chromatography (100% EtOAc to 27:2:1 EtOAc/MeOH/H<sub>2</sub>O). A white solid was obtained that was recrystallized from Et<sub>2</sub>O/MeOH to afford white needles (0.77 g, 3.01 mmol, 71%). M.p. =

151-153°C. Rf (27:2:1 EtOAc/MeOH/H<sub>2</sub>O) = 0.23. Anal. calcd. for C<sub>12</sub>H<sub>16</sub>O<sub>6</sub> · 1/4 H<sub>2</sub>O (256.26 + 4.50): C, 55.27; H, 6.20. Found: C, 55.52; H, 6.42.

**Table 3-3:**  $^1\text{H}$  NMR data for aryl 2,3:4,6-di-*O*-cyclohexylidene  $\beta$ -D-mannopyranosides (400 MHz,  $\text{CDCl}_3$ ). Multiplicity and coupling constants (Hz) are given in parentheses. Chemical shifts referenced internally to the solvent. For 2  $\times$  cyclohexylidene:  $\delta$  2.0-1.3 (m, 20 H).

	2,4-dinitro	2,5-dinitro	4-chloro, 2-nitro	4-nitro	3-nitro
<b>H-2 Ph</b>	-	-	-	7.09 (d, 9.2)	7.87 (s)
<b>H-3 Ph</b>	8.67 (d, 2.8)	7.86 (d, 8.8)	7.77 (d, 2.6)	8.19 (d, 9.2)	-
<b>H-4 Ph</b>	-	7.95 (dd, 2.3, 8.8)	-	-	7.88 (d, 8.1)
<b>H-5 Ph</b>	8.37 (dd, 2.8, 9.3)	-	7.44 (dd, 2.6, 9.0)	as for H-3	7.43 (dd, 8.0, 8.0)
<b>H-6 Ph</b>	7.33 (d, 9.3)	8.09 (d, 2.2)	7.17 (d, 9.0)	as for H-2	7.34 (d, 8.0)
<b>H-1</b>	5.81 (d, 3.2)	5.76 (d, 3.2)	5.56 (d, 3.2)	5.57 (d, 3.1)	5.53 (d, 3.0)
<b>H-2</b>	4.48 (dd, 3.2, 7.9)	4.49 (dd, 3.2, 7.8)	4.44 (dd, 3.2, 7.7)	4.44 (dd, 3.2, 6.9)	4.43 (dd, 3.1, 6.6)
<b>H-3</b>	4.40 (dd, 7.5, 7.5)	4.40 (dd, 7.4, 7.4)	4.35 (dd, 7.4, 7.4)	4.36 (m)	4.35 (m)
<b>H-4</b>	4.64 (dd, 7.3, 10.2)	4.58 (dd, 7.1, 10.3)	4.59 (dd, 7.1, 10.7)	4.36 (m)	4.35 (m)
<b>H-5</b>	3.58 (m)	3.56 (ddd, 4.5, 10.3, 10.3)	3.49 (ddd, 5.3, 10.5, 10.5)	3.51 (ddd, 4.8, 10.1, 10.1)	3.51 (ddd, 5.1, 10.1, 10.1)
<b>H-6<sub>eq</sub></b>	3.87 (m)	3.90 (dd, 4.5, 10.2)	3.85 (dd, 5.3, 10.7)	3.90 (dd, 4.1, 9.6)	3.91 (dd, 5.1, 10.6)
<b>H-6<sub>ax</sub></b>	3.58 (m)	3.61 (dd, 10.3, 10.3)	3.65 (dd, 10.5, 10.5)	3.56 (dd, 10.3, 10.3)	3.61 (dd, 10.4, 10.4)

	4-chloro	4-bromo	4-cyano	phenyl
<b>H-2 Ph</b>	6.95 (d, 9.0)	6.91 (d, 8.9)	7.07 (d, 8.9)	7.02 (m)
<b>H-3 Ph</b>	7.23 (d, 9.0)	7.37 (d, 8.9)	7.57 (d, 8.9)	7.28 (dd, 7.3, 8.8)
<b>H-4 Ph</b>	-	-	-	7.02 (m)
<b>H-5 Ph</b>	as for H-3	as for H-3	as for H-3	as for H-3
<b>H-6 Ph</b>	as for H-2	as for H-2	as for H-2	7.02 (m)
<b>H-1</b>	5.38 (d, 3.0)	5.39 (d, 3.0)	5.52 (d, 3.1)	5.42 (d, 3.0)
<b>H-2</b>	4.39 (dd, 3.0, 6.7)	4.39 (dd, 3.1, 6.5)	4.42 (dd, 3.1, 6.9)	4.41 (dd, 3.0, 6.7)
<b>H-3</b>	4.32 (m)	4.32 (m)	4.34 (m)	4.31 (dd, 6.9, 6.9)
<b>H-4</b>	4.32 (m)	4.32 (m)	4.34 (m)	4.36 (dd, 7.1, 10.2)
<b>H-5</b>	3.44 (ddd, 5.3, 10.1, 10.1)	3.44 (ddd, 5.3, 10.2, 10.2)	3.50 (ddd, 4.8, 9.9, 9.9)	3.44 (ddd, 5.4, 10.2, 10.2)
<b>H-6<sub>eq</sub></b>	3.89 (dd, 5.3, 10.8)	3.89 (dd, 5.3, 10.8)	3.88 (dd, 4.9, 10.4)	3.90 (dd, 5.4, 10.8)
<b>H-6<sub>ax</sub></b>	3.64 (dd, 10.5, 10.5)	3.62 (dd, 10.4, 10.4)	3.58 (dd, 10.3, 10.3)	3.67 (dd, 10.5, 10.5)

**Table 3-4:**  $^{13}\text{C}$  NMR data<sup>49</sup> for aryl 2,3:4,6-di-*O*-cyclohexylidene  $\beta$ -D-mannopyranosides (100 MHz,  $\text{CDCl}_3$ ). Assignments based on APT experiments. Chemical shifts internally referenced to the solvent.

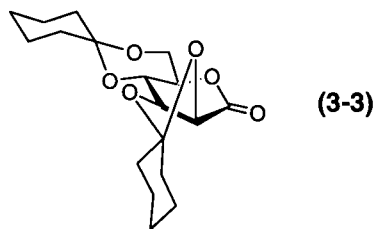
	<b>4-nitro</b>	<b>3-nitro</b>	<b>4-bromo</b>	<b>4-cyano</b>	<b>phenyl</b>
<b>C-R phenyl</b>	161.7, 142.6	157.5, 149.2	156.3, 114.9	160.2, 118.8	157.2
<b>C-H phenyl</b>	126.1, 116.3	130.1, 123.2, 117.4, 111.8	132.4, 118.8	134.0, 117.2	129.4, 122.5, 117.0
<b>C-1</b>	95.6	96.8	96.8	96.0	96.8
<b>C-2,3,4,5</b>	75.2, 72.8, 70.4, 66.4	75.7, 73.0, 70.5, 66.5	75.8, 73.2, 70.6, 66.4	75.6, 72.8, 70.4, 66.5	75.8, 73.4, 70.7, 66.3
<b>C-6</b>	62.6	62.4	62.4	62.4	62.4
<b>C cyclohexyl</b>	112.7, 99.9	112.5, 99.8	112.3, 99.8	112.5, 99.8	112.2, 99.8
<b>CH<sub>2</sub> cyclohexyl</b>	37.8, 36.5, 34.9, 27.7, 25.5, 25.0, 23.9, 23.6, 22.6, 22.4	37.8, 36.4, 35.0, 27.7, 25.6, 25.1, 24.0, 23.6, 22.7, 22.5	37.9, 36.6, 35.2, 27.7, 25.6, 25.1, 24.0, 23.6, 22.7, 22.4	37.8, 36.4, 35.0, 27.7, 25.6, 25.0, 23.9, 23.6, 22.7, 22.4	37.9, 36.7, 35.2, 27.7, 25.6, 25.1, 23.9, 23.6, 22.7, 22.4
<b>other</b>				105.8 (cyano)	

**Table 3-5:**  $^1\text{H}$  NMR data for aryl  $\beta$ -D-mannopyranosides (400 MHz,  $\text{CD}_3\text{OD}$ ). Multiplicity and coupling constants (Hz) are given in parentheses. Chemical shifts are referenced internally to the solvent.

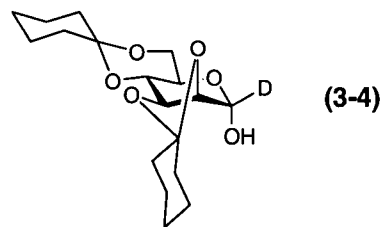
	2,4-dinitro	2,5-dinitro	4-chloro, 2-nitro	4-nitro	3-nitro
<b>H-2 Ph</b>	-	-	-	7.22 (d, 9.3)	7.92 (dd, 2.2, 2.2)
<b>H-3 Ph</b>	8.71 (d, 2.8)	8.00 (d, 8.8)	7.85 (d, 2.6)	8.21 (d, 9.3)	-
<b>H-4 Ph</b>	-	8.04 (dd, 2.0, 8.8)	-	-	7.88 (ddd, 1.2, 2.1, 7.9)
<b>H-5 Ph</b>	8.46 (dd, 2.8, 9.3)	-	7.59 (dd, 2.6, 9.0)	as for H-3	7.53 (dd, 8.1, 8.1)
<b>H-6 Ph</b>	7.64 (d, 9.4)	8.29 (d, 2.0)	7.49 (d, 9.0)	as for H-2	7.47 (ddd, 1.2, 2.4, 8.3)
<b>H-1</b>	5.50 (d, 0.8)	5.46 (d, < 1)	5.27 (d, 1.0)	5.35 (d, 0.9)	5.32 (d, 0.9)
<b>H-2</b>	4.12 (dd, 0.7, 3.0)	4.12 (dd, <1, 2.3)	4.10 (dd, 0.9, 3.1)	4.09 (dd, 0.9, 3.0)	4.10 (dd, 0.8, 3.1)
<b>H-3</b>	3.58 (dd, 3.0, 9.3)	3.59 (dd, 3.0, 9.3)	3.55 (dd, 3.1, 9.4)	3.59 (dd, 3.1, 9.4)	3.60 (dd, 3.0, 9.6)
<b>H-4</b>	3.65 (dd, 9.4, 9.4)	3.65 (dd, 9.3, 9.3)	3.64 (dd, 9.4, 9.4)	3.66 (dd, 9.4, 9.4)	3.67 (dd, 9.4, 9.4)
<b>H-5</b>	3.49 (ddd, 2.3, 6.2, 9.4)	3.48 (ddd, 2.3, 6.2, 9.4)	3.39 (ddd, 2.3, 6.1, 9.5)	3.45 (ddd, 2.3, 6.0, 9.3)	3.45 (ddd, 2.4, 6.0, 9.3)
<b>H-6<sub>eq</sub></b>	3.92 (dd, 2.3, 12.0)	3.92 (dd, 2.2, 12.1)	3.91 (dd, 2.3, 12.0)	3.91 (dd, 2.3, 12.0)	3.91 (dd, 2.3, 12.0)
<b>H-6<sub>ax</sub></b>	3.72 (dd, 6.2, 12.0)	3.73 (dd, 6.2, 12.1)	3.72 (dd, 6.1, 12.0)	3.72 (dd, 6.0, 12.0)	3.73 (dd, 6.0, 12.0)

	4-chloro	phenyl
<b>H-2 Ph</b>	7.05 (d, 9.1)	7.07 (d, 7.7)
<b>H-3 Ph</b>	7.25 (d, 9.1)	7.27 (dd, 7.4, 8.7)
<b>H-4 Ph</b>	-	6.98 (dd, 7.3, 7.3)
<b>H-5 Ph</b>	as for H-3	as for H-3
<b>H-6 Ph</b>	as for H-2	as for H-2
<b>H-1</b>	5.16 (d, 0.9)	5.19 (d, 0.8)
<b>H-2</b>	4.04 (dd, 0.7, 3.1)	4.05 (dd, 0.7, 3.1)
<b>H-3</b>	3.56 (dd, 3.2, 9.4)	3.56 (dd, 3.1, 9.4)
<b>H-4</b>	3.64 (dd, 9.5, 9.5)	3.66 (dd, 9.5, 9.5)
<b>H-5</b>	3.37 (ddd, 2.4, 5.9, 9.4)	3.38 (ddd, 2.4, 5.8, 9.5)
<b>H-6<sub>eq</sub></b>	3.89 (dd, 2.3, 12.0)	3.90 (dd, 2.4, 11.9)
<b>H-6<sub>ax</sub></b>	3.72 (dd, 5.9, 12.0)	3.73 (dd, 5.8, 12.0)

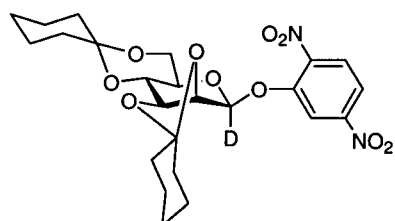
**2,3:4,6-Di-O-cyclohexylidene-D-mannolactone (3-3)**

Oxalyl chloride (8.57g, 67.5 mmol, 1.1 eq.) was dissolved in dry DCM (100 mL) and cooled to  $-78^{\circ}\text{C}$  under dry  $\text{N}_2$  in a 3-neck round bottom flask. From an addition funnel DMSO (10.0 mL, 116 mmol, 2 eq.) diluted in dry DCM (30 mL) was added dropwise with stirring. Subsequently 20 g (58.8 mmol) of **3-1** in DCM (275 mL) was added via canula over a period of 5 min. After stirring for 25 min., triethylamine (40 mL,  $\sim 5$  eq.) was added via syringe and the reaction mixture allowed to warm to room temperature. TLC (4:1 PE/EtOAc) indicated essentially complete conversion of **3-1** to a product with a higher  $R_f$  value. The reaction mixture was washed with water and brine then dried over  $\text{MgSO}_4$ . Evaporation of the solvent afforded a yellow solid. Recrystallization from PE/EtOAc afforded large, granular, transparent crystals of the lactone (**3-3**) (14.45 g, 42.7 mmol, 73%).  $R_f$  (4:1 PE/EtOAc) = 0.45;  $^1\text{H}$  NMR (400 MHz,  $\text{CDCl}_3$ ):  $\delta$  4.71 (d, 1 H,  $J = 8.4$  Hz, H-2), 4.56 (dd, 1 H,  $J = 6.2, 8.3$  Hz, H-3), 4.04 (m, 1 H, H-6eq.), 4.03 (ddd, 1 H,  $J = 5.6, 9.7, 11.4$  Hz, H-5), 3.88 (dd, 1 H,  $J = 6.3, 9.5$  Hz, H-4), 3.83 (m, 1 H, H-6ax), 2.05 (m, 1 H, cyclohexylidene), 1.85 (m, 1 H, cyclohexylidene), 1.75-1.33 (m, 18 H,  $2 \times$  cyclohexylidene);  $^{13}\text{C}$  NMR (100 MHz,  $\text{CDCl}_3$ ):  $\delta$  168.9 (C-1), 113.6, 100.2 ( $2 \times$  ROCOR' cyclohexylidene), 76.7, 72.0, 72.9, 67.5 (C-2,3,4,5), 60.7 (C-6), 37.5, 36.3, 34.7, 27.5, 25.4, 24.8, 23.7, 23.5, 22.6, 22.4 ( $\text{CH}_2$  cyclohexylidene); Anal. calcd. for  $\text{C}_{18}\text{H}_{26}\text{O}_6$  (338.4): C, 63.89; H, 7.74. Found: C, 63.99; H, 7.99.

**2,3:4,6-Di-O-cyclohexylidene- $\alpha$ -D-[1- $^2\text{H}$ ]-mannopyranose (3-4)<sup>298</sup>**

The mannlactone (**3-3**) (15.12 g, 44.7 mmol) was dissolved in dry THF (200 mL) and cooled to 0°C under dry N<sub>2</sub>. A solution of sodium borodeuteride (0.765 g, 20.2 mmol, 0.45 eq.) in D<sub>2</sub>O (6 mL) was added dropwise and the reaction stirred for 3 hrs.. The solvent was evaporated and the crude product redissolved in DCM, washed with water and brine, then dried over MgSO<sub>4</sub>. Evaporation of the solvent afforded deuterium labeled **3-4** as a white solid (13.7 g, 40.2 mmol, 90%) that was used without further purification. R<sub>f</sub> (4:1 PE/EtOAc) = 0.30; <sup>1</sup>H NMR (400 MHz, CDCl<sub>3</sub>) agreed with that of **3-1**. Integration of δ 5.43 (H-1) indicated 97% incorporation of deuterium at C-1.

**2,5-Dinitrophenyl 2,3:4,6-di-O-cyclohexylidene-β-D-[1-<sup>2</sup>H]-mannopyranoside**



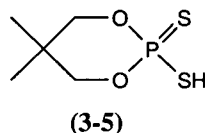
Deuterium labeled **3-4** (3.0 g, 8.79 mmol) was reacted with 2,5-dinitrophenol using the Mitsunobu protocol described above. Following the usual work-up the crude product was purified by silica gel chromatography (9:1 to 8:1 PE/EtOAc). Evaporation of the solvent afforded β- and α-anomers as brittle foams (2.42 g β-anomer, 0.49 g α-anomer, 2.91 g total, 5.73 mmol, 65%, β/α = 4.9:1). <sup>1</sup>H NMR (400 MHz, CDCl<sub>3</sub>): δ 8.09 (d, 1 H, *J* = 2.2 Hz, H-6 Ph), 7.95 (dd, 1 H, *J* = 2.2, 8.8 Hz, H-4 Ph), 7.86 (d, 1 H, *J* = 8.8 Hz, H-3 Ph), 5.76 (d, 3% abundant, *J* = 3 Hz, H-1), 4.59 (dd, 1 H, *J* = 7.2, 10.3 Hz, H-4), 4.48 (d, 1 H, *J* = 7.9 Hz, H-2), 4.40 (dd, 1 H, *J* = 7.4, 7.4 Hz, H-3), 3.89 (m, 1 H, H-6eq), 3.62 (dd, 1-H, *J* = 10.3, 10.3 Hz, H-6ax), 3.57 (ddd, 1 H, *J* = 4.5, 10.3, 10.3 Hz, H-5), 1.7-1.3 (m, 20 H, 2 × cyclohexylidene). Anal. calcd. for C<sub>24</sub>H<sub>29</sub>DN<sub>2</sub>O<sub>10</sub> (507.5): C, 56.8; H + D, 6.16; N, 5.52. Found: C, 57.18; H + D, 6.17; N, 5.30.

**2,5-Dinitrophenyl β-D-[1-<sup>2</sup>H]-mannopyranoside**

Deprotection of 2.41 g (4.75 mmol) deuterium labelled **3-4** in 4% HCl/MeOH was complete in 9 hrs. at 0°C. Evaporation of the solvent afforded a yellow solid that was recrystallized from EtOH to afford off white small needles (0.693 g, 1.99 mmol, 42%). M.p. = 145-148°C; R<sub>f</sub> (7:2:1 EtOAc/MeOH/H<sub>2</sub>O) = 0.67; <sup>1</sup>H NMR (400 MHz, CD<sub>3</sub>OD): δ 8.29 (d, 1 H, *J* = 2.1 Hz, H-6 Ph), 8.04 (dd, 1 H, *J* = 2.1, 8.8 Hz, H-4 Ph), 8.00 (d, 1 H, *J* = 8.8 Hz, H-3 Ph), 5.47 (d, 3% abundant,

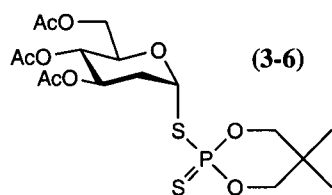
$J = 3$  Hz, H-1), 4.12 (d, 1 H,  $J = 3$  Hz, H-2), 3.92 (dd, 1 H,  $J = 2.3, 12.1$  Hz, H-6a), 3.73 (dd, 1 H,  $J = 6.3, 12.1$  Hz, H-6b), 3.66 (dd, 1 H,  $J = 9.3, 9.3$  Hz, H-4), 3.59 (dd, 1 H,  $J = 3.1, 9.3$  Hz, H-3), 3.48 (ddd, 1 H,  $J = 2.3, 6.3, 9.0$  Hz, H-5). Anal. calcd. for  $C_{12}H_{13}DN_2O_{10}$  (347.26): C, 41.51; H + D, 4.35; N, 8.07. Found: C, 41.13; H + D, 4.18; N, 7.89.

**2-Mercapto-5,5-dimethyl-2-thioxo-1,3,2-dioxaphosphorinane (3-5)**<sup>145</sup>



Phosphorus pentasulfide (24.1 g, 108 mmol) was stirred as a suspension in dry toluene (80 mL) at 70°C. 2,2-Dimethyl-1,3-propanediol (22.6 g, 217 mmol, 2 eq.) was partially dissolved in hot toluene (130 mL) and added portion-wise. The mixture was then refluxed for 2.5 hrs, during which time the solution clarified. The solvent was evaporated to afford **3-5** as an off white solid which was recrystallized from PE/toluene to afford large cubes and needles (27.8 g, 140 mmol, 65% based on propanediol). M.p. = 76-78°C (lit. 81-82°C);<sup>145</sup>  $^1\text{H}$  NMR (200 MHz,  $\text{CDCl}_3$ ):  $\delta$  4.05 (d, 4 H,  $J_{P,H} = 15.7$  Hz,  $2 \times \text{CH}_2$ ), 3.00 (s, 1 H, RSH), 1.08 (s, 6 H,  $2 \times \text{CH}_3$ );  $^{31}\text{P}$  NMR (81 MHz,  $\text{CDCl}_3$ , H-coupled, referenced to  $\text{H}_3\text{PO}_4$ )  $\delta$  76.5 (quintet,  $J_{P,H} = 15.3$  Hz).

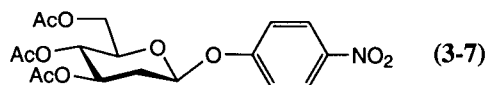
**5,5-Dimethyl-2-thioxo-2-(3,4,6-tri-O-acetyl-2-deoxy- $\alpha$ -D-arabino-hexopyranosylthio)-1,3,2-dioxaphosphorinane (3-6)**<sup>146</sup>



Tri-*O*-acetyl-D-glucal (20 g, 73.4 mmol) was dissolved in dry benzene (200 mL) and cooled to 0°C. A solution of the phosphorodithioic acid (**3-5**) in benzene (100 mL) was gradually added via canula. Clean conversion of D-glucal was noted after 24 hrs.. The solvent was evaporated and the resulting residue redissolved in EtOAc (400 mL), washed with saturated sodium bicarbonate and water, then dried over  $\text{MgSO}_4$ . Pure **3-6** was obtained by recrystallization ( $2 \times$ ) from PE/EtOAc (11.6 g, 23.8 mmol, 32%). The remaining pale yellow solid was a mixture of anomers (21.5g, 44.2 mmol, 60%). Rf  $\beta$ -anomer (1:2 PE/EtOAc) = 0.78; Rf  $\alpha$ -anomer (1:2

PE/EtOAc) = 0.83;  $^1\text{H}$  NMR (400 MHz,  $\text{CDCl}_3$ ):  $\delta$  6.11 (ddd, 1 H,  $J_{\text{H1,P}} = 10.4$  Hz,  $J_{\text{H1,H2ax}} = 4.6$  Hz,  $J_{\text{H1,H2eq}} < 1$  Hz, H-1), 5.22 (ddd, 1 H,  $J_{\text{H3,H2eq}} = 5.2$  Hz,  $J_{\text{H3,H4}} = 9.5$  Hz,  $J_{\text{H3,H2ax}} = 11.6$  Hz, H-3), 5.01 (dd, 1 H,  $J = 9.8, 9.8$  Hz, H-4), 4.32 (dd, 1 H,  $J = 4.9, 12.2$  Hz, H-6a), 4.13 (m, 3 H, H-5,  $\text{RCH}_2\text{OP}$ ), 4.03 (dd, 1 H,  $J = 2.4, 12.2$  Hz, H-6b), 3.96 (m, 2 H,  $\text{RCH}_2\text{OP}$ ), 2.42 (ddd, 1 H,  $J_{\text{H2eq,H2ax}} = 13.7$  Hz,  $J_{\text{H2eq,H3}} = 5.0$  Hz,  $J_{\text{H2eq,H1}} < 1$  Hz, H-2eq), 2.28 (dddd,  $J_{\text{H2ax,P}} = 3.0$  Hz,  $J_{\text{H2ax,H1}} = 5.2$  Hz,  $J_{\text{H2ax,H3}} = 11.6$  Hz,  $J_{\text{H2eq,H2ax}} = 13.7$  Hz, H-2ax), 2.05, 2.03, 2.01 (3  $\times$  s, 9 H, 3  $\times$  OAc), 1.24, 0.93 (2  $\times$  s, 6 H, 2  $\times$  Me);  $^{13}\text{C}$  NMR (100 MHz,  $\text{CDCl}_3$ ):  $\delta$  170.5, 170.0, 169.5 (3  $\times$  C=O), 84.3 (s, C-1), 78.09 (d,  $J_{\text{C,P}} = 9.1$  Hz,  $\text{CH}_2\text{OP}$ ), 77.2 (d,  $J_{\text{C,P}} = 9.2$  Hz,  $\text{CH}_2\text{OP}$ ), 70.9, 69.1, 68.9 (C-3,4,5), 62.0 (C-6), 36.6 (d,  $J_{\text{C,P}} = 8.1$  Hz, C-2), 32.4 (d,  $J_{\text{C,P}} = 6.5$  Hz,  $\text{C}(\text{CH}_3)_2$ ), 22.03, 20.87, 20.76, 20.62, 20.56 (5  $\times$  s, 5  $\times$   $\text{CH}_3$ );  $^{31}\text{P}$  NMR (121.5 MHz,  $\text{CDCl}_3$ , ref. to  $\text{H}_3\text{PO}_4$ ):  $\delta$  84.3; Anal. calcd. for  $\text{C}_{17}\text{H}_{27}\text{O}_9\text{PS}_2$  (470.49): C, 43.40; H, 5.78. Found: C, 43.63; H, 5.94.

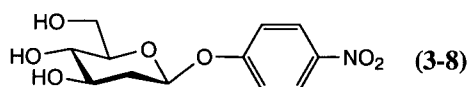
**4-Nitrophenyl 3,4,6-tri-O-acetyl-2-deoxy- $\beta$ -D-arabino-hexopyranoside (3-7)**<sup>143</sup>



The dioxaphosphorinane (**3-6**) (2.24 g, 4.76 mmol) was suspended in 10:1 dry isopropanol / benzene (55 mL) along with 4-nitrophenolate bound to Amberlyst A-26 resin (2.9 g,  $\sim 1.7$  mmol phenoxide/g resin).<sup>299</sup> The mixture was stirred under argon for 7 days whereupon a second portion of phenoxide resin was added (2.7 g). The reaction was stirred for another 6 days when TLC indicated completion. The reaction mixture was filtered through Celite and the solvent evaporated. The concentrate was redissolved in DCM, washed with saturated sodium bicarbonate and water, then dried over  $\text{MgSO}_4$ . Evaporation of the solvent afforded a residue that was recrystallized from PE/EtOAc to obtain white flakes of pure **3-7** (1.07 g, 2.60 mmol, 55%). A second crop of white crystals obtained from EtOH proved to be a mixture of anomers (0.16 g, 0.39 mmol, 8%) Pure  $\alpha$ -anomer could be obtained by further recrystallization. **Data for 3-7:** Rf (2:1 toluene/EtOAc) = 0.58;  $^1\text{H}$  NMR for (400 MHz,  $\text{CDCl}_3$ ):  $\delta$  8.18 (d, 2 H,  $J = 9.3$  Hz, H-3,5 Ph), 7.05 (d, 2 H,  $J = 9.0$  Hz, H-2,6 Ph), 5.30 (dd, 1 H,  $J = 2.3, 9.3$  Hz, H-1), 5.11 (ddd, 1 H,  $J = 5.2, 9.2, 11.1$  Hz, H-3), 5.04 (dd, 1 H,  $J = 9.2, 9.2$  Hz, H-4), 4.28 (dd, 1 H,  $J = 5.8, 12.2$  Hz, H-6a), 4.14 (dd, 1 H,  $J = 2.7, 12.2$  Hz, H-6b), 3.82 (ddd, 1 H,  $J = 2.4, 5.8, 8.9$  Hz, H-5), 2.54 (ddd, 1 H,  $J = 2.3, 5.0, 12.7$  Hz, H-2eq), 2.06 (ddd, 1 H,  $J = 9.4, 11.0, 12.8$  Hz, H-2ax), 2.049, 2.044, 2.038 (all s, 9 H, 3  $\times$  OAc);  $^{13}\text{C}$  NMR (100 MHz,  $\text{CDCl}_3$ ):  $\delta$  170.4, 170.1, 169.6 (3  $\times$

CH<sub>3</sub>CO), 161.3 (C-4'), 143.0 (C-1'), 125.7 (C-3',5'), 116.4 (C-2',6'), 96.6 (C-1), 72.6, 69.8, 68.6 (C-3,4,5), 62.4 (C-6), 35.4 (C-2), 20.8, 20.6 (2 lines) (3 × CH<sub>3</sub>CO). **Data for α-anomer:** R<sub>f</sub> (2:1 toluene/EtOAc) = 0.64; <sup>1</sup>H NMR (400 MHz, CDCl<sub>3</sub>): δ 8.18 (d, 2 H, *J* = 9.2 Hz, H-3,5 Ph), 7.16 (d, 2 H, *J* = 9.1 Hz, H-2,6 Ph), 5.74 (app. d, 1 H, *J* = 2.4 Hz, H-1), 5.47 (ddd, 1 H, *J* = 5.3, 9.4, 11.4 Hz, H-3), 5.08 (dd, 1 H, *J* = 9.8, 9.8 Hz, H-4), 4.25 (dd, 1 H, *J* = 5.0, 12.5 Hz, H-6<sub>a</sub>), 3.97 (dd, 1 H, *J* = 2.2, 12.1 Hz, H-6<sub>b</sub>), 3.94 (ddd, 1 H, *J* = 2.1, 4.8, 10.1 Hz, H-5), 2.50 (ddd, *J* = 1.3, 5.3, 13.3 Hz, H-2<sub>eq</sub>), 2.04 (m, 1 H, H-2<sub>ax</sub>), 2.03, 2.02, 1.99 (all s, 9 H, 3 × OAc); <sup>13</sup>C NMR (100 MHz, CDCl<sub>3</sub>): δ 170.4, 170.1, 169.7 (3 × CH<sub>3</sub>CO), 160.9 (C-4'), 142.8 (C-1'), 125.7 (C-3',5'), 116.3 (C-2',6'), 95.5 (C-1), 69.3, 68.8, 68.4 (C-3,4,5), 61.9 (C-6), 34.7 (C-2), 20.9, 20.6 (2 lines) (3 × CH<sub>3</sub>CO). Anal. calcd. for C<sub>18</sub>H<sub>21</sub>NO<sub>10</sub> (411.36): C, 52.56; H, 5.15; N, 3.40. Found: C, 52.70; H, 5.20; N, 3.43.

#### ***4-Nitrophenyl 2-deoxy-β-D-arabino-hexopyranoside (3-8)***



The per-*O*-acetylated **3-7** (1.01 g, 2.47 mmol) was dissolved in dry MeOH (50 mL). A catalytic fragment of sodium was added at room temperature with stirring (basic litmus test observed). After 35 min. TLC indicated completion of reaction. The reaction was neutralized with Amberlite IR-120 resin (H<sup>+</sup> form). After filtration and evaporation white crystals of **3-8** formed spontaneously. These were recrystallized from ethanol (0.490 g, 1.72 mmol, 70%). R<sub>f</sub> (20:1 acetonitrile/water) = 0.80; <sup>1</sup>H NMR (400 MHz, D<sub>2</sub>O): δ 8.24 and 7.20 (d, 4 H, *J* = 9.0 Hz, H-3,5 Ph and H-2,6 Ph), 5.55 (dd, 1 H, *J* = ~1, 9.5 Hz, H-1), 3.93 (dd, 1 H, *J* = 1.5, 12.3 Hz, H-6<sub>eq</sub>), 3.84 (ddd, 1 H, *J* = 4.9, 9.2, 12.0 Hz, H-3), 3.76 (dd, 1 H, *J* = 5.6, 12.3 Hz, H-6<sub>ax</sub>), 3.60 (ddd, 1 H, *J* = 1.4, 5.8, 9.2 Hz, H-5), 3.40 (dd, 1 H, *J* = 9.3, 9.3 Hz, H-4), 2.48 (ddd, 1 H, *J* = 1.5, 4.4, 12.0 Hz, H-2<sub>eq</sub>), 1.85 (apparent quartet, 1 H, *J* ~ 11 Hz, H-2<sub>ax</sub>); Anal. calcd. for C<sub>12</sub>H<sub>15</sub>NO<sub>7</sub> (285.25): C, 50.53; H, 5.30; N, 4.91. Found: C, 50.68; H, 5.29; N, 4.88.

#### **Steady-State Kinetic Analyses of Man2A and Man2AE429A**

Steady-state kinetics were performed on Unicam UV-4 or Unicam 8700 UV-Vis spectrometers equipped with thermo-equilibrated cell blocks. All reactions were performed at 25°C, pH 7, in acrylic cuvettes unless otherwise noted. A typical reaction cuvette contained substrate, 50 mM NaPi (pH 7) and 1 mg/mL BSA in a total volume of 750 μL. After pre-equilibrating the cuvette

at 25°C a small aliquot of appropriately diluted Man2A (5-10  $\mu\text{L}$  in 1 mg/mL BSA) was added and mixed briefly. Release of the phenol was monitored continuously at the appropriate wavelength. Initial rates ( $V_0$ ) were determined from linear fits of these plots in regions corresponding to 5-15% consumption of the substrate. Substrate concentrations were varied typically from 1/5 to  $5 \times$  the  $K_M$  value, whenever possible, for Michaelian kinetics. Higher substrate concentrations were assayed when substrate inhibition was observed. Steady-state kinetic parameters were derived by fits of the data to the Michaelis Menten equation or the substrate inhibition equation 2-1 using GraFit.<sup>292</sup>

The wavelengths and extinction coefficients used for assays of aryl  $\beta$ -mannosides and calculation of  $k_{cat}$  are the same as those reported previously.<sup>33</sup> The substrate 4-methylumbelliferyl  $\beta$ -mannoside, was assayed at 365 nm ( $5136 \text{ M}^{-1} \cdot \text{cm}^{-1}$ ).<sup>149</sup>

Assays with 4-chlorophenyl and phenyl  $\beta$ -mannoside were performed in quartz cuvettes (500 mL total volume). Stock solutions of 2,4-dinitrophenyl  $\beta$ -mannoside were prepared immediately before use in an acidic buffer (pH 5-6) and concentrated aliquots (5-50  $\mu\text{L}$ ) of the substrate were used to initiate reaction with Man2A in pH 7 buffer. In neutral solutions, 2,4-dinitrophenyl  $\beta$ -mannoside slowly rearranges to a new species, presumably through a migration of the phenol group to the 2-hydroxyl, which inhibits Man2A. This migration is virtually instantaneous above pH 7. The rearranged species can be observed by TLC (UV and charring):  $R_f$  2,4DNPMAN (7:2:1 EtOAc/MeOH/H<sub>2</sub>O) = 0.65;  $R_f$  migration product (7:2:1) = 0.74.

Concentrations of Man2A and Man2A E429A stock solutions were determined by absorbance at 280 nm using the extinction coefficient  $2.2 \text{ mL} \cdot \text{mg}^{-1} \cdot \text{cm}^{-1}$  (calculated from the amino acid sequence). A molecular weight of 95 000 Da was used in the determination of  $k_{cat}$ .

### **pH-Rate Studies**

The pH dependence of  $k_{cat}/K_M$  for wild type Man2A was determined by the substrate depletion method. Cuvettes were charged with the appropriate buffer, 1 mg/mL BSA and a concentration of substrate that was 1/10 or less of the corresponding  $K_M$  value (9.3  $\mu\text{M}$  PNPMAN, 205  $\mu\text{M}$  PhMAN). After equilibration at 25°C an aliquot of Man2A (10  $\mu\text{L}$ ) was added to afford a final concentration of enzyme (0.12  $\mu\text{M}$  Man2A for PNPMAN, 2.1  $\mu\text{M}$  Man2A for PhMAN) sufficient to generate a first order rate of phenol release within 10 to 20 min.. Phenol release was monitored continuously on a Unicam UV-4 spectrometer ( $\lambda = 400 \text{ nm}$  for PNPMAN, 280 nm for PhMAN) until a limiting absorbance was reached. Using GraFit, the curves generated at each pH

were fit with a first order rate equation (Equation 3-3) to determine the rate constant  $k$ , which corresponds to  $V_{max}/K_M$ .

$$A_t = A_{\infty} (1 - e^{-kt}) + offset \quad (3-3)$$

The following buffers (50 mM) were used for the following pH ranges: citric acid, pH 6-6.8; sodium phosphate, pH 6.8-8.4. Man2A retained at least 90% activity in these buffers at each pH over a period of 30 minutes. Rates were obtained at overlapping buffer pH values and buffer concentrations were varied to reveal buffer effects, none of which were observed. The  $k_{cat}/K_M$  values determined at each pH were fit with a function describing a single ionisation using GraFit (Equation 3-4).

$$k_{cat} / K_M = \frac{Limit_1 + Limit_2 \cdot 10^{(pH-pKa)}}{10^{(pH-pKa)} + 1} \quad (3-4)$$

In the case of Man2A E429A the pH dependence of  $k_{cat}/K_M$  for the reaction with 2,5-dinitrophenyl  $\beta$ -mannoside could not be determined owing to the very low  $K_M$  value ( $< 1 \mu\text{M}$ ) with this substrate. Therefore  $k_{cat}$  was determined from initial rates at various pH values using a single saturating concentration of 2,5DNPMAN (2 mM). An extinction coefficient of  $4288 \text{ M}^{-1} \cdot \text{cm}^{-1}$  ( $\lambda = 440 \text{ nm}$ ) for 2,5-dinitrophenol ( $\text{pK}_a^{\text{lg}} = 5.15$ ) was used for pH values between 6 and 9, and a value of  $2290 \text{ M}^{-1} \cdot \text{cm}^{-1}$  for pH 5.5, in order to determine  $k_{cat}$ . The following buffers (50 mM) were used: MES, pH 5.5-6.9; sodium phosphate, pH 6.75-8.2; AMPSO, pH 8.85-9.1. A dramatic buffer effect was observed for 50 mM citric acid between pH 5.5 and 7 that was also dependent on the concentration of citrate. The  $k_{cat}$  values at each pH were fit with a function describing a bell shaped pH profile (Equation 3-5) using GraFit.

$$k_{cat} = \frac{Limit \cdot 10^{(pH-pKa_1)}}{10^{(2 \times pH - pKa_1 - pKa_2)} + 10^{(pH-pKa_1)} + 1} \quad (3-5)$$

### Azide Rescue of Man2A E429A

A stock solution of sodium azide (0.5 M) in 50 mM sodium phosphate, pH 7, was prepared within a day of use and stored at 0-4°C. Initially Man2A E429A was assayed in the usual way (1 mg/mL BSA, pH 7, 25°C) with a single saturating concentration of 2,5-dinitrophenyl  $\beta$ -

mannoside (2 mM) while varying the concentration of azide (1.6  $\mu\text{M}$  to 4 mM). Apparent  $k_{cat}$  and  $K_M$  values were obtained by fixing azide at 100 mM and varying the concentration of 2,5DNPMan from 1/5 to 5  $\times$  the  $K_M$  value. Spontaneous hydrolysis of 2,5DNPMan was negligible at all concentrations.

#### **Synthesis of $\beta$ -D-Mannopyranosyl Azide with Man2A E429A**

2,5-Dinitrophenyl  $\beta$ -mannoside (10.5 mg) was dissolved in 150 mM ammonium bicarbonate (1 mL, pH 7.9) containing 64 mM sodium azide. Man2A was added to afford a final enzyme concentration of 0.37 mg/mL (3.9  $\mu\text{M}$ ) and the reaction incubated at RT overnight. TLC analysis indicated reasonably clean conversion to a new product that was not UV active. The reaction mixture was concentrated *in vacuo* and purified by silica gel chromatography (17:2:1 to 7:2:1 EtOAc/MeOH/H<sub>2</sub>O). Evaporation of the solvent afforded a white film that was determined to be  $\beta$ -mannosyl azide.  $R_f$  (7:2:1 EtOAc/MeOH/H<sub>2</sub>O) = 0.61; <sup>1</sup>H NMR (200 MHz, CD<sub>3</sub>OD):  $\delta$  4.58 (d, 1 H,  $J$  = 1.0 Hz, H-1), 3.91 (dd, 1 H,  $J$  = 2.3, 12.0, H-6a), 3.86 (dd, 1 H,  $J$  = 1.0, 3.1, H-2), 3.73 (dd,  $J$  = 6.0, 11.9 Hz, H-6b), 3.58 (dd, 1 H,  $J$  = 9.3, 9.3 Hz, H-4), 3.45 (dd, 1 H,  $J$  = 3.0, 9.3 Hz, H-3), 3.32 (ddd, 1 H,  $J$  = 2.3, 6.0, 9.3, H-5).

#### **Kinetic Isotope Effects with Man2A E429A**

$\alpha$ -DKIE's were determined on  $k_{cat}$  for Man2A E429A using virtually identical and saturating concentrations of 2,5-DNP  $\beta$ -mannoside and 2,5-DNP  $\beta$ -[1-2H]-mannoside (2 mM). A stock solution containing Man2A E429A (0.11 mg/mL, 1.1  $\mu\text{M}$ ), 1 mg/mL BSA, and 50 mM NaPi, pH 7 was prepared. 700  $\mu\text{L}$  aliquots of the stock solution were then measured into quartz cuvettes and individually weighed on an analytical balance. After pre-equilibration at 25°C, reaction was initiated by the addition of substrate (50  $\mu\text{L}$  of 30 mM), also pre-equilibrated at 25°C. The reaction was monitored spectrophotometrically, as described above. A total of 6-8 measurements were made with each substrate, alternating between each to eliminate bias. All initial rates (protio and deuterio) were corrected according to the corresponding masses of the reaction solutions. Measurements with 100 mM sodium azide or 100 mM NaCl were performed in the same fashion, with the corresponding stock solutions containing these salts.

## Chapter 5: Engineering Enhanced Glycosynthase Activity in *Agrobacterium* sp. $\beta$ -glucosidase

### General

Mutagenesis and expression of Abg E358 mutants has been described elsewhere.<sup>206,244</sup> The mutagenesis was performed by Dr. Christoph Mayer and Dr. David Jakeman. The per-*O*-acetylated oligosaccharide products were characterized by  $^1\text{H}$  NMR (400 MHz, Bruker) and  $^{13}\text{C}$  NMR (100 MHz, Varian) spectroscopy as well as high resolution MS. Individual resonances were assigned by  $^1\text{H}$ - $^1\text{H}$  COSY and APT experiments. Glycosidic linkages were assigned on the basis of the considerable upfield chemical shift experienced by sugar ring protons residing on carbons bearing hydroxyl groups that form glycosidic bonds. Ring protons whose hydroxyl groups are *O*-acetylated are typically shifted downfield due to the electron withdrawing effects of the acetate. The anomeric configuration of the glycosidic linkages formed were assigned on the basis of the corresponding  $J_{\text{H1-H2}}$  coupling constants.

### Transglycosylation Kinetics

Concentrations of mutant enzyme solutions were quantified directly by absorbance at 280 nm ( $\epsilon_{280}^{0.1\%} = 2.20$ ). All transglycosylation kinetic studies were conducted in a water bath manually maintained at 25°C ( $\pm 1^\circ\text{C}$ ). Assay solutions consisted of  $\alpha$ -glycosyl fluoride donor ( $\alpha$ -galactosyl fluoride or  $\alpha$ -glucosyl fluoride) and acceptor (PNP  $\beta$ -glucoside or PNP  $\beta$ -cellobioside) in 150 mM NaPi, 150 mM NaCl, pH 7. Assays with  $\alpha$ -galactosyl fluoride were supplemented with 1 mg/mL BSA, but not assays with  $\alpha$ -glucosyl fluoride. BSA (or an  $\alpha$ -glucosidase contaminant within BSA) rapidly hydrolyzes  $\alpha$ -glucosyl fluoride. The total reaction volume was 400-420  $\mu\text{L}$ . An Orion fluoride electrode (model 96-09BN), interfaced with LoggerPro software,<sup>300</sup> was used to monitor fluoride release following addition of a small aliquot of Abg E358A, E358C, E358S or E358G (10-50  $\mu\text{L}$ ). A micro stir-bar (5 mm long), fashioned from a plastic coated paper clip, was used to stir the solution during the course of the reaction. All enzymatic rates were corrected for the spontaneous hydrolysis rate of the glycosyl fluoride donor. Initially the concentration of  $\alpha$ -glycosyl fluoride was fixed (57 mM  $\alpha$ -galactosyl fluoride) and the concentration of acceptor varied. Substrate inhibition behaviour was observed with both acceptors and was fit with the appropriate equation (see Chapter 3, equation 3-1). Next, the complementary experiment was carried out in which the acceptor was held at a

constant concentration (22 mM PNP  $\beta$ -glucoside, 11 mM PNP  $\beta$ -cellobioside) and the concentration of  $\alpha$ -glucosyl fluoride was varied. Standard saturation kinetics were obtained with  $\alpha$ -glucosyl fluoride. Very high concentrations of  $\alpha$ -galactosyl fluoride (800-1000 mM) were required to achieve saturation, and saturation may in fact be due to viscosity effects. Therefore  $k_{cat}/K_M$ , derived from data at low concentrations of donor, is a more reliable parameter for  $\alpha$ -galactosyl fluoride. Apparent values of  $k_{cat}$ ,  $K_M$ , and  $k_{cat}/K_M$  for donor and acceptor were derived from fits to the appropriate equations using GraFit.<sup>292</sup>

In studies of the dependence of reaction rate upon pH the following buffers were used: pH 5-6, 100 mM sodium citrate; pH 7-8, 100 mM NaPi, pH 8-9, 100 mM AMPSO. Apparent values of  $k_{cat}/K_M$  for  $\alpha$ -galactosyl fluoride were determined from the linear dependence of rates ( $V_o = k_{cat}E_o/K_M$ ) measured at 3 low concentrations of  $\alpha$ -galactosyl fluoride (5, 10, and 15 mM) at a fixed concentration of PNP  $\beta$ -glucoside (22 mM).

#### **Chemical Rescue of Abg E358 Nucleophile Mutants**

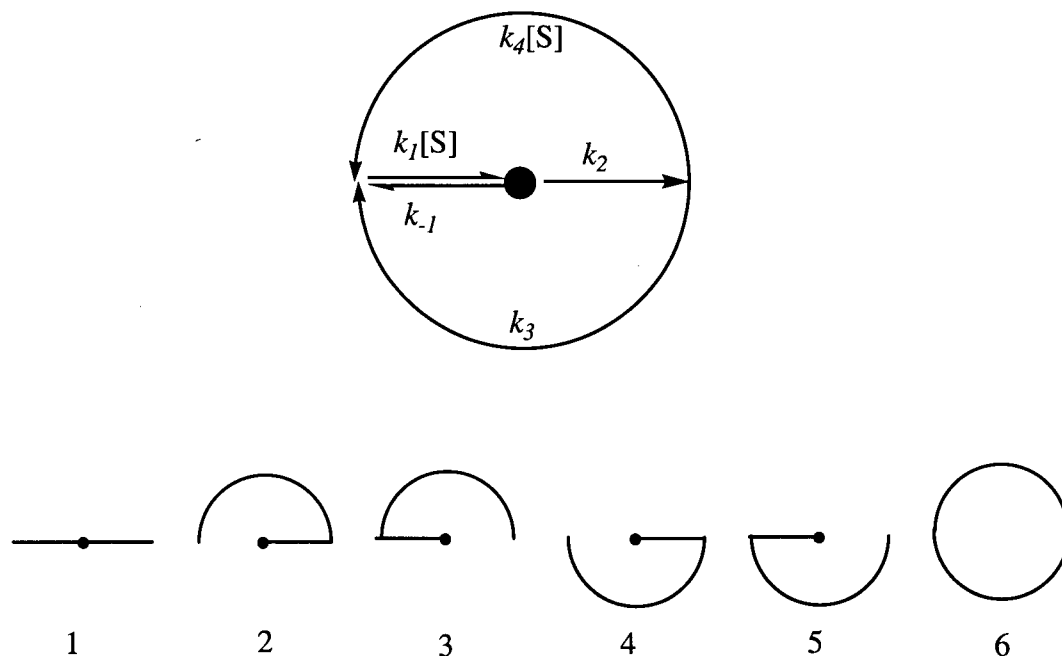
The reaction of Abg E358 nucleophile mutants with 2,4-dinitrophenyl  $\beta$ -glucoside and formate (2 M or 5 M) or azide (2 M) was performed at 37°C or 25°C. Azide or formate stock solutions were used within 2-3 days of preparation. Assays were buffered with 100 mM NaPi, pH 7 or 100 mM citrate, pH 6, supplemented with 1 mg/mL BSA. The total reaction volume was 750  $\mu$ L. Reactions were initiated by the addition of a small aliquot of enzyme (10-20  $\mu$ L) to pre-equilibrated assay solution. The release of dinitrophenol was monitored spectrophotometrically at 400 nm ( $\Delta\epsilon = 10\,900\text{ M}^{-1}\text{ cm}^{-1}$ ). The 2,4-dinitrophenyl  $\beta$ -glucoside concentration was varied from 1/5 the final  $K_M$  value (when possible) to 3-6 mM. Enzymatic rates were corrected for spontaneous hydrolysis of the substrate, which was negligible at 25°C, pH 6. The non-saturating rate curves shown in Figures 5-4 and 5-5 have not been reported previously for chemical rescue of other retaining glycosidase nucleophile mutants. This includes Abg E358A.<sup>30</sup> The kinetic parameters derived from the curves shown in Figures 5-4 and 5-5 require fits of the Michaelis Menten equation to data points at low substrate concentrations (< 0.5 mM) where transglycosylation is minimal. This does not appear to have been done in the past with E358A, thus the  $K_M$  values reported here for azide and formate rescue (Tables 5-2 and 5-3) are considerably lower than those reported previously.<sup>30</sup>

The following buffers were used to determine a pH-rate profile for the reaction of Abg E358G with azide (2 M) and 2,4-dinitrophenyl  $\beta$ -glucoside (1.1 mM): 100 mM citrate (pH 5.5-6.5), 100 mM NaPi (pH 6.5-7.95), 100 mM AMPSO (pH 7.95-8.95).

The following wavelengths and extinction coefficients were used to assay of the reaction of Abg E358G with formate and other aryl  $\beta$ -glucoside or aryl 2-deoxy- $\beta$ -glucoside substrates (pH 6, 25°C): 2,5-dinitrophenyl (440 nm, 3780 M<sup>-1</sup>·cm<sup>-1</sup>), 4-chloro, 2-nitrophenyl (425 nm, 1000 M<sup>-1</sup>·cm<sup>-1</sup>), 4-nitrophenyl (400 nm, 1220 M<sup>-1</sup>·cm<sup>-1</sup>). These values were determined by allowing the enzymatic reaction to run to completion (supplemented with additional mutant or wild type enzyme) and plotting the final absorbance value of the solution (at the appropriate wavelength) against the concentration of substrate. The slope from the resulting linear plot afforded the extinction coefficient ( $A = \epsilon cL$ ). This value was corrected by the slope obtained from the same plot prior to addition of enzyme (typically this was negligible).

### Modelling Chemical Rescue

The steady-state equation for the chemical rescue scheme shown in Figure 5-10 is readily derived using the King-Altman method. The 4 steps in the scheme result in  $(4!)/(3-1)!(5-4+1)! = 6$  basic patterns that represent all possible pathways between enzyme species.



Pathway 6 can be excluded because it is a closed loop. From these patterns the following rate equations can be derived for the formation of each enzyme species.

$$d[E]/dt = 0 + k_2k_4[S] + k_{-1}k_4[S] + k_2k_3 + k_{-1}k_3$$

$$d[ES]/dt = 0 + 0 + k_1k_4[S]^2 + 0 + k_1k_3[S]$$

$$d[ES^*]/dt = k_1k_2[S] + 0 + 0 + 0 + 0$$

The rate of dinitrophenol release is  $d[\text{DNP}]/dt = k_2[ES]$ , thus the steady state equation becomes:

$$\frac{V}{Et} = \frac{k_2[ES]}{[E] + [ES] + [ES^*]}$$

$$\frac{V}{Et} = \frac{k_2(k_1k_4[S]^2 + k_1k_3[S])}{k_2k_4[S] + k_{-1}k_4[S] + k_2k_3 + k_{-1}k_3 + k_1k_4[S]^2 + k_1k_3[S] + k_1k_2[S]}$$

Dividing the numerator and denominator by  $k_1$  and simplification yields a final steady state equation.<sup>214</sup>

$$\frac{V}{Et} = \frac{\left( \frac{k_2(k_3 + k_4[S])}{k_2 + k_3 + k_4[S]} \right) [S]}{\left( \frac{k_{-1} + k_2}{k_1} \right) \left( \frac{k_3 + k_4[S]}{k_2 + k_3 + k_4[S]} \right) + [S]}$$

Generally the chemical step  $k_2$  will be much slower than binding or dissociation steps  $k_1$  and  $k_{-1}$ , thus the term  $(k_{-1} + k_2)/k_1$  reduces to  $K_d$  as shown in equation (5-1).<sup>148</sup> Curves were generated from equation (5-1) using Mathematica.<sup>301</sup>

## Synthesis of Glycosyl Fluorides

### *$\alpha$ -Galactosyl fluoride*

Galactose per-*O*-acetate (8.9 g, 22.7 mmol) was dissolved in 15 mL DCM in a Nalgene bottle (125 mL volume) and flushed with  $N_2$ . Acetic anhydride (1.5 mL) was added, followed by 70% HF-pyridine (25 g). The reaction was maintained at 4°C for 24 hrs. then RT for another 24 hrs. whereupon TLC (2:1 PE/EtOAc) indicated completion. The reaction mixture was diluted with DCM (100 mL) and poured into ice water. The organic layer was washed with saturated

bicarbonate and water, dried over  $\text{MgSO}_4$ , then the solvent evaporated. The crude was purified by silica gel chromatography (5:1 to 2:1 PE/EtOAc). Following evaporation of the solvent,  $\alpha$ -galactosyl fluoride, per-*O*-acetate, was isolated as an oil (5.27g, 15.0 mmol, 66%).  $R_f$  (2:1 PE/EtOAc) = 0.34.  $^1\text{H}$  NMR (200 MHz,  $\text{CDCl}_3$ ):  $\delta$  5.78 (dd, 1 H,  $J = 2.4, 53$  Hz, H-1), 5.50 (dd, 1 H,  $J = 2.9, 1$  Hz, H-4), 5.34 (dd, 1 H,  $J = 3.2, 10.7$  Hz, H-3), 5.16 (ddd, 1 H,  $J = 2.9, 10.7, 23.2$  Hz, H-2), 4.38 (m, 1 H, H-5), 4.11 (m, 2 H, 2 x H-6),  $^{19}\text{F}$  NMR (188 MHz,  $\text{CDCl}_3$ , referenced to  $\text{CF}_3\text{CO}_2\text{H}$ ):  $\delta$  -75.1 (dd,  $J = 53.4, 22.9$  Hz).

The per-*O*-acetate (5.27 g, 15.0 mmol) was subsequently dissolved in dry MeOH (100 mL) and a catalytic amount of sodium methoxide added such that the solvent was strongly basic (by litmus). After 45 min. TLC (5:2:1 EtOAc/MeOH/ $\text{H}_2\text{O}$ ) indicated completion of the reaction. The methoxide was neutralized with Amberlite IR-120 ( $\text{H}^+$ ) resin and the solvent evaporated. Recrystallization of the crude from MeOH / acetone / hexanes afforded white crystals (2.35 g, 12.9 mmol, 86%). Selected data for  $\alpha$ -galactosyl fluoride:  $R_f$  (5:2:1 EtOAc/MeOH/ $\text{H}_2\text{O}$ ) = 0.58;  $^1\text{H}$  NMR (200 MHz,  $\text{CD}_3\text{OD}$ ):  $\delta$  5.56 (dd, 1 H,  $J = 2.7, 54.3$  Hz, H-1), 3.95 (m, 2 H), 3.81 (ddd, 1 H,  $J = 2.9, 10.0, 22.9$  Hz, H-2), 3.73 (m, 3 H).

#### *$\alpha$ -Glucosyl fluoride*

$\beta$ -D-Glucose per-*O*-acetate (10.0 g, 25.6 mmol) was treated with 70% HF/pyridine as described above. Reaction was complete overnight at 4°C. After work-up the crude product was recrystallized from PE/EtOAc to afford white crystals of  $\alpha$ -glucosyl fluoride per-*O*-acetate (7.56 g, 21.6 mmol, 84%).  $R_f$  (1:1 PE/EtOAc) = 0.58. Deprotection of the per-*O*-acetate (6.77 g, 19.3 mmol) with sodium methoxide in methanol followed by recrystallization from MeOH / acetone / EtOAc afforded  $\alpha$ -glucosyl fluoride as a white powder (3.17 g, 17.4 mmol, 90%).  $R_f$  (5:2:1 EtOAc/MeOH/ $\text{H}_2\text{O}$ ) = 0.54;  $^1\text{H}$  NMR (300 MHz,  $\text{D}_2\text{O}$ ):  $\delta$  5.73 (dd, 1 H,  $J = 2.2, 53.5$  Hz, H-1), 3.94-3.82 (m, 3 H, H-6a,b and H-5), 3.78 (dd, 1 H,  $J = 9.4, 9.4$  Hz, H-3), 3.65 (ddd, 1 H,  $J = 2.4, 9.9, 26.1$  Hz, H-2), 3.55 (dd, 1 H,  $J = 9.4, 9.4$  Hz, H-4);  $^{19}\text{F}$  NMR (188 MHz,  $\text{D}_2\text{O}$ , ref. to  $\text{CF}_3\text{CO}_2\text{H}$ ):  $\delta$  -74.3 (dd,  $J = 25.1, 52.6$  Hz).

#### **Oligosaccharide Synthesis with AbgE358S**

In a typical reaction the acceptor glycoside was dissolved in approximately 2.5 mL 150 mM ammonium hydrogen carbonate (pH 7.9). An aliquot of a concentrated solution (~1 M) containing  $\alpha$ -glucosyl fluoride or  $\alpha$ -galactosyl fluoride was then added (1-2 eq.) followed by

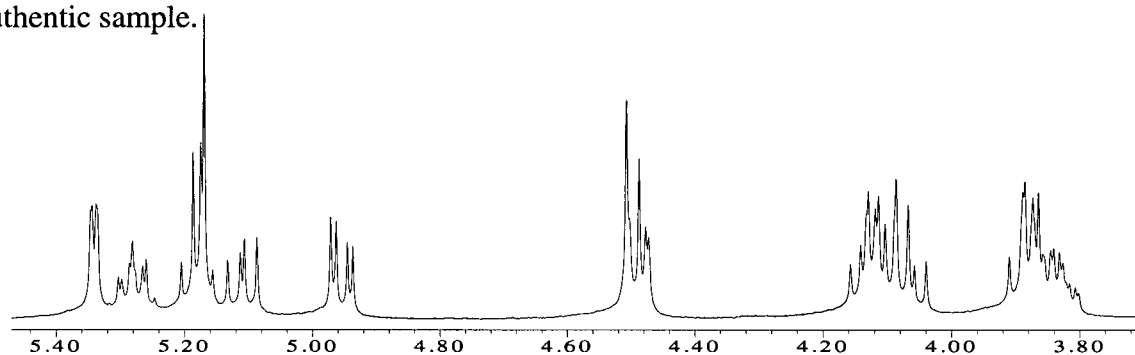
Abg E358S. Final acceptor concentrations ranged from 20 to 40 mM, donor concentrations from 30 to 80 mM, and Abg E358S concentrations from 0.25 - 1 mg/mL (4.85 - 20  $\mu$ M). Reaction times ranged from 2 hrs to 7 days. Reactions were monitored by TLC (silica gel 60 F<sub>254</sub>, aluminum backed, Merck) using 7:2:1 EtOAc/MeOH/water. Plates were visualized by exposure to 10% sulphuric acid in methanol followed by charring.

### Oligosaccharide Purification

Upon completion, reaction solutions were lyophilized, re-dissolved in 1 mL water, and the mutant enzyme removed by ultrafiltration (Centricon-30, Amicon). Reaction products were purified by preparative HPLC on a TosoHaas Amide-80 column (21.5 mm  $\times$  30 cm, # 14460). A BioSeptra ProSys workstation (Beckman Coulter) was used to generate a linear gradient of 80:20 to 60:40 acetonitrile/water at a flow rate of 5 mL/min. Products were detected using a UV/Vis detector. Product fractions were concentrated *in vacuo* then lyophilized. Reaction yields were determined by integration of the peaks within the HPLC chromatograms using an analysis program developed by BioSeptra. Molecular weights of oligosaccharide products were confirmed by ESI-MS (Perkin Elmer API 300, Sciex, Thornhill, Ontario, Canada). The oligosaccharide products were then acetylated with acetic anhydride and pyridine (2:3) followed by purification by silica gel chromatography.

### *Gal* $\beta$ 1,4*Glu* $\beta$ 1-OPNP (5-1)

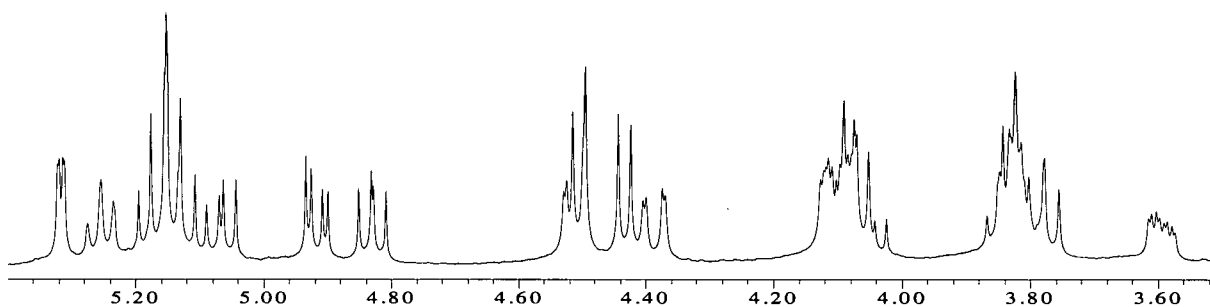
PNP  $\beta$ -glucoside (34.6 mg, 115  $\mu$ mol),  $\alpha$ -galactosyl fluoride (172  $\mu$ mol, 1.5 eq.) and Abg E358S (0.75 mg) were combined in 3 mL buffer. After 48 hrs. the reaction mixture was worked up as described above to yield PNP  $\beta$ -lactoside **5-1** (98% by HPLC, 44.5 mg, 96  $\mu$ mol, 84% isolated). The <sup>1</sup>H NMR spectrum (400 MHz, CDCl<sub>3</sub>) of the per-*O*-acetylated product matched that of an authentic sample.



Partial <sup>1</sup>H NMR spectrum of per-*O*-acetylated **5-1** (400 MHz, CDCl<sub>3</sub>).

***Galβ1-4Gluβ1-4Gluβ1-OPNP (5-2)***

PNP β-cellobioside (34.3 mg, 74 μmol), α-galactosyl fluoride (89 μmol, 1.2 eq.) and Abg E358S (0.75 mg) were combined in 3 mL buffer. The reaction was complete in 2 hrs. After the usual work up, 33.8 mg (54 μmol, 73%) of **5-2** was obtained (98% by HPLC). Data for the per-*O*-acetate: <sup>1</sup>H NMR (400 MHz, CDCl<sub>3</sub>): δ 8.17 (d, 2 H, *J* = 9.3 Hz, Ph H-3,5), 7.02 (d, 2 H, *J* = 9.3 Hz, Ph H-2,6), 5.32 (dd, 1 H, *J* = 3.4, 1.1 Hz, H-4<sup>3</sup>), 5.25 (dd, 1 H, *J* = 7.9, 7.9 Hz, H-3<sup>1</sup>), 5.20-5.10 (m, 3 H, H-1<sup>1</sup>,2<sup>1</sup>,3<sup>2</sup>), 5.07 (dd, 1 H, *J* = 7.9, 10.5 Hz, H-2<sup>3</sup>), 4.92 (dd, 1 H, *J* = 3.3, 10.4 Hz, H-3<sup>3</sup>), 4.83 (dd, 1 H, *J* = 8.1, 9.2 Hz, H-2<sup>2</sup>), 4.51 (dd, 1 H, *J* = 2.0, 12.0 Hz, H-6), 4.50 (d, 1 H, *J* = 8.1 Hz, H-1<sup>2</sup>), 4.43 (d, 1 H, *J* = 8.1 Hz, H-1<sup>3</sup>), 4.39 (dd, 1 H, *J* = 2.0, 12.0 Hz, H-6), 4.13-4.02 (m, 4 H, 4 × H-6), 3.88-3.80 (m, 3 H, H-4<sup>1</sup>,5<sup>1</sup>,5<sup>3</sup>), 3.78 (dd, 1 H, *J* = 9.8, 9.8 Hz, H-4<sup>2</sup>), 3.59 (ddd, 1 H, *J* = 1.8, 4.9, 9.7 Hz, H-5<sup>2</sup>); 2.12-1.94 (lines, 30 H, 10 × Ac); <sup>13</sup>C NMR (100 MHz, CDCl<sub>3</sub>): δ 170.3-169.1 (lines, 10 × CH<sub>3</sub>CO), 161.1 (Ph C-4), 143.2 (Ph C-1), 125.7 (Ph C-3,5), 116.6 (Ph C-2,6), 101.1 (C-1), 100.4 (C-1), 97.8 (C-1), 76.0, 75.8, 73.2, 72.9, 72.8, 72.1, 71.8, 71.2, 70.9, 70.7, 69.0, 66.5, 62.1 (C-6), 61.7 (C-6), 60.7 (C-6), 20.8-20.5 (lines, 10 × CH<sub>3</sub>CO); HRMS (DCI+): *m/z* = 1063.3254; calcd. for C<sub>44</sub>H<sub>59</sub>O<sub>28</sub>N<sub>2</sub> [M + NH<sub>4</sub>]<sup>+</sup>: *m/z* = 1063.3254.

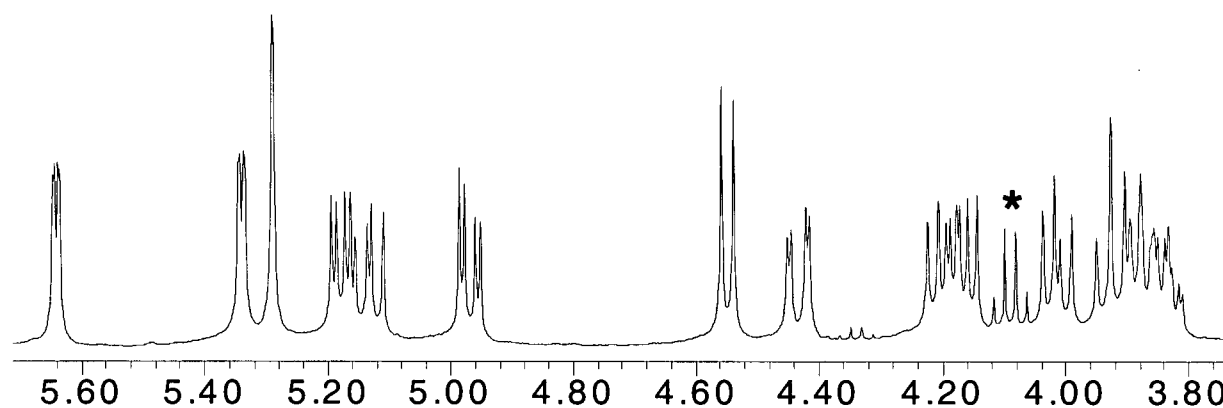


Partial <sup>1</sup>H NMR spectrum of per-*O*-acetylated **5-2** (400 MHz, CDCl<sub>3</sub>).

***Galβ1,4Manβ1-OPNP (5-3)***

PNP β-mannoside (31.5 mg, 104 μmol) was dissolved in 3 mL buffer. α-Galactosyl fluoride (189 μmol, 1.8 eq.) and Abg E358S (1.51 mg) were added portion wise over 30 hrs.. After 56 hrs. at RT the reaction mixture was worked up in the usual way. HPLC and evaporation of the solvent afforded **5-3** (31.3 mg, 67.5 μmol, 65%, 80.3% by HPLC). Selected data for per-*O*-acetylated **5-3**: <sup>1</sup>H NMR (400 MHz, CDCl<sub>3</sub>): δ 5.64 (dd, 1 H, *J* = 1.1, 3.3 Hz, H-2<sup>1</sup>), 5.34 (dd, 1 H, *J* = 1.0, 3.3 Hz, H-4<sup>2</sup>), 5.29 (d, 1 H, *J* = 1.1 Hz, H-1<sup>1</sup>), 5.18 (dd, 1 H, *J* = 3.4, 9.0 Hz, H-3<sup>1</sup>),

5.13 (dd, 1 H,  $J = 7.9, 10.4$  Hz, H-2<sup>2</sup>), 4.97 (dd, 1 H,  $J = 3.3, 10.5$  Hz, H-3<sup>2</sup>), 4.55 (d, 1 H,  $J = 7.9$  Hz, H-1<sup>2</sup>), 4.43 (dd, 1 H,  $J = 2.4, 11.8$  Hz, H-6), 4.20 (dd, 1 H,  $J = 6.8, 11.8$  Hz, H-6), 4.16 (dd, 1 H,  $J = 6.2, 11.2$  Hz, H-6), 4.01 (dd, 1 H,  $J = 7.5, 11.1$  Hz, H-6), 3.93 (dd, 1 H,  $J = 9.2, 9.2$  Hz, H-4<sup>1</sup>), 3.88 (m, 1 H, H-5<sup>2</sup>), 3.83 (ddd, 1 H,  $J = 2.4, 6.9, 9.3$  Hz, H-5<sup>1</sup>); <sup>13</sup>C NMR (100 MHz, CDCl<sub>3</sub>):  $\delta$  167.2-166.1 (lines, 7  $\times$  CH<sub>3</sub>CO), 158.1 (Ph C-4), 140.9 (Ph C-1), 124.0 (Ph C-3,5), 115.1 (Ph C-2,6), 100.3 (C-1), 95.1 (C-1), 74.1, 73.4, 71.1, 71.0, 70.8, 69.3, 68.5, 66.9, 63.0 (C-6), 61.3 (C-6), 22.6-22.4 (lines, 7  $\times$  CH<sub>3</sub>CO); HRMS (DCI<sup>+</sup>):  $m/z = 775.2412$ ; calcd. for C<sub>32</sub>H<sub>43</sub>O<sub>20</sub>N<sub>2</sub> [M + NH<sub>4</sub>]<sup>+</sup>:  $m/z = 775.2409$ .



Partial <sup>1</sup>H NMR spectrum of per-*O*-acetylated **5-3** (400 MHz, CDCl<sub>3</sub>). \* Residual EtOAc.

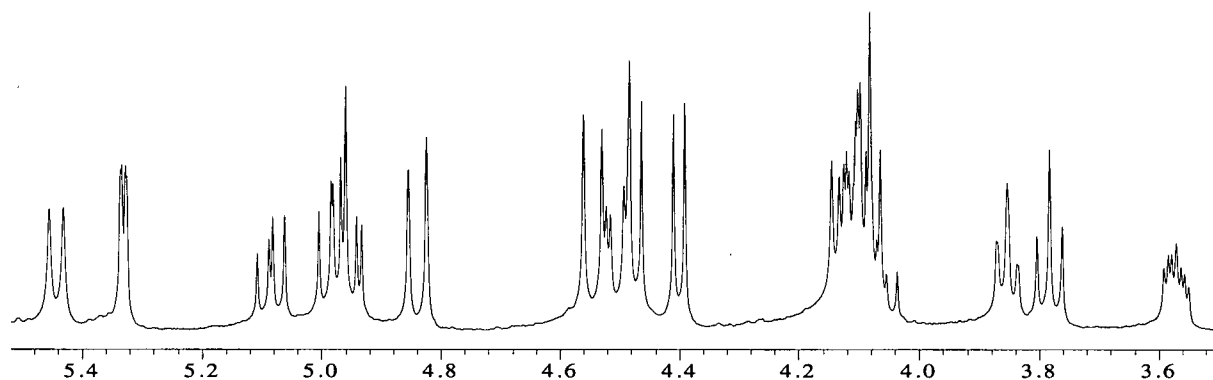
#### ***Gal*β1,4*GlcNAc*β1-*OPNP* (**5-4**)**

PNP *N*-acetyl-β-glucosaminide (10.3 mg, 30.1 μmol) was dissolved in 2 mL buffer. Abg E358S (1.8 mg total) and α-galactosyl fluoride (121 μmol total, 4 eq.) were added portion-wise over 48 hrs. After 72 hrs. at RT the reaction was worked up in the usual way. HPLC and evaporation of the solvent afforded PNP β-lactosaminide (**5-4**) (8.2 mg, 16.2 μmol, 54%, 63% by HPLC). Selected data for per-*O*-acetylated **5-4**: <sup>1</sup>H NMR (400 MHz, CDCl<sub>3</sub>):  $\delta$  6.13 (d, 1 H,  $J = 9.2$  Hz, NHAc), 5.37 (dd, 1 H,  $J = 0.8, 3.4$  Hz, H-4<sup>2</sup>), 5.26 (d, 1 H,  $J = 5.9$  Hz, H-1<sup>1</sup>), 5.18 (dd, 1 H,  $J = 7.0, 7.0$  Hz, H-3<sup>1</sup>), 5.13 (dd, 1 H,  $J = 8.0, 10.6$  Hz, H-2<sup>2</sup>), 5.00 (dd, 1 H,  $J = 3.4, 10.3$  Hz, H-3<sup>2</sup>), 4.49 (d, 1 H,  $J = 7.8$  Hz, H-1<sup>2</sup>), 4.45 (dd, 1 H,  $J = 4.0, 11.8$  Hz, H-6), 4.37 (ddd, 1 H,  $J = 5.5, 7.3, 9.2$  Hz, H-2<sup>1</sup>), 4.14 (m, 2 H, 2  $\times$  H-6), 4.08 (dd, 1 H,  $J = 7.3, 11.6$  Hz, H-6), 3.90 (m, 2 H, 2  $\times$  H-5), 3.86 (dd, 1 H,  $J = 6.4, 6.4$ , H-4<sup>1</sup>); <sup>13</sup>C NMR (100 MHz, CDCl<sub>3</sub>):  $\delta$  170.3-169.7 (lines, 7  $\times$  CH<sub>3</sub>CO), 161.3 (Ph C-4), 142.8 (Ph C-1), 125.7 (Ph C-3,5), 116.4 (Ph C-2,6), 100.8 (C-1), 97.8 (C-1), 74.0, 73.0, 71.0, 70.5, 70.3, 69.0, 66.6, 62.5 (C-6), 60.8 (C-6), 51.1 (C-2<sup>1</sup>), 23.1 (CH<sub>3</sub>CO,

amide), 20.9-20.5 (lines, 6 × CH<sub>3</sub>CO); HRMS (DCI+):  $m/z = 757.2314$ ; calcd. for C<sub>32</sub>H<sub>41</sub>O<sub>19</sub>N<sub>2</sub> [M + H]<sup>+</sup>:  $m/z = 757.2303$ .

### *Galβ1,4GlcNAcβ1-OBn (5-5)*

Benzyl *N*-acetyl-β-glucosaminide (31.9 mg, 102.5 μmol) was dissolved in 2.5 mL buffer. α-Galactosyl fluoride (160 μmol, 1.6 eq.) and Abg E358S (1.1 mg) were added portion-wise over 3 days. After 6 days at RT the reaction mixture was worked up in the usual way. HPLC of the crude product and evaporation of the solvent afforded benzyl β-lactosaminide (**5-5**) (32 mg, 68 μmol, 66%). Selected data for per-*O*-acetylated **5-5**: <sup>1</sup>H NMR (400 MHz, CDCl<sub>3</sub>): δ 7.34-7.24 (m, 5 H, Ph-H), 5.44 (d, 1 H,  $J = 9.4$  Hz, NHAc), 5.33 (dd, 1 H,  $J = 0.9, 3.4$  Hz, H-4<sup>2</sup>), 5.08 (dd, 1 H,  $J = 8.0, 10.5$  Hz, H-2<sup>2</sup>), 4.98 (dd, 1 H,  $J = 8.4, 9.7$  Hz, H-3<sup>1</sup>), 4.95 (dd, 1 H,  $J = 3.4, 10.7$  Hz, H-3<sup>2</sup>), 4.84 (d, 1 H,  $J = 12.0$  Hz, BnCH<sub>2</sub>), 4.54 (d, 1 H,  $J = 12.5$  Hz, BnCH<sub>2</sub>), 4.51 (dd, 1 H,  $J = 2.6, 12.0$ , H-6), 4.47 (d, 1 H,  $J = 8.2$  Hz, H-1<sup>2</sup>), 4.40 (d, 1 H,  $J = 7.3$  Hz, H-1<sup>1</sup>), 4.15-4.06 (m, 4 H, H-2<sup>1</sup>, 3 × H-6), 3.85 (m, 1 H, H-5<sup>2</sup>), 3.78 (dd, 1 H,  $J = 8.6, 8.6$  Hz, H-4<sup>1</sup>), 3.57 (ddd, 1 H,  $J = 2.6, 5.0, 8.2$  Hz, H-5<sup>1</sup>); <sup>13</sup>C NMR (100 MHz, CDCl<sub>3</sub>): δ 170.7-169.3 (lines, 7 × CH<sub>3</sub>CO), 136.9 (Ph C-1), 128.5 (2 lines, 2 × Ph CH), 128.0 (Ph CH), 127.9 (2 lines, 2 × Ph CH), 100.9 (C-1), 99.4 (C-1), 75.6, 72.7, 72.3, 70.8, 70.7, 70.3 (CH<sub>2</sub> benzyl), 69.1, 66.6, 62.3 (C-6), 60.8 (C-6), 53.1 (C-2<sup>1</sup>), 23.2 (CH<sub>3</sub>CO amide), 20.9-20.5 (lines, 6 × CH<sub>3</sub>CO); HRMS (DCI+):  $m/z = 726.2617$ ; calcd. for C<sub>33</sub>H<sub>44</sub>O<sub>17</sub>N [M + H]<sup>+</sup>:  $m/z = 726.2609$ .



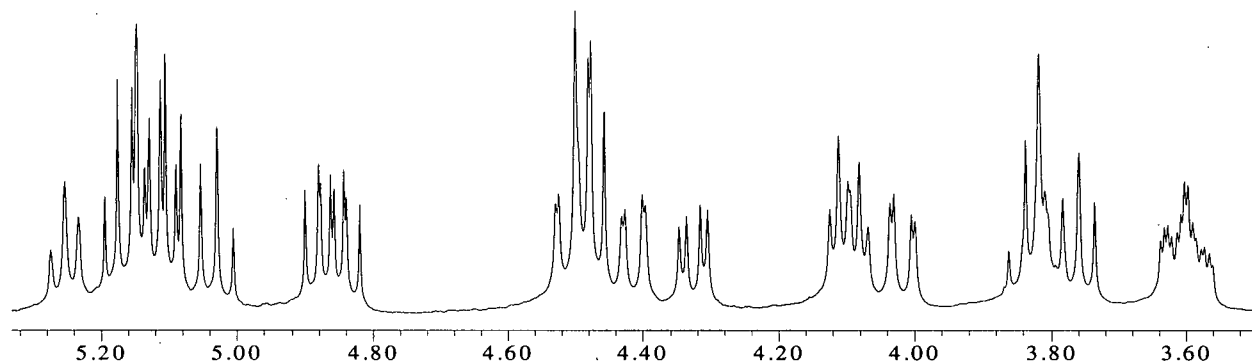
Partial <sup>1</sup>H NMR spectrum for per-*O*-acetylated **5-5** (400 MHz, CDCl<sub>3</sub>).

**PNP  $\beta$ -glucoside as acceptor,  $\alpha$ -glucosyl fluoride as donor:** PNP  $\beta$ -glucoside (34.5 mg, 114.5  $\mu$ mol) was combined with 0.38 mg Abg E358S in 2.7 mL buffer.  $\alpha$ -Glucosyl fluoride (250  $\mu$ mol, 2.2 eq.) was added in 3 portions over 48 hrs. Following the usual work-up and HPLC of the crude material, PNP  $\beta$ -celotrioside (**5-6a**) was isolated as the major product (38.3 mg, 61.2  $\mu$ mol, 53%). The total yield of tri- and tetrasaccharides was 96% by HPLC.

**PNP  $\beta$ -cellobioside as acceptor,  $\alpha$ -glucosyl fluoride as donor:** PNP  $\beta$ -cellobioside (32.8 mg, 70.8  $\mu$ mol) was dissolved in 2.8 mL buffer. Abg E358S was added (0.75 mg) followed by an aliquot of  $\alpha$ -glucosyl fluoride (78  $\mu$ mol, 1.1 eq.). After 2 hrs. complete conversion of the acceptor was observed by TLC. After the usual work-up and purification by HPLC, the trisaccharide **5-6a** (30.9 mg, 49.4  $\mu$ mol, 70%, 88.3% by HPLC) and tetrasaccharide **5-6b** (2.1 mg, 2.66  $\mu$ mol, 3.7%, 7.0% by HPLC) were isolated as the major products.

***Glu $\beta$ 1,4Glu $\beta$ 1,4Glu $\beta$ 1-OPNP (5-6a)***

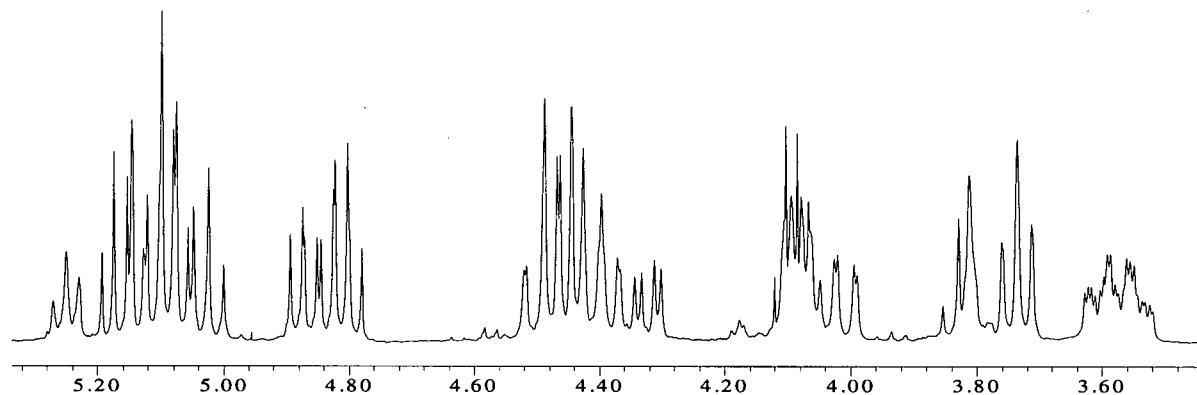
Selected data for per-*O*-acetylated **5-6a**:  $^1\text{H}$  NMR (400 MHz,  $\text{CDCl}_3$ ):  $\delta$  5.25 (dd, 1 H,  $J = 8.0, 8.0$  Hz, H-3<sup>1</sup>), 5.18 (dd, 1 H,  $J = 7.3, 8.5$  Hz, H-2<sup>1</sup>), 5.14 (d, 1 H,  $J = 7.3$  Hz, H-1<sup>1</sup>), 5.11 and 5.10 (dd, 2 H,  $J = 9.2, 9.2$  Hz, H-3<sup>2</sup>, H-4<sup>3</sup>), 5.03 (dd, 1 H,  $J = 9.6, 9.6$  Hz, H-3<sup>3</sup>), 4.88 and 4.84 (dd, 2 H,  $J = 8.1, 9.2$  Hz, H-2<sup>2,3</sup>), 4.51 (dd, 1 H,  $J = 1.8, 11.8$  Hz, H-6), 4.49 (d, 1 H,  $J = 7.7$  Hz, H-1), 4.47 (d, 1 H,  $J = 8.1$  Hz, H-1), 4.41 (dd, 1 H,  $J = 1.8, 12.1$  Hz, H-6), 4.32 (dd, 1 H,  $J = 4.4, 12.5$  Hz, H-6), 4.10 (m, 2 H, 2  $\times$  H-6), 4.02 (dd, 1 H,  $J = 2.2, 12.5$  Hz, H-6), 3.84 (dd, 1 H,  $J = 9.9, 9.9$  Hz, H-4<sup>1</sup>), 3.81 (m, 1 H, H-5<sup>1</sup>), 3.76 (dd, 1 H,  $J = 9.4, 9.4$  Hz, H-4<sup>2</sup>), 3.62 (ddd, 1 H,  $J = 2.2, 4.4, 9.9$  Hz, H-5), 3.58 (ddd, 1 H,  $J = 1.8, 4.8, 9.9$  Hz, H-5);  $^{13}\text{C}$  NMR (100 MHz,  $\text{CDCl}_3$ ):  $\delta$  170.5-169.0 (lines, 10  $\times$   $\text{CH}_3\text{CO}$ ), 161.1 (Ph C-4), 143.2 (Ph C-1), 125.7 (Ph C-3,5), 116.6 (Ph C-2,6), 100.7 (C-1), 100.5 (C-1), 97.8 (C-1), 76.1, 76.0, 73.2, 72.8 (2 lines), 72.5, 72.1, 72.0, 71.7, 71.6, 71.2, 67.7, 62.0 (C-6), 61.7 (C-6), 61.5 (C-6), 20.8-20.4 (lines, 10  $\times$   $\text{CH}_3\text{CO}$ ); HRMS (DCI+):  $m/z = 1063.3206$ ; calcd. for  $\text{C}_{44}\text{H}_{59}\text{O}_{28}\text{N}_2$  [ $\text{M} + \text{NH}_4$ ]<sup>+</sup>:  $m/z = 1063.3254$ .



Partial  $^1\text{H}$  NMR spectrum of per-*O*-acetylated **5-6a** (400 MHz,  $\text{CDCl}_3$ ).

***Glu* $\beta$ 1,4*Glu* $\beta$ 1,4*Glu* $\beta$ 1,4*Glu* $\beta$ 1-OPNP (**5-6b**)**

Selected data for per-*O*-acetylated **5-6b**:  $^1\text{H}$  NMR (400 MHz,  $\text{CDCl}_3$ ):  $\delta$  5.25 (broad dd, 1 H,  $J = 8.0, 8.0$  Hz, H-3 $^1$ ), 5.17 (dd, 1 H,  $J = 8.5, 7.3$  Hz, H-2 $^1$ ), 5.15-5.05 (m, 4 H, H-3 $^{2,3,4}$ , H-1 $^1$ ), 5.02 (dd, 1 H,  $J = 9.5, 9.5$  Hz, H-4 $^4$ ), 4.87, 4.82, and 4.80 (all dd, 3 H,  $J = 7.9, 9.1$  Hz, H-2 $^{2,3,4}$ ), 4.53-4.36 (m, 6 H, H-1 $^{2,3,4}$ , 3  $\times$  H-6), 4.32 (dd, 1 H,  $J = 4.6, 12.8$  Hz, H-6), 4.12-4.04 (m, 3 H, 3  $\times$  H-6), 4.01 (dd, 1 H,  $J = 2.1, 12.5$  Hz, H-6), 3.82 (m, 2 H, H-4 $^1$ , H-5 $^1$ ), 3.74 (broad dd, 2 H,  $J = 9.8, 9.8$  Hz, H-4 $^{2,3}$ ), 3.63-3.51 (m, 3 H, H-5 $^{2,3,4}$ );  $^{13}\text{C}$  NMR (100 MHz,  $\text{CDCl}_3$ ):  $\delta$  170.4-169.0 (lines, 13  $\times$   $\text{CH}_3\text{CO}$ ), 161.1 (C-4 Ph), 143.2 (C-1 Ph), 125.7 (C-3,5 Ph), 116.6 (C-2,6 Ph), 100.8 (C-1), 100.4 (2 lines, 2  $\times$  C-1), 97.8 (C-1), 76.1, 76.0 (2 lines), 73.2, 72.9 (2 lines), 72.8, 72.6, 72.4, 72.0 (2 lines), 71.9, 71.8, 71.6, 71.2, 67.8, 62.0 (2 lines, 2  $\times$  C-6), 61.7 (C-6), 61.5 (C-6), 20.8-20.4 (lines, 13  $\times$   $\text{CH}_3\text{CO}$ ); HRMS (DCI $^+$ ):  $m/z = 1351.4097$ ; calcd. for  $\text{C}_{56}\text{H}_{75}\text{O}_{36}\text{N}_2$  [ $\text{M} + \text{NH}_4$ ] $^+$ :  $m/z = 1351.4099$ .



Partial  $^1\text{H}$  NMR spectrum of per-*O*-acetylated **5-6b** (400 MHz,  $\text{CDCl}_3$ ).

**PNP  $\beta$ -mannoside as acceptor,  $\alpha$ -glucosyl fluoride as donor:** PNP  $\beta$ -mannoside (32.8 mg, 109  $\mu$ mol) was dissolved in 3 mL buffer. Abg E358S (3.77 mg) and  $\alpha$ -glucosyl fluoride (224 mmol, 2.1 eq.) were added portion-wise over 72 hrs.. Following the usual work-up and HPLC of the crude material, di-, tri-, and tetrasaccharides were isolated as the major products. The total oligosaccharide yield was 59% by HPLC. The total isolated yield of oligosaccharides was 42.5%.

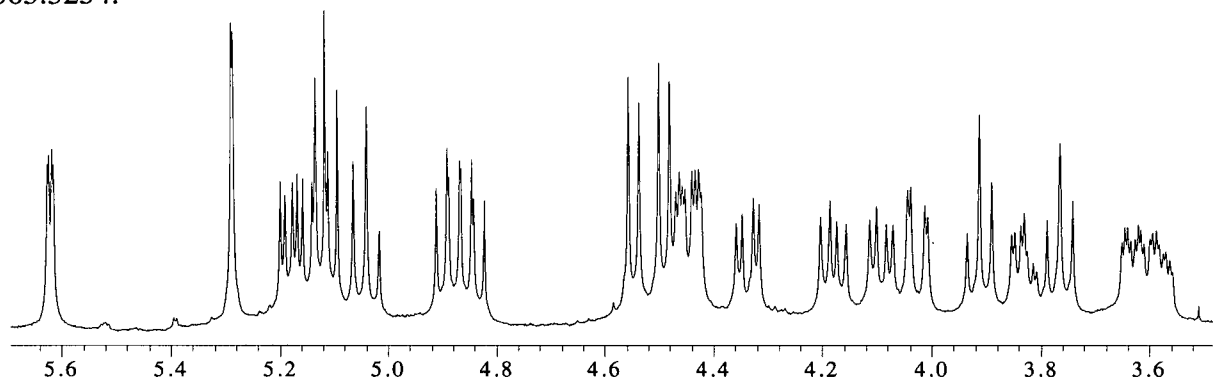
***Glu $\beta$ 1,4Man $\beta$ 1-OPNP (5-7a)***

5.9 mg (12.7 mmol, 11.7%) was isolated (17.2% by HPLC). Selected data for per-*O*-acetylated **5-7a**:  $^1\text{H}$  NMR (400 MHz,  $\text{CDCl}_3$ ):  $\delta$  5.64 (dd, 1 H,  $J = 1.1, 3.4$  Hz, H-2 $^1$ ), 5.28 (d, 1 H,  $J = 1.3$  Hz, H-1 $^1$ ), 5.18 (dd, 1 H,  $J = 3.4, 9.1$  Hz, H-3 $^1$ ), 5.16 (dd, 1 H,  $J = 9.5, 9.5$  Hz, H-4 $^2$ ), 5.06 (dd, 1 H,  $J = 9.6, 9.6$  Hz, H-3 $^2$ ), 4.93 (dd, 1 H,  $J = 7.9, 9.3$  Hz, H-2 $^2$ ), 4.58 (d, 1 H,  $J = 7.8$  Hz, H-1 $^2$ ), 4.45 (dd, 1 H,  $J = 2.6, 11.7$  Hz, H-6), 4.31 (dd, 1 H,  $J = 4.6, 12.7$  Hz, H-6), 4.20 (dd, 1 H,  $J = 6.9, 11.8$  Hz, H-6), 4.05 (dd, 1 H,  $J = 2.5, 12.2$  Hz, H-6), 3.92 (dd, 1 H,  $J = 9.2, 9.2$  Hz, H-4 $^1$ ), 3.83 (ddd, 1 H,  $J = 2.5, 6.9, 9.4$  Hz, H-5 $^1$ ), 3.67 (ddd, 1 H,  $J = 2.4, 4.4, 9.8$  Hz, H-5 $^2$ );  $^{13}\text{C}$  NMR (100 MHz,  $\text{CDCl}_3$ ):  $\delta$  170.5-169.1 (lines,  $7 \times \text{CH}_3\text{CO}$ ), 161.0 (Ph C-4), 143.2 (Ph C-1), 125.7 (Ph C-3,5), 116.4 (Ph C-2,6), 100.7 (C-1), 95.8 (C-1), 74.0, 73.4, 72.7, 71.9, 71.6, 70.6, 68.4, 67.9, 62.5 (C-6), 61.8 (C-6), 20.7-20.5 (lines,  $7 \times \text{CH}_3\text{CO}$ ); HRMS (DCI+):  $m/z = 775.2422$ ; calcd. for  $\text{C}_{32}\text{H}_{43}\text{O}_{20}\text{N}_2$   $[\text{M} + \text{NH}_4]^+$ :  $m/z = 775.2409$ .

***Glu $\beta$ 1,4Glu $\beta$ 1,4Man $\beta$ 1-OPNP (5-7b)***

11.9 mg (19  $\mu$ mol, 17.4%) was isolated (25% by HPLC). Selected data for per-*O*-acetylated **5-7b**:  $^1\text{H}$  NMR (400 MHz,  $\text{CDCl}_3$ ):  $\delta$  5.62 (dd, 1 H,  $J = 1.2, 3.4$  Hz, H-2 $^1$ ), 5.29 (d, 1 H,  $J = 1.1$  Hz, H-1 $^1$ ), 5.18 (dd, 1 H,  $J = 3.4, 9.0$  Hz, H-3 $^1$ ), 5.14 and 5.12 (dd, 2 H,  $J = 9.2, 9.2$  Hz, H-3 $^2, 4^3$ ), 5.04 (dd, 1 H,  $J = 9.2, 9.2$  Hz, H-3 $^3$ ), 4.89 and 4.84 (dd, 2 H,  $J = 8.0, 9.2$  Hz, H-2 $^2, 3$ ), 4.55 and 4.49 (d, 2 H,  $J = 7.7$  Hz, H-1 $^2, 3$ ), 4.45 (dd, 1 H,  $J = 2.6, 11.8$  Hz, H-6), 4.44 (dd, 1 H,  $J = 2.2, 12.1$  Hz, H-6), 4.34 (dd, 1 H,  $J = 4.4, 12.5$  Hz, H-6), 4.18 (dd, 1 H,  $J = 6.6, 11.8$  Hz, H-6), 4.09 (dd, 1 H,  $J = 5.0, 12.0$  Hz, H-6), 4.02 (dd, 1 H,  $J = 2.2, 12.5$  Hz, H-6), 3.91 (dd, 1 H,  $J = 9.2, 9.2$  Hz, H-4 $^1$ ), 3.83 (ddd, 1 H,  $J = 2.2, 6.7, 9.2$  Hz, H-5 $^1$ ), 3.76 (dd, 1 H,  $J = 9.4, 9.4$  Hz, H-4 $^2$ ), 3.63 (ddd, 1 H,  $J = 2.2, 4.0, 9.6$  Hz, H-5), 3.58 (ddd, 1 H,  $J = 2.2, 4.8, 9.9$  Hz, H-5);  $^{13}\text{C}$  NMR (100 MHz,  $\text{CDCl}_3$ ):  $\delta$  170.5-169.0 (lines,  $10 \times \text{CH}_3\text{CO}$ ), 161.0 (Ph C-4), 143.1 (Ph C-1), 125.7 (Ph C-3,5), 116.4 (Ph C-2,6), 100.8 (C-1), 100.3 (C-1), 95.7 (C-1), 76.0, 73.9, 73.4, 72.8 (2 lines), 72.4,

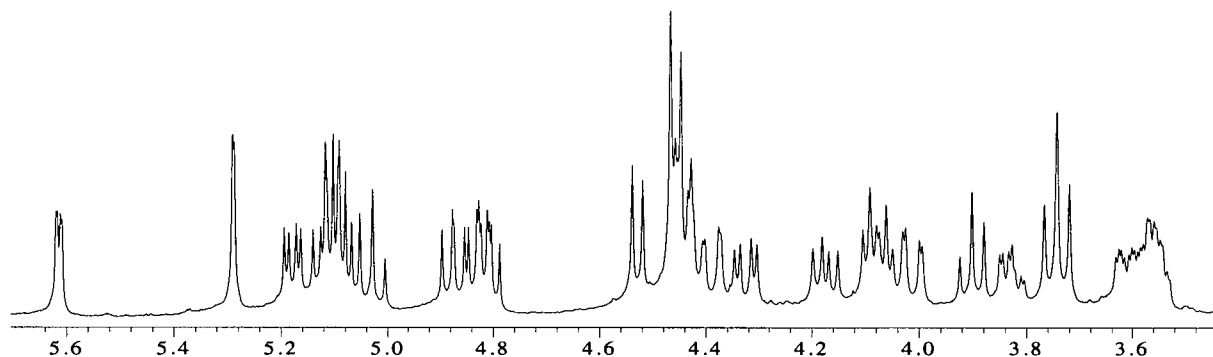
72.0, 71.8, 71.6, 70.3, 68.3, 67.7, 62.5 (C-6), 61.9 (C-6), 61.5 (C-6), 20.7-20.5 (lines,  $10 \times \text{CH}_3\text{CO}$ ); HRSMS (DCI+):  $m/z = 1063.3229$ ; calcd. for  $\text{C}_{44}\text{H}_{59}\text{O}_{28}\text{N}_2$   $[\text{M} + \text{NH}_4]^+$ :  $m/z = 1063.3254$ .



Partial  $^1\text{H}$  NMR spectrum of per-*O*-acetylated **5-7b** (400 MHz,  $\text{CDCl}_3$ ).

***Glu* $\beta$ 1,4*Glu* $\beta$ 1,4*Glu* $\beta$ 1,4*Man* $\beta$ 1-*OPNP* (**5-7c**)**

11.5 mg (14.6  $\mu\text{mol}$ , 13.4%) was isolated (17% by HPLC). Selected data for per-*O*-acetylated **5-7c**:  $^1\text{H}$  NMR (400 MHz,  $\text{CDCl}_3$ ):  $\delta$  5.61 (dd, 1 H,  $J = 1.1, 3.3$  Hz, H-2 $^1$ ), 5.29 (d, 1 H,  $J = 1.1$  Hz, H-1 $^1$ ), 5.18 (dd, 1 H,  $J = 3.3, 9.0$  Hz, H-3 $^1$ ), 5.12, 5.10, and 5.09 (dd, 3 H,  $J = 9.2, 9.2$  Hz, H-3 $^{2,3}$ , H-4 $^4$ ), 5.03 (dd, 1 H,  $J = 9.6, 9.6$  Hz, H-3 $^4$ ), 4.88, 4.82, and 4.81 (dd, 3 H,  $J = 7.7, 9.2$  Hz, H-2 $^{2,3,4}$ ), 4.53 (d, 1 H,  $J = 7.7$  Hz, H-1), 4.45 (m, 3 H,  $2 \times$  H-1, H-6), 4.39 (dd, 1 H,  $J = 1.8, 12.1$  Hz, H-6), 4.32 (dd, 1 H,  $J = 4.2, 12.5$  Hz, H-6), 4.17 (dd, 1 H,  $J = 6.8, 12.0$  Hz, H-6), 4.08 (m, 2 H,  $2 \times$  H-6), 4.01 (dd, 1 H,  $J = 2.1, 12.3$  Hz, H-6), 3.90 (dd, 1 H,  $J = 9.0, 9.0$  Hz, H-4 $^1$ ), 3.83 (ddd, 1 H,  $J = 2.2, 6.6, 9.2$  Hz, H-5 $^1$ ), 3.74 (dd, 2 H,  $J = 9.4, 9.4$  Hz, H-4 $^{2,3}$ ), 3.61 (ddd, 1 H,  $J = 2.2, 4.0, 9.9$  Hz, H-5), 3.59-3.52 (m, 2 H,  $2 \times$  H-5); HRMS (DCI+):  $m/z = 1351.4068$ ; calcd. for  $\text{C}_{56}\text{H}_{75}\text{O}_{36}\text{N}_2$   $[\text{M} + \text{NH}_4]^+$ :  $m/z = 1351.4099$ .



Partial  $^1\text{H}$  NMR spectrum for per-*O*-acetylated **5-7c** (400 MHz,  $\text{CDCl}_3$ ).

## Chapter 6: Development of a Mannosynthase from *Cellulomonas fimi* Man2A

### General

The mutagenesis and expression of Man2A E519A and E519S, performed by Dr. Oyekanmi Nashiru, has been described elsewhere.<sup>273</sup>  $^1\text{H}$  NMR (Bruker Avance, 400 MHz),  $^{19}\text{F}$  NMR (Bruker, 188 MHz) and  $^{13}\text{C}$  NMR (Varian, 100 MHz) spectra of the per-*O*-acetylated oligosaccharide products listed in Table 6-1 were acquired in  $\text{CDCl}_3$  at 300 K.  $^1\text{H}$  and  $^{13}\text{C}$  chemical shifts are internally referenced to the solvent.  $^{19}\text{F}$  chemical shifts are referenced to  $\text{CF}_3\text{CO}_2\text{H}$ . Chemical shifts were assigned on the basis of  $^1\text{H}$ - $^1\text{H}$  COSY and APT experiments. Glycosidic linkages were assigned on the basis of the considerable upfield shift experienced by sugar ring protons residing on carbons bearing hydroxyl groups that form glycosidic bonds (relative to ring protons whose hydroxyl groups are *O*-acetylated). For the branched oligosaccharide products **6-6a** and **6-6b**, TOCSY analysis was used to assign proton resonances to specific sugar rings and HMBC was performed to verify the position of the glycosidic linkages. The anomeric configurations of the glycosidic linkages formed in products **6-1a** and **6-1b** were established from  $J_{(C-1, H-1)}$  coupling constants measured from the corresponding proton coupled  $^{13}\text{C}$  NMR spectra (100 MHz, 0.76 Hz / point resolution). NOE intensities described for product **6-4b** were estimated (by peak integration) from the corresponding 1-dimensional NOE difference spectrum (400 MHz).

### Miscellaneous Syntheses

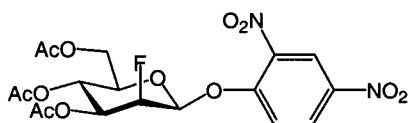
#### *$\alpha$ -Mannosyl fluoride*

D-Mannose per-*O*-acetate (7.64 g, 19.6 mmol) was dissolved in dry DCM (10 mL) in a 125 mL Nalgene™ bottle and flushed with dry nitrogen. HF-pyridine (70%, approx. 15 mL) was added and the vessel sealed. The reaction mixture was maintained at 4°C overnight then at RT for 5 hrs. whereupon TLC analysis (2:1 PE/EtOAc) indicated essentially complete consumption of starting material. The reaction mixture was diluted in DCM (125 mL), poured into ice water, and the organic layer washed with saturated sodium bicarbonate. After drying over  $\text{MgSO}_4$  and the solvent was evaporated to produce a gum. White needles of  $\alpha$ -mannosyl fluoride per-*O*-acetate were produced after prolonged storage of the gum at 4°C (5.43 g, 15.5 mmol, 79%). Rf (2:1 PE/EtOAc) = 0.53;  $^1\text{H}$  NMR (200 MHz,  $\text{CDCl}_3$ ):  $\delta$  5.55 (dd, 1 H,  $J = 48.3, 1.7$  Hz, H-1),

5.40-5.30 (m, 3 H, H-2,3,4), 4.29 (dd, 1 H,  $J = 12.7, 5.4$  Hz, H-6ax), 4.14 (m, 2 H, H-5, H-6eq);  $^{19}\text{F}$  NMR (188 MHz,  $\text{CDCl}_3$ , referenced to  $\text{CF}_3\text{CO}_2\text{H}$ ):  $\delta$  -62.5 (d,  $J = 49.2$  Hz).

The per-*O*-acetate was quantitatively de-acetylated in 10 min. (RT) with sodium methoxide in methanol. The reaction solution was neutralized with Amberlite IR-120 ( $\text{H}^+$ ) and the solvent evaporated to obtain a gum. The crude material was purified by flash chromatography on silica gel (30:2:1 EtOAc/MeOH/ $\text{H}_2\text{O}$ ) to obtain  $\alpha$ -mannosyl fluoride as a gum that would not crystallize.  $R_f$  (4:1 acetonitrile/ $\text{H}_2\text{O}$ ) = 0.55;  $^1\text{H}$  NMR (200 MHz,  $\text{D}_2\text{O}$ ):  $\delta$  5.60 (dd, 1 H,  $J = 1.9, 49.3$  Hz, H-1), 4.07 (ddd, 1 H,  $J = 0.8, 1.9, 3.1$  Hz, H-2), 3.91-3.6 (m, 5 H, H-3,4,5,6a,6b);  $^{19}\text{F}$  NMR (188 MHz,  $\text{D}_2\text{O}$ , referenced to  $\text{CF}_3\text{CO}_2\text{H}$ ,  $^1\text{H}$  decoupled):  $\delta$  -62.6.

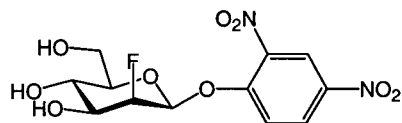
**2,4-Dinitrophenyl 3,4,6-tri-*O*-acetyl-2-deoxy-2-fluoro- $\beta$ -D-mannopyranoside**<sup>302,303</sup>



3,4,6-*Tri-O*-acetyl-D-glucal (5.62 g, 20.6 mmol) was dissolved in 3:1 DMF /  $\text{H}_2\text{O}$  (200 mL) followed by Selectfluor<sup>TM</sup> (10.5 g, 29.7 mmol, 1.4 eq.) and the whole mixture stirred overnight at  $50^\circ\text{C}$ . TLC analysis (1:1 PE/EtOAc) indicated complete conversion of the D-glucal to 2-deoxy-2-fluoro hexopyranoses at this time. The solvent was evaporated and the residue redissolved in EtOAc (300 mL), washed with brine and water, then dried over  $\text{MgSO}_4$ . The solvent was evaporated and the crude, without further purification, redissolved in DMF (200 mL). DABCO (7.0 g, 62.4 mmol,  $\sim 3$  eq.) was added and dissolved, followed by 2,4-dinitrofluorobenzene (6.0 g, 32.2 mmol,  $\sim 1.5$  eq.). The vessel was purged with argon and stirred in the dark overnight at room temperature, whereupon TLC analysis (3:4 EtOAc / PE) indicated complete conversion to 2,4-dinitrophenyl 2-deoxy-2-fluoro-glycosides. The solvent was evaporated and the residue redissolved in EtOAc (300 mL). The organic was washed with 0.2 M  $\text{H}_2\text{SO}_4$ , saturated sodium bicarbonate and water, then dried over  $\text{MgSO}_4$ . A dark, brown oil was obtained upon evaporation of the solvent. Chromatography on silica gel (4:3 to 1:1 EtOAc / PE) and evaporation of the solvent afforded  $\alpha$ - (1.49 g, 3.13 mmol, 15.1%) and  $\beta$ - (1.55 g, 3.26 mmol, 15.7%,  $\beta/\alpha = 1:1$ ) anomers of 2,4-dinitrophenyl 2-fluoro-mannosides, and a  $\beta/\alpha$  mixture of 2,4-dinitrophenyl 2-fluoro-glucosides (2.58 g, 5.43 mmol, 26%,  $\beta/\alpha = 3.7:1$  by  $^{19}\text{F}$  NMR) as pale yellow crystalline solids.  $^1\text{H}$  and  $^{19}\text{F}$  NMR spectral data matched that reported previously.<sup>302</sup>

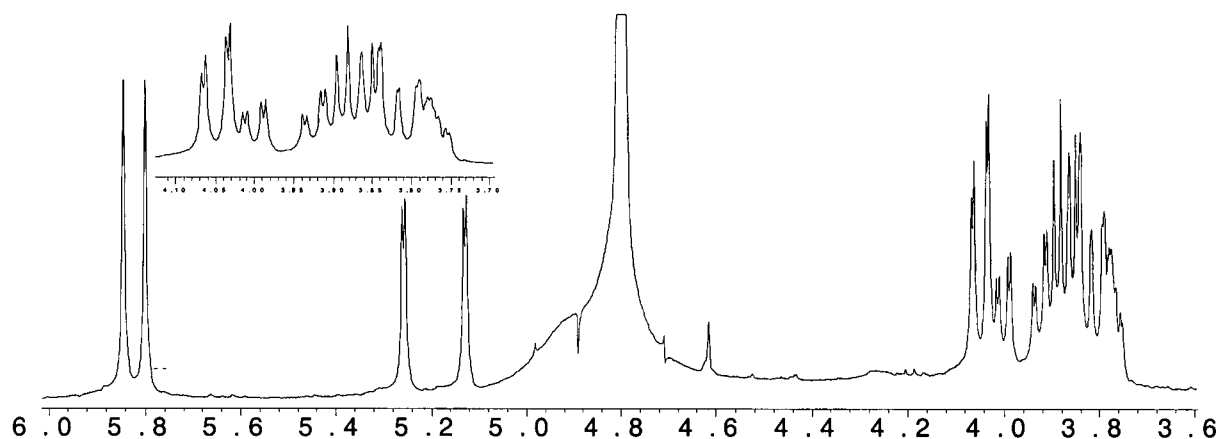
**Data for 2,4-Dinitrophenyl 2-deoxy-2-fluoro- $\beta$ -D-mannopyranoside:** Rf (3:4 EtOAc / PE) = 0.20; M.p. = 189.5-190.5°C;  $^1\text{H}$  NMR (400 MHz,  $\text{CDCl}_3$ ):  $\delta$  8.74 (d, 1 H,  $J$  = 2.5 Hz, H-3 Ph), 8.42 (dd, 1 H,  $J$  = 2.5, 9.2 Hz, H-5 Ph), 7.48 (d, 1 H,  $J$  = 9.5 Hz, H-6 Ph), 5.38 (dd, 1 H,  $J$  = 14.6, < 1 Hz, H-1), 5.37 (dd, 1 H,  $J$  = 9.5, 9.5 Hz, H-4), 5.14 (ddd, 1 H,  $J$  = 24.3, 9.1, 2.6 Hz, H-3), 5.12 (ddd, 1 H,  $J$  = 51.4, 2.5, < 1 Hz, H-2), 4.27 (apparent d, 2 H,  $J$  = 4.4 Hz, H-6<sub>a,b</sub>), 3.87 (ddd, 1 H,  $J$  = 4.4, 4.4, 8.8 Hz, H-5), 2.14, 2.07, 2.06 (all s, 9 H, 3  $\times$  OAc);  $^{19}\text{F}$  NMR (188.3 MHz,  $\text{CDCl}_3$ , referenced to  $\text{CF}_3\text{CO}_2\text{H}$ ):  $\delta$  -142.4 (ddd,  $J_{F,H}$  = 50.3, 24.4, 15.2 Hz);  $^{13}\text{C}$  NMR (100 MHz,  $\text{CDCl}_3$ ):  $\delta$  170.4, 170.0, 169.2 (3  $\times$   $\text{CH}_3\text{CO}$ ), 153.5, 142.6, 140.7 (3  $\times$  C-Ph), 128.5, 121.6, 119.9 (3  $\times$  CH-Ph), 97.2 (d,  $J_{C,F}$  = 16.7 Hz, C-1), 85.7 (d,  $J_{C,F}$  = 194.7 Hz, C-2), 73.3 (C-5), 70.2 (d,  $J_{C,F}$  = 17.2 Hz, C-3), 65.5 (C-4), 61.9 (C-6), 20.6 (3 lines, 3  $\times$   $\text{CH}_3\text{CO}$ ); HRMS (DCI+):  $m/z$  = 492.1269; calcd. for  $\text{C}_{18}\text{H}_{23}\text{FN}_3\text{O}_{12}$  [ $\text{M} + \text{NH}_4$ ] $^+$ :  $m/z$  = 492.1266; Anal. calcd. for  $\text{C}_{18}\text{H}_{19}\text{FN}_2\text{O}_{12}$  (474.35): C, 45.58; H, 4.04; N, 5.91; Found: C, 45.68; H, 4.15; N, 6.03. **Data for 2,4-Dinitrophenyl 2-deoxy-2-fluoro- $\alpha$ -D-mannopyranoside:** Rf (3:4 EtOAc / PE) = 0.70; M.p. = 217-219°C;  $^1\text{H}$  NMR (200 MHz,  $\text{CDCl}_3$ ):  $\delta$  8.80 (d, 1 H,  $J$  = 2.7 Hz, H-3 Ph), 8.45 (dd, 1 H,  $J$  = 2.7, 9.3 Hz, H-5 Ph), 7.54 (d, 1 H,  $J$  = 9.3 Hz, H-6 Ph), 5.92 (dd, 1 H,  $J$  = 1.9, 6.1 Hz, H-1), 5.47 (dd, 1 H,  $J$  = 10.0, 10.0 Hz, H-4), 5.41 (ddd,  $J$  = 2.2, 10.0, 29.5 Hz, H-3), 5.08 (ddd, 1 H,  $J$  = 2.1, 2.1, 48.8 Hz, H-2), 4.25 (dd, 1 H,  $J$  = 5.1, 12.7 Hz, H-6<sub>a</sub>), 4.07 (m, 2 H, H-5, H-6<sub>b</sub>), 2.11, 2.05, 2.03 (all s, 9 H, 3  $\times$  OAc);  $^{19}\text{F}$  NMR (188.3 MHz,  $\text{CDCl}_3$ , referenced to  $\text{CF}_3\text{CO}_2\text{H}$ ):  $\delta$  -129.5 (ddd,  $J_{F,H}$  = 48.8, 29.0, 6.1 Hz); HRMS (DCI+):  $m/z$  = 492.1262; ; calcd. for  $\text{C}_{18}\text{H}_{23}\text{FN}_3\text{O}_{12}$  [ $\text{M} + \text{NH}_4$ ] $^+$ :  $m/z$  = 492.1266. **Data for 2,4-Dinitrophenyl 2-deoxy-2-fluoro-D-glucopyranosides:** Rf (3:4 EtOAc / PE) = 0.44;  $^{19}\text{F}$  NMR (188.3 MHz,  $\text{CDCl}_3$ , referenced to  $\text{CF}_3\text{CO}_2\text{H}$ ):  $\delta$  -122.5 ( $\beta$ -anomer), -125.6 ( $\alpha$ -anomer).

**2,4-Dinitrophenyl 2-deoxy-2-fluoro- $\beta$ -D-mannopyranoside**



The per-*O*-acetate (1.69 g, 3.57 mmol) was suspended in dry MeOH (50 mL) and cooled to 0°C under argon. Acetyl chloride (2 mL) was added dropwise to afford a 4% solution of HCl. The mixture was stirred for 2 days at 4°C. The solvent was evaporated followed by repeated evaporation of dry diethyl ether from the residue to remove excess HCl. The crude was

columned on silica gel (95:5 EtOAc/MeOH). Subsequent evaporation of the solvent and recrystallization of the residue from acetone / PE to afforded white needles (1.08 g, 3.10 mmol, 87%).  $R_f$  (30:2:1 EtOAc/MeOH/H<sub>2</sub>O = 0.50; <sup>1</sup>H NMR (400 MHz, D<sub>2</sub>O):  $\delta$  8.95 (d, 1 H,  $J$  = 2.8 Hz, H-3 Ph), 8.59 (dd, 1 H,  $J$  = 2.8, 9.4 Hz, H-5 Ph), 7.67 (d, 1 H,  $J$  = 9.6 Hz, H-6 Ph), 5.82 (dd, 1 H,  $J$  = 18.4, < 1 Hz, H-1) 5.19 (ddd, 1 H,  $J$  = 51.5, 2.2, < 1 Hz, H-2), 4.05 (dd, 1 H,  $J$  = 2.2, 12.5 Hz, H-6a), 3.96 (ddd, 1 H,  $J$  = 30.1, 9.4, 2.4 Hz, H-3), 3.87 (dd, 1 H,  $J$  = 5.9, 12.5 Hz, H-6b), 3.84 (ddd,  $J$  = 1.1, 9.7, 9.7 Hz, H-4), 3.78 (m, 1 H, H-5); <sup>19</sup>F NMR (188 MHz, D<sub>2</sub>O, ref. to CF<sub>3</sub>CO<sub>2</sub>H):  $\delta$  -144.8 (ddd,  $J$  = 48.8, 29.2, 18.4 Hz); <sup>13</sup>C NMR (100 MHz, D<sub>2</sub>O):  $\delta$  154.1, 142.0, 139.1 (C-1',2',4'), 130.1, 122.5, 118.1 (C-3',5',6'), 96.9 (d,  $J_{C,F}$  = 14.9 Hz, C-1), 90.2 (d,  $J_{C,F}$  = 183.9 Hz, C-2), 77.1 (C-5), 71.7 (d,  $J_{C,F}$  = 17.5 Hz, C-3), 66.6 (C-4), 60.7 (C-6). Anal. calcd. for C<sub>12</sub>H<sub>13</sub>FN<sub>2</sub>O<sub>9</sub> (348.24) + 0.4 mol acetone: C, 42.92; H, 4.87; N, 7.59. Found: C, 42.92; H, 4.27; N, 7.26.



Partial <sup>1</sup>H NMR spectrum (400 MHz, D<sub>2</sub>O) of 2,4-dinitrophenyl 2-deoxy-2-fluoro  $\beta$ -D-mannopyranoside.

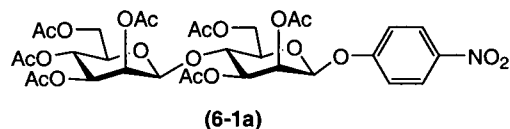
### **Oligosaccharide Synthesis with Man2A E519S**

The following describes synthetic and selected physical data for the per-*O*-acetylated oligosaccharide products listed in Table 6-1. Yields quoted are for purified, per-*O*-acetylated products and based on the acceptor. HPLC purification of oligosaccharide products was performed as described in the experimental for Chapter 5.

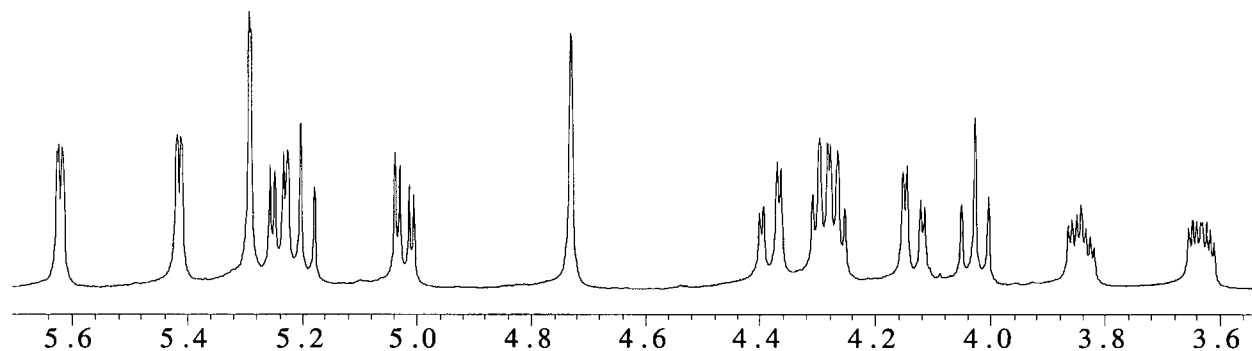
***p*-Nitrophenyl  $\beta$ -D-mannopyranoside as an acceptor:** PNP- $\beta$ -mannoside (30.3 mg, 100.6  $\mu$ mol) was dissolved in 2 mL 150 mM sodium citrate, pH 6. Man2a E519S was added to a final concentration of 1 mg/mL followed by 2 eq. of  $\alpha$ -mannosyl fluoride added in portions over time.

The reaction was maintained at room temperature. After 48 hrs. TLC (7:2:1 EtOAc/MeOH/H<sub>2</sub>O) indicated no further consumption of acceptor. Products were separated by HPLC, acetylated, then further purified by chromatography on silica gel.

***Man*β1-4*Man*β1-*OPNP*, *per-O*-acetate (**6-1a**)**

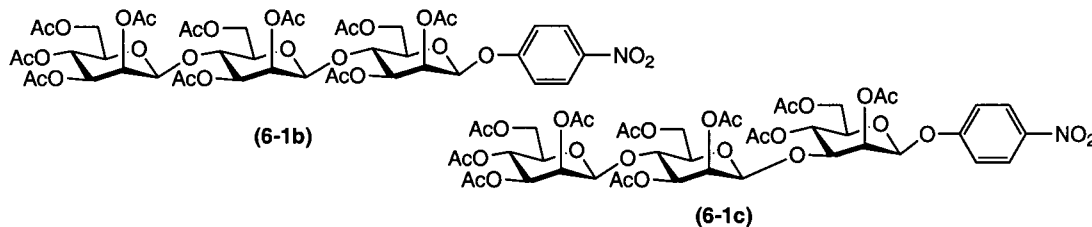


10.2 mg (13.5 μmol, 13.4 %); <sup>1</sup>H NMR (400 MHz, CDCl<sub>3</sub>): δ 5.62 (dd, 1 H, *J* = 0.8, 3.5 Hz, H-2<sup>1</sup>), 5.41 (dd, 1 H, *J* = 0.8, 3.4 Hz, H-2<sup>2</sup>), 5.29 (d, 1 H, *J* = 0.8 Hz, H-1<sup>1</sup>), 5.24 (dd, 1 H, *J* = 3.4, 9.4 Hz, H-3<sup>1</sup>), 5.20 (dd, 1 H, *J* = 9.8, 9.8 Hz, H-4<sup>2</sup>), 5.02 (dd, 1 H, *J* = 3.6, 9.9 Hz, H-3<sup>2</sup>), 4.73 (d, 1 H, *J* < 1.0 Hz, H-1<sup>2</sup>), 4.38 (dd, 1 H, *J* = 2.4, 12.0 Hz, H-6), 4.30-4.26 (m, 2 H, 2 × H-6), 4.13 (dd, 1 H, *J* = 2.5, 12.1 Hz, H-6), 4.03 (dd, 1 H, *J* = 9.5, 9.5 Hz, H-4<sup>1</sup>), 3.84 (ddd, 1 H, *J* = 2.7, 6.1, 9.1 Hz, H-5<sup>1</sup>), 3.63 (ddd, 1 H, *J* = 2.7, 5.3, 9.4 Hz, H-5<sup>2</sup>); <sup>13</sup>C NMR (100 MHz, CDCl<sub>3</sub>): δ 97.78 (*J*<sub>C,H</sub> = 161.3 Hz, C-1<sup>2</sup>), 95.89 (*J*<sub>C,H</sub> = 159.8 Hz, C-1<sup>1</sup>), 73.29 (C-5<sup>1</sup>), 72.70 (C-4<sup>1</sup>), 72.66 (C-5<sup>2</sup>), 70.56 (C-3<sup>2</sup>), 70.23 (C-3<sup>1</sup>), 68.60 (C-2<sup>1</sup>), 68.30 (C-2<sup>2</sup>), 65.78 (C-4<sup>1</sup>), 62.64 (C-6), 62.40 (C-6); HRMS (DCI<sup>+</sup>): *m/z*: 775.2414, calcd. for C<sub>32</sub>H<sub>43</sub>O<sub>20</sub>N<sub>2</sub> [M+NH<sub>4</sub>]<sup>+</sup>: 775.2409.

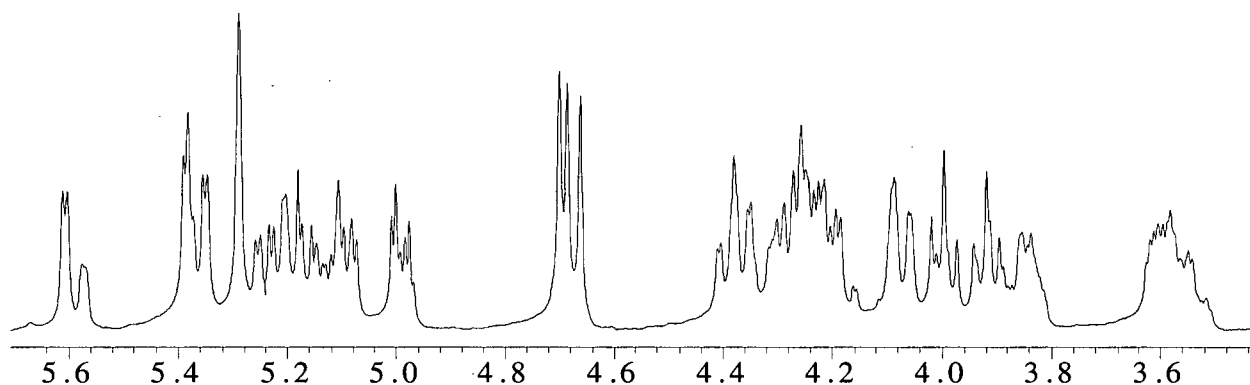


Partial <sup>1</sup>H NMR spectrum of **6-1a** (400 MHz, CDCl<sub>3</sub>).

*Man* $\beta$ 1-4*Man* $\beta$ 1-4*Man* $\beta$ 1-OPNP, *per*-O-acetate (6-1b) and *Man* $\beta$ 1-4*Man* $\beta$ 1-3*Man* $\beta$ 1-OPNP, *per*-O-acetate (6-1c), an inseparable 5:2 mixture

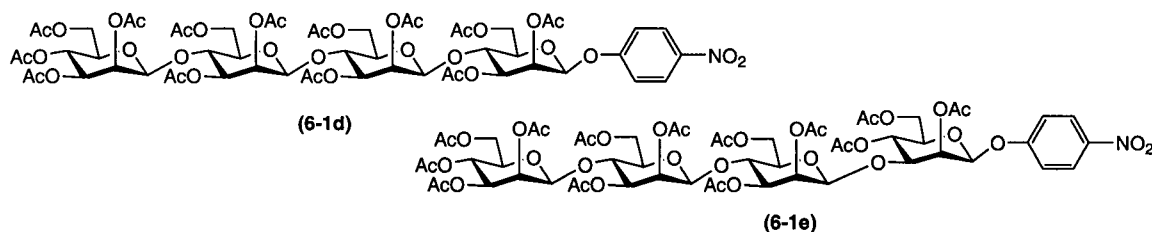


16.1 mg (15.4  $\mu$ mol, 15.3%); **Data for 6-1b:**  $^1\text{H}$  NMR (400 MHz,  $\text{CDCl}_3$ ):  $\delta$  5.61 (dd, 1 H,  $J = 1.4, 3.4$  Hz, H-2 $^1$ ), 5.39 (dd, 1 H,  $J = 3.4, \approx 1$  Hz, H-2 $^3$ ), 5.35 (dd, 1 H,  $J = 3.4, \approx 1$  Hz, H-2 $^2$ ), 5.29 (d, 1 H,  $J \approx 1$  Hz, H-1 $^1$ ), 5.21 (dd, 1 H,  $J = 3.4, 9.5$  Hz, H-3 $^1$ ), 5.19 (dd, 1 H,  $J = 9.5, 9.5$  Hz, H-4 $^3$ ), 5.09 (dd, 1 H,  $J = 3.4, 9.5$  Hz, H-3 $^2$ ), 4.99 (dd, 1 H,  $J = 3.4, 9.5$  Hz, H-3 $^3$ ), 4.71 (d, 1 H,  $J = 1.4$  Hz, H-1 $^3$ ), 4.69 (d, 1 H,  $J = 1.4$  Hz, H-1 $^2$ ), 4.37 (m, 2 H, 2  $\times$  H-6), 4.32-4.17 (m, 3 H, 3  $\times$  H-6), 4.06 (dd, 1 H,  $J = 12.3, 2.7$  Hz, H-6), 4.00 (dd, 1 H,  $J = 9.5, 9.5$  Hz, H-4 $^1$ ), 3.92 (dd, 1 H,  $J = 9.5, 9.5$  Hz, H-4 $^2$ ), 3.84 (m, 1 H, H-5 $^1$ ), 3.63-3.53 (m, 2H, H-5 $^{2,3}$ );  $^{13}\text{C}$  NMR (100 MHz,  $\text{CDCl}_3$ ):  $\delta$  97.95, 97.66, 95.78, 73.22, 72.98, 72.75, 72.65, 72.55, 70.65, 70.46, 70.14, 68.68, 68.52, 68.30, 65.72, 62.61, 62.53, 62.45. **Data for 6-1c:**  $^1\text{H}$  NMR (400 MHz,  $\text{CDCl}_3$ ):  $\delta$  5.58 (dd, 1 H,  $J = 1.4, 3.4$  Hz, H-2 $^1$ ), 5.38 (dd, 1 H,  $J \approx 1, 3.5$  Hz, H-2 $^3$ ), 5.29 (d, 1 H,  $J \approx 1$  Hz, H-1 $^1$ ), 5.25 (dd, 1 H,  $J \approx 1, 3.5$  Hz, H-2 $^2$ ), 5.18 (dd, 1 H,  $J = 9.5, 9.5$  Hz, H-4 $^3$ ), 5.13 (dd, 1 H,  $J = 3.4, 9.5$  Hz, H-3 $^2$ ), 5.11 (dd, 1 H,  $J = 9.5, 9.5$  Hz, H-4 $^1$ ), 4.98 (dd, 1 H,  $J = 3.4, 9.5$  Hz, H-3 $^3$ ), 4.66 (2  $\times$  d, 2 H,  $J \approx 1$  Hz each, H-1 $^{2,3}$ ), 4.35-4.15 (m, 6 H, 6  $\times$  H-6), 4.00 (dd, 1 H,  $J = 3.4, 9.5$  Hz, H-3 $^1$ ), 3.91 (dd, 1 H,  $J = 9.5, 9.5$  Hz, H-4 $^2$ ), 3.86 (m, 1 H, H-5 $^1$ ), 3.63-3.50 (m, 2 H, H-5 $^{2,3}$ );  $^{13}\text{C}$  NMR (100 MHz,  $\text{CDCl}_3$ ):  $\delta$  97.85, 74.72, 72.88, 72.62, 72.46, 70.70, 69.97, 68.57, 68.27, 66.87, 66.32, 65.80, 62.68; HRMS (DCI+) on mixture:  $m/z$ : 1063.3215, calcd. for  $\text{C}_{44}\text{H}_{59}\text{O}_{28}\text{N}_2$   $[\text{M}+\text{NH}_4]^+$ : 1063.3254.



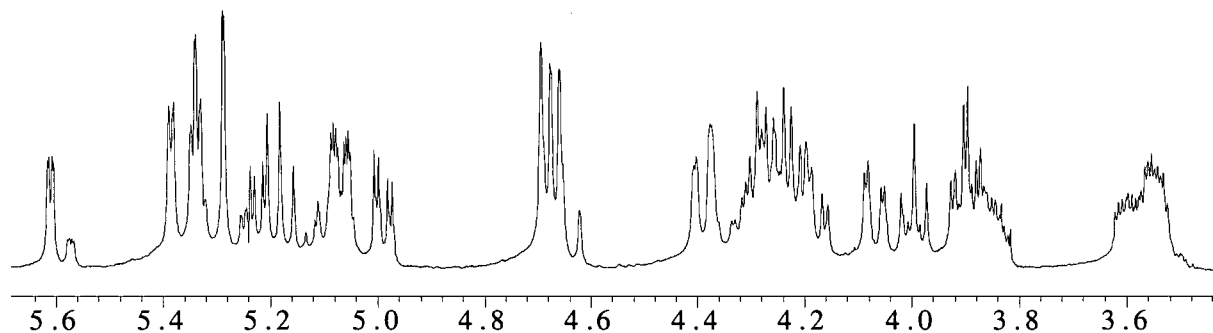
Partial  $^1\text{H}$  NMR spectrum of the mixture of **6-1b** and **6-1c** (400 MHz,  $\text{CDCl}_3$ ).

**Man $\beta$ 1-4Man $\beta$ 1-4Man $\beta$ 1-4Man $\beta$ 1-OPNP, per-O-acetate (6-1d) and Man $\beta$ 1-4Man $\beta$ 1-4Man $\beta$ 1-3Man $\beta$ 1-OPNP, per-O-acetate (6-1e), an inseparable 5:1 mixture**



5.6 mg (4.2 mmol, 4.2%); **Data for 6-1d:**  $^1\text{H}$  NMR (400 MHz,  $\text{CDCl}_3$ ):  $\delta$  5.61 (dd, 1 H,  $J = 3.3, 1.1$  Hz, H-2 $^1$ ), 5.39 (dd, 1 H,  $J = 3.3, < 1$  Hz, H-2), 5.34 (m, 2 H, 2  $\times$  H-2), 5.29 (d, 1 H,  $J = 1.1$  Hz, H-1 $^1$ ), 5.22 (dd, 1 H,  $J = 9.6, 3.7$  Hz, H-3 $^1$ ), 5.18 (dd, 1 H,  $J = 9.8, 9.8$  Hz, H-4 $^4$ ), 5.07 (m, 2 H, 2  $\times$  H-3), 4.99 (dd, 1 H,  $J = 3.3, 9.9$  Hz, H-3 $^4$ ), 4.69, 4.67, 4.66 (3  $\times$  d, 3 H,  $J < 1$  Hz each, 3  $\times$  H-1), 4.39 (2  $\times$  dd, 2 H,  $J \approx 2, 12$  Hz, H-6, H-6 $^1$ ), 4.34-4.15 (m, 5 H, 5  $\times$  H-6), 4.07 (dd, 1 H,  $J = 2.7, 12.2$  Hz, H-6), 4.00 (dd, 1 H,  $J = 9.4, 9.4$  Hz, H-4 $^1$ ), 3.90 (dd, 1 H,  $J = 9.4, 9.4$  Hz, H-4), 3.89 (dd, 1 H,  $J = 9.4, 9.4$  Hz, H-4), 3.85 (m, 1 H, H-5 $^1$ ), 3.60 (ddd, 1 H,  $J = 2.6, 5.5, 9.6$  Hz, H-5), 3.55 (m, 2 H, 2  $\times$  H-5);  $^{13}\text{C}$  NMR (100 MHz,  $\text{CDCl}_3$ ):  $\delta$  97.99, 97.95, 97.59 (3  $\times$  C-1), 95.80 (C-1 $^1$ ), 73.24, 73.01, 72.92, 72.78, 72.72 (2 lines), 72.57 (3  $\times$  C-4, 4  $\times$  C-5), 70.66 (2 lines), 70.47, 70.08 (4  $\times$  C-3), 68.73, 68.61, 68.55, 68.30 (4  $\times$  C-2), 65.74 (C-4 $^4$ ), 62.73 (C-6), 62.65 (C-6), 62.50 (2 lines, 2  $\times$  C-6). **Data for 6-1e:**  $^1\text{H}$  NMR (400 MHz,  $\text{CDCl}_3$ ):  $\delta$  5.57 (dd, 1 H,  $J = 3.3, 1.5$  Hz, H-2 $^1$ ), 5.32 (dd, 1 H,  $J = 3.3, < 1$  Hz, H-2), 5.29 (d, 1 H,  $J < 1$  Hz, H-1 $^1$ ), 5.25 (dd, 1 H,  $J = 3.3, < 1$  Hz, H-2), 5.12 (dd, 1 H,  $J = 9.5, 9.5$  Hz, H-4 $^1$ ), 5.10 (dd, 1 H,  $J = 3.3, 9.5$  Hz, H-3), 4.65 (d, 1 H,  $J < 1$  Hz, H-1), 4.62 (d, 1 H,  $J < 1$  Hz, H-1), 4.00 (dd, 1 H,  $J = 3.7, 9.5$  Hz, H-

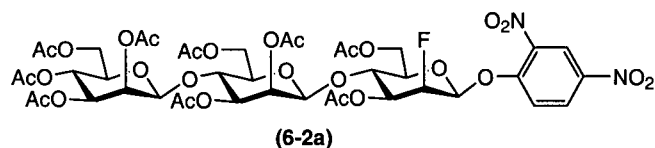
3<sup>1</sup>); HRMS (DCI+) on mixture:  $m/z$ : 1351.4072, calcd. for C<sub>56</sub>H<sub>75</sub>O<sub>36</sub>N<sub>2</sub> [M+NH<sub>4</sub>]<sup>+</sup>: 1351.4099.



Partial <sup>1</sup>H NMR spectrum of the mixture of **6-1d** and **6-1e** (400 MHz, CDCl<sub>3</sub>).

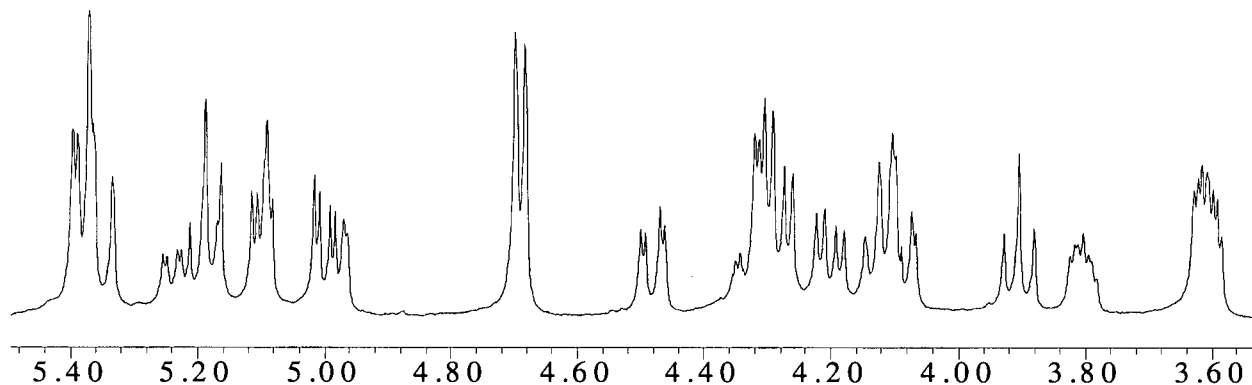
**2,4-Dinitrophenyl 2-deoxy-2-fluoro-β-D-mannopyranoside as an acceptor:** 23 mg (66 μmol) of acceptor was dissolved in 3 mL 150 mM sodium citrate, pH 6, and Man2a E519S was added to a final concentration of 2 mg/mL. α-Mannosyl fluoride was added in portions over time (3 eq. total) with the reaction mixture maintained at room temperature. At 120 hrs. TLC analysis (7:2:1 EtOAc/MeOH/H<sub>2</sub>O) indicated no further consumption of acceptor. Products were isolated and acetylated as described above.

***Manβ(1-4)Manβ(1-4)-2FManβ1-ODNP, per-O-acetate (6-2a)***



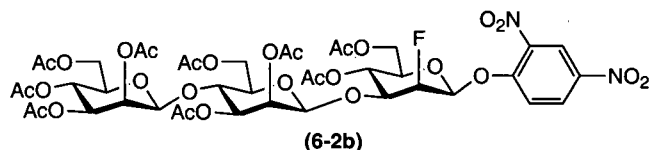
6.8 mg (6.5 μmol, 9.8%); R<sub>f</sub> (2:1 EtOAc/PE) = 0.37; <sup>1</sup>H NMR (400 MHz, CDCl<sub>3</sub>): δ 8.72 (d, 1 H,  $J = 2.7$  Hz, H-3 Ph), 8.41 (dd, 1 H,  $J = 2.7, 9.2$  Hz, H-5 Ph), 7.46 (d, 1 H,  $J = 9.1$  Hz, H-6 Ph), 5.39 (dd, 1 H,  $J = 3.1, < 1$  Hz, H-2<sup>3</sup>), 5.37 (m, 1 H, H-2<sup>2</sup>), 5.35 (dd, 1 H,  $J = 14.6, < 1$  Hz, H-1<sup>1</sup>), 5.21 (ddd, 1 H,  $J = 2.5, 9.1, 25.2$  Hz, H-3<sup>1</sup>), 5.19 (dd, 1 H,  $J = 9.8, 9.8$  Hz, H-4<sup>3</sup>), 5.10 (dd, 1 H,  $J = 3.4, 9.4$  Hz, H-3<sup>2</sup>), 5.03 (ddd, 1 H,  $J = 50.3, 2.3, < 1$  Hz, H-2<sup>1</sup>), 5.00 (dd, 1 H,  $J = 3.3, 9.9$  Hz, H-3<sup>3</sup>), 4.70 (d, 1 H,  $J < 1$  Hz, H-1<sup>3</sup>), 4.68 (d, 1 H,  $J < 1$  Hz, H-1<sup>2</sup>), 4.48 (dd, 1 H,  $J = 2.9, 12.2$  Hz, H-6a<sup>1</sup>), 4.30 (m, 3 H, 3 × H-6), 4.20 (dd, 1 H,  $J = 5.5, 12.4$  Hz, H-6b<sup>1</sup>), 4.12 (dd, 1 H,  $J = 8.7, 8.7$  Hz, H-4<sup>1</sup>), 4.08 (dd, 1 H,  $J = 2.5, 12.6$  Hz, H-6), 3.90 (dd, 1 H,  $J = 9.5, 9.5$  Hz, H-4<sup>2</sup>), 3.80 (ddd, 1 H,  $J = 3.1, 5.0, 8.3$  Hz, H-5<sup>1</sup>), 3.60 (m, 2 H, H-5<sup>2</sup>, H-5<sup>3</sup>); <sup>13</sup>C NMR (100 MHz,

CDCl<sub>3</sub>):  $\delta$  97.89, 97.86 (C-1<sup>2,3</sup>), 97.00 (d,  $J_{C,F}$  = 16.9 Hz, C-1<sup>1</sup>), 86.15 (d,  $J_{C,F}$  = 193.5 Hz, C-2<sup>1</sup>), 73.67, 73.02, 72.79, 72.57, 72.18 (d,  $J_{C,F}$   $\approx$  2 Hz, C-4<sup>1</sup>), 70.63, 70.55, 69.70 (d,  $J_{C,F}$  = 17.2 Hz, C-3<sup>1</sup>), 68.72, 68.30, 65.73 (C-4<sup>3</sup>), 62.52 (C-6), 62.46 (C-6), 61.90 (C-6); <sup>19</sup>F NMR (188 MHz, CDCl<sub>3</sub>, <sup>1</sup>H decoupled):  $\delta$  -141.61; HRMS (DCI+):  $m/z$ : 1068.2920, calcd. for C<sub>42</sub>H<sub>55</sub>O<sub>28</sub>N<sub>3</sub>F [M+NH<sub>4</sub>]<sup>+</sup>: 1068.2956.



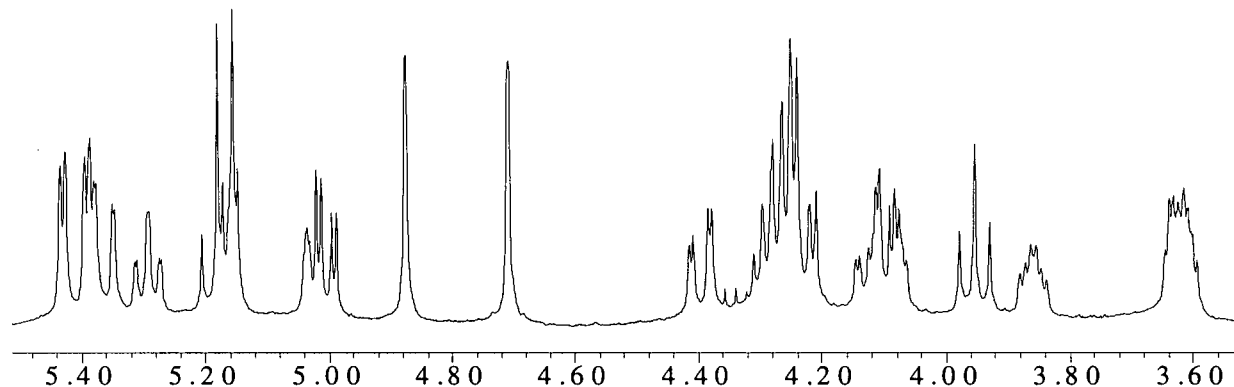
Partial <sup>1</sup>H NMR spectrum of **6-2a** (400 MHz, CDCl<sub>3</sub>).

***Man* $\beta$ (1-4)*Man* $\beta$ (1-3)-2*FMan* $\beta$ 1-ODNP, *per-O*-acetate (**6-2b**)**



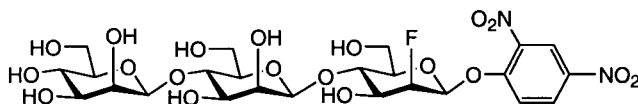
5.1 mg (4.9  $\mu$ mol, 7.4%); R<sub>f</sub> (2:1 EtOAc/PE) = 0.18; <sup>1</sup>H NMR (400 MHz, CDCl<sub>3</sub>):  $\delta$  8.73 (d, 1 H,  $J$  = 2.6 Hz, H-3 Ph), 8.39 (dd, 1 H,  $J$  = 2.6, 9.2 Hz, H-5 Ph), 7.51 (d, 1 H,  $J$  = 9.2 Hz, H-6 Ph), 5.43 (dd, 1 H,  $J$  = 2.9, < 1 Hz, H-2<sup>2</sup>), 5.39 (dd, 1 H,  $J$  = 3.3, < 1 Hz, H-2<sup>3</sup>), 5.36 (dd, 1 H,  $J$  = 12.1, 1.3 Hz, H-1<sup>1</sup>), 5.29 (ddd, 1 H,  $J$  = 1.5, 8.3, 8.3 Hz, H-4<sup>1</sup>), 5.18 (dd, 1 H,  $J$  = 9.9, 9.9 Hz, H-4<sup>3</sup>), 5.16 (dd, 1 H,  $J$  = 3.5, 9.7 Hz, H-3<sup>2</sup>), 5.10 (ddd, 1 H,  $J$  = 48.2,  $\approx$  2, < 1 Hz, H-2<sup>1</sup>), 5.00 (dd, 1 H,  $J$  = 3.3, 9.9 Hz, H-3<sup>3</sup>), 4.88 (d, 1 H,  $J$  < 1 Hz, H-1<sup>2</sup>), 4.71 (d, 1 H,  $J$  < 1 Hz, H-1<sup>3</sup>), 4.40 (dd, 1 H,  $J$  = 2.6, 12.1 Hz, H-6), 4.25 (m, 4 H, 4  $\times$  H-6), 4.10 (ddd, 1 H,  $J$  = 2.2, 8.1, 21.7 Hz, H-3<sup>1</sup>), 4.09 (dd, 1 H,  $J$  = 2.6, 12.1 Hz, H-6), 3.98 (dd, 1 H,  $J$  = 9.6, 9.6 Hz, H-4<sup>2</sup>), 3.86 (m, 1 H, H-5<sup>1</sup>), 3.62 (m, 2 H, H-5<sup>2,3</sup>); <sup>13</sup>C NMR (100 MHz, CDCl<sub>3</sub>):  $\delta$  97.80 (C-1), 97.62 (d,  $J_{C,F}$  = 17.8 Hz, C-1<sup>1</sup>), 95.89 (C-1), 85.35 (d,  $J_{C,F}$  = 195.7 Hz, C-2<sup>1</sup>), 73.40, 73.37 (d,  $J_{C,F}$  = 17.0 Hz, C-3<sup>1</sup>), 73.13, 72.83, 72.60, 70.71, 70.46, 68.85, 68.37, 66.27 (d,  $J_{C,F}$   $\approx$  2 Hz, H-4<sup>1</sup>), 65.83 (C-4<sup>3</sup>), 62.50 (2

lines,  $2 \times$  C-6), 62.23 (C-6);  $^{19}\text{F}$  NMR (188 MHz,  $\text{CDCl}_3$ ,  $^1\text{H}$  decoupled):  $\delta$  -139.92; HRMS (DCI+):  $m/z$ : 1068.2909, calcd. for  $\text{C}_{42}\text{H}_{55}\text{O}_{28}\text{N}_3\text{F}$   $[\text{M}+\text{NH}_4]^+$ : 1068.2956.



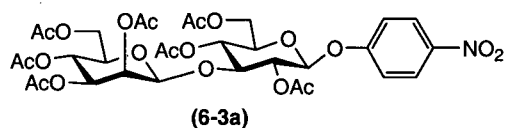
Partial  $^1\text{H}$  NMR spectrum of **6-2b** (400 MHz,  $\text{CDCl}_3$ ).

#### **2,4-Dinitrophenyl 2-deoxy-2-fluoro- $\beta$ -mannotrioside**

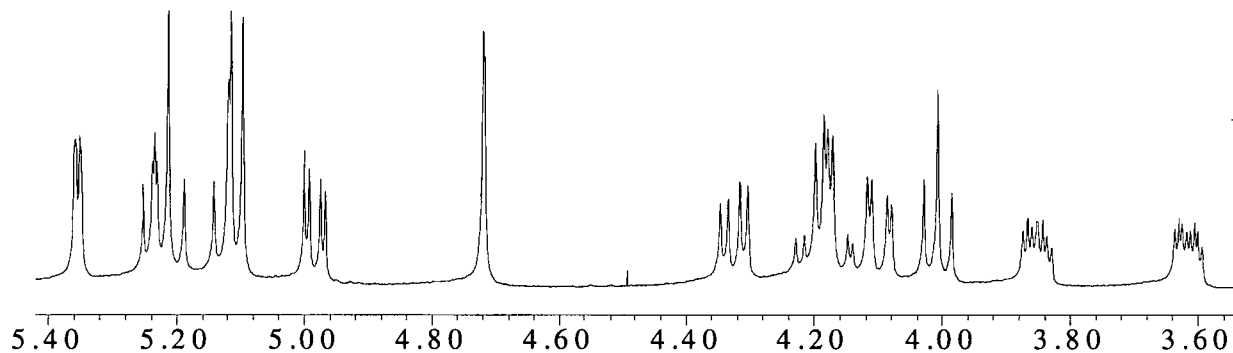


2,4-Dinitrophenyl 2-deoxy-2-fluoro- $\beta$ -mannoside (403 mg, 1.16 mmol) was dissolved in 47 mL 100 mM citrate (pH 6). An aliquot of  $\alpha$ -mannosyl fluoride was then added (181 mg, 0.99 mmol, 0.86 eq., in 2 mL citrate buffer) followed by 51 mg of Man2A E519S (4.5 mL of 11.4 mg/mL). The reaction was maintained at room temperature for 20 hrs., whereupon a further 38 mg of Man2A E519S was added. After 24 hrs. at room temperature complete consumption of  $\alpha$ -mannosyl fluoride was observed by TLC (30:2:1 EtOAc/MeOH/ $\text{H}_2\text{O}$ ). The reaction mixture was clarified by centrifugation and the Man2A E519S removed by ultrafiltration (30 kDa NMW membrane). After evaporating the water in vacuo and drying the resulting residue over  $\text{P}_2\text{O}_5$  the crude oligosaccharide mixture was acetylated with 100 mL 2:1  $\text{Ac}_2\text{O}$ /pyridine over 24 hrs.. The solvent was then evaporated in vacuo and the crude mixture purified by flash chromatography on silica gel (3:2 to 3:1 EtOAc/PE on a 5 cm  $\times$  20 cm column). The per-*O*-acetylated trisaccharides **6-2a** (105 mg, 0.1 mmol, 10.1% based on  $\alpha$ -ManF) and **6-2b** (84 mg, 0.08 mmol, 8.1%) were obtained as the major products. **6-2a** (64 mg, 0.061 mmol) was then deprotected in acidic methanol (25 mL, 2% HCl) over 2 days at  $4^\circ\text{C}$ . After evaporation of the solvent the crude product was purified by HPLC (TosoHaas Amide 80, 21.5  $\times$  30 cm, 4:1 to 3:2 acetonitrile/ $\text{H}_2\text{O}$ , 5 mL/min) then lyophilized to obtain a white solid (28.4 mg, 0.042 mmol, 69%).  $R_f$  (7:2:1

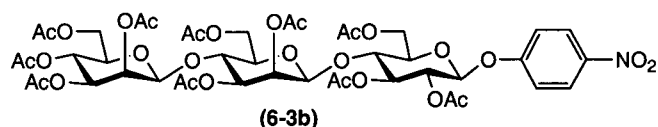


**Man $\beta$ 1-3Glu $\beta$ 1-OPNP, per-O-acetate (6-3a)**

10.3 mg (13.6  $\mu$ mol, 8.6%); Rf (1:1 EtOAc/PE) = 0.24;  $^1\text{H}$  NMR (400 MHz,  $\text{CDCl}_3$ ):  $\delta$  5.35 (dd, 1 H,  $J = 0.9, 3.3$  Hz, H-2 $^2$ ), 5.23 (dd, 1 H,  $J = 7.2, 8.6$  Hz, H-2 $^1$ ), 5.21 (dd, 1 H,  $J = 9.9, 9.9$  Hz, H-4 $^2$ ), 5.12 (dd, 1 H,  $J = 9.0, 9.0$  Hz, H-4 $^1$ ), 5.10 (d, 1 H,  $J = 7.2$  Hz, H-1 $^1$ ), 4.98 (dd, 1 H,  $J = 3.4, 10.1$  Hz, H-3 $^2$ ), 4.72 (d, 1 H,  $J = 1.0$  Hz, H-1 $^2$ ), 4.32 (dd, 1 H,  $J = 4.9, 12.3$  Hz, H-6), 4.21 (dd, 1 H,  $J = 5.5, 12.2$  Hz, H-6), 4.16 (dd, 1 H,  $J = 2.8, 12.1$  Hz, H-6), 4.10 (dd, 1 H,  $J = 2.8, 12.3$  Hz, H-6), 4.01 (dd, 1 H,  $J = 8.8, 8.8$  Hz, H-3 $^1$ ), 3.85 (ddd, 1 H,  $J = 3.0, 5.5, 9.5$  Hz, H-5 $^1$ ), 3.61 (ddd, 1 H,  $J = 2.7, 4.8, 9.8$  Hz, H-5 $^2$ );  $^{13}\text{C}$  NMR (100 MHz,  $\text{CDCl}_3$ ): 98.37 ( $J_{\text{C,H}} = 158.8$  Hz, C-1), 98.02 ( $J_{\text{C,H}} = 163.8$  Hz, C-1), 78.16, 72.59, 72.49, 71.89, 70.84, 68.25, 67.74, 65.72, 62.27 (C-6), 62.09 (C-6); HRMS (DCI $^+$ ):  $m/z$ : 775.2408, calcd. for  $\text{C}_{32}\text{H}_{43}\text{O}_{20}\text{N}_2$  [ $\text{M}+\text{NH}_4$ ] $^+$ : 775.2409.

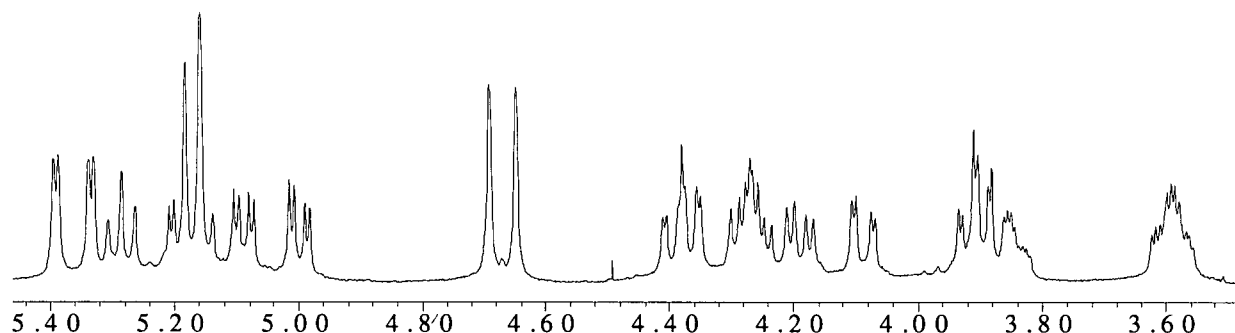


Partial  $^1\text{H}$  NMR spectrum of **6-3a** (400 MHz,  $\text{CDCl}_3$ ).

**Man $\beta$ 1-4Man $\beta$ 1-4Glu $\beta$ 1-OPNP, per-O-acetate (6-3b)**

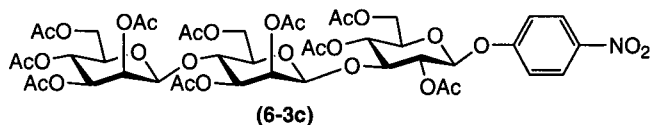
3.6 mg (3.4  $\mu$ mol, 2.2%); Rf (2:1 EtOAc/PE) = 0.85;  $^1\text{H}$  NMR (400 MHz,  $\text{CDCl}_3$ ):  $\delta$  5.39 (dd, 1 H,  $J = <1.0, 3.0$  Hz, H-2 $^3$ ), 5.33 (dd, 1 H,  $J = <1.0, 3.1$  Hz, H-2 $^2$ ), 5.28 (dd, 1 H,  $J = 8.7, 8.7$  Hz, H-3 $^1$ ), 5.21-5.13 (m, 3 H, H-1 $^1$ , H-2 $^1$ , H-4 $^3$ ), 5.09 (dd, 1 H,  $J = 3.3, 9.5$  Hz, H-3 $^2$ ), 5.00 (dd, 1 H,

$J = 3.4, 10.0$  Hz, H-3<sup>3</sup>), 4.69 (d, 1 H,  $J < 1.0$  Hz, H-1<sup>3</sup>), 4.65 (d, 1 H,  $J < 1.0$  Hz, H-1<sup>2</sup>), 4.39 (dd, 1 H,  $J = 2.3, 12.1$  Hz, H-6), 4.36 (dd, 1 H,  $J = 2.5, 12.2$  Hz, H-6), 4.27 (dd, 1 H,  $J = 5.4, 12.3$  Hz, H-6), 4.25 (dd, 1 H,  $J = 4.7, 12.2$  Hz, H-6), 4.19 (dd, 1 H,  $J = 4.8, 12.5$  Hz, H-6<sup>1</sup>), 4.09 (dd, 1 H,  $J = 2.7, 12.3$  Hz, H-6), 3.91 (m, 2 H,  $J \approx 9.5, 9.5$  Hz, H-4<sup>1</sup>, H-4<sup>2</sup>), 3.84 (ddd, 1 H,  $J = 2.2, 4.6, 9.8$  Hz, H-5<sup>1</sup>), 3.59 (m, 2 H, H-5<sup>2</sup>, H-5<sup>3</sup>); <sup>13</sup>C NMR (100 MHz, CDCl<sub>3</sub>):  $\delta$  97.92 (2 lines, 2  $\times$  C-1), 97.30 (C-1), 74.57, 73.04, 73.02, 72.77, 72.61, 71.67, 71.15, 70.69, 70.50, 68.64, 68.34, 65.80, 62.48 (2 lines, 2  $\times$  C-6), 62.07 (C-6); HRMS (DCI<sup>+</sup>):  $m/z$ : 1063.323, calcd. for C<sub>44</sub>H<sub>59</sub>O<sub>28</sub>N<sub>2</sub> [M+NH<sub>4</sub>]<sup>+</sup>: 1063.325.



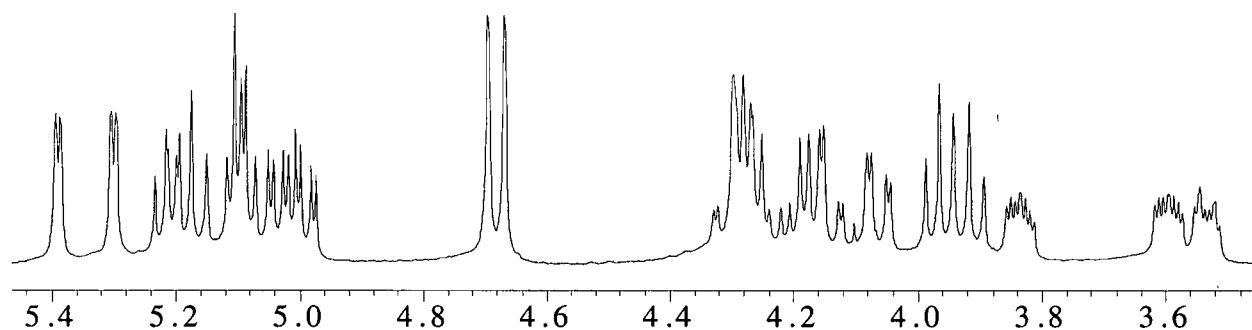
Partial <sup>1</sup>H NMR spectrum of **6-3b** (400 MHz, CDCl<sub>3</sub>).

**Man $\beta$ 1-4Man $\beta$ 1-3Glu $\beta$ 1-OPNP, per-O-acetate (6-3c)**



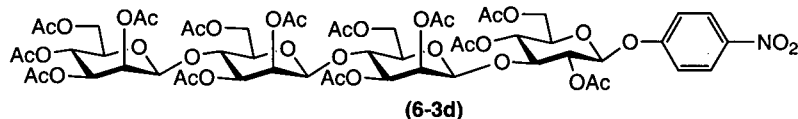
66.4 mg (63.5  $\mu$ mol, 40%); Rf (2:1 EtOAc/PE) = 0.73; <sup>1</sup>H NMR (400 MHz, CDCl<sub>3</sub>):  $\delta$  5.39 (dd, 1 H,  $J = 2.4, < 1.0$  Hz, H-2<sup>3</sup>), 5.30 (dd, 1 H,  $J = 2.7, < 1.0$  Hz, H-2<sup>2</sup>), 5.21 (dd, 1 H,  $J = 7.3, 8.6$  Hz, H-2<sup>1</sup>), 5.17 (dd, 1 H,  $J = 9.8, 9.8$  Hz, H-4<sup>3</sup>), 5.09 (d, 1 H,  $J = 7.3$  Hz, H-1<sup>1</sup>), 5.09 (dd, 1 H,  $J = 9.1, 9.1$  Hz, H-4<sup>1</sup>), 5.03 (dd, 1 H,  $J = 3.4, 9.9$  Hz, H-3<sup>2</sup>), 4.99 (dd, 1 H,  $J = 3.1, 9.8$  Hz, H-3<sup>3</sup>), 4.69 (d, 1 H,  $J < 1.0$  Hz, H-1<sup>3</sup>), 4.67 (d, 1 H,  $J < 1.0$  Hz, H-1<sup>2</sup>), 4.33-4.23 (m, 3 H, 3  $\times$  H-6), 4.20 (dd, 1 H,  $J = 5.4, 12.1$  Hz, H-6), 4.14 (dd, 1 H,  $J = 2.8, 12.3$  Hz, H-6), 4.06 (dd, 1 H,  $J = 2.7, 12.5$  Hz, H-6), 3.96 (dd, 1 H,  $J = 9.0, 9.0$  Hz, H-3<sup>1</sup>), 3.92 (dd, 1 H,  $J = 9.4, 9.4$  Hz, H-4<sup>2</sup>), 3.83 (ddd, 1 H,  $J = 2.7, 5.6, 8.9$  Hz, H-5<sup>1</sup>), 3.59 (ddd, 1 H,  $J = 2.7, 5.5, 9.6$  Hz, H-5<sup>3</sup>), 3.53 (ddd, 1 H,  $J = 2.9, 3.8, 9.5$  Hz, H-5<sup>2</sup>); <sup>13</sup>C NMR (100 MHz, CDCl<sub>3</sub>):  $\delta$  98.42 (C-1), 98.08 (C-1), 97.97 (C-1), 78.23, 72.84, 72.76, 72.54, 72.51, 71.84, 70.96, 70.67, 68.62, 68.35, 67.76, 65.75, 62.60 (C-

6), 62.50 (C-6), 62.08 (C-6); HRMS (DCI+):  $m/z$ : 1063.323, calcd. for  $C_{44}H_{59}O_{28}N_2$   $[M+NH_4]^+$ : 1063.325.

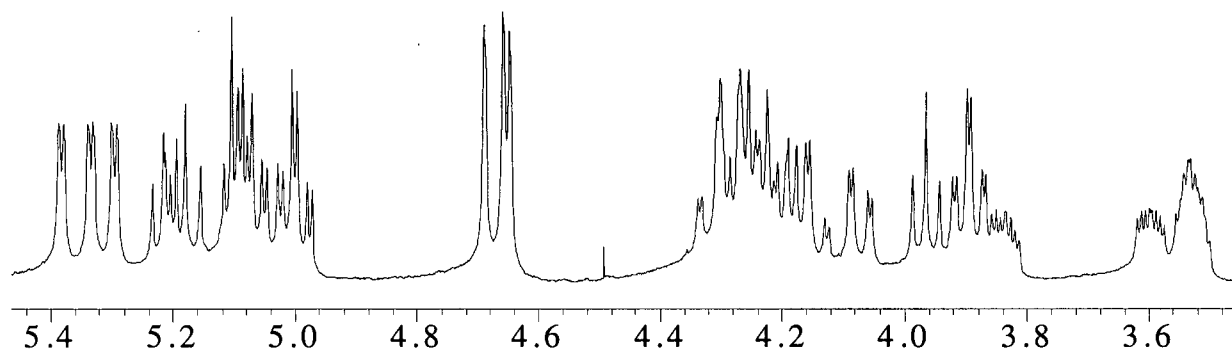


Partial  $^1H$  NMR spectrum of **6-3c** (400 MHz,  $CDCl_3$ ).

***Man* $\beta$ 1-4*Man* $\beta$ 1-4*Man* $\beta$ 1-3*Glu* $\beta$ 1-*OPNP*, *per-O*-acetate (**6-3d**)**



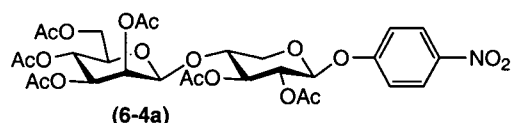
5.7 mg (4.3  $\mu$ mol, 2.7%) Rf (2:1 EtOAc/PE) = 0.24;  $^1H$  NMR (400 MHz,  $CDCl_3$ ):  $\delta$  5.38, 5.33, 5.29 (3  $\times$  dd, 3 H,  $J$  = 3.3, < 1.0 Hz, H-2<sup>2,3,4</sup>), 5.21 (dd, 1 H,  $J$  = 7.2, 8.6 Hz, H-2<sup>1</sup>), 5.18 (dd, 1 H,  $J$  = 9.8, 9.8 Hz, H-4<sup>4</sup>), 5.09 (d, 1 H,  $J$  = 7.3 Hz, H-1<sup>1</sup>), 5.09 (dd, 1 H,  $J$  = 9.1, 9.1 Hz, H-4<sup>1</sup>), 5.06, 5.01 (2  $\times$  dd, 2 H,  $J$  = 3.4, 9.4 Hz, H-3<sup>2,3</sup>), 4.98 (dd, 1 H,  $J$  = 3.4, 9.8 Hz, H-3<sup>4</sup>), 4.69, 4.65, 4.64 (3  $\times$  s, 3 H,  $J$  < 1.0 Hz, H-1<sup>2,3,4</sup>), 4.34-4.17 (m, 6 H, 6  $\times$  H-6), 4.14 (dd, 1 H,  $J$  = 2.8, 12.4 Hz, H-6), 4.07 (dd, 1 H,  $J$  = 2.6, 12.3 Hz, H-6), 3.96 (dd, 1 H,  $J$  = 8.7, 8.7 Hz, H-3<sup>1</sup>), 3.89 (2  $\times$  dd, 2 H,  $J$  = 9.6, 9.6 Hz, H-4<sup>2,3</sup>), 3.83 (ddd, 1 H,  $J$  = 2.9, 5.4, 9.3 Hz, H-5<sup>1</sup>), 3.60 (ddd, 1 H,  $J$  = 2.7, 5.5, 9.6 Hz, H-5<sup>4</sup>), 3.53 (m, 2 H, H-5<sup>2,3</sup>);  $^{13}C$  NMR (100 MHz,  $CDCl_3$ ):  $\delta$  98.41 (C-1), 98.00 (3 lines, 3  $\times$  C-1), 78.19, 72.89 (2 lines), 72.84, 72.74, 72.57 (2 lines), 71.88, 70.90, 70.67 (2 lines), 68.80, 68.59, 68.31, 67.77, 65.75, 62.76 (C-6), 62.59 (C-6), 62.51 (C-6), 62.10 (C-6); HRMS (DCI+):  $m/z$ : 1351.410, calcd. for  $C_{56}H_{75}O_{36}N_2$   $[M+NH_4]^+$ : 1351.410.



Partial  $^1\text{H}$  NMR spectrum of **6-3d** (400 MHz,  $\text{CDCl}_3$ ).

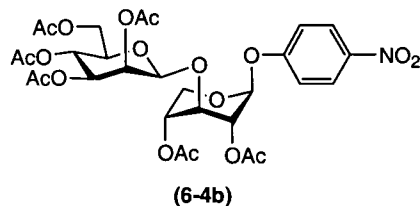
***p*-Nitrophenyl  $\beta$ -D-xylopyranoside as an acceptor:** 32 mg (118  $\mu\text{mol}$ ) acceptor was dissolved in 4 mL 150 mM sodium citrate, pH 6. Man2a E519S added to a final concentration of 1 mg/mL.  $\alpha$ -Mannosyl fluoride (4 eq.) was added portion-wise over time while maintaining the reaction at room temperature. At 70 hrs. TLC analysis (7:2:1 EtOAc/MeOH/ $\text{H}_2\text{O}$ ) indicated no further consumption of acceptor. The products were isolated and acetylated in the usual manner.

***Man* $\beta$ 1-4*Xyl*( $^4\text{C}_1$ ) $\beta$ 1-*OPNP*, *per-O*-acetate (**6-4a**)**



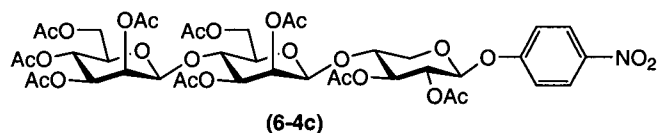
1.0 mg (1.5  $\mu\text{mol}$ , 1.3%); Rf (1:1 EtOAc/PE) = 0.51;  $^1\text{H}$  NMR (400 MHz,  $\text{CDCl}_3$ ):  $\delta$  5.42 (dd, 1 H,  $J = 3.2, < 1.0$  Hz, H-2 $^2$ ), 5.22 (dd, 1 H,  $J = 7.7, 7.7$  Hz, H-3 $^1$ ), 5.21 (dd, 1 H,  $J = 10.0, 10.0$  Hz, H-4 $^2$ ), 5.19 (dd, 1 H,  $J = 6.1$  Hz, H-1 $^1$ ), 5.12 (dd, 1 H,  $J = 6.1, 7.9$  Hz, H-2 $^1$ ), 5.00 (dd, 1 H,  $J = 3.3, 10.1$  Hz, H-3 $^2$ ), 4.72 (d, 1 H,  $J = < 1.0$  Hz, H-1 $^2$ ), 4.29 (dd, 1 H,  $J = 5.6, 12.2$  Hz, H-6 $^2$ ), 4.11 (dd, 1 H,  $J = 2.5, 12.2$  Hz, H-6 $^2$ ), 4.08 (dd, 1 H,  $J = 4.6, 12.1$  Hz, H-5 $^1$ ), 3.96 (ddd, 1 H,  $J = 4.6, 7.9, 7.9$  Hz, H-4 $^1$ ), 3.65 (ddd, 1 H,  $J = 2.5, 5.5, 9.8$  Hz, H-5 $^2$ ), 3.56 (dd, 1 H,  $J = 8.2, 12.1$  Hz, H-5 $^1$ ); HRMS (DCI $^+$ ):  $m/z$ : 703.2189, calcd. for  $\text{C}_{29}\text{H}_{39}\text{O}_{18}\text{N}_2$  [ $\text{M}+\text{NH}_4$ ] $^+$ : 703.2198.

***Man* $\beta$ 1-3*Xyl*( $^1C_4$ ) $\beta$ 1-*OPNP*, per-*O*-acetate (6-4b)**

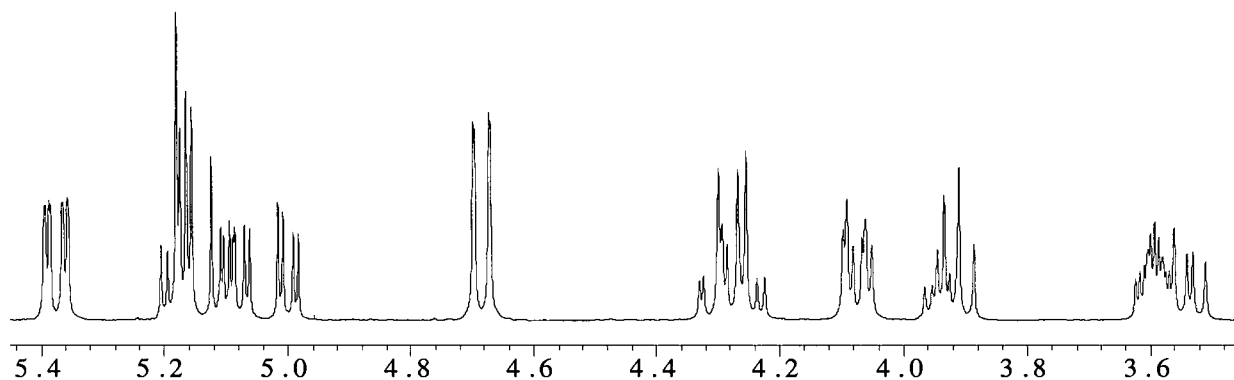


1.0 mg (1.5  $\mu$ mol, 1.3%); Rf (1:1 EtOAc/PE) = 0.25;  $^1\text{H}$  NMR (400 MHz,  $\text{CDCl}_3$ ):  $\delta$  5.55 (dd, 1 H,  $J = 3.3, < 1.0$  Hz, H-2<sup>2</sup>), 5.43 (d, 1 H,  $J = 2.8$  Hz, H-1<sup>1</sup>), 5.25 (dd, 1 H,  $J = 10.0, 10.0$  Hz, H-4<sup>2</sup>), 5.06 (dd, 1 H,  $J = 10.1, 3.3$  Hz, H-3<sup>2</sup>), 5.02 (m, 1 H, H-2<sup>1</sup>), 4.98 (m, 1 H, H-4<sup>1</sup>), 4.89 (d, 1 H,  $J < 1.0$  Hz, H-1<sup>2</sup>), 4.32 (dd, 1 H,  $J = 5.4, 12.3$  Hz, H-6<sup>2</sup>), 4.12 (dd, 1 H,  $J = 2.7, 12.3$  Hz, H-6<sup>2</sup>), 4.11 (dd, 1 H,  $J = 2.7, 12.8$  Hz, H-5<sup>1</sup>), 4.04 (dd, 1 H,  $J \approx 4.5, 4.5$  Hz, H-3<sup>1</sup>), 3.68 (ddd, 1 H,  $J = 2.6, 5.3, 9.8$  Hz, H-5<sup>2</sup>), 3.63 (dd, 1 H,  $J = 3.2, 13.0$  Hz, H-5<sup>1</sup>); NOE's observed upon irradiation of  $\delta$  5.43 (H-1<sup>1</sup>):  $\delta$  7.10 (15%, Ph H-2,6), 5.02 (5%, H-2<sup>1</sup>), 4.04 (2%, H-3<sup>1</sup>), 3.63 (1%, H-5<sup>1</sup>); HRMS (DCI<sup>+</sup>):  $m/z$ : 703.2192, calcd. for  $\text{C}_{29}\text{H}_{39}\text{O}_{18}\text{N}_2$   $[\text{M}+\text{NH}_4]^+$ : 703.2198.

***Man* $\beta$ 1-4*Man* $\beta$ 1-4*Xyl*( $^4C_1$ ) $\beta$ 1-*OPNP*, per-*O*-acetate (6-4c)**

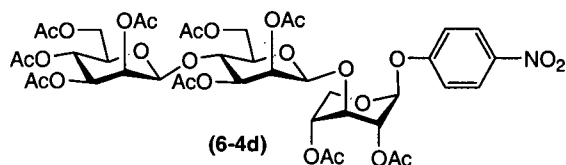


10 mg (10.3  $\mu$ mol, 8.7%); Rf (2:1 EtOAc/PE) = 0.48;  $^1\text{H}$  NMR (400 MHz,  $\text{CDCl}_3$ ):  $\delta$  5.39 (dd, 1 H,  $J = 0.9, 3.3$  Hz, H-2<sup>3</sup>), 5.36 (dd, 1 H,  $J = 0.9, 3.3$  Hz, H-2<sup>2</sup>), 5.17 (m, 3 H, H-1<sup>1</sup>, H-3<sup>1</sup>, H-4<sup>3</sup>), 5.10 (dd, 1 H,  $J = 6.2, 7.9$  Hz, H-2<sup>1</sup>), 5.08 (dd, 1 H,  $J = 3.4, 9.6$  Hz, H-3<sup>2</sup>), 5.00 (dd, 1 H,  $J = 3.2, 9.9$  Hz, H-3<sup>3</sup>), 4.70 (d, 1 H,  $J = 1.2$  Hz, H-1<sup>3</sup>), 4.67 (d, 1 H,  $J = 0.9$  Hz, H-1<sup>2</sup>), 4.31 (dd, 1 H,  $J = 2.7, 12.2$  Hz, H-6), 4.28 (dd, 1 H,  $J = 5.6, 12.5$  Hz, H-6), 4.24 (dd, 1 H,  $J = 5.0, 12.2$  Hz, H-6), 4.08 (dd, 1 H,  $J = 2.3, 12.2$  Hz, H-6), 4.07 (dd, 1 H,  $J = 4.1, 12.2$  Hz, H-5a<sup>1</sup>), 3.94 (ddd, 1 H,  $J = 4.6, 7.9, 7.9$  Hz, H-4<sup>1</sup>), 3.91 (dd, 1 H,  $J = 9.5, 9.5$  Hz, H-4<sup>2</sup>), 3.60 (m, 2 H, H-5<sup>2,3</sup>), 3.53 (dd, 1 H,  $J = 8.3, 12.0$  Hz, H-5b<sup>1</sup>);  $^{13}\text{C}$  NMR (100 MHz,  $\text{CDCl}_3$ ):  $\delta$  98.03 (C-1), 97.95 (C-1), 96.56 (C-1), 72.98, 72.85 (2 lines), 72.55, 70.80, 70.70, 70.64, 69.79, 68.96, 68.33, 65.83, 62.65 (C-6), 62.51 (C-6), 62.27 (C-5<sup>1</sup>); HRMS (DCI<sup>+</sup>):  $m/z$ : 991.3081, calcd. for  $\text{C}_{41}\text{H}_{55}\text{O}_{26}\text{N}_2$   $[\text{M}+\text{NH}_4]^+$ : 991.3043.

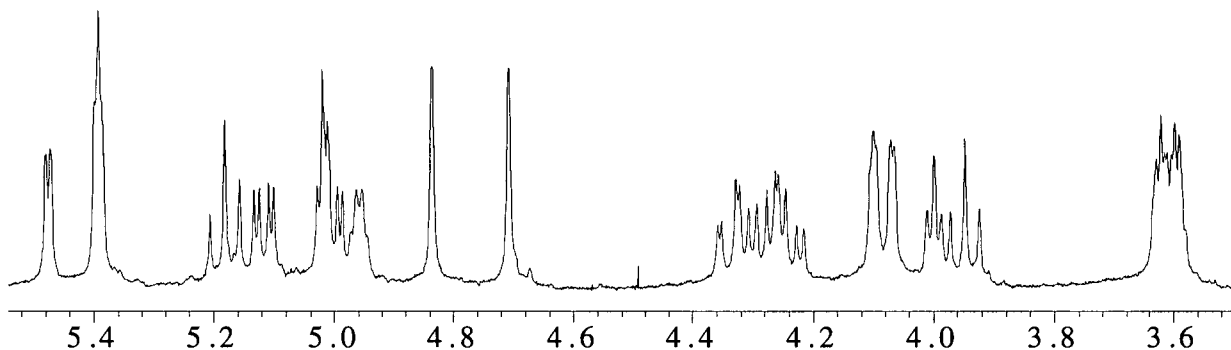


Partial  $^1\text{H}$  NMR spectrum of **6-4c** (400 MHz,  $\text{CDCl}_3$ ).

***Man $\beta$ 1-4Man $\beta$ 1-3Xyl( $^1\text{C}_4$ ) $\beta$ 1-OPNP, per-O-acetate (6-4d)***

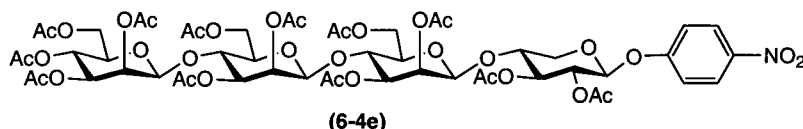


22 mg (22.6  $\mu\text{mol}$ , 19.1%); Rf (2:1 EtOAc/PE) = 0.37;  $^1\text{H}$  NMR (400 MHz,  $\text{CDCl}_3$ ):  $\delta$  5.47 (dd, 1 H,  $J = 3.3$ ,  $< 1$  Hz, H-2<sup>2</sup>), 5.39 (m, 2 H, H-1<sup>1</sup>, H-2<sup>3</sup>), 5.18 (dd, 1 H,  $J = 9.7$ , 9.7 Hz, H-4<sup>3</sup>), 5.11 (dd, 1 H,  $J = 3.3$ , 9.5 Hz, H-3<sup>2</sup>), 5.01 (m, 1 H, H-2<sup>1</sup>), 4.99 (dd, 1 H,  $J = 3.0$ , 9.7 Hz, H-3<sup>3</sup>), 4.95 (m, 1 H, H-4<sup>1</sup>), 4.83 (d, 1 H,  $J < 1$  Hz, H-1<sup>2</sup>), 4.71 (d, 1 H,  $J < 1$  Hz, H-1<sup>3</sup>), 4.33 (dd, 1 H,  $J = 2.7$ , 12.2 Hz, H-6), 4.28 (dd, 1 H,  $J = 5.5$ , 12.2 Hz, H-6), 4.23 (dd, 1 H,  $J = 4.9$ , 12.2 Hz, H-6), 4.08 (m, 2 H, H-6, H-5a<sup>1</sup>), 3.99 (dd, 1 H,  $J \approx 4.7$ , 4.7 Hz, H-3<sup>1</sup>), 3.95 (dd, 1 H,  $J = 9.7$ , 9.7 Hz, H-4<sup>2</sup>), 3.60 (m, 3 H, H-5<sup>2,3</sup>, H-5b<sup>1</sup>);  $^{13}\text{C}$  NMR (100 MHz,  $\text{CDCl}_3$ ):  $\delta$  98.12 (C-1), 97.98 (C-1), 96.23 (C-1<sup>1</sup>), 73.55, 72.98, 72.87, 72.54, 70.76, 70.67, 68.95, 68.33, 68.30, 68.14, 65.82, 62.63 (C-6), 62.54 (C-6), 59.98 (C-5<sup>1</sup>); HRMS (DCI<sup>+</sup>):  $m/z$ : 991.3033, calcd. for  $\text{C}_{41}\text{H}_{55}\text{O}_{26}\text{N}_2$   $[\text{M}+\text{NH}_4]^+$ : 991.3043.

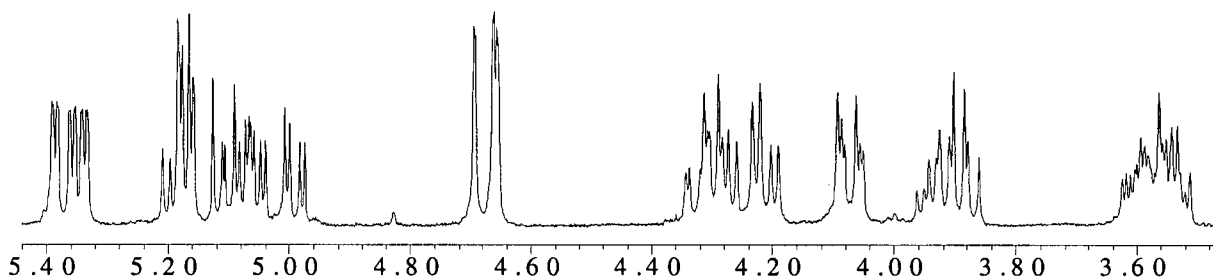


Partial  $^1\text{H}$  NMR spectrum of **6-4d** (400 MHz,  $\text{CDCl}_3$ ).

***Man* $\beta$ 1-4*Man* $\beta$ 1-4*Man* $\beta$ 1-4*Xyl*( $^4\text{C}_1$ ) $\beta$ 1-*OPNP*, *per-O*-acetate (**6-4e**)**

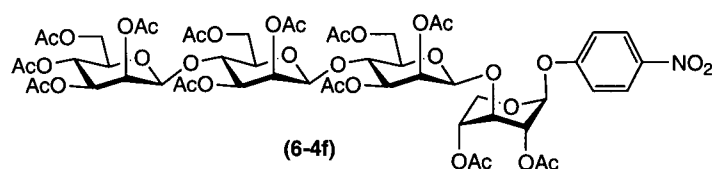


1.5 mg (1.2  $\mu\text{mol}$ , 1%); Rf (5:2 EtOAc/PE) = 0.52;  $^1\text{H}$  NMR (400 MHz,  $\text{CDCl}_3$ ):  $\delta$  5.39 (dd, 1 H,  $J = 3.3$ ,  $< 1$  Hz, H-2 $^4$ ), 5.36 and 5.34 (2  $\times$  dd, 2 H,  $J = 3.3$ ,  $< 1$  Hz, H-2 $^{2,3}$ ), 5.18 (m, 3 H, H-1 $^1$ , H-3 $^1$ , H-4 $^4$ ), 5.11 (dd, 1 H,  $J = 6.4$ , 7.9 Hz, H-2 $^1$ ), 5.08 and 5.05 (2  $\times$  dd, 2 H,  $J = 3.3$ , 9.4 Hz and 3.3, 9.7 Hz, respectively, H-3 $^{2,3}$ ), 4.99 (dd, 1 H,  $J = 3.3$ , 9.7 Hz, H-3 $^4$ ), 4.69 (d, 1 H,  $J < 1$  Hz, H-1 $^4$ ), 4.66 (2  $\times$  d, 2 H,  $J < 1$  Hz, H-1 $^{2,3}$ ), 4.35-4.25 (m, 3 H, 3  $\times$  H-6), 4.21 (2  $\times$  dd, 2 H,  $J = 4.9$ , 12.2 Hz, 2  $\times$  H-6), 4.07 (dd, 1 H,  $J = 2.7$ , 12.2 Hz, H-6), 4.07 (dd, 1 H,  $J = 4.6$ , 12.2 Hz, H-5a $^1$ ), 3.94 (ddd, 1 H,  $J = 4.6$ , 7.9, 7.9 Hz, H-4 $^1$ ), 3.90 and 3.88 (2  $\times$  dd, 2H,  $J = 9.4$ , 9.4 Hz and 9.7, 9.7 Hz, respectively, H-4 $^{2,3}$ ), 3.57 (m, 4H, H-5 $^{2,3,4}$ , H-5b $^1$ ); HRMS (APCI+):  $m/z$ : 1279.3885, calcd. for  $\text{C}_{53}\text{H}_{71}\text{O}_{34}\text{N}_2$   $[\text{M}+\text{NH}_4]^+$ : 1279.3888.

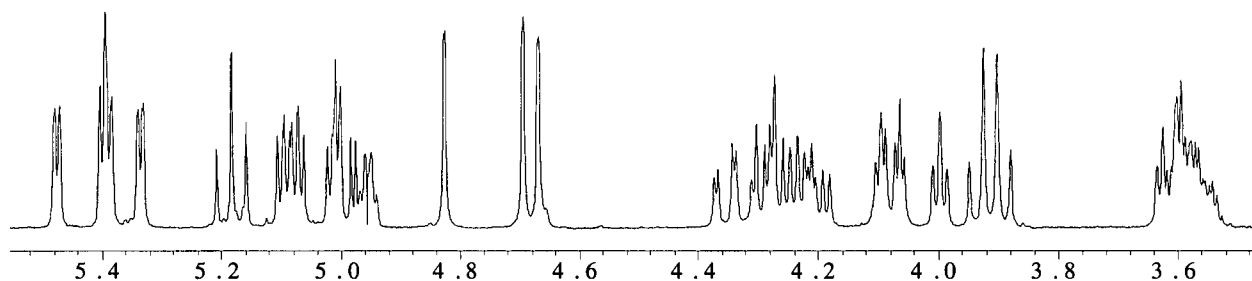


Partial  $^1\text{H}$  NMR spectrum of **6-4e** (400 MHz,  $\text{CDCl}_3$ ).

*Man* $\beta$ 1-4*Man* $\beta$ 1-4*Man* $\beta$ 1-3*Xyl*(<sup>1</sup>*C*<sub>4</sub>) $\beta$ 1-*OPNP*, *per-O*-acetate (**6-4f**)

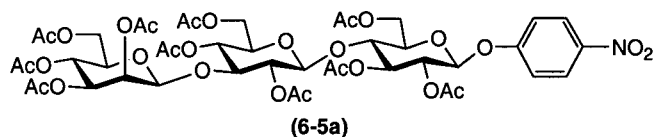


1.5 mg (1.2  $\mu$ mol, 1%); Rf (5:2 EtOAc/PE) = 0.31; <sup>1</sup>H NMR:  $\delta$  5.47 (dd, 1 H,  $J = 3.3$ ,  $< 1$  Hz, H-2<sup>man</sup>), 5.39 (m, 2 H, H-1<sup>1</sup>, H-2<sup>man</sup>), 5.33 (dd, 1 H,  $J = 3.3$ ,  $< 1$  Hz, H-2<sup>man</sup>), 5.18 (dd, 1 H,  $J = 9.9$ , 9.9 Hz, H-4<sup>4</sup>), 5.09 (dd, 1 H,  $J = 3.3$ , 9.4 Hz, H-3<sup>man</sup>), 5.08 (dd, 1 H,  $J = 3.6$ , 9.4 Hz, H-3<sup>man</sup>), 5.01 (m, 1 H, H-2<sup>1</sup>), 4.99 (dd, 1 H,  $J = 3.0$ , 10.0 Hz, H-3<sup>man</sup>), 4.95 (m, 1 H, H-4<sup>1</sup>), 4.83, 4.69, 4.67 (3  $\times$  d, 3 H,  $J < 1$  Hz, H-1<sup>2,3,4</sup>), 4.35 (dd, 1 H,  $J = 2.7$ , 12.2 Hz, H-6), 4.32-4.17 (m, 4 H, 4  $\times$  H-6), 4.08 (m, 2 H, H-6, H-5a<sup>1</sup>), 4.00 (dd, 1 H,  $J \approx 4.9$ , 4.9 Hz, H-3<sup>1</sup>), 3.92, 3.90 (2  $\times$  dd, 2 H,  $J = 9.4$ , 9.4 Hz and 9.1, 9.1 Hz, respectively, H-4<sup>2,3</sup>), 3.64-3.53 (m, 4 H, H-5<sup>2,3,4</sup>, H-5b<sup>1</sup>); HRMS (APCI<sup>+</sup>):  $m/z$ : 1279.3892, calcd. for C<sub>53</sub>H<sub>71</sub>O<sub>34</sub>N<sub>2</sub> [M+NH<sub>4</sub>]<sup>+</sup>: 1279.3888.

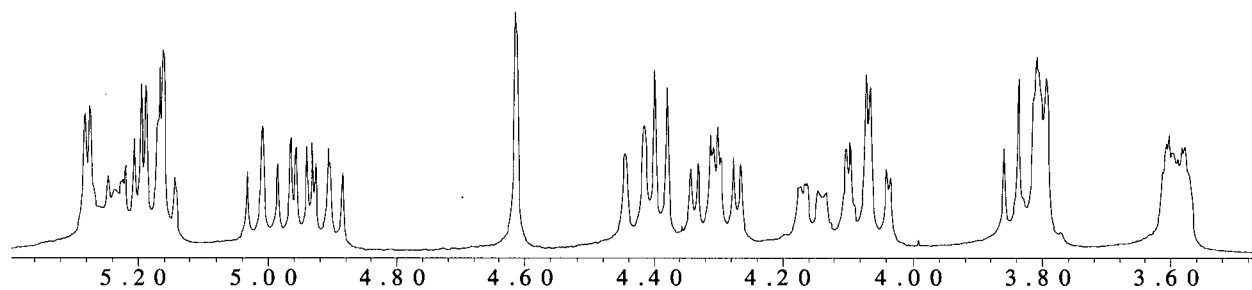


Partial <sup>1</sup>H NMR spectrum of **6-4f** (400 MHz, CDCl<sub>3</sub>).

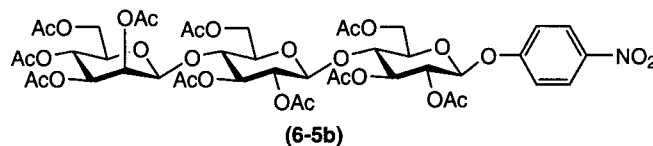
***p*-Nitrophenyl  $\beta$ -cellobioside as an acceptor:** 41.7 mg (90  $\mu$ mol) acceptor was dissolved in 4 mL 150 mM sodium citrate, pH 6.  $\alpha$ -Mannosyl fluoride (2 eq.) was added, followed by Man2a E519S to a final concentration of 1 mg/mL. The reaction was maintained at room temperature for 24 hrs. whereupon TLC analysis (7:2:1 EtOAc/MeOH/H<sub>2</sub>O) indicated essentially complete consumption of acceptor. Products were isolated and acetylated in the usual manner.

**Man $\beta$ 1-3Glu $\beta$ 1-4Glu $\beta$ 1-OPNP, per-O-acetate (6-5a)**

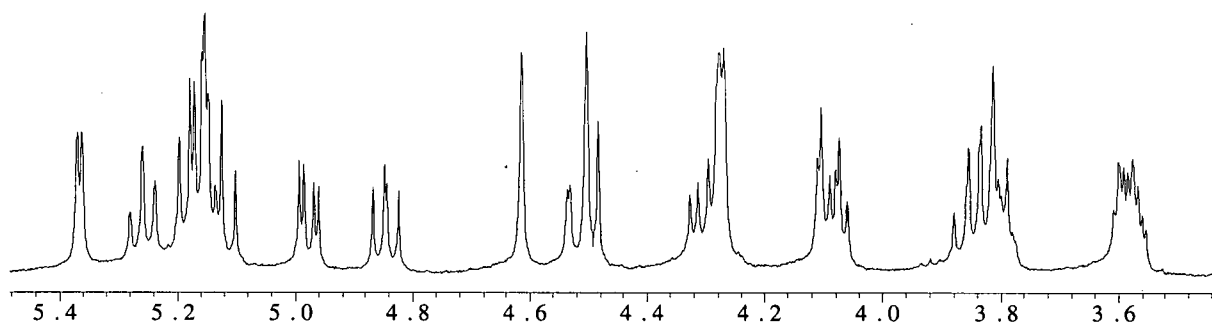
7.3 mg (7  $\mu$ mol, 7.8%); Rf (3:1 EtOAc/PE) = 0.64;  $^1\text{H}$  NMR (400 MHz,  $\text{CDCl}_3$ ):  $\delta$  5.28 (dd, 1 H,  $J = 3.3, < 1.0$  Hz, H-2 $^3$ ), 5.26-5.14 (m, 4 H, H-1 $^1$ , H-2 $^1$ , H-3 $^1$ , H-4 $^3$ ), 5.01 (dd, 1 H,  $J = 9.5, 9.5$  Hz, H-4 $^2$ ), 4.95 (dd, 1 H,  $J = 3.3, 9.6$  Hz, H-3 $^3$ ), 4.90 (dd, 1 H,  $J = 8.1, 9.1$  Hz, H-2 $^2$ ), 4.61 (d, 1 H,  $J < 1.0$  Hz, H-1 $^3$ ), 4.43 (broad d, 1 H,  $J \approx 12$  Hz, H-6), 4.39 (d, 1 H,  $J = 7.7$  Hz, H-1 $^2$ ), 4.32 (dd, 1 H,  $J = 4.6, 12.4$  Hz, H-6), 4.28 (dd, 1 H,  $J = 4.6, 12.5$  Hz, H-6), 4.15 (dd, 1 H,  $J = 3.7, 12.1$  Hz, H-6), 4.08 (dd, 1 H,  $J = 2.7, 12.4$  Hz, H-6), 4.05 (dd, 1 H,  $J = 2.2, 12.3$  Hz, H-6), 3.84 (dd, 1 H,  $J = 9.4, 9.4$  Hz, H-3 $^2$ ), 3.80 (m, 2 H, H-5 $^1$ , H-4 $^1$ ), 3.59 (m, 2 H, H-5 $^2$ , H-5 $^3$ );  $^{13}\text{C}$  NMR (100 MHz,  $\text{CDCl}_3$ ):  $\delta$  100.73 (C-1), 98.31 (C-1), 97.87 (C-1), 78.63, 75.79, 73.31, 72.61, 72.43, 72.23, 72.18, 71.06, 70.86, 68.25, 67.59, 65.70, 62.23 (C-6), 61.98 (C-6), 61.83 (C-6); HRMS (DCI+):  $m/z$ : 1063.322, calcd. for  $\text{C}_{44}\text{H}_{59}\text{O}_{28}\text{N}_2$   $[\text{M}+\text{NH}_4]^+$ : 1063.325.



Partial  $^1\text{H}$  NMR spectrum for **6-5a** (400 MHz,  $\text{CDCl}_3$ ).

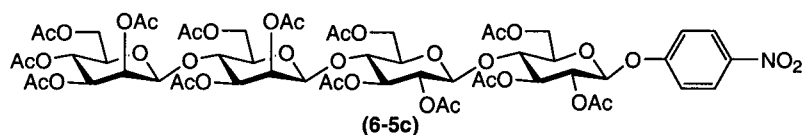
**Man $\beta$ 1-4Glu $\beta$ 1-4Glu $\beta$ 1-OPNP, per-O-acetate (6-5b)**

2.3 mg (2.2  $\mu$ mol, 2.4%); Rf (2:1 EtOAc/PE) = 0.50;  $^1\text{H}$  NMR (400 MHz,  $\text{CDCl}_3$ ):  $\delta$  5.36 (dd, 1 H,  $J = < 1.0, 3.2$  Hz, H-2<sup>3</sup>), 5.26 (dd, 1 H,  $J = 8.6, 8.6$  Hz, H-3<sup>1</sup>), 5.20-5.13 (m, 3 H, H-1<sup>1</sup>, H-2<sup>1</sup>, H-4<sup>3</sup>), 5.12 (dd, 1 H,  $J = 9.4, 9.4$  Hz, H-3<sup>2</sup>), 4.97 (dd, 1 H,  $J = 3.1, 9.7$  Hz, H-3<sup>3</sup>), 4.84 (dd, 1 H,  $J = 7.9, 9.4$  Hz, H-2<sup>2</sup>), 4.61 (d, 1 H,  $J = < 1.0$  Hz, H-1<sup>3</sup>), 4.52 (dd, 1 H,  $J = 2.0, 12.1$  Hz, H-6), 4.49 (d, 1 H,  $J = 7.9$  Hz, H-1<sup>2</sup>), 4.30 (dd, 1 H,  $J = 5.2, 12.4$  Hz, H-6), 4.27 (m, 2 H, 2  $\times$  H-6), 4.09 (dd, 1 H,  $J = 2.5, 12.3$  Hz, H-6), 4.08 (dd, 1 H,  $J = 5.5, 12.1$  Hz, H-6), 3.85 (dd, 1 H,  $J = 9.6, 9.6$  Hz, H-4<sup>1</sup>), 3.81 (dd, 1 H,  $J = 9.5, 9.5$  Hz, H-4<sup>2</sup>), 3.80 (m, 1 H, H-5<sup>1</sup>), 3.58 (m, 2 H, H-5<sup>2</sup>, H-5<sup>3</sup>);  $^{13}\text{C}$  NMR (100 MHz,  $\text{CDCl}_3$ ):  $\delta$  100.65 (C-1), 97.91 (C-1), 97.56 (C-1), 76.12, 74.47, 73.30, 72.75, 72.72, 72.32, 72.25, 71.74, 71.33, 70.76, 68.25, 65.87,  $\delta$  62.26 (2 lines, 2  $\times$  C-6), 61.77 (C-6); HRMS (DCI+):  $m/z$ : 1063.3261, calcd. for  $\text{C}_{44}\text{H}_{59}\text{O}_{28}\text{N}_2$   $[\text{M}+\text{NH}_4]^+$ : 1063.3254.



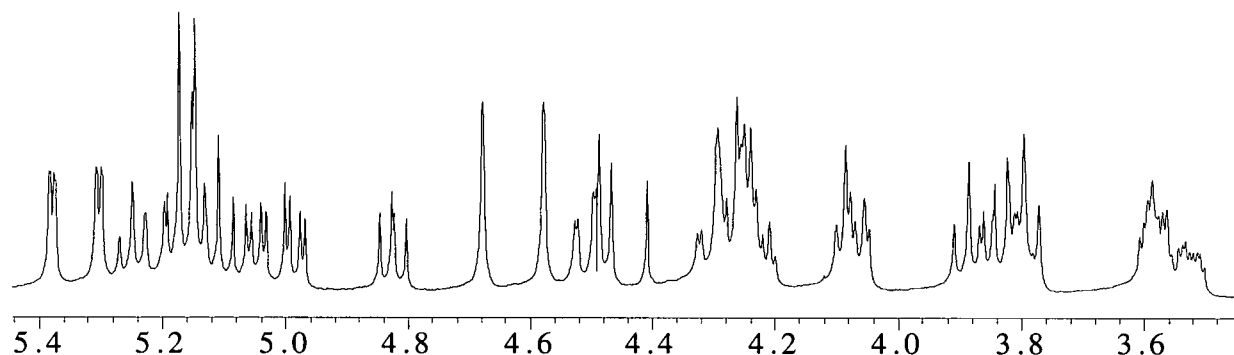
Partial  $^1\text{H}$  NMR spectrum for **6-5b** (400 MHz,  $\text{CDCl}_3$ ).

***Man $\beta$ 1-4Man $\beta$ 1-4Glu $\beta$ 1-4Glu $\beta$ 1-OPNP, per-O-acetate (6-5c)***



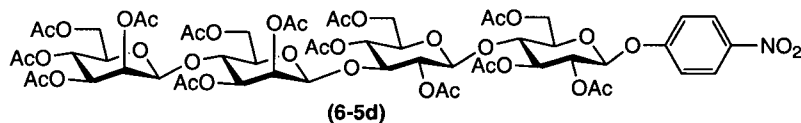
41.3 mg (31  $\mu$ mol, 34.4%); Rf (2:1 EtOAc/PE) = 0.42;  $^1\text{H}$  NMR (400 MHz,  $\text{CDCl}_3$ ):  $\delta$  5.38 (dd, 1 H,  $J = 3.3, 0.9$  Hz, H-2<sup>4</sup>), 5.30 (dd, 1 H,  $J = 3.3, < 1$  Hz, H-2<sup>3</sup>), 5.25 (dd, 1 H,  $J = 8.5, 8.5$  Hz, H-3<sup>1</sup>), 5.16 (m, 3 H, H-1<sup>1</sup>, H-2<sup>1</sup>, H-4<sup>4</sup>), 5.11 (dd, 1 H,  $J = 9.3, 9.3$  Hz, H-3<sup>2</sup>), 5.05 (dd, 1 H,  $J = 3.3, 9.5$  Hz, H-3<sup>3</sup>), 4.98 (dd, 1 H,  $J = 3.3, 10.1$  Hz, H-3<sup>4</sup>), 4.82 (dd, 1 H,  $J = 7.9, 9.5$  Hz, H-2<sup>2</sup>), 4.68 (d, 1 H,  $J < 1$  Hz, H-1<sup>4</sup>), 4.58 (d, 1 H,  $J < 1$  Hz, H-1<sup>3</sup>), 4.51 (dd, 1 H,  $J = 2.1, 12.2$  Hz, H-6a<sup>1</sup>), 4.48 (d, 1 H,  $J = 7.9$  Hz, H-1<sup>2</sup>), 4.33-4.19 (m, 5 H, 5  $\times$  H-6), 4.07 (m, 2 H, H-6, H-6b<sup>1</sup>), 3.88 (dd, 1 H,  $J = 9.6, 9.6$  Hz, H-4<sup>3</sup>), 3.84 (dd, 1 H,  $J = 8.5, 9.8$  Hz, H-4<sup>1</sup>), 3.80 (dd, 1 H,  $J = 9.5, 9.5$  Hz, H-4<sup>2</sup>), 3.80 (m, 1 H, H-5<sup>1</sup>), 3.58 (m, 2 H, H-5<sup>2,4</sup>), 3.52 (ddd, 1 H,  $J = 2.7, 4.6, 9.6$  Hz, H-5<sup>3</sup>);  $^{13}\text{C}$  NMR (100 MHz,  $\text{CDCl}_3$ ):  $\delta$  100.60 (C-1), 97.89 (C-1), 97.81 (C-1), 97.39 (C-1), 76.05,

74.44, 73.23, 72.97, 72.71, 72.58 (2 lines), 72.19 (2 lines), 71.74, 71.19, 70.67, 70.63, 68.64, 68.31, 65.77, 62.54 (C-6), 62.47 (C-6), 62.19 (C-6), 61.70 (C-6); HRMS (DCI+):  $m/z$ : 1351.4101, calcd. for  $C_{56}H_{75}O_{36}N_2$   $[M+NH_4]^+$ : 1351.4099.

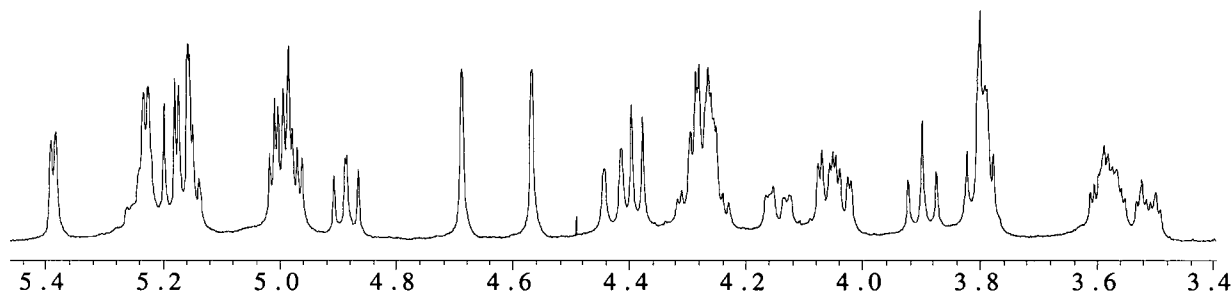


Partial  $^1H$  NMR spectrum for **6-5c** (400 MHz,  $CDCl_3$ ).

***Man $\beta$ 1-4Man $\beta$ 1-3Glu $\beta$ 1-4Glu $\beta$ 1-OPNP, per-O-acetate (6-5d)***

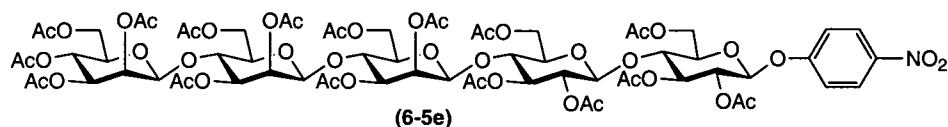


5.5 mg (4.1  $\mu$ mol, 4.6%);  $R_f$  (2:1 EtOAc/PE) = 0.37;  $^1H$  NMR (400 MHz,  $CDCl_3$ ):  $\delta$  5.39 (dd, 1 H,  $J$  = 3.3, < 1 Hz, H-2<sup>4</sup>), 5.27-5.13 (m, 5 H, H-1<sup>1</sup>, H-2<sup>1</sup>, H-3<sup>1</sup>, H-2<sup>3</sup>, H-4<sup>4</sup>), 4.99 (m, 3 H, H-4<sup>2</sup>, H-3<sup>3,4</sup>), 4.89 (dd, 1 H,  $J$  = 7.6, 8.8 Hz, H-2<sup>2</sup>), 4.69 (d, 1 H,  $J$  < 1 Hz, H-1<sup>4</sup>), 4.57 (d, 1 H,  $J$  < 1 Hz, H-1<sup>3</sup>), 4.43 (dd, 1 H,  $J$   $\approx$  2, 12 Hz, H-6a<sup>1</sup>), 4.39 (d, 1 H,  $J$  = 7.6 Hz, H-1<sup>2</sup>), 4.32-4.22 (m, 4 H, 4  $\times$  H-6), 4.14 (dd, 1 H,  $J$   $\approx$  5, 12 Hz, H-6b<sup>1</sup>), 4.06 (dd, 1 H,  $J$  = 2.7, 12.2 Hz, H-6), 4.04 (dd, 1 H,  $J$  = 2.2, 12.2 Hz, H-6), 3.90 (dd, 1 H,  $J$  = 9.7, 9.7 Hz, H-4<sup>3</sup>), 3.80 (m, 3 H, H-4<sup>1</sup>, H-5<sup>1</sup>, H-3<sup>2</sup>), 3.58 (m, 2 H, H-5<sup>2,4</sup>), 3.51 (ddd, 1 H,  $J$  = 2.8, 3.8, 9.8 Hz, H-5<sup>3</sup>);  $^{13}C$  NMR (100 MHz,  $CDCl_3$ ):  $\delta$  100.69 (C-1), 98.39 (C-1), 98.14 (C-1), 97.94 (C-1), 78.79, 75.79, 73.38, 72.87 (2 lines), 72.68, 72.60, 72.28 (2 lines), 71.19, 71.03, 70.75, 68.70, 68.43, 67.80, 65.91, 62.69 (C-6), 62.59 (C-6), 61.96 (2 lines, 2  $\times$  C-6); HRMS (APCI+):  $m/z$ : 1351.4072, calcd. for  $C_{56}H_{75}O_{36}N_2$   $[M+NH_4]^+$ : 1351.4099.

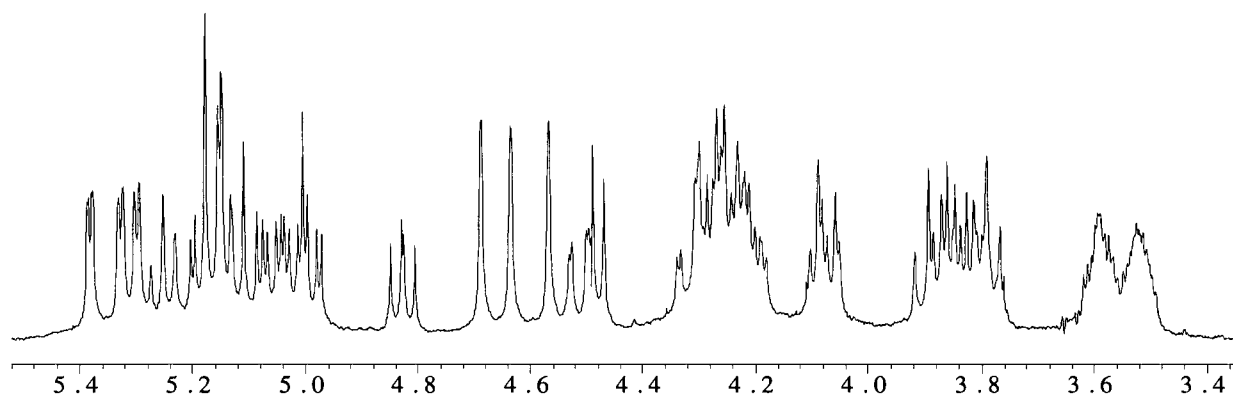


Partial  $^1\text{H}$  NMR spectrum for **6-5d** (400 MHz,  $\text{CDCl}_3$ ).

***Man $\beta$ 1-4Man $\beta$ 1-4Man $\beta$ 1-4Glu $\beta$ 1-4Glu $\beta$ 1-OPNP, per-O-acetate (6-5e)***



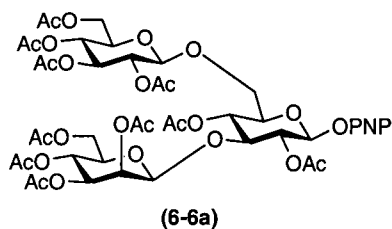
2 mg (1.2  $\mu\text{mol}$ , 1.8%); Rf (3:1 EtOAc/PE) = 0.39;  $^1\text{H}$  NMR (400 MHz,  $\text{CDCl}_3$ ):  $\delta$  5.38 (dd, 1 H,  $J = 3.3$ ,  $< 1$  Hz, H-2<sup>5</sup>), 5.33, 5.30 (2  $\times$  dd, 2 H,  $J = 3.3$ ,  $< 1$  Hz each, 2  $\times$  H-2<sup>man</sup>), 5.25 (dd, 1 H,  $J = 8.7$ , 8.7 Hz, H-3<sup>1</sup>), 5.21-5.12 (m, 3 H, H-1<sup>1</sup>, H-2<sup>1</sup>, H-4<sup>5</sup>), 5.11 (dd, 1 H,  $J = 9.5$ , 9.5 Hz, H-3<sup>2</sup>), 5.06, 5.02 (2  $\times$  dd, 2 H,  $J = 3.3$ , 9.8 Hz each, 2  $\times$  H-3<sup>man</sup>), 4.99 (dd, 1 H,  $J = 3.3$ , 10.1 Hz, H-3<sup>5</sup>), 4.83 (dd, 1 H,  $J = 7.9$ , 9.5 Hz, H-2<sup>2</sup>), 4.69 (d, 1 H,  $J < 1$  Hz, H-1<sup>5</sup>), 4.63, 4.57 (2  $\times$  d, 2 H,  $J < 1$  Hz each, 2  $\times$  H-1<sup>man</sup>), 4.51 (dd, 1 H,  $J = 1.8$ , 11.9 Hz, H-6a<sup>1</sup>), 4.48 (d, 1 H,  $J = 7.9$  Hz, H-1<sup>2</sup>), 4.34-4.17 (m, 7 H, 7  $\times$  H-6), 4.08 (m, 2 H, H-6, H-6b<sup>1</sup>), 3.89 (dd, 1 H,  $J = 9.5$ , 9.5 Hz, H-4<sup>man</sup>), 3.86 (dd, 1 H,  $J = 9.7$ , 9.7 Hz, H-4<sup>man</sup>), 3.85 (dd, 1 H,  $J = 8.8$ , 8.8 Hz, H-4<sup>1</sup>), 3.79 (dd, 1 H,  $J = 9.5$ , 9.5 Hz, H-4<sup>2</sup>), 3.79 (m, 1 H, H-5<sup>1</sup>), 3.62-3.48 (m, 4 H, H-5<sup>2,3,4,5</sup>);  $^{13}\text{C}$  NMR (100 MHz,  $\text{CDCl}_3$ ):  $\delta$  100.61, 97.99, 97.91, 97.84, 97.36 (5  $\times$  C-1), 76.06, 74.43, 73.25, 73.04, 72.98, 72.84, 72.72, 72.60 (2 lines), 72.22, 72.15, 71.77, 71.21, 70.68 (3 lines), 68.75, 68.58, 68.32, 65.77, 62.73 (C-6), 62.52 (2 lines, 2  $\times$  C-6), 62.23 (C-6), 61.72 (C-6); MS (DCI<sup>+</sup>):  $m/z$ : 1639, calcd. for  $\text{C}_{68}\text{H}_{91}\text{O}_{44}\text{N}_2$   $[\text{M}+\text{NH}_4]^+$ : 1639.5.



Partial  $^1\text{H}$  NMR spectrum for **6-5e** (400 MHz,  $\text{CDCl}_3$ ).

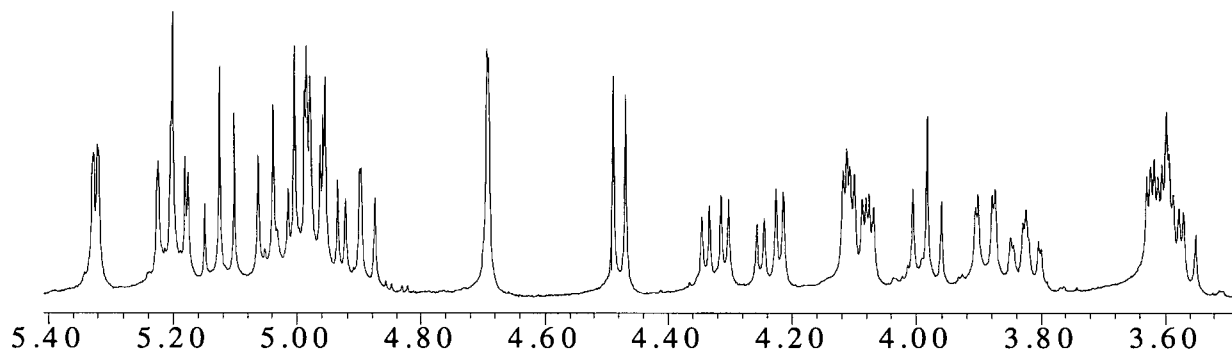
***p*-Nitrophenyl  $\beta$ -gentiobioside as an acceptor:** 20 mg (43.1  $\mu\text{mol}$ ) acceptor was dissolved in 2 mL 150 mM sodium citrate buffer, pH 6.  $\alpha$ -Mannosyl fluoride (2 eq.) was added, followed by Man2a E519S (1 mg/mL final concentration). The reaction was maintained at room temperature for 24 hrs. whereupon TLC analysis (7:2:1 EtOAc/MeOH/ $\text{H}_2\text{O}$ ) indicated complete consumption of the acceptor. Products were isolated and acetylated in the usual manner.

***Man* $\beta$ (1,3)[*Glu* $\beta$ (1,6)]*Glu* $\beta$ 1-OPNP, *per*-*O*-acetate (**6-6a**)**



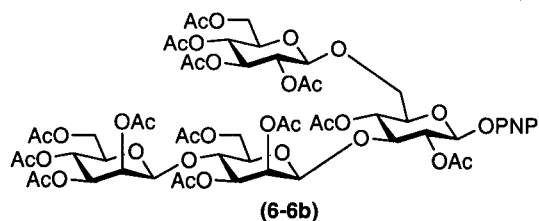
7.7 mg (7.4  $\mu\text{mol}$ , 17.2%);  $R_f$  (2:1 EtOAc/PE) = 0.42;  $^1\text{H}$  NMR (400 MHz,  $\text{CDCl}_3$ ):  $\delta$  5.33 (dd, 1 H,  $J = 3.2, 0.9$  Hz, H-2<sup>3</sup>), 5.20 (dd, 1 H,  $J = 9.4, 9.4$  Hz, H-4<sup>3</sup>), 5.20 (dd, 1 H,  $J = 7.9, 9.1$  Hz, H-2<sup>1</sup>), 5.12 (dd, 1 H,  $J = 9.5, 9.5$  Hz, H-3<sup>2</sup>), 5.04 (dd, 1 H,  $J = 9.7, 9.7$  Hz, H-4<sup>2</sup>), 4.99 (d, 1 H,  $J = 7.6$  Hz, H-1<sup>1</sup>), 4.97 (dd, 1 H,  $J = 3.3, 10.0$  Hz, H-3<sup>3</sup>), 4.95 (dd, 1 H,  $J = 7.9, 9.5$  Hz, H-2<sup>2</sup>), 4.90 (dd, 1 H,  $J = 9.1, 9.8$  Hz, H-4<sup>1</sup>), 4.69 (d, 1 H,  $J = 0.9$  Hz, H-1<sup>3</sup>), 4.48 (d, 1 H,  $J = 7.9$  Hz, H-1<sup>2</sup>), 4.32 (dd, 1 H,  $J = 4.9, 12.2$  Hz, H-6), 4.23 (dd, 1 H,  $J = 4.9, 12.2$  Hz, H-6), 4.10 (dd, 1 H,  $J = 2.4, 12.2$  Hz, H-6), 4.09 (dd, 1 H,  $J = 2.7, 12.2$  Hz, H-6), 3.98 (dd, 1 H,  $J = 9.1, 9.1$  Hz, H-3<sup>1</sup>), 3.89 (dd, 1 H,  $J = 1.7, 10.8$  Hz, H-6a<sup>1</sup>), 3.82 (ddd, 1 H,  $J = 1.8, 7.9, 9.9$  Hz, H-5<sup>1</sup>), 3.61 (m, 2 H, H-5<sup>2,3</sup>), 3.57 (dd, 1 H,  $J = 7.9, 10.7$  Hz, H-6b<sup>1</sup>);  $^{13}\text{C}$  NMR (100 MHz,  $\text{CDCl}_3$ ):  $\delta$  100.49 (C-1), 98.45 (C-1), 98.36 (C-1), 78.56 (C-3<sup>1</sup>), 74.02, 72.58, 72.54, 72.04, 71.98, 71.06, 70.84, 68.40,

68.30, 68.25, 68.07 (C-6), 65.70, 62.30 (C-6), 61.74 (C-6); HRMS (DCI+):  $m/z$ : 1063.323, calcd. for  $C_{44}H_{59}O_{28}N_2$   $[M+NH_4]^+$ : 1063.325. The HMBC spectrum indicated that C-3<sup>1</sup> coupled with H-1<sup>3</sup> (mannoside ring) as well as H-2<sup>1</sup>, and H-4<sup>1</sup> (PNP glucoside ring). Coupling was also observed between C-1<sup>3</sup> and H-3<sup>1</sup>. The HMBC data thus supports the  $\beta$ -(1,3) branch linkage proposed.



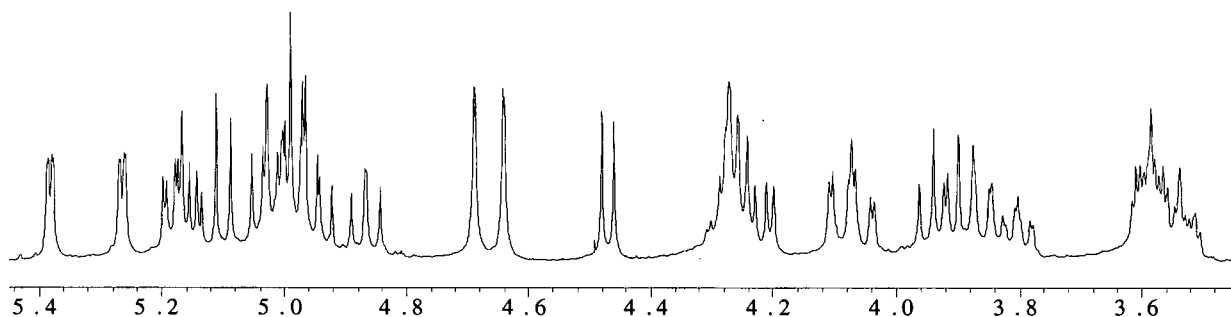
Partial  $^1H$  NMR spectrum for **6-6a** (400 MHz,  $CDCl_3$ ).

***Man $\beta$ (1,4)Man $\beta$ (1,3)[Glu $\beta$ (1,6)]Glu $\beta$ 1-OPNP, per-O-acetate (6-6b)***



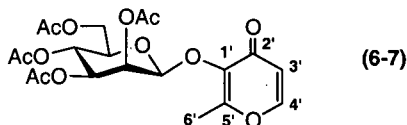
24.6 mg (18.5  $\mu$ mol, 43%); Rf (2:1 EtOAc/PE) = 0.24;  $^1H$  NMR (400 MHz,  $CDCl_3$ ):  $\delta$  5.38 (dd, 1 H,  $J$  = 3.3, 0.9 Hz, H-2<sup>4</sup>), 5.27 (dd, 1 H,  $J$  = 3.3, 0.9 Hz, H-2<sup>3</sup>), 5.18 (dd, 1 H,  $J$  = 7.9, 9.5 Hz, H-2<sup>1</sup>), 5.17 (dd, 1 H,  $J$  = 9.9, 9.9 Hz, H-4<sup>4</sup>), 5.11 (dd, 1 H,  $J$  = 9.5, 9.5 Hz, H-3<sup>2</sup>), 5.03 (dd, 1 H,  $J$  = 10.0, 10.0, H-4<sup>2</sup>), 5.02 (dd, 1 H,  $J$  = 3.3, 9.8 Hz, H-3<sup>3</sup>), 4.98 (d, 1 H,  $J$  = 7.9 Hz, H-1<sup>1</sup>), 4.98 (dd, 1 H,  $J$  = 3.2, 9.9 Hz, H-3<sup>4</sup>), 4.94 (dd, 1 H,  $J$  = 7.9, 9.5 Hz, H-2<sup>2</sup>), 4.87 (dd, 1 H,  $J$  = 9.1, 9.8 Hz, H-4<sup>1</sup>), 4.69 (d, 1 H,  $J$  = 0.9 Hz, H-1<sup>4</sup>), 4.64 (d, 1 H,  $J$  = 0.9 Hz, H-1<sup>3</sup>), 4.47 (d, 1 H,  $J$  = 7.9 Hz, H-1<sup>2</sup>), 4.27 (m, 3 H, 3  $\times$  H-6), 4.22 (dd, 1 H,  $J$  = 4.9, 12.2 Hz, H-6), 4.09 (dd, 1 H,  $J$  = 2.4, 12.2 Hz, H-6), 4.05 (dd, 1 H,  $J$  = 2.4, 12.2 Hz, H-6), 3.94 (dd, 1 H,  $J$  = 9.1, 9.1 Hz, H-3<sup>1</sup>), 3.90 (dd, 1 H,  $J$  = 9.7, 9.7 Hz, H-4<sup>3</sup>), 3.86 (dd, 1 H,  $J$  = 1.5, 10.4 Hz, H-6a<sup>1</sup>), 3.80 (ddd, 1 H,  $J$  = 1.8, 7.9, 9.8 Hz, H-5<sup>1</sup>), 3.61-3.50 (m, 4H, H-5<sup>2,3,4</sup>, H-6b<sup>1</sup>);  $^{13}C$  NMR (100 MHz,  $CDCl_3$ ):  $\delta$  100.47 (C-1), 98.49 (C-1), 98.31 (C-1), 98.05 (C-1), 78.67, 73.99, 72.88, 72.71, 72.57, 72.53, 72.00,

71.91, 71.03, 70.95, 70.67, 68.66, 68.48, 68.35, 68.22, 68.03 (C-6), 65.77, 62.65 (C-6), 62.50 (C-6), 61.70 (C-6); HRMS (DCI+):  $m/z$ : 1351.412, calcd. for  $C_{44}H_{59}O_{28}N_2$   $[M+NH_4]^+$ : 1351.410. The HMBC spectrum indicated coupling between C-3<sup>1</sup> and H-1<sup>3</sup>, as well as between H-3<sup>1</sup> and C-1<sup>3</sup>, thus confirming the presence of a  $\beta$ -(1,3) branch linkage. Coupling was also observed between C-4<sup>3</sup> and H-1<sup>4</sup>, as well as between C-1<sup>4</sup> and H-4<sup>3</sup>. This further confirms that the terminal mannose residue is  $\beta$ -(1,4) linked.



Partial  $^1H$  NMR spectrum for **6-6b** (400 MHz,  $CDCl_3$ ).

**Maltol  $\beta$ -D-mannopyranoside, per-O-acetate (6-7)**



Maltol (20.6 mg, 0.18 mmol) was dissolved in 3 mL citrate buffer (100 mM, pH 6). An aliquot of  $\alpha$ -ManF was added (356  $\mu$ L of 0.509 M, 0.18 mmol, 1 eq.) followed by 6 mg of Man2A E519S. The reaction was maintained at room temperature for 20 hrs. whereupon a second aliquot of  $\alpha$ -ManF was added (0.113 mmol, 0.6 eq.). After 44 hrs. complete conversion of maltol to a new UV active product was noted by TLC ( $R_f$  (7:2:1 EtOAc/MeOH/ $H_2O$ ) = 0.30). The product was purified by HPLC, per-O-acetylated, then further purified by silica gel chromatography to obtain an off white solid (38 mg, 0.085 mmol, 47%).  $^1H$  NMR (400 MHz,  $CDCl_3$ ):  $\delta$  7.61 (d, 1 H,  $J$  = 5.5 Hz, H-4'), 6.32 (d, 1 H,  $J$  = 5.8 Hz, H-3'), 5.72 (dd, 1 H,  $J$  = 0.9, 3.3 Hz, H-2), 5.67 (d, 1 H,  $J$  = 0.9 Hz, H-1), 5.22 (dd, 1 H,  $J$  = 9.9, 9.9 Hz, H-4), 5.10 (dd, 1 H,  $J$  = 10.0, 3.0 Hz, H-3), 4.23 (dd, 1 H,  $J$  = 12.2, 5.5 Hz, H-6a), 4.06 (dd, 1 H,  $J$  = 12.2, 2.7 Hz, H-6b), 3.59 (ddd, 1 H,  $J$  = 2.7, 5.5, 9.9 Hz, H-5), 2.27, 2.18, 2.01, 1.99, 1.98 (all s, 15 H,  $5 \times CH_3$ );  $^{13}C$  NMR (100 MHz,  $CDCl_3$ ):  $\delta$  173.87 (C-2'), 170.37, 169.92, 169.73, 169.69 ( $4 \times CH_3CO$ ),

160.78 (C-1'), 153.69 (C-4'), 140.75 (C-5'), 117.18 (C-3'), 96.12 (C-1), 72.51, 70.84, 68.57, 66.20 (C-2,3,4,5), 62.21 (C-6), 20.76-20.53 (lines,  $4 \times \text{CH}_3\text{CO}$ ), 14.82 (C-6').

### **Transglycosylation kinetics**

Transglycosylation kinetic analysis of Man2A E519A and E519S was performed in a manner similar to the protocol described in the Chapter 5 experimental.  $\alpha$ -Mannosyl fluoride was used as donor and PNP  $\beta$ -cellobioside as acceptor. All kinetics were performed at 25°C in 100 mM citrate, 150 mM NaCl, 1 mg/mL BSA, pH 6. Final enzyme concentrations of 5  $\mu\text{M}$  E519S and 70  $\mu\text{M}$  E519A were used. Because  $\alpha$ -mannosyl fluoride could only be prepared as a gum, solution concentrations were determined by boiling appropriately diluted samples (~ 50 mM) for 30 min. and measuring the total fluoride released with the fluoride electrode.

### **Azide rescue of Man2A E519A and E519S**

Kinetic analysis of the chemical rescue of Man2A E519A and E519S mutants was performed in a manner similar to the rescue protocol described in the Chapter 5 experimental. Solutions of 2,4-dinitrophenyl  $\beta$ -mannoside and azide, buffered at pH 6, were prepared fresh prior to use. Reactions were performed at 25°C in 1 M azide, 100 mM citrate, 1 mg/mL BSA, pH 6. Final enzyme concentrations of 184 nM E519A and 71 nM E519S were used. Man2A E519S displayed transglycosylation behaviour, therefore kinetic parameters were derived from a fit of the data at low substrate concentrations to the Michaelis Menten equation using GraFit. Man2A E519A displayed substrate inhibition, thus the whole data set was fit to the substrate inhibition equation.

## Chapter 7: Development of a 'Cellulosynthase' from *Streptomyces lividans* endoglucanase CelB

### General

The syntheses of DNPC and 2FDNPC have been described previously.<sup>304</sup> The expression and purification of CelB has also been published elsewhere.<sup>248</sup> This is a truncated form of the enzyme, lacking a signal peptide and cellulose binding domain, corresponding to D41 through G274 of the sequence listed in the National Center for Biotechnology Information (NCBI) database (accession number 2462718). CelB nucleophile mutants were constructed, expressed and purified by the lab of Professor Claude Dupont (Centre de recherche en microbiologie appliquée, Institut Armand-Frappier, Université du Québec). Enzyme concentrations were determined using the extinction coefficient  $\epsilon_{280} = 54.6 \text{ mM}^{-1}\cdot\text{cm}^{-1}$  ( $\epsilon_{280}^{0.1\%} = 2.2$ ), which was calculated from the content of tyrosine and tryptophan residues.<sup>305</sup>

### Steady-State Kinetics

Steady state kinetic studies were performed on a Unicam 8700 UV-Vis spectrometer equipped with a circulating water bath. Appropriate concentrations of DNPC were diluted in 50 mM sodium citrate, 0.1% BSA, pH 6.5 (200  $\mu\text{l}$ ) and equilibrated at 37°C in micro quartz cuvettes. An aliquot of CelB (10  $\mu\text{l}$ ,  $8.1 \times 10^{-4}$  mg/ml, diluted in 50 mM sodium citrate, 0.1% BSA, pH 6.5) was added to initiate hydrolysis whereupon the release of 2,4-dinitrophenol was monitored continuously at  $\lambda = 400 \text{ nm}$  ( $\Delta\epsilon_{400} = 10\,910 \text{ M}^{-1}\cdot\text{cm}^{-1}$ ).<sup>33</sup> Enzymatic hydrolysis rates were measured for DNPC concentrations ranging from 1/5 to 40 times the estimated  $K_M$  value. These enzymatic hydrolysis rates were corrected for the significant spontaneous hydrolysis rate of DNPC (measured prior to the addition of CelB). The resulting velocity curve was fit according to substrate inhibition (Chapter 3, equation 3-1) using GraFit.<sup>292</sup>

### Inactivation Kinetics

CelB (100  $\mu\text{l}$ , 0.02 mg/ml 50 mM sodium citrate, 0.1% BSA, pH 6.5) was incubated at 37°C in the presence of various concentrations of 2FDNPC (0.057-11.38 mM). Aliquots (10  $\mu\text{l}$ ) were removed from the inactivation mix at appropriate intervals and added to cuvettes pre-equilibrated at 37°C with 0.5 mM solutions of DNPC (900  $\mu\text{l}$ , 50 mM sodium citrate, 0.1% BSA, pH 6.5), whereupon the hydrolysis rates were measured as described above. Each inactivation reaction

was monitored for a minimum of 3 half lives and the resulting curve of fractional activity ( $V/V_0$ ) over time was fit according to single exponential kinetics ( $V/V_0 = \exp(-k_{obs(inact)} \cdot t) + C$ ) using GraFit. The resulting values of  $k_{obs(inact)}$  were subsequently plotted against the corresponding concentrations of 2FDNPC and fit with the substrate inhibition equation (Chapter 3, equation 3-1) using GraFit. In this case  $k_{cat}$  becomes  $k_{inact}$ , and  $K_M$  becomes  $K_{inact}$ . A control reaction (no inactivator) indicated that the spontaneous loss of enzyme activity was negligible within the time range considered.

Protection against inactivation was demonstrated by reacting CelB with 2FDNPC (2.84 mM) in the presence and absence of 47 mM cellobiose, a competitive inhibitor. When the concentration of 2FDNPC is sufficiently low to neglect uncompetitive inhibition, the ratio of observed rate constants with and without a competitive inhibitor present is given by equation 6-1 where P is the competitive inhibitor with a dissociation constant  $K_d$ .

$$\frac{k_{obs(inact)}^{prot}}{k_{obs(inact)}} = \frac{K_{inact} + [I]}{K_{inact} \left( 1 + \frac{[P]}{K_d} \right) + [I]} \quad (6-1)$$

### **Reactivation kinetics**

CelB was diluted to 0.1 mg/ml in 50 mM sodium citrate, pH 6.5 (without BSA) to a total volume of 120  $\mu$ L and incubated for 60 minutes at 37°C with 0.5 mM 2FDNPC. This resulted in >95% inactivation of the enzyme, as determined by the residual activity assay described above. Excess inactivator was removed by dilution with BSA free buffer (to 400  $\mu$ L) and subsequent ultrafiltration (to a final volume of ~100  $\mu$ L) using a Millipore Ultrafree-MC centrifugal concentrator (10 kDa nominal molecular weight cut-off). This was performed at 4°C to minimize premature reactivation. After 3 such cycles, the final retentate was diluted to ~0.025 mg/ml inactivated CelB with buffer containing 0.1% BSA (650  $\mu$ L total volume). The inactivated enzyme was then incubated at 37°C in the presence of various concentrations of cellobiose (0 to 43 mM) and assayed for activity as described above. To compensate for loss of activity through denaturation of the enzyme a control reaction involving incubation of CelB in the absence of 2FDNPC was carried through the same steps. The increase in fractional activity ( $V/V_0$ ) was monitored over 20 hours, and the resulting time courses fit according to single exponential kinetics ( $V/V_0 = A(1 - \exp(k_{obs(react)} \cdot t)) + C$ ) using GraFit. The rate constants ( $k_{obs(react)}$ ) so derived were corrected for reactivation in the absence of cellobiose ( $k_{H_2O}$ ) then

plotted against the corresponding concentrations of cellobiose and fit according to standard saturation kinetics to derive  $k_{react}$  and  $K_{react}$ .

### **Labeling of CelB with 2FDNPC and proteolysis**

CelB (120  $\mu$ l, 3.7 mg/ml in 50 mM sodium citrate without BSA) was incubated with 0.5 mM 2FDNPC for 60 minutes at 37°C. Residual activity was reduced to 5% by this time. The sample was then used immediately for proteolysis or for ESI-MS analysis of the intact protein. Alternatively the samples were stored over dry ice until required.

The labeled CelB was highly resistant to proteolysis as judged by HPLC profiles of peptic digests over time, thus it was necessary to denature the enzyme (by boiling) prior to digestion. Immediately following incubation with 2FDNPC, CelB (100  $\mu$ l, 3.7 mg/ml labeled or native) was mixed with 200 mM sodium phosphate, pH 2 (200  $\mu$ l) and boiled for 3 minutes. The resulting enzyme precipitates were rapidly clarified upon the addition of pepsin (2  $\mu$ l, 5.6 mg/ml, 200 mM sodium phosphate, pH 2). Labeled and native digests were incubated overnight at room temperature and immediately analyzed by ESI-MS or frozen until required.

### **ESI-MS/MS analysis of labelled CelB**

All mass spectra (intact LC/MS, MS/MS neutral loss, and MS/MS daughter ion spectra) were recorded using a PE-Sciex API 300 triple quadrupole mass spectrometer (Sciex, Thornhill, Ontario, Canada) equipped with an electrospray ionization source. For the intact mass spectra, CelB (4  $\mu$ g, 2F-cellobiosyl labeled or unlabeled) was introduced into the mass spectrometer through a microbore PLRP-5 column (1  $\times$  50 mm) on a Michrom HPLC system. The quadrupole mass analyzer was scanned over a  $m/z$  range of 600 to 2400 Da, with a step size of 0.5 Da and a dwell time of 1 ms/step. The ion source voltage was set at 5 kV, and the orifice energy was 50 V. The molecular weights of the CelB species were determined using the deconvolution software, Multiview 1.1, supplied by Sciex.

Following proteolysis of the labelled enzyme, peptides were separated by reverse phase HPLC on an Ultra-fast Microprotein Analyzer (Michrom BioResources Inc., Pleasanton, CA, USA) directly interfaced with the mass spectrometer. In each of the MS experiments, the proteolytic digest was loaded onto a C18 column (Reliasil, 1  $\times$  150 mm), then eluted with a gradient of 0-60% solvent B over 60 min, followed by 100% B over 2 min. at a flow rate of 50  $\mu$ l/min. (solvent A: 0.05% trifluoroacetic acid, 2% acetonitrile in water: solvent B: 0.045%

trifluoroacetic acid, 80% acetonitrile in water). A post-column splitter sent 80% of the sample into a fraction collector and 20% into the mass spectrometer. The total ion current (TIC) was initially detected in single-quadrupole scan mode (LC-MS) to produce an HPLC chromatogram for the whole digest. A mass range of  $m/z = 300-2200$  Da was scanned using mass spectrometer settings identical to those used for the intact protein. The TIC for a second HPLC run was subsequently collected in neutral loss mode, scanning for the loss of the 2-fluorocellobiosyl label (327 Da) from a singly charged peptide. The collision gas consisted of 90% argon and 10%  $N_2$ . HPLC fractions corresponding to the labeled peptide were saved for sequencing.

The MS/MS daughter ion spectrum of the labeled peptide isolated above was obtained in the triple-quadrupole scan mode by selectively introducing the  $m/z$  947.5 Da peptide from the first quadrupole (Q1) into the collision cell (Q2) and observing the daughter ions in the third quadrupole (Q3). The following settings were used: Q1 was locked on  $m/z = 947.5$  Da; Q3 scan range:  $m/z = 50-970$  Da; step size: 0.5 Da; dwell time: 1 ms/step; ion source voltage: 5.5 kV; orifice voltage: 50 V; RNG = 400 V; Q0 = -10; R02 = -55 V; collision gas =  $N_2$ .

### **Transglycosylation kinetics with CelB nucleophile mutants**

The polymerization of  $\alpha$ -cellobiosyl fluoride by CelB nucleophile mutants was monitored with a fluoride electrode. The apparatus and software used were the same as that described in the experimental for Chapter 5. Reaction cuvettes were charged with  $\alpha$ -cellobiosyl fluoride in 150 mM NaPi, 150 mM NaCl, 1 mg/mL BSA, pH 7 (500  $\mu$ L total volume) and equilibrated at 25°C. The reaction was initiated by addition of an aliquot of CelB nucleophile mutant (20-150  $\mu$ L) and subsequently monitored over 7-10 min.. Final enzyme concentrations were as follows: CelB E120S, 0.57 mg/mL (23.3  $\mu$ M); E120A, 0.62 mg/mL (25.4  $\mu$ M); E120G, 4.5 mg/mL (183  $\mu$ M). Enzymatic rates were corrected for spontaneous hydrolysis of  $\alpha$ -cellobiosyl fluoride. Plots of reaction velocity vs substrate concentration were fit according to standard Michaelis Menton kinetics using GraFit.

### **Synthesis**

#### ***$\alpha$ -Cellobiosyl fluoride, per-O-acetate***

$\alpha$ -Cellobiosyl fluoride, per-O-acetate was synthesized according to a published procedure.<sup>306</sup> Cellobiose per-O-acetate (8.02 g, 11.8 mmol) was dissolved in dry DCM (25 mL) in a 125 mL

Nalgene™ bottle. The flask was flushed with dry argon and then 70% HF/pyridine (25 g) and acetic anhydride (1 mL) added. The container was sealed and the reaction maintained at room temperature for 36 hrs. at which time TLC analysis (1:1 EtOAc/PE) indicated complete conversion to  $\alpha$ -cellobiosyl fluoride per-*O*-acetate. The reaction was diluted with DCM (125 mL) and poured into ice-water (200 mL). The organic layer was washed with saturated sodium bicarbonate and water then dried over MgSO<sub>4</sub>. After evaporation of the solvent  $\alpha$ -cellobiosyl fluoride per-*O*-acetate was obtained as white crystals (7.12 g, 11.1 mmol, 94%). <sup>1</sup>H NMR data was in agreement with that reported previously.<sup>306</sup> Rf (1:1 EtOAc/PE) = 0.38; <sup>1</sup>H NMR (400 MHz, CDCl<sub>3</sub>):  $\delta$  5.65 (dd, 1 H, *J* = 2.6, 53.1 Hz, H-1<sup>1</sup>), 5.45 (dd, 1 H, *J* = 9.8, 9.8 Hz, H-3<sup>1</sup>), 5.13 (dd, 1 H, *J* = 9.3, 9.3 Hz, H-3<sup>2</sup>), 5.05 (dd, 1 H, *J* = 9.6, 9.6 Hz, H-4<sup>2</sup>), 4.91 (dd, 1 H, *J* = 7.8, 9.4 Hz, H-2<sup>2</sup>), 4.87 (ddd, 1 H, *J* = 2.8, 10.1, 24.4 Hz, H-2<sup>1</sup>), 4.53 (dd, 1 H, *J* = 2.1, 12.5 Hz, H-6), 4.52 (d, 1 H, *J* = 7.8 Hz, H-1<sup>2</sup>), 4.34 (dd, 1 H, *J* = 4.6, 12.5 Hz, H-6), 4.12 (dd, 1 H, *J* = 4.1, 12.3 Hz, H-6), 4.09 (m, 1 H, H-5<sup>1</sup>), 4.03 (dd, 1 H, *J* = 2.1, 12.5 Hz, H-6), 3.81 (dd, 1 H, *J* = 9.7, 9.7 Hz, H-4<sup>1</sup>), 3.65 (ddd, 1 H, *J* = 2.1, 4.3, 9.8 Hz, H-5<sup>2</sup>); <sup>19</sup>F NMR (188 MHz, CDCl<sub>3</sub>, ref. to CF<sub>3</sub>CO<sub>2</sub>H):  $\delta$  -73.4 (dd, *J* = 24.4, 53.4 Hz).

#### *$\alpha$ -Cellobiosyl fluoride*

$\alpha$ -Cellobiosyl fluoride was obtained by treatment of the per-*O*-acetate (7.06 g, 11 mmol) with catalytic sodium methoxide in dry methanol for 45 min.. Neutralization of the reaction with Amberlite IR-120(H<sup>+</sup>) resin caused the product to crystallize spontaneously (3.02 g, 8.77 mmol, 80%). Rf (5:2:1 EtOAc/MeOH/H<sub>2</sub>O) = 0.46; <sup>1</sup>H NMR (400 MHz, D<sub>2</sub>O):  $\delta$  5.68 (dd, 1 H, *J* = 2.7, 53.4 Hz, H-1<sup>1</sup>), 4.51 (d, 1 H, *J* = 8.0 Hz, H-1<sup>2</sup>), 3.95 (m, 1 H, H-5<sup>1</sup>), 3.94-3.87 (m, 3 H, H-6<sup>1</sup>a,b and H-6<sup>2</sup>a), 3.85 (dd, 1 H, *J* = 9.4, 9.4 Hz, H-3<sup>1</sup>), 3.75 (dd, 1 H, *J* = 9.5, 9.5 Hz, H-4<sup>1</sup>), 3.71 (dd, 1 H, *J* = 5.9, 12.6 Hz, H-6<sup>2</sup>b), 3.65 (ddd, 1 H, *J* = 2.7, 9.7, 26.3 Hz, H-2<sup>1</sup>), 3.50 (dd, 1 H, *J* = 9.1, 9.1 Hz, H-3<sup>2</sup>), 3.47 (m, 1 H, H-5<sup>2</sup>), 3.40 (dd, 1 H, *J* = 9.2, 9.2 Hz, H-4<sup>2</sup>), 3.31 (dd, 1 H, *J* = 8.0, 9.0 Hz, H-2<sup>2</sup>), <sup>19</sup>F NMR (188 MHz, D<sub>2</sub>O, ref. to CF<sub>3</sub>CO<sub>2</sub>H):  $\delta$  -74.6 (dd, *J* = 25.9, 53.4 Hz).

#### *Synthesis of cellulose with CelB E120S*

$\alpha$ -Cellobiosyl fluoride (49 mg, 142  $\mu$ mol) was dissolved in 1 mL 500 mM ammonium bicarbonate, pH 7.9. CelB E120S (0.75 mg) was added and the reaction maintained at room temperature. In 1 hr. a white precipitate formed. After 24 hrs. a second portion of E120S was added (0.35 mg). TLC analysis (5:2:1 EtOAc/MeOH/H<sub>2</sub>O) indicated complete consumption of

$\alpha$ -cellobiosyl fluoride after 36 hrs.. The white precipitate was collected by centrifugation then washed repeatedly with water. Upon drying *in vacuo* over  $P_2O_5$  a white powder was obtained (40.5 mg, 85%).

The polysaccharide product was per-*O*-acetylated in a fashion similar to the Miles' method for the synthesis of triacetyl cellulose.<sup>253</sup> The product (38 mg) was suspended in 0.5 mL acetic anhydride / acetic acid /  $H_2SO_4$  (1:1: 0.025) and the mixture maintained at 35°C for 24 hrs. whereupon a clear, pale brown solution was obtained. This solution was poured into cold water (4 mL) to obtain a white precipitate which was subsequently stirred vigorously for 24 hrs.. The precipitate was collected by centrifugation, washed repeatedly with water, then dried over  $P_2O_5$  *in vacuo* to obtain a white powder (36 mg). TLC analysis (2:1 EA/PE) and ESI-MS indicated an entire series of per-*O*-acetylated oligosaccharides had been formed, with degrees of polymerization ranging from 3 to at least 8 monosaccharide units in length. The method of acetylation described above will result in glycosidic bond cleavage, producing the odd numbered polymeric products, but produces a form of cellulose tri-*O*-acetate that is soluble in chloroform.  $^1H$  NMR (400 MHz,  $CDCl_3$ , chemical shifts assigned by  $^1H$ - $^1H$  COSY analysis):  $\delta$  6.21 (d,  $J = 4.1$  Hz, H-1 $^1$   $\alpha$ -anomer), 5.61 (d,  $J = 8.9$  Hz, H-1 $^1$   $\beta$ -anomer,  $\alpha/\beta = 10:2$ ), 5.37 (broad dd,  $J = 9.6, 9.6$  Hz, H-3 $^1$ ), 5.04 (m, H-3), 4.95 (dd,  $J = 4.1, 10.2$  Hz, H-2 $^1$   $\alpha$ -anomer), 4.90-4.73 (m, H-2), 4.38 (m, H-1, H-6a), 4.10-3.91 (m, H-6b), 3.69 (m, H-4), 3.62-3.47 (m, H-5);  $^{13}C$  NMR (100 MHz,  $CDCl_3$ , resonances assigned from ref. <sup>254</sup>), major resonances:  $\delta$  170.16, 169.69 and 169.24 ( $3 \times CH_3CO$ ), 100.45 (C-1), 76.03 (C-4), 72.79 (C-5), 72.48 (C-3), 71.81 (C-2), 61.99 (C-6), 20.74, 20.52 and 20.43 ( $3 \times CH_3CO$ ); minor resonances:  $\delta$  100.75 and 88.91 (C-1), 70.72 (C-5), 69.34 and 69.31 (C-2, C-3), 67.73 (C-4), 61.49 and 61.23 (C-6); ESI-MS: observed  $m/z = 331.3$  (glucosyl) 619.7 (cellobiosyl), 907.8 (cellotriaosyl), 1195.9 (cellotetraosyl), 1484.5 (cellopentaosyl), 1772.0 (cellohexaosyl), 2060.4 (celloheptaosyl), and 2349.1 (cellooctaose, per-*O*-acetate  $[M - CH_3CO + H]^+$ ).

## Chapter 8: Enzymatic Synthesis of Carbon-Fluorine Bonds

### Kinetic analysis of enzymatic halogenation reactions

All halogenation reactions by Man2A and Abg nucleophile mutants (as well as wild type enzymes) were performed with 2 M halide, 1 mg/mL BSA, 100 mM citrate at pH 6, 25°C. Because concentrated fluoride solutions destroy pH electrodes, the pH values of fluoride solutions were determined with precision litmus paper. 2,4-Dinitrophenyl  $\beta$ -glucoside or 2,4-dinitrophenyl  $\beta$ -mannoside served as substrates for Abg and Man2A nucleophile mutant halogenation reactions. The  $\beta$ -mannoside was prepared fresh in pH 6 buffer prior to use. The release of 2,4-dinitrophenol was monitored spectrophotometrically ( $\lambda$  400 nm,  $\Delta\epsilon = 10\,900\text{ M}^{-1}\text{ cm}^{-1}$ ) and corrected for spontaneous hydrolysis of the substrate, which was generally negligible at the concentrations of substrate used. Data points prior to the onset of transglycosylation in plots of reaction velocity versus substrate concentration were fit with the Michaelis-Menten equation to derive  $k_{cat}$  and  $K_M$  values.

The fluorination of 2,5-dinitrophenyl  $\beta$ -mannoside with Man2A E429A was performed with 1 M KF, 1 mg/mL BSA, 100 mM sodium phosphate at pH 7, 25°C. Reactions with chloride or bromide were performed under the same conditions. The release of 2,5-dinitrophenol was monitored spectrophotometrically at 440 nm ( $\Delta\epsilon = 4288\text{ M}^{-1}\text{ cm}^{-1}$ ).

### Kinetic isotope effects

The  $\alpha$ -deuterium kinetic isotope effect was measured on  $k_{cat}/K_M$  for the Abg E358A, E358S and E358G fluorination reactions (2 M KF, 1 mg/mL BSA, pH 6, 25°C) using the substrate depletion method (see Chapter 3 experimental). The following concentrations of 2,4-dinitrophenyl  $\beta$ -glucoside (protio and 1-deuterio labelled) and mutant were used to generate a first order rate of 2,4-dinitrophenol release over a period of 10 to 30 minutes: E358S ( $E_0 = 0.45\ \mu\text{M}$ ,  $[\text{S}] = 4.3\ \mu\text{M}$ ); E358A ( $E_0 = 0.86\ \mu\text{M}$ ,  $[\text{S}] = 13.3\ \mu\text{M}$ ); E358G ( $E_0 = 0.18\ \mu\text{M}$ ,  $[\text{S}] = 13.3\ \mu\text{M}$ ). The Abg mutants retained complete activity under these assay conditions for over 8 hrs. The  $\alpha$ DKIE value was derived from an average of 8 measurements with each protio and deuterio substrate.

### **TLC and ESI-MS characterization of transglycosylation products**

2,4-Dinitrophenyl  $\beta$ -glucoside (5 mg) was dissolved in 2 M anion (fluoride, chloride, or bromide), 100 mM citrate, pH 6. Abg nucleophile mutant was added to afford a final enzyme concentration of 0.5-1 mg/mL. The total reaction volume was 0.5 mL (yielding 29 mM 2,4-DNPGlu). After 5-7 hrs. at room temperature an aliquot of the reaction mixture (50  $\mu$ L) was diluted 3 fold with acetonitrile, applied to a plug of silica gel (2.5 cm) in a Pasteur pipette and eluted with 1 column volume of acetonitrile. The desalted sample was then concentrated *in vacuo* and analyzed by TLC (7:2:1 EtOAc/MeOH/H<sub>2</sub>O). Di- and trisaccharide products were observed for the fluorination reaction. Interestingly, the chlorination and bromination reactions afforded only disaccharide products. The samples were then dissolved in 80% acetonitrile/H<sub>2</sub>O and analyzed by direct infusion into a Perkin Elmer API-300 ESI-MS/MS instrument operating in positive ion mode. Masses corresponding to 2,4-dinitrophenyl  $\beta$ -cellobioside ( $m/z = 531.1$ ,  $[M + Na]^+$ ) and 2,4-dinitrophenyl  $\beta$ -cellotrioside ( $m/z = 693.2$   $[M + Na]^+$ ) were observed for the fluorination reaction; only 2,4-dinitrophenyl  $\beta$ -cellobioside was observed for the chlorination or bromination reactions.

### **Synthesis of $\beta$ -Mannosyl Fluoride Standard**

$\beta$ -Mannosyl fluoride was obtained by deacetylation of  $\beta$ -mannosyl fluoride per-*O*-acetate with sodium methoxide in methanol. The crude sample was used as a <sup>19</sup>F NMR standard without further purification. Selected data for  $\beta$ -mannosyl fluoride, per-*O*-acetate: <sup>1</sup>H NMR (200 MHz, CDCl<sub>3</sub>):  $\delta$  5.53 (dd, 1 H,  $J = 1.9, 49.3$  Hz, H-1), 5.43 (ddd, 1 H,  $J = 1.9, 3.2, 10.7$  Hz, H-2), 5.22 (dd, 1 H,  $J = 7.8, 7.8$  Hz, H-4), 5.16 (dd, 1 H,  $J = 7.8, 3.0$  Hz, H-3), 4.33 (m, 2 H, 2  $\times$  H-6), 3.90 (m, 1 H, H-5); <sup>19</sup>F NMR (188 MHz, CDCl<sub>3</sub>, ref. to CF<sub>3</sub>CO<sub>2</sub>H):  $\delta$  66.1 (dd,  $J = 10.7, 50.3$  Hz). Data for  $\beta$ -mannosyl fluoride: <sup>19</sup>F NMR (282 MHz, referenced to CFC<sub>3</sub>):  $\delta$  -146.7 (d,  $J = 49$  Hz).

### **Enzymatic synthesis of glycosyl halides**

#### ***$\alpha$ -D-Mannopyranosyl fluoride***

Man2A E519S or E519A (1 mg/mL) was reacted with 2,4-dinitrophenyl  $\beta$ -D-mannoside (19 mM) and 2 M KF in 100 mM citrate, pH 6 in a total volume of 1.5 mL. After 6 hrs. the samples were desalted on silica gel (as described above). TLC analysis of each reaction mixture

indicated the formation of  $\alpha$ -D-mannosyl fluoride as the major product; Rf (7:2:1 EtOAc/MeOH/H<sub>2</sub>O) = 0.58. The samples were dried *in vacuo*, acetylated with 3:2 pyridine / acetic anhydride and purified by silica gel chromatography (3:1 PE / EtOAc). <sup>1</sup>H and <sup>19</sup>F NMR spectra of the isolated, per-*O*-acetylated product agreed with those of an authentic sample of  $\alpha$ -mannosyl fluoride per-*O*-acetate (see Chapter 6 experimental for data). An analogous reaction with wild type Man2A (0.12 mg/mL) monitored by <sup>19</sup>F NMR did not show any signals corresponding to the formation of  $\alpha$ - or  $\beta$ -mannosyl fluoride.

#### ***$\alpha$ -D-Glucopyranosyl fluoride***

Abg E358G (0.18 mg/mL) was reacted with 2,4-dinitrophenyl  $\beta$ -glucoside (22 mM) and 2 M KF in 100 mM citrate, 10% D<sub>2</sub>O, pH 6 (total reaction volume of 0.56 mL) at 300 K. The reaction was monitored directly by <sup>19</sup>F NMR (282 MHz, referenced to CF<sub>3</sub>CO<sub>2</sub>H). After 10 min. a resonance corresponding to  $\alpha$ -glucosyl fluoride was observed:  $\delta$  -74.3 (dd,  $J$  = 55.4, 24.9 Hz). An analogous reaction with wild type Abg (0.11 mg/mL) monitored by <sup>19</sup>F NMR did not show any signals corresponding to the formation of  $\alpha$ - or  $\beta$ -glucosyl fluoride.

#### ***$\alpha$ -D-Galactopyranosyl fluoride***

Abg E358G (1 mg/mL) was reacted with 2,4-dinitrophenyl  $\beta$ -galactoside (23 mM) and 2 M KF in 100 mM citrate, pH 6. After 8 hrs. the sample was desalted on silica gel. TLC analysis indicated the formation of  $\alpha$ -galactosyl fluoride as the major product; Rf (7:2:1 EtOAc/MeOH/H<sub>2</sub>O) = 0.46. The sample was dried *in vacuo*, acetylated with 3:2 pyridine / acetic anhydride, and purified on silica gel. <sup>1</sup>H and <sup>19</sup>F NMR spectra of the isolated, per-*O*-acetylated product agreed with those of an authentic sample (see Chapter 5 experimental).

#### ***$\alpha$ -D-Galactopyranosyl chloride***

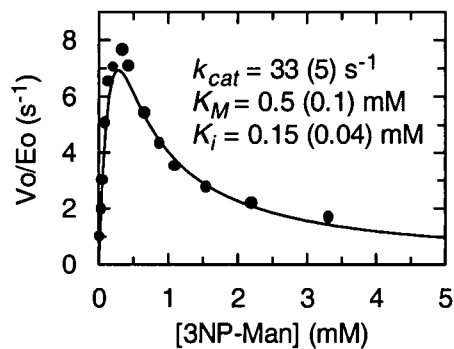
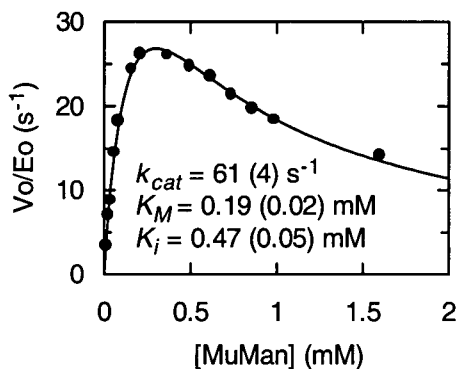
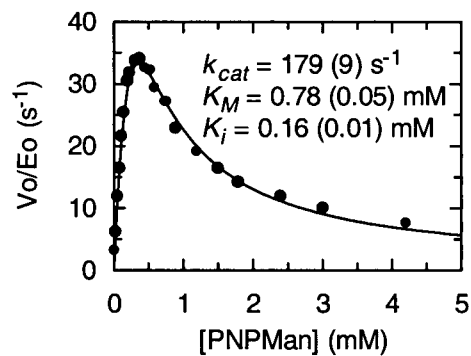
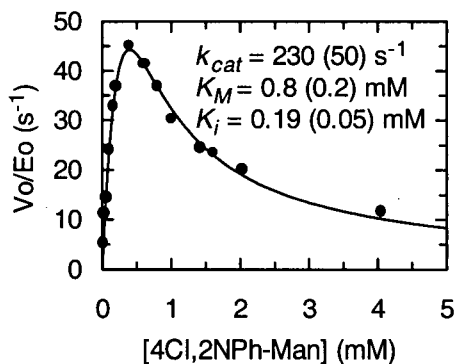
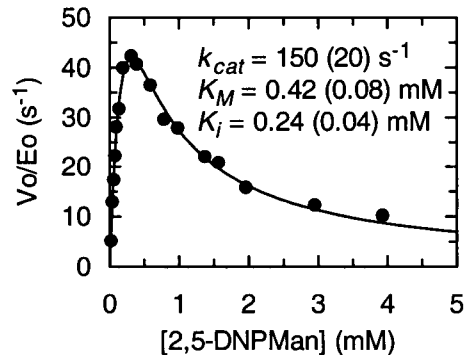
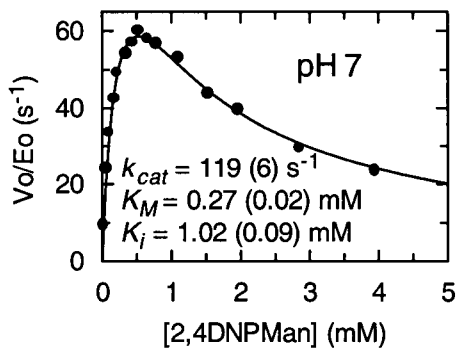
Abg E358G (1 mg/mL) was reacted with 2,4-dinitrophenyl  $\beta$ -galactoside (7.5 mM) and 1.7 M NaCl in 100 mM citrate (99.8% D<sub>2</sub>O), pD 5.65. After 145 min. at room temperature the sample was analyzed by <sup>1</sup>H NMR (300 MHz, referenced to HDO). A small doublet was observed ( $\delta$  5.45,  $J$  = 3.1 Hz) which may correspond to the anomeric proton of  $\alpha$ -galactosyl chloride. A control reaction (no E358G) did not show appreciable formation of this signal.

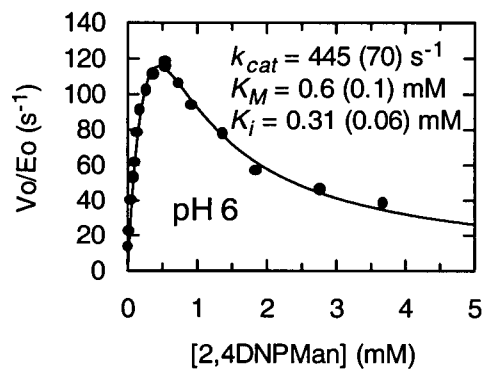
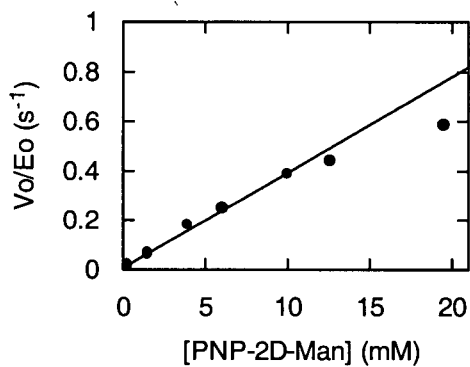
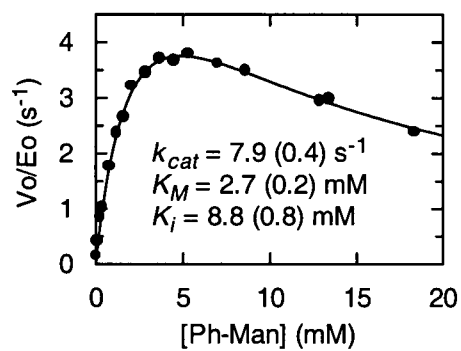
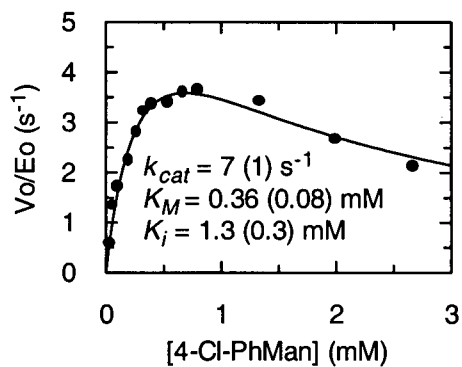
***$\beta$ -D-Mannopyranosyl fluoride***

Man2A E429A (0.38 mg/mL, 4  $\mu$ M) was reacted with 2,5-dinitrophenyl  $\beta$ -D-mannoside (23 mM) in 1 M KF, 100 mM sodium phosphate, 10% D<sub>2</sub>O, pH 7 (total reaction volume of 0.6 mL), at 300K. After 20 min. an apparent doublet was observed by <sup>19</sup>F NMR (282 MHz, referenced to CFCl<sub>3</sub>):  $\delta$  -146.7 (d,  $J$  = 49 Hz). This agreed with an authentic sample of  $\beta$ -D-mannosyl fluoride prepared by deprotection of  $\beta$ -mannosyl fluoride per-*O*-acetate with sodium methoxide in methanol.<sup>307</sup> For  $\alpha$ -D-mannosyl fluoride:  $\delta$  -139.0 (d,  $J$  = 49 Hz, referenced to CFCl<sub>3</sub>).

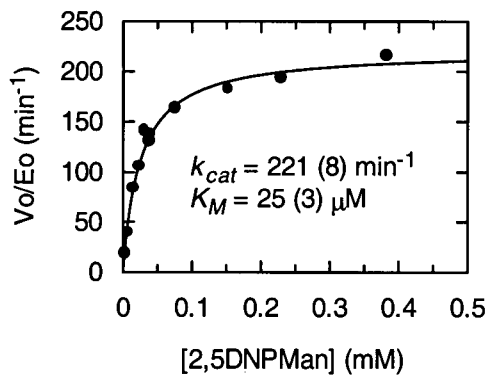
## Appendix A

Plots of reaction rate vs substrate concentration for the reaction of wild type Man2A and Man2A E429A with aryl  $\beta$ -mannosides (pH 7, 25°C, unless indicated otherwise).





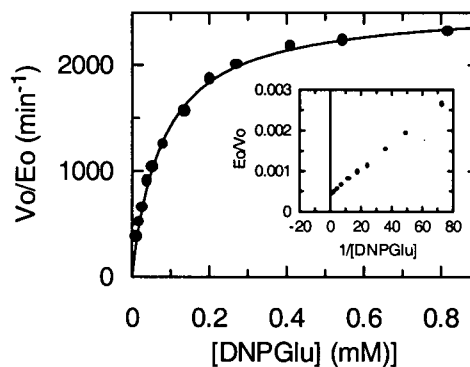
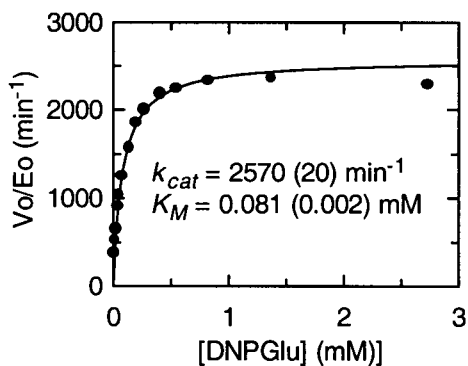
Man2A E429A, 100 mM azide,  
pH 7, 25°C



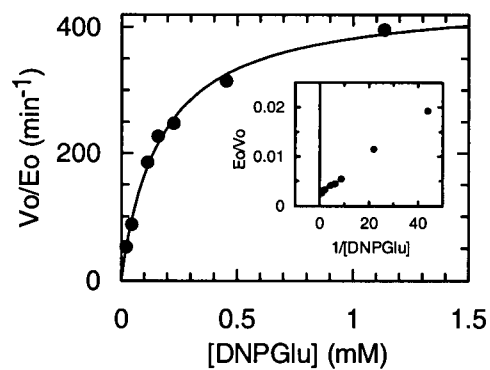
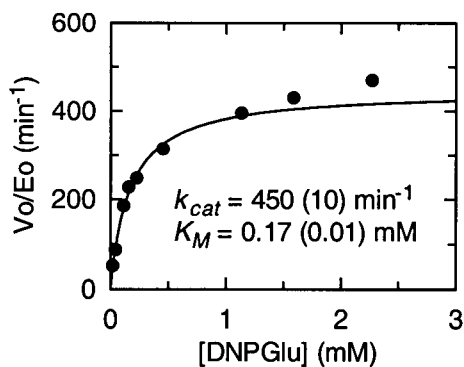
## Appendix B

Plots of reaction rate vs substrate concentration for the reaction of Abg nucleophile mutants with 2,4-DNP  $\beta$ -glucoside and formate or azide. Overall plots and corresponding expansions are shown.

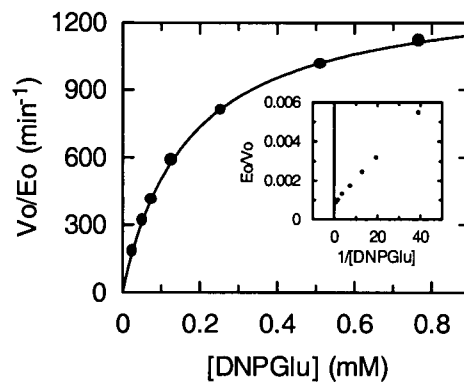
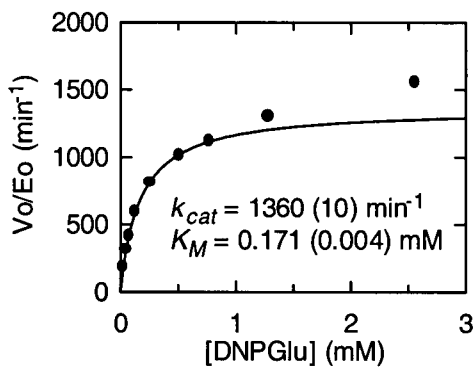
**Abg E358G + 2 M formate, pH 6, 25°C**



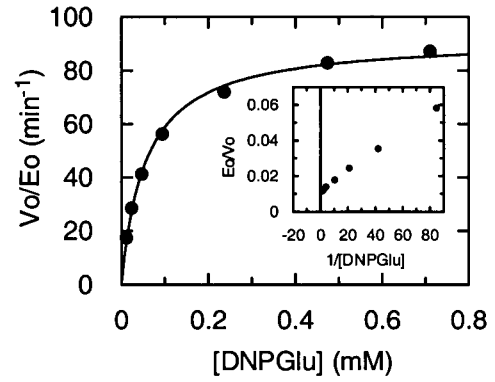
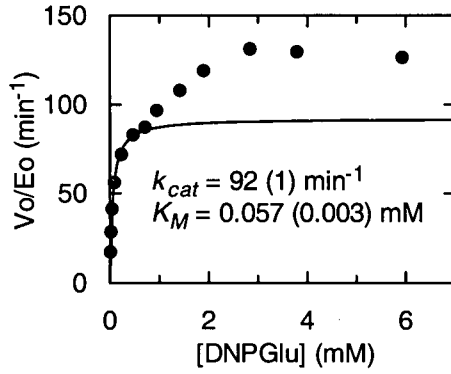
**Abg E358G + 2 M azide, pH 7, 37°C**



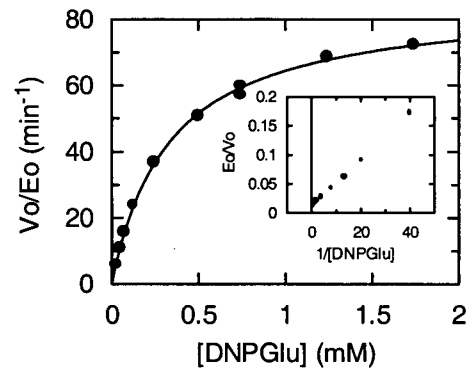
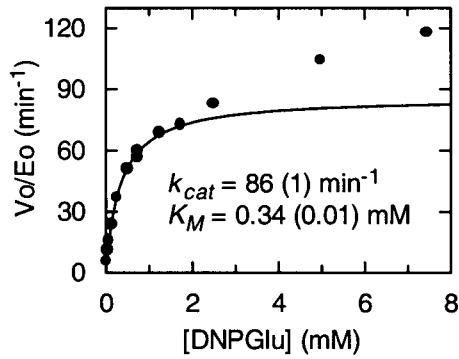
**Abg E358G + 2 M azide, pH 6, 25°C**



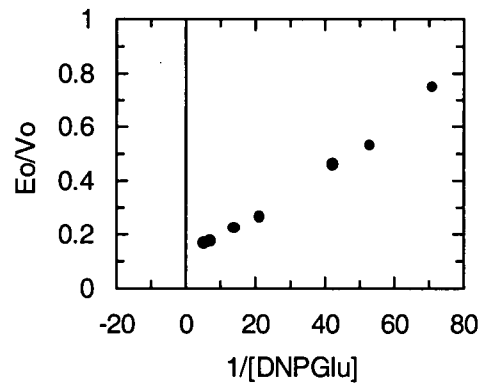
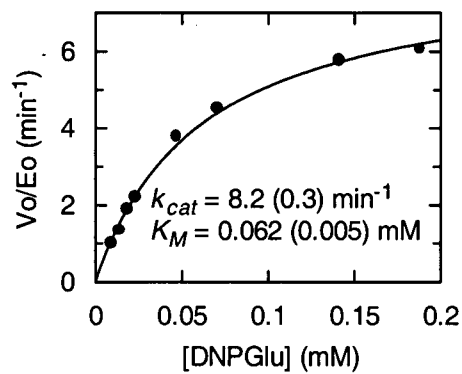
## AbgE358A + 5 M formate pH 7, 37°C



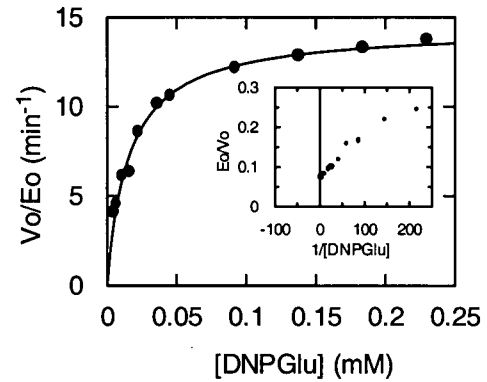
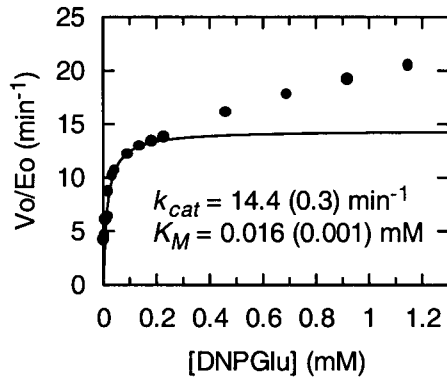
## Abg E358A + 2 M azide, pH 6, 25°C



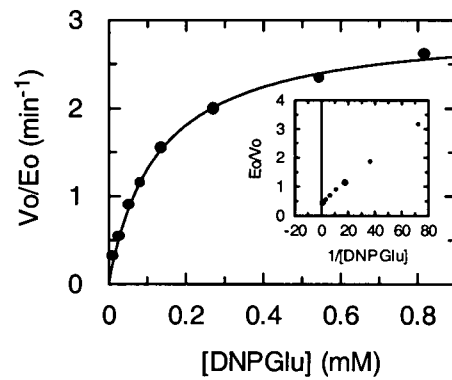
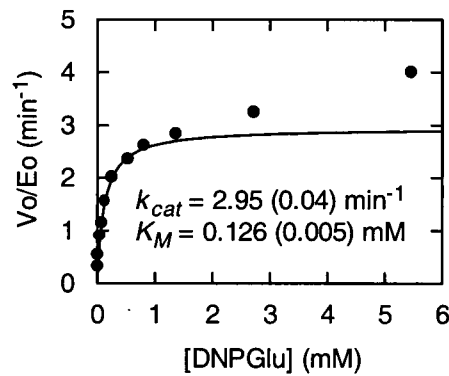
## Abg E358S + 2 M formate, pH 7, 37°C



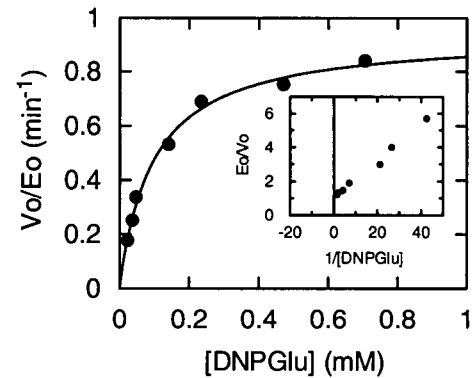
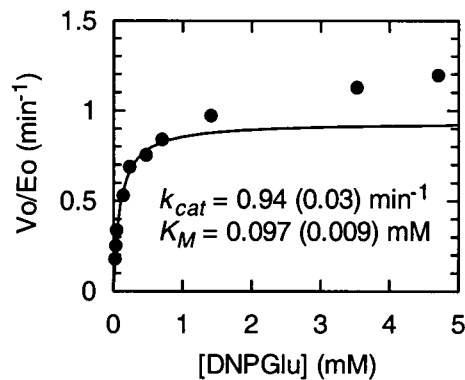
## Abg E358S, 5 M formate, pH 7, 37°C



## Abg E358S + 2 M azide, pH 6, 25°C

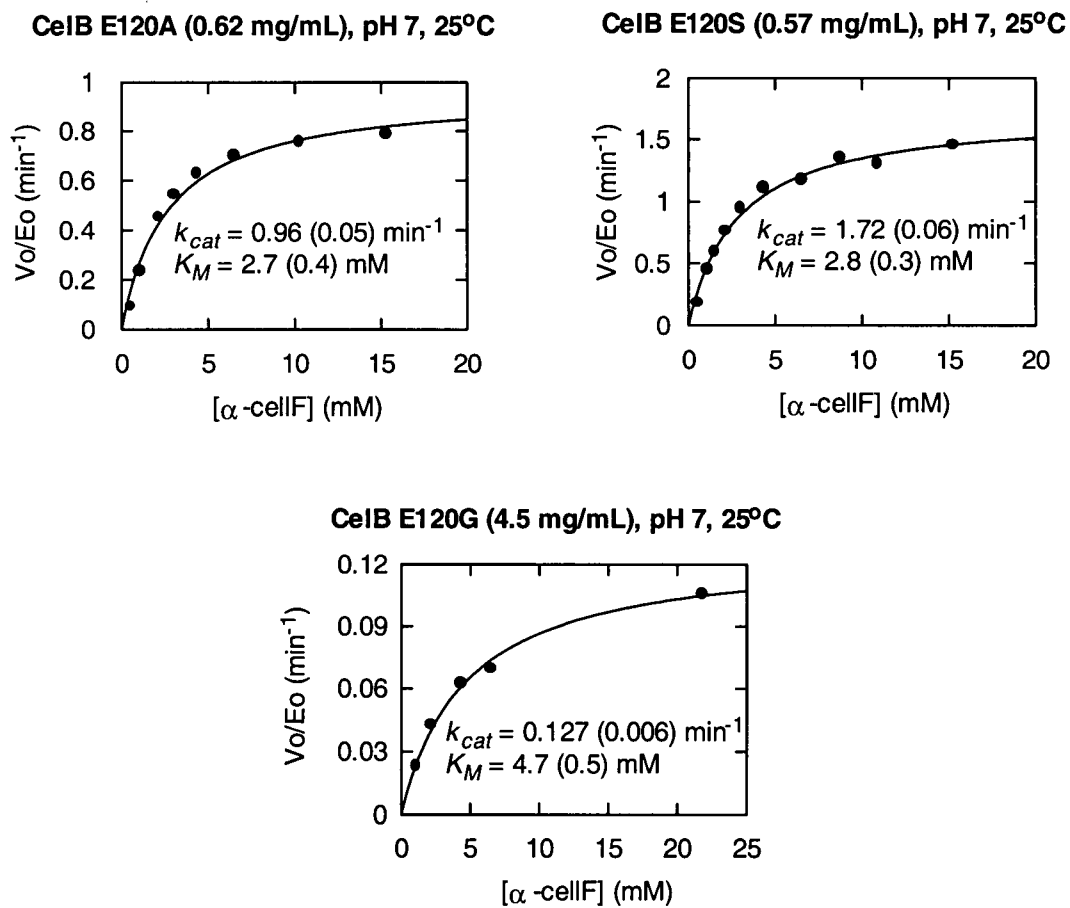


## Abg E358S + 2 M azide, pH 7, 37°C



## Appendix C

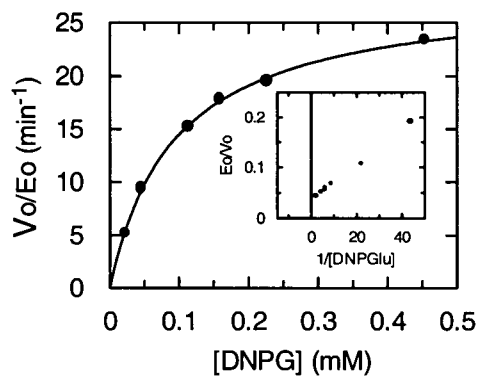
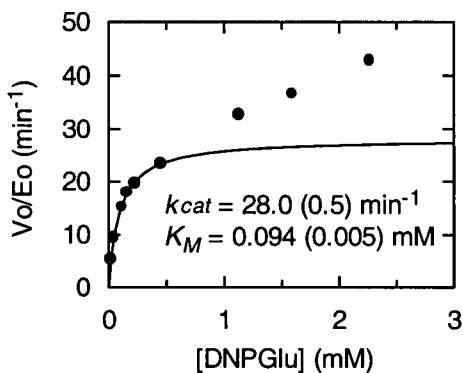
Plots of reaction rate vs substrate concentration for the reaction of CelB nucleophile mutants with  $\alpha$ -cellobiosyl fluoride.



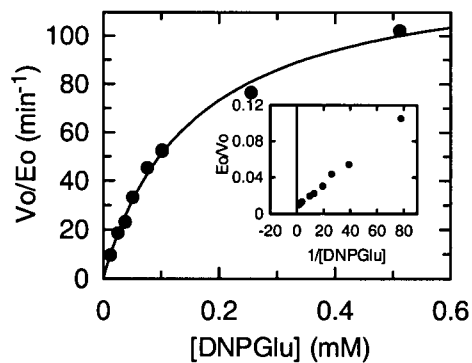
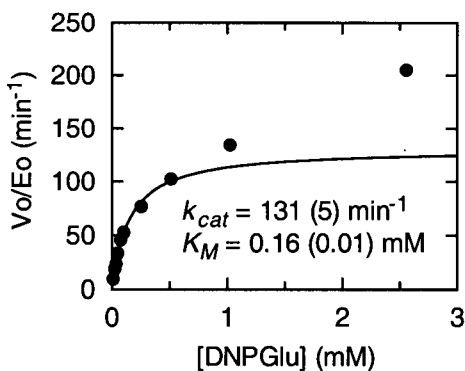
## Appendix D

Plots of reaction rate vs substrate concentration for the reaction of Abg nucleophile mutants with 2,4-DNP  $\beta$ -glucoside and halides. Overall plots and corresponding expansions are shown.

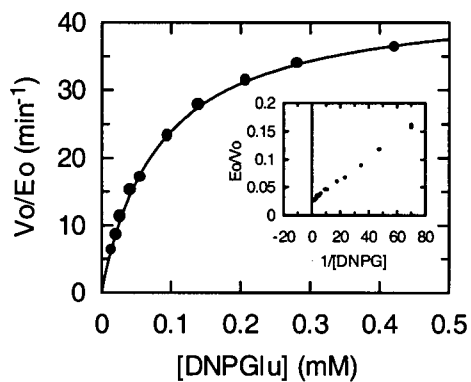
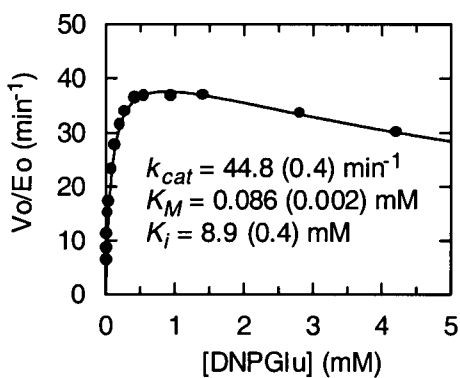
**Abg E358G + 2 M KF, pH 7, 37°C**



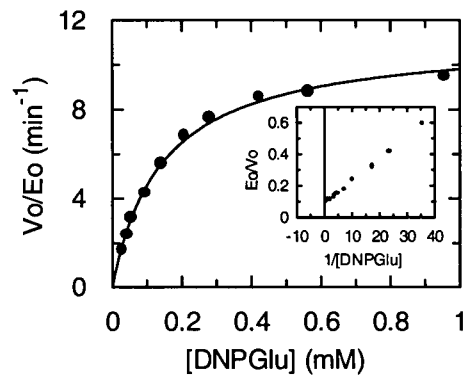
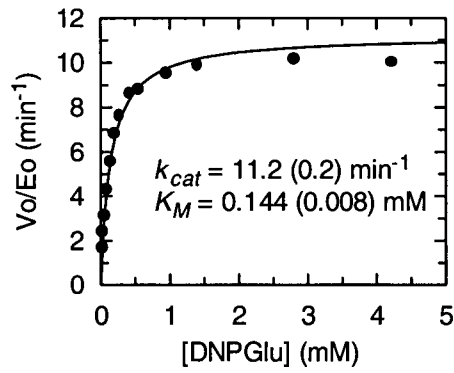
**Abg E358G + 2 M KF, pH 6, 25°C**



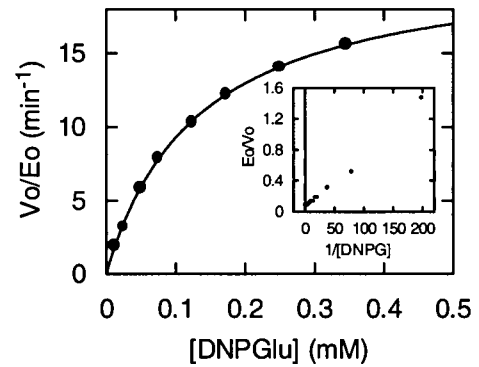
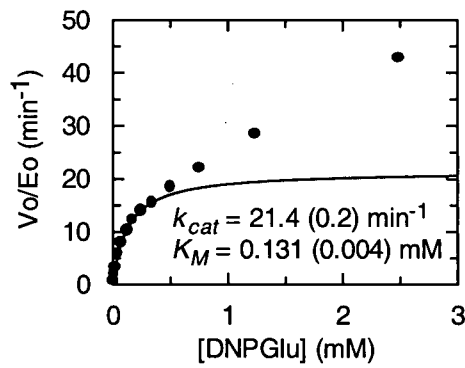
**Abg E358G + 2 M NaCl, pH 6, 25°C**



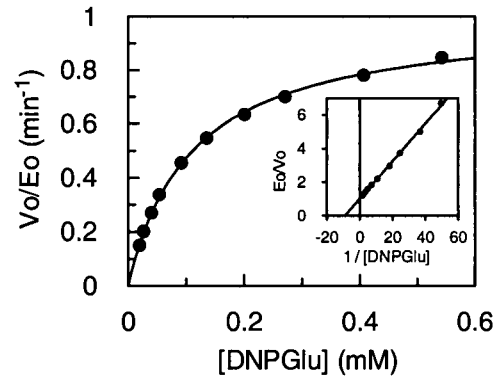
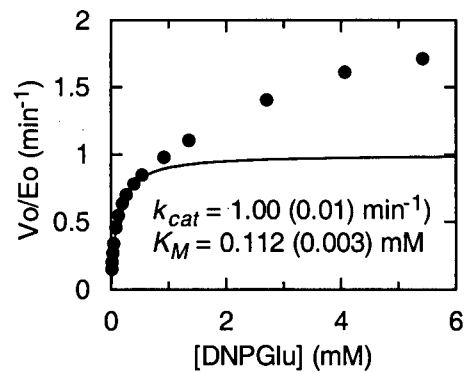
## Abg E358G + 2 M NaBr, pH 6, 25°C



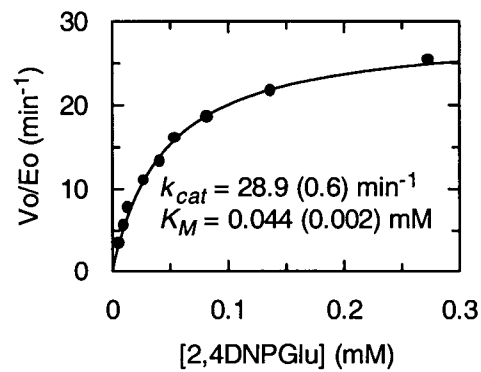
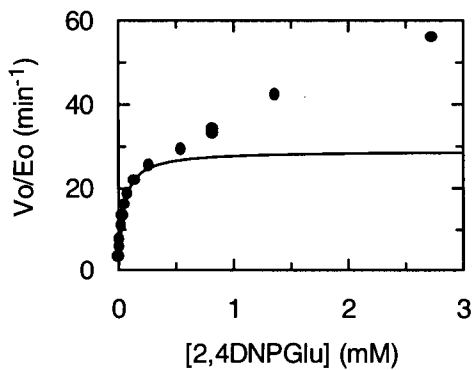
## Abg E358A + 2 M KF, pH 6, 25°C



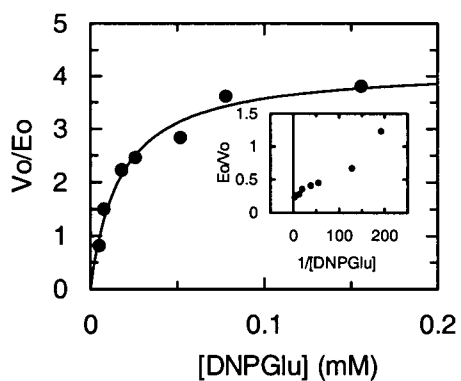
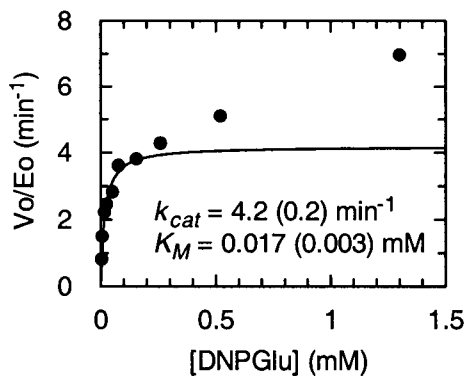
## Abg E358A + 2 M NaCl, pH 6, 25°C



Abg E358S + 2 M KF, pH 6, 25°C



Abg E358S + 4 M KF, pH 7, 37°C



## References

- (1) Wolfenden, R.; Lu, X.; Young, G. *J. Am. Chem. Soc.* **1998**, *120*, 6814-6815.
- (2) Phillips, D. C. *Proc. Natl. Acad. Sci. U.S.A.* **1967**, *57*, 484-495.
- (3) Imoto, T.; Johnson, L.; North, A.; Phillips, D.; Rupley, J. *The Enzymes*; Academic Press: New York, 1972.
- (4) Deslongchamps, P. *Stereoelectronic Effects in Organic Chemistry*; Pergamon Press: New York, 1983.
- (5) Strynadka, N. C. J.; James, M. N. G. *J. Mol. Biol.* **1991**, *220*, 401-424.
- (6) Huang, X.; Surry, C.; Hiebert, T.; Bennet, A. J. *J. Am. Chem. Soc.* **1995**, *117*, 10614-10621.
- (7) Banait, N. S.; Jencks, W. P. *J. Am. Chem. Soc.* **1991**, *113*, 7951-7958.
- (8) Banait, N. S.; Jencks, W. P. *J. Am. Chem. Soc.* **1991**, *113*, 7958-7961.
- (9) Amyes, T. L.; Jencks, W. P. *J. Amer. Chem. Soc.* **1989**, *111*, 7888.
- (10) Young, P. R.; Jencks, W. P. *J. Am. Chem. Soc.* **1977**, *99*, 8238-8247.
- (11) Sinnott, M. L. *Chem. Rev.* **1990**, *90*, 1171-1202.
- (12) Rosenberg, S.; Kirsch, J. F. *Biochemistry* **1981**, *20*, 3189-3195.
- (13) Rosenberg, S.; Kirsch, J. F. *Biochemistry* **1981**, *20*, 3196-3204.
- (14) Dahlquist, F. W.; Rand-Meir, T.; Raftery, M. A. *Biochemistry* **1969**, *8*, 4214-21.
- (15) Koshland, D. E. *Biol. Rev.* **1953**, *28*, 416-436.
- (16) Lowe, G.; Sheppard, G.; Sinnott, M.L.; Williams, A. *Biochem. J.* **1967**, *104*, 893-9.
- (17) Lowe, G.; Sheppard, G. *Chem. Commun.* **1968**, 529.
- (18) Piszkiwicz, D.; Bruice, T. C. *J. Am. Chem. Soc.* **1967**, *89*, 6237.
- (19) Piszkiwicz, D.; Bruice, T. C. *J. Am. Chem. Soc.* **1968**, *90*, 2156.
- (20) Mark, B. L.; Vocadlo, D. J.; Knapp, S.; Triggs-Raine, B. L.; Withers, S. G.; James, M. N. G. *J. Biol. Chem.* **2001**, *276*, 10330-10337.
- (21) Knapp, S.; Vocadlo, D.; Gao, Z.; Kirk, B.; Lou, J.; Withers, S. G. *J. Am. Chem. Soc.* **1996**, *118*.
- (22) Rand-Meir, T.; Dahlquist, F. W.; Raftery, M. A. *Biochemistry* **1969**, *8*, 4206-4214.
- (23) Raftery, M. A.; Rand-Meir, T. *Biochemistry* **1968**, *7*, 3281.
- (24) Henrissat, B.; Bairoch, A. *Biochem. J.* **1996**, *316*, 695-696.
- (25) Henrissat, B.; Davies, G. *Curr. Opin. Struct. Biol.* **1997**, *7*, 637-644.

- (26) Davies, G.; Henrissat, B. *Structure* **1995**, *3*, 853-859.
- (27) White, A.; Rose, D. R. *Curr. Opin. Struct. Biol.* **1997**, *7*, 645-651.
- (28) Gebler, J.; Gilkes, N. R.; Claeysens, M.; Wilson, D. B.; Beguin, P.; Wakarchuk, W. W.; Kilburn, D. G.; Miller, R. C., Jr.; Warren, R. A. J.; Withers, S. G. *J. Biol. Chem.* **1992**, *267*, 12559-12561.
- (29) McCarter, J.; Withers, S. G. *Curr. Opin. Struct. Biol.* **1994**, *4*, 885-892.
- (30) Wang, Q.; Graham, R. W.; Trimbur, D.; Warren, R. A. J.; Withers, S. G. *J. Am. Chem. Soc.* **1994**, *116*, 11594-11595.
- (31) Nath, R. L.; Rydon, H. N. *Biochem. J.* **1954**, *57*, 1-10.
- (32) Sinnott, M. L.; Souchard, I. J. L. *Biochem. J.* **1973**, *133*, 89-98.
- (33) Kempton, J. B.; Withers, S. G. *Biochemistry* **1992**, *31*, 9961-9969.
- (34) Namchuk, M. N.; Withers, S. G. *Biochemistry* **1995**, *34*, 16194-16202.
- (35) McCarter, J.; Adam, M.; Withers, S. G. *Biochem. J.* **1992**, *286*, 721-727.
- (36) Davies, G.; Sinnott, M. L.; Withers, S. G. "Glycosyl Transfer" in *Comprehensive Biological Catalysis*; Sinnott, M.L., Ed., Academic Press Ltd.: London, 1998, Vol. 1, pp 119-209.
- (37) Withers, S. G.; Namchuk, M.; Mosi, R. "Potent glycosidase inhibitors: transition state mimics or simply fortuitous binders?" in *Iminosugars as glycosidase inhibitors: nojirimycin and beyond.*; Stutz, A. E., Ed.; Wiley-VCH: Weinheim, 1999, pp 188-206.
- (38) Schimdt, D. D.; Frommer, W.; Muller, L.; Truscheit, E. *Naturwissenschaften* **1979**, *66*, 584.
- (39) Hohenschutz, L. D.; Bell, E. A.; Jewess, P. J.; Leworthy, D. P.; Pyrcce, R. J.; Arnold, E.; Clardy, J. *Phytochemistry* **1981**, *20*, 811.
- (40) Legler, G. *Adv. Carbohydr. Chem. Biochem.* **1990**, *48*, 319-384.
- (41) Ganem, B. *Acc. Chem. Res.* **1996**, *29*, 340-347.
- (42) Bols, M. *Acc. Chem. Res.* **1998**, *31*, 1-8.
- (43) Ichikawa, Y.; Igarashi, Y.; Ichikawa, M.; Suhara, Y. *J. Am. Chem. Soc.* **1998**, *120*, 3007-3018.
- (44) Bols, M.; Hazell, R. G.; Thomsen, I. B. *Chem. Eur. J.* **1997**, *3*, 940-947.
- (45) Tanaka, K. S. E.; Winters, G. C.; Batchelor, R. J.; Einstein, F. W. B.; Bennet, A. J. *J. Am. Chem. Soc.* **2001**, *123*, 998-999.

- (46) Takayama, S.; Martin, R.; Wu, J.; Laslo, K.; Siuzdak, G.; Wong, C.-H. *J. Am. Chem. Soc.* **1997**, *119*, 8146-8151.
- (47) Heightman, T. D.; Vasella, A. T. *Angew. Chem. Int. Ed.* **1999**, *38*, 750-770.
- (48) Williams, S. J.; Notenboom, V.; Wicki, J.; Rose, D. R.; Withers, S. G. *J. Am. Chem. Soc.* **2000**, *122*, 4229-4230.
- (49) Zechel, D. L.; Withers, S. G. *Acc. Chem. Res.* **2000**, *33*, 11-18.
- (50) Uitdehaag, J. C. M.; Mosi, R.; Kalk, K. H.; van der Veen, B. A.; Dijkhuisen, L.; Withers, S. G.; Dijkstra, B. W. *Nat. Struct. Biol.* **1999**, *6*, 432-436.
- (51) Williams, S. J.; Hoos, R.; Withers, S. G. *J. Am. Chem. Soc.* **2000**, *122*, 2223-2235.
- (52) Notenboom, V.; Williams, S. J.; Hoos, R.; Withers, S. G.; Rose, D. R. *Biochemistry* **2000**, *39*, 11553-11563.
- (53) Varrot, A.; Schulein, M.; Pipelier, M.; Vasella, A. T.; Davies, G. J. *J. Am. Chem. Soc.* **1999**, *121*, 2621-2622.
- (54) Frick, J.; Wolfenden, R. *Design of Enzyme Inhibitors as Drugs*; Sandler, M.; Smith, J. H., eds.; Oxford University Press: New York, 1989, p. 19.
- (55) Bartlett, P. A.; Mader, M. M. *Chem. Rev.* **1997**, *97*, 1281-1301.
- (56) Berland, C. R.; Sigurskjold, B. W.; Stoffer, B.; Frandsen, T. P.; Svensson, B. *Biochemistry* **1995**, *34*, 10153-10161.
- (57) Mosi, R.; Sham, H.; Uitdehaag, J. C. M.; Ruiterkamp, R.; Dijkstra, B. W.; Withers, S. G. *Biochemistry* **1998**, *37*, 17192-17198.
- (58) Ermert, P.; Vasella, A.; Weber, M.; Rupitz, K.; Withers, S. G. *Carbohydr. Res.* **1993**, *250*, 113-128.
- (59) Ly, H. D.; Withers, S. G. *Annu. Rev. Biochem.* **1999**, *68*, 487-522.
- (60) MacLeod, A. M.; Lindhorst, T.; Withers, S. G.; Warren, R. A. *Biochemistry* **1994**, *33*, 6371-6376.
- (61) Richard, J. P.; Huber, R. E.; Heo, C.; Amyes, T. L.; Lin, S. *Biochemistry* **1996**, *35*, 12387-12401.
- (62) MacLeod, A. M.; Tull, D.; Rupitz, K.; Warren, R. A. J.; Withers, S. G. *Biochemistry* **1996**, *35*, 13165-13172.
- (63) Lawson, S. L.; Wakarchuk, W. W.; Withers, S. G. *Biochemistry* **1997**, *36*, 2257-2265.
- (64) Wang, Q.; Trimbur, D.; Graham, R.; Warren, R. A. J.; Withers, S. G. *Biochemistry* **1995**, *34*, 14554-14562.

- (65) Wang, Q.; Withers, S. G. *J. Am. Chem. Soc.* **1995**, *117*, 10137-10138.
- (66) Burmeister, W. P.; Cottaz, S.; Driguez, H.; Iori, R.; Palmieri, S.; Henrissat, B. *Structure* **1997**, *5*, 663-675.
- (67) Burmeister, W. P.; Cottaz, S.; Rollin, P.; Vasella, A.; Henrissat, B. *J. Biol. Chem.* **2000**, *275*, 39385-39393.
- (68) Fierobe, H.-P.; Clarke, A. J.; Tull, D.; Svensson, B. *Biochemistry* **1998**, *37*, 3753-3759.
- (69) McIntosh, L. P.; Hand, G.; Johnson, P. E.; Joshi, M. D.; Korner, M.; Plesniak, L. A.; Ziser, L.; Wakarchuk, W. W.; Withers, S. G. *Biochemistry* **1996**, *35*, 9958-9966.
- (70) Richard, J. P. *Biochemistry* **1998**, *37*, 4305-4309.
- (71) Davies, G. J.; Mackenzie, L.; Varrot, A.; Dauter, M.; Brzozowski, A. M.; Schulein, M.; Withers, S. G. *Biochemistry* **1998**, *37*, 11707-13.
- (72) Sulzenbacher, G.; Driguez, H.; Henrissat, B.; Schulein, M.; Davies, G. J. *Biochemistry* **1996**, *35*, 15280-15287.
- (73) Tews, I.; Perrakis, A.; Oppenheim, A.; Dauter, Z.; Wilson, K. S.; Vorgias, C. E. *Nat. Struct. Biol.* **1996**, *3*, 638-648.
- (74) Vocadlo, D. J.; Davies, G. J.; Withers, S. G. *Nature* **2001**, In press.
- (75) Withers, S. G.; Rupitz, K.; Street, I. P. *J. Biol. Chem.* **1988**, *263*, 7929-7932.
- (76) McCarter, J. D.; Withers, S. G. *J. Am. Chem. Soc.* **1996**, *118*, 241-242.
- (77) McCarter, J. D.; Yeung, W.; Chow, J.; Dolphin, D.; Withers, S. G. *J. Am. Chem. Soc.* **1997**, *119*, 5792-5297.
- (78) Withers, S. G.; Aebersold, R. *Protein Sci.* **1995**, *4*, 361-372.
- (79) Withers, S. G.; Street, I. P. *J. Am. Chem. Soc.* **1988**, *110*, 8551-8553.
- (80) White, A.; Tull, D.; Johns, K.; Gilkes, N. R.; Withers, S. G.; Rose, D. R. *Nat. Struct. Biol.* **1996**, *3*, 149-154.
- (81) Vocadlo, D. J.; Mayer, C.; He, S. M.; Withers, S. G. *Biochemistry* **2000**, *39*, 117-126.
- (82) Zechel, D. L.; Withers, S. G. "Mechanisms of Glycosyl Transfer" in *Comprehensive Natural Products Chemistry*; Poulter, C. D., Ed.; Elsevier: New York, 1999; Vol. 5, pp 279-314.
- (83) Sulzenbacher, G.; Mackenzie, L. F.; Wilson, K. S.; Withers, S. G.; Dupont, C.; Davies, G. J. *Biochemistry* **1999**, *38*, 4826-33.
- (84) Notenboom, V.; Birsan, C.; Warren, R. A. J.; Withers, S. G.; Rose, D. R. *Biochemistry* **1998**, *37*, 4751-4758.

- (85) Notenboom, V.; Birsan, C.; Nitz, M.; Rose, D. R.; Warren, R. A. J.; Withers, S. G. *Nat. Struct. Biol.* **1998**, *5*, 812-818.
- (86) Cleland, W. W.; Kreevoy, M. M. *Science* **1994**, *264*, 1887-90.
- (87) Sidhu, G.; Withers, S. G.; Nguyen, N. T.; McIntosh, L. P.; Ziser, L.; Brayer, G. D. *Biochemistry* **1999**, *38*, 5346-5354.
- (88) Hosie, L.; Sinnot, M. L. *Biochem. J.* **1985**, *226*, 437-446.
- (89) Siuzdak, G. *Mass Spectrometry for Biotechnology*; Academic Press: San Diego, 1996.
- (90) Loo, J. A.; He, J. X.; Cody, W. L. *J. Am. Chem. Soc.* **1998**, *120*, 4542-4543.
- (91) Fenn, J. B.; Mann, M.; Meng, C. K.; Wong, S. F.; Whitehouse, C. M. *Science* **1989**, *246*, 64-71.
- (92) Mann, M.; Wilm, M. *Trends Biochem. Sci.* **1995**, *20*, 219-224.
- (93) Loo, J. A. *Mass Spectrom. Rev.* **1997**, *16*, 1-23.
- (94) Chowdhury, S. K.; Katta, V.; Chait, B. T. *J. Am. Chem. Soc.* **1990**, *112*, 9012-9013.
- (95) Miranker, A.; Robinson, C. V.; Radford, S. E.; Aplin, R.; Dobson, C. M. *Science* **1993**, *262*, 896-900.
- (96) Konermann, L.; Douglas, D. J. *Biochemistry* **1997**, *36*, 12296-12302.
- (97) Wood, T. D.; Chorush, R. A.; Wampler, F. M.; Little, D. P.; O'Connor, P. B.; McLafferty, F. M. *Proc. Natl. Acad. Sci. USA* **1995**, *92*, 2451-2454.
- (98) Clemmer, D. E.; Hudgins, R. R.; Jarrold, M. F. *J. Am. Chem. Soc.* **1995**, *117*, 10141-10142.
- (99) Collings, B. A.; Douglas, D. J. *J. Am. Chem. Soc.* **1996**, *118*, 4488-4489.
- (100) Konermann, L.; Collings, B. A.; Douglas, D. J. *Biochemistry* **1997**, *36*, 5554-5559.
- (101) Konermann, L.; Rosell, F. I.; Mauk, A. G.; Douglas, D. J. *Biochemistry* **1997**, *36*, 6448-6454.
- (102) Northrop, D. B.; Simpson, F. B. *Bioorg. Med. Chem.* **1997**, *5*, 641-644.
- (103) Cheng, X.; Chen, R.; Bruce, J. E.; Schwartz, B. L.; Anderson, G. A.; Hofstadler, S. A.; Gale, D. C.; Smith, R. D.; Gao, J.; Sigal, G. B.; Mammem, M.; Whitesides, G. M. *J. Am. Chem. Soc.* **1995**, *117*, 8859-8860.
- (104) Ganem, B.; Li, Y.-T.; Henion, J. D. *J. Am. Chem. Soc.* **1991**, *113*, 7818-7819.
- (105) Ashton, D. S.; Beddell, C. R.; Cooper, D. J.; Green, B. N.; Oliver, R. W. A.; Welham, K. J. *FEBS Lett.* **1991**, *292*, 201-204.

- (106) Knight, W. B.; Swiderek, K. M.; Sakuma, T.; Calaycay, J.; Shively, J. E.; Lee, T. D.; Covey, T. R.; Shushan, B.; Green, B. G.; Chabin, R.; Shah, S.; Mumford, R.; Dickinson, T. A.; Griffin, P. R. *Biochemistry* **1993**, *32*, 2031-2035.
- (107) Aplin, R. T.; Baldwin, J. E.; Schofield, C. J.; Waley, S. G. *FEBS Lett.* **1990**, *277*, 212-214.
- (108) Brown, R. P.; Aplin, R. T.; Schofield, C. J. *Biochemistry* **1996**, *35*, 12421-12432.
- (109) Brown, R. P.; Aplin, R. T.; Schofield, C. J.; Frydrych, C. H. *J. Antibiot. (Tokyo)* **1997**, *50*, 184-185.
- (110) Lee, E. D.; Muck, W.; Henion, J. D.; Covey, T. R. *J. Am. Chem. Soc.* **1989**, *111*, 4600-4604.
- (111) Paiva, A. A.; Tilton, R. F.; Crooks, G. P.; Huang, L. Q.; Anderson, K. S. *Biochemistry* **1997**, *36*, 15472-15476.
- (112) Northrop, D. B.; Simpson, F. B. *FASEB J.* **1997**, *11*, A1021.
- (113) Hiromi, K. *Kinetics of Fast Enzyme Reactions*; John Wiley & Sons: New York, 1979.
- (114) Fersht, A. *Structure and Mechanism in Protein Science: A Guide to Enzyme Catalysis and Protein Folding*; W.H. Freeman and Co.: New York, 1999.
- (115) Johnson, K. A. *Methods Enzymology* **1995**, *249*, 38-61.
- (116) Fierke, C. A.; Hammes, G. G. *Methods Enzymology* **1995**, *249*, 3-37.
- (117) Tull, D.; Withers, S. G. *Biochemistry* **1994**, *33*, 6363-70.
- (118) Gebler, J. C.; Trimbur, D. E.; Warren, R. A. J.; Aebersold, R.; Namchuk, M.; Withers, S. G. *Biochemistry* **1995**, *34*, 14547-14553.
- (119) Fink, A. L.; Angelides, K. J. *Biochem. Biophys. Res. Commun.* **1975**, *64*, 701-708.
- (120) Withers, S. G. *The Mechanism of Action of Glycosidases*, Ph.D. Thesis, Department of Chemistry, University of Bristol, 1977.
- (121) Deschavanne, P. J.; Viratelle, O. M.; Yon, J. M. *Proc. Natl. Acad. Sci. USA* **1978**, *75*, 1892-1896.
- (122) Hakulinen, N.; Paavilainen, S.; Korpela, T.; Rouvinen, J. *J. Struct. Biol.* **2000**, *129*, 69-79.
- (123) Miao, S.; Ziser, L.; Aebersold, R.; Withers, S. G. *Biochemistry* **1994**, *33*, 7027-7032.
- (124) Wakarchuk, W. W.; Campbell, R. L.; Sung, W. L.; Davoodi, J.; Yaguchi, M. *Protein Sci.* **1994**, *3*, 467-475.
- (125) Connelly, G. P.; Withers, S. G.; McIntosh, L. P. *Protein Sci.* **2000**, *9*, 512-524.

- (126) Joshi, M. D.; Sidhu, G.; Pot, I.; Brayer, G. D.; Withers, S. G.; McIntosh, L. P. *J. Mol. Biol.* **2000**, *299*, 255-279.
- (127) Ziser, L.; Setyawati, I.; Withers, S. G. *Carbohydr. Res.* **1995**, *274*, 137-153.
- (128) Kraunsoe, J. A.; Aplin, R. T.; Green, B.; Lowe, G. *FEBS Lett.* **1996**, *396*, 108-112.
- (129) Fabris, D. *J. Am. Chem. Soc.* **2000**, *122*, 8779-8780.
- (130) Bothner, B.; Chavez, R.; Wei, J.; Strupp, C.; Phung, Q.; Schneemann, A.; Siuzdak, G. *J. Biol. Chem.* **2000**, *275*, 13455-13459.
- (131) Gerber, S. A.; Scott, C. R.; Turecek, F.; Gelb, M. H. *J. Am. Chem. Soc.* **1999**, *121*, 1102-1103.
- (132) Lu, W. P.; Sun, Y. P.; Bauer, M. D.; Paule, S.; Koenigs, P. M.; Kraft, W. G. *Biochemistry* **1999**, *38*, 6537-6546.
- (133) Norris, A. J.; Whitelegge, J. P.; Faull, K. F.; Toyokuni, T. *Biochemistry* **2001**, *40*, 3774-3779.
- (134) Houston, C. T.; Taylor, W. P.; Widlanski, T. S.; Reilly, J. P. *Anal. Chem.* **2000**, *72*, 3311-3319.
- (135) Gross, J. W.; Hegeman, A. D.; Vestling, M. M.; Frey, P. A. *Biochemistry* **2000**, *39*, 13633-13640.
- (136) Stoll, D. *Characterization of the Mannan Degradation System of Cellulomonas fimi*, Ph.D. Thesis, Department of Microbiology, University of British Columbia, 1999.
- (137) Stoll, D.; Stalbrand, H.; Warren, R. A. *J. Appl. Environ. Microbiol.* **1999**, *65*, 2598-2605.
- (138) Stoll, D.; He, S.; Withers, S. G.; Warren, R. A. *J. Biochem. J.* **2000**, *351*, 833-838.
- (139) Brockhaus, M.; Dettinger, H.-M.; Kurz, G.; Lehmann, J.; Wallenfels, K. *Carbohydr. Res.* **1979**, *69*, 264-268.
- (140) Garegg, P. J.; Iversen, T.; Norberg, T. *Carbohydr. Res.* **1979**, *73*, 313-314.
- (141) Roush, W. R.; Bennett, C. E. *J. Am. Chem. Soc.* **1999**, *121*, 3541-3542.
- (142) Bielawska, H.; Michalska, M. *J. Carbohydr. Chem.* **1991**, *10*, 107-112.
- (143) Bielawska, H.; Michalska, M. *J. Carbohydr. Chem.* **1986**, *5*, 445-458.
- (144) Michalska, M.; Borowiecka, J. *J. Carbohydr. Chem.* **1983**, *2*, 99-103.
- (145) Edmundson, R. S. *Tetrahedron* **1965**, *21*, 2379-2387.
- (146) Borowiecka, J.; Michalska, M. *Carbohydr. Res.* **1979**, *68*, C8-C10.

- (147) Collins, P. M.; Ferrier, R. J. *Monosaccharides: Their Chemistry and Their Roles In Natural Products*; John Wiley and Sons: Toronto, 1995.
- (148) Fersht, A. *Enzyme Structure and Mechanism*; 2nd ed.; W.H. Freeman and Company: New York, 1985.
- (149) Malet, C.; Planas, A. *Biochemistry* **1997**, *36*, 13838-13848.
- (150) Zechel, D. L.; He, S.; Dupont, C.; Withers, S. G. *Biochem. J.* **1998**, *336*, 139-145.
- (151) Richard, J. P.; Huber, R. E.; Lin, S.; Heo, C.; Amyes, T. L. *Biochemistry* **1996**, *35*, 12377-12386.
- (152) Zhang, Y.; Bommuswamy, J.; Sinnott, M. L. *J. Am. Chem. Soc.* **1994**, *116*, 7557-7563.
- (153) Umezurike, G. M. *Biochem. J.* **1988**, *254*, 73.
- (154) Li, Y.-K.; Chir, J.; Chen, F.-Y. *Biochem. J.* **2001**, *355*, 835-840.
- (155) Crout, H. G.; Vic, G. *Curr. Opin. Chem. Biol.* **1998**, *2*, 98-111.
- (156) Davies, G. J. *Nat. Struct. Biol.* **2001**, *8*, 98-100.
- (157) Persson, K.; Ly, H. D.; Dieckelmann, M.; Wakarchuk, W. W.; Withers, S. G.; Strynadka, N. C. J. *Nat. Struct. Biol.* **2001**, *8*, 166-175.
- (158) Murray, B.; Shuichi, T.; Schultz, J.; Wong, C. *Biochemistry* **1996**, *35*, 11183-11195.
- (159) Murray, B. W.; Wittmann, V.; Burkart, M. D.; Hung, S.-C.; Wong, C.-H. *Biochemistry* **1997**, *36*, 823.
- (160) Qiao, L.; Murray, B.; Shimazaki, M.; Schultz, J.; Wong, C. *J. Am. Chem. Soc.* **1996**, *118*, 7653-7662.
- (161) Unligil, U. M.; Zhou, S. H.; Yuwaraj, S.; Sarkar, M.; Schachter, H.; Rini, J. M. *Glycobiology* **2000**, *10*, 103.
- (162) Charnock, S. J.; Davies, G. J. *Biochemistry* **1999**, *38*, 6380-6385.
- (163) Wong, C.-H.; Halcomb, R. L.; Ichikawa, Y.; Kajimoto, T. *Angew. Chem. Int. Ed. Engl.* **1995**, *34*, 521-546.
- (164) Ichikawa, Y.; Lin, Y.-C.; Dumas, D. P.; Shen, G.-J.; Garcia-Junceda, E.; Williams, M. A.; Bayer, R.; Ketcham, C.; Walker, L. E.; Paulson, J. C.; Wong, C.-H. *J. Am. Chem. Soc.* **1992**, *114*, 9283-9298.
- (165) Thiem, J.; Kren, V. *J. Am. Chem. Soc.* **1995**, *34*, 893-895.
- (166) De Luca, C.; Lansing, M.; Martini, I.; Crescenzi, F.; Shen, G.-J.; O'Regan, M.; Wong, C.-H. *J. Am. Chem. Soc.* **1995**, *117*, 5869-5870.

- (167) Endo, T.; Koizumi, S.; Tabata, K.; Kakita, S.; Ozaki, A. *Carbohydr. Res.* **1999**, *316*, 179-183.
- (168) Endo, T.; Koizumi, S.; Tabata, K.; Ozaki, A. *Appl. Microbiol. Biotechnol.* **2000**, *53*, 257-261.
- (169) Lougheed, B.; Ly, H. D.; Wakarchuk, W. W.; Withers, S. G. *J. Biol. Chem.* **1999**, *274*, 37 717-37 722.
- (170) Blanco, G.; Patallo, E. P.; Braña, A. F.; Trefzer, A.; Bechthold, A.; Rohr, J.; Méndez, C.; Salas, J. A. *Chem. Biol.* **2001**, *8*, 253-263.
- (171) Losey, H. C.; Peczuh, M. W.; Chen, Z.; Eggert, U. S.; Dong, S. D.; Pelczer, I.; Kahne, D.; Walsh, C. T. *Biochemistry* **2001**, *40*, 4745-4755.
- (172) Blixt, O.; Brown, J.; Schur, M. J.; Wakarchuk, W.; Paulson, J. C. *J. Org. Chem.* **2001**, *66*, 2442-2448.
- (173) Koeller, K. M.; Wong, C.-H. *Chem. Rev.* **2000**, *100*, 4465-4494.
- (174) Palcic, M. M. *Curr. Opin. Biotech.* **1999**, *10*, 616-624.
- (175) Wohlert, S.-E.; Blanco, G.; Lombo, F.; Fernandez, E.; Brana, A. F.; Reich, S.; Udvarnoki, G.; Mendez, C.; Decker, H.; Frevert, J.; Salas, J. A.; Rohr, J. *J. Am. Chem. Soc.* **1998**, *120*, 10596-10601.
- (176) Wong, C.-H.; Dumas, D. P.; Ichikawa, Y.; Koseki, K.; Danishefsky, S. J.; Weston, B. W.; Lowe, J. B. *J. Am. Chem. Soc.* **1992**, *114*, 7321-7322.
- (177) van der Veen, B. A.; Uitdehaag, J. C. M.; Dijkstra, B. W.; Dijkhuizen, L. *Biochim. Biophys. Acta* **2000**, *1543*, 336-360.
- (178) Mitchell, E. P.; Withers, S. G.; Ermert, P.; Vasella, A. T.; Garman, E. F.; Oikonomakos, N. G.; Johnson, L. N. *Biochemistry* **1996**, *35*, 7341-7355.
- (179) Vocadlo, D. J.; Withers, S. G. "Glycosidase Catalysed Oligosaccharide Synthesis" in *Carbohydrates in Chemistry and Biology*; Ernst, B., Hart, G. W. and Sinay, P., Ed.; Wiley-VCH GmbH: Weinheim, Germany, 2000; Vol. 2, pp 723-844.
- (180) Williams, S. J.; Withers, S. G. *Carbohydr. Res.* **2000**, *327*, 27-46.
- (181) Nidetzky, B.; Eis, C.; Albert, M. *Biochem. J.* **2000**, *351*, 649-659.
- (182) Kasumi, T.; Brewer, C. F.; Reese, E. T.; Hehre, E. J. *Carbohydr Res* **1986**, *146*, 39-49.
- (183) Mori, T.; Okahata, Y. *Tetrahedron Lett.* **1997**, *38*, 1971-1974.
- (184) Mori, T.; Fujita, S.; Okahata, Y. *Carbohydr. Res* **1997**, *298*, 65-73.

- (185) Ajisaka, K.; Matsuo, I.; Isomura, M.; Fujimoto, H.; Shirakabe, M. *Carbohydr. Res.* **1995**, *270*, 123-130.
- (186) Vic, G.; Crout, D. H. G. *Carbohydr. Res.* **1995**, *279*, 315-319.
- (187) Kobayashi, S.; Kiyosada, T.; Shoda, S. *J. Am. Chem. Soc.* **1996**, *118*, 13113-13114.
- (188) Singh, S.; Scigelova, M.; Crout, D. H. G. *Chem. Commun.* **1996**, 993-994.
- (189) Kobayashi, S.; Kashiwa, K.; Kawasaki, T.; Shoda, S. *J. Am. Chem. Soc.* **1991**, *113*, 3079-3084.
- (190) Takegawa, K.; Tabuchi, M.; Yamaguchi, S.; Kondo, A.; Kato, I.; Iwahara, S. *J. Biol. Chem.* **1995**, *270*, 3094-3099.
- (191) Fairweather, J. K.; Stick, R. V.; Tilbrook, D. M. G.; Driguez, H. *Tetrahedron* **1999**, *55*, 3695-3706.
- (192) Kuroki, R.; Weaver, L. H.; Matthews, B. W. *Proc. Nat. Acad. Sci., USA* **1999**, *96*, 8949-8954.
- (193) Padre, H.; Mackenzie, L. F.; Withers, S. G. *Carbohydr. Res.* **1997**, *305*, 371-381.
- (194) Mackenzie, L. F.; Wang, Q.; Warren, R. A. J.; Withers, S. G. *J. Am. Chem. Soc.* **1998**, *120*, 5583-5584.
- (195) Mackenzie, L. F.; Davies, G. J.; Schulein, M.; Withers, S. G. *Biochemistry* **1997**, *36*, 5893-901.
- (196) Mackenzie, L. F.; Brooke, G. S.; Cutfield, J. F.; Sullivan, P. A.; Withers, S. G. *J Biol Chem* **1997**, *272*, 3161-7.
- (197) Mackenzie, L. F.; Sulzenbacher, G.; Divne, C.; Jones, T. A.; Woldike, H. F.; Schulein, M.; Withers, S. G.; Davies, G. J. *Biochem J* **1998**, *335*, 409-16.
- (198) Johnson, P. E.; Brun, E.; MacKenzie, L. F.; Withers, S. G.; McIntosh, L. P. *J Mol Biol* **1999**, *287*, 609-25.
- (199) Trincone, A.; Perugino, G.; Rossi, M.; Moracci, M. *Biorg. Med. Chem. Lett.* **2000**, *10*, 365-368.
- (200) Malet, C.; Planas, A. *FEBS Lett.* **1998**, *440*, 208-212.
- (201) Fort, S.; Boyer, V.; Greffe, L.; Davies, G. J.; Moroz, O.; Christiansen, L.; Schülein, M.; Cottaz, S.; Driguez, H. *J. Am. Chem. Soc.* **2000**, *122*, 5429-5437.
- (202) Armand, S.; Vieille, C.; Gey, C.; Heyraud, A.; Zeikus, J. G.; Henrissat, B. *Eur. J. Biochem.* **1996**, *236*, 706-13.

- (203) Gabin, V.; Hastings, J. J.; Howarth, O. W.; Crout, D. H. G. *Tetrahedron: Asymmetry* **1996**, *7*, 709-720.
- (204) Blanchard, J.; Withers, S. G. *Chem. Biol.* **2001**, In Press.
- (205) Houseman, B. T.; Mrksich, M. *Angew. Chem. Int. Ed.* **1999**, *38*, 782-785.
- (206) Mayer, C.; Jakeman, D. L.; Mah, M.; Karjala, G.; Gal, L.; Warren, R. A. J.; Withers, S. G. *Chem. Biol.* **2001**, *8*, 437-43.
- (207) Dunitz, J. D.; Taylor, R. *Chem. Eur. J.* **1997**, *3*, 89-98.
- (208) Viladot, J.-L.; de Ramon, E.; Durany, O.; Planas, A. *Biochemistry* **1998**, *37*, 11332-11342.
- (209) Moracci, M.; Trincone, A.; Perugino, G.; Ciaramella, M.; Rossi, M. *Biochemistry* **1998**, *37*, 17262-17270.
- (210) O'Hagan, D.; Rzepa, H. S. *Chem. Commun.* **1997**, 645-652.
- (211) Hibbert, F.; Emsley, J. *Adv. Phys. Org. Chem.* **1990**, *26*, 255-379.
- (212) Barnett, J. E. G. *Carbohydr. Res.* **1969**, *9*, 21-31.
- (213) Sinnott, M. L.; Jencks, W. P. *J. Am. Chem. Soc.* **1980**, *102*, 2026-2032.
- (214) Sinnott, M. L.; Viratelle, O. M. *Biochem. J.* **1973**, *133*, 81-88.
- (215) Street, I. P.; Kempton, J. B.; Withers, S. G. *Biochemistry* **1992**, *31*, 9970-9978.
- (216) Gebler, J. C.; Aebersold, R.; Withers, S. G. *J. Biol. Chem.* **1992**, *267*, 11126-11130.
- (217) Vocadlo, D. J.; Mackenzie, L. F.; He, S.; Zeikus, G. J.; Withers, S. G. *Biochem. J.* **1998**, *335*, 449-445.
- (218) Dwek, R. A. *Chem. Rev.* **1996**, *96*, 683-720.
- (219) Vinogradov, D.; Petersen, B. O.; Duus, J. O. *Carbohydr. Res* **2000**, *325*, 216-221.
- (220) Trinel, P.-A.; Plancke, Y.; Gerold, P.; Jouault, T.; Delplace, F.; Schwarz, R. T.; Strecker, G.; Poulain, D. *J. Biol. Chem.* **1999**, *274*, 30520-30526.
- (221) Martinez, J. P.; Gil, M. L.; Lopez-Ribot, J. L.; Chaffin, W. L. *Clin. Microbiol. Rev.* **1998**, *11*, 121-141.
- (222) Lindberg, B.; Leontein, K.; Lindquist, U.; Svenson, S. B.; Wrangsell, G.; Dell, A.; Rogers, M. *Carbohydr. Res.* **1988**, *174*, 313-322.
- (223) Riggs, M. W.; McNeil, M. R.; Perryman, L. E.; Stone, A. L.; Scherman, M. S.; O'Connor, R. M. *Infect. Immun.* **1999**, *67*, 1317-1322.
- (224) Sugita, M.; Sanai, Y.; Itonori, S.; Hori, T. *Biochim. Biophys. Acta* **1988**, *962*, 159-165.

- (225) Barresi, F.; Hindsgaul, O. "Synthesis of  $\beta$ -D-Mannose Containing Oligosaccharides" in *Modern Methods in Carbohydrate Synthesis*; Khan, S. H. and O'Neill, R. A., Ed.; Harwood Academic Publishers: Amsterdam, 1996, pp 251-276.
- (226) Gridley, J. J.; Osborn, H. M. I. *J. Chem. Soc., Perkin Trans. I* **2000**, 1471-1492.
- (227) Paulsen, H.; Lebuhn, R.; Lockhoff, O. *Carbohydr. Res.* **1982**, *103*, C7-C11.
- (228) Lichtenthaler, F. W.; Klares, U.; Lergenmuller, M.; Schwidetzky, S. *Synthesis* **1992**, 179-184.
- (229) Ekborg, G.; Lindberg, B.; Lonngren, J. *Acta. Chem. Scan.* **1972**, *26*, 3287.
- (230) Alais, J.; David, S. *Carbohydr. Res.* **1990**, *201*, 69-77.
- (231) Gunther, W.; Kunz, H. *Carbohydr. Res.* **1992**, *228*, 217-241.
- (232) Barresi, F.; Hindsgaul, O. *Can. J. Chem.* **1994**, *72*, 1447-1465.
- (233) Ziegler, T.; Lemanski, G. *Angew. Chem. Int. Ed.* **1998**, *37*, 3129-3132.
- (234) Crich, D.; Sun, S. *Tetrahedron* **1998**, *54*, 8321-8348.
- (235) Scigelova, M.; Singh, S.; Crout, D. H. G. *J. Chem. Soc., Perkin Trans. I* **1999**, 777-782.
- (236) Taubken, N.; Thiem, J. *Glyconj. J.* **1998**, *15*, 757-767.
- (237) Usui, T.; Suzuki, M.; Sato, T.; Kawagishi, H.; Adachi, K.; Sano, H. *Glyconjugate J.* **1994**, *11*, 105-110.
- (238) Kyosaka, S.; Murata, S.; Tsuda, Y.; Tanaka, M. *Chem. Pharm. Bull.* **1986**, *34*, 5140-5143.
- (239) Revers, L.; Bill, R. M.; Wilson, I. B. H.; Watt, G. M.; Flitsch, S. L. *Biochim. Biophys. Acta* **1999**, *1428*, 88-98.
- (240) Watt, G. M.; Revers, L.; Webberley, M. C.; Wilson, I. B. H.; Flitsch, S. L. *Carbohydr. Res* **1998**, *305*, 533-541.
- (241) Watt, G. M.; Revers, L.; Webberlyey, M. C.; Wilson, I. B. H.; Flitsch, S. L. *Angew. Chem. Int. Ed.* **1997**, *36*, 2354-2356.
- (242) Zhao, Y.; Biggins, J. B.; Thorson, J. S. *J. Am. Chem. Soc.* **1998**, *120*, 12986-12987.
- (243) Zhao, Y.; Thorson, J. S. *Carbohydr. Res.* **1999**, *319*, 184-191.
- (244) Mayer, C.; Zechel, D. L.; Reid, S. P.; Warren, R. A. J.; Withers, S. G. *FEBS Lett.* **2000**, *466*, 40-44.
- (245) Bock, K.; Pedersen, C. *J. Chem. Soc., Perkin Trans. II* **1974**, 293-297.
- (246) Capon, B. *Chem. Rev.* **1969**, *69*, 407-498.

- (247) Wittmann, S.; Shareck, F.; Kluepfel, D.; Morosoli, R. *Appl. Environ. Microbiol.* **1994**, *60*, 1701-1703.
- (248) Sulzenbacher, G.; Shareck, F.; Morosoli, R.; Dupont, C.; Davies, G. J. *Biochemistry* **1997**, *36*, 16032-16039.
- (249) Torronen, A.; Kubicek, C. P.; Henrissat, B. *FEBS Lett.* **1993**, *321*, 135-139.
- (250) Wang, Q.; Tull, D.; Meinke, A.; Gilkes, N. R.; Warren, R. A. J.; Aebersold, R.; Withers, S. G. *J. Biol. Chem.* **1993**, *268*, 14096-14102.
- (251) Sinnott, M. L. *FEBS Lett.* **1978**, *94*, 1-9.
- (252) Vemuri, S.; Lee, T. D. *MacProMass*, Beckman Research Institute of the City of Hope, 1992.
- (253) Dorée, C. *The Methods of Cellulose Chemistry*; 2nd ed.; Chapman and Hall, Ltd.: London, 1947, p. 278.
- (254) Capon, B.; Rycroft, D. S.; Thomson, J. W. *Carbohydr. Res.* **1979**, *70*, 145-149.
- (255) Gribble, G. W. *Chem. Soc. Rev.* **1999**, *28*, 335-346.
- (256) Gribble, G. W. *Acc. Chem. Res.* **1998**, *31*, 141-152.
- (257) O'Hagan, D.; Harper, D. B. *J. Fluorine Chem.* **1999**, *100*, 127-133.
- (258) Cotton, F. A.; Wilkinson, G. *Advanced Inorganic Chemistry*; 5th ed.; John Wiley and Sons: New York, 1988.
- (259) Harper, D. B.; O'Hagan, D. *Nat. Prod. Rep.* **1994**, 123-133.
- (260) Butler, A. *Coord. Chem. Rev.* **1999**, *187*, 17-35.
- (261) Littlechild, J. *Curr. Opin. Chem. Biol.* **1999**, *3*, 28-34.
- (262) Hofmann, B.; Tölzer, S.; Pelletier, I.; Altenbuchner, J.; van Pée, K.-H.; Hecht, H. J. *J. Mol. Biol.* **1998**, *279*, 889-900.
- (263) van Pée, K.-H. *Annu. Rev. Microbiol.* **1996**, *50*, 375-399.
- (264) Sitachitta, N.; Rossi, J.; Roberts, M. A.; Gerwick, W. H.; Fletcher, M. D.; Willis, C. L. *J. Am. Chem. Soc.* **1998**, *120*, 7131-7132.
- (265) Hartung, J. *Angew. Chem. Int. Ed.* **1999**, *38*, 1209-1211.
- (266) van Pée, K.-H.; Keller, S.; Wage, T.; Wynands, I.; Schnerr, H.; Zehner, S. *Biol. Chem.* **2000**, *381*, 1-5.
- (267) *CRC Handbook of Chemistry and Physics*; 71st ed.; CRC Press: Boston, 1990-1991.
- (268) Wuosmaa, A. M.; Hager, L. P. *Science* **1990**, *249*, 160-162.

- (269) Keller, S.; Wage, T.; Hohaus, K.; Hölzer, M.; Eichhorn, E.; van Pée, K.-H. *Angew. Chem. Int. Ed.* **2000**, *39*, 2300-2302.
- (270) Hamilton, J. T. G.; Murphy, C. D.; Amin, M. A.; O'Hagan, D.; Harper, D. B. *J. Chem. Soc. Perkin Trans. I* **1998**, 759-767.
- (271) Reid, K. A.; Hamilton, J. T. G.; Bowden, R. D.; O'Hagan, D.; Dasaradhi, L.; Amin, M. R.; Harper, D. B. *Microbiology* **1995**, *141*, 1385-1393.
- (272) Hayden, B. M.; Dean, J. L. E.; Martin, S. R.; Engel, P. C. *Biochem. J.* **1999**, *340*, 555-560.
- (273) Nashiru, O.; Zechel, D. L.; Stoll, D.; Mohammadzadeh, T.; Warren, R. A. J.; Withers, S. G. *Angew. Chem. Int. Ed.* **2001**, *40*, 417-419.
- (274) Olmstead, W. N.; Brauman, J. I. *J. Am. Chem. Soc.* **1977**, *99*, 4219-4228.
- (275) Parker, A. J. *J. Chem. Soc.* **1961**, 1328-1337.
- (276) Pearson, R. G.; Songstad, J. *J. Org. Chem.* **1967**, *32*, 2899-2900.
- (277) Bennet, A. J.; Sinnott, M. L. *J. Am. Chem. Soc.* **1986**, *108*, 7287-7294.
- (278) Gerlt, J. A.; Babbitt, P. C. *Curr. Opin. Chem. Biol.* **1998**, *2*, 607-612.
- (279) O'Brien, P. J.; Herschlag, D. *Chem. Biol.* **1999**, *6*, R91-R105.
- (280) Song, Y.; Yang, C.; Kluger, R. *J. Am. Chem. Soc.* **1993**, *115*, 4365-4366.
- (281) Benkovic, S. J.; Lutz, S. *Curr. Opin. Biotech.* **2000**, *11*, 319-324.
- (282) Griffiths, A. D.; Tawfik, D. S. *Curr. Opin. Biotech.* **2000**, *11*, 338-353.
- (283) Cedrone, F.; Ménez, A.; Quéméneur, E. *Curr. Opin. Struct. Biol.* **2000**, *10*, 405-410.
- (284) Petrounia, I. P.; Arnold, F. H. *Curr. Opin. Biotech.* **2000**, *11*, 325-330.
- (285) Quéméneur, E.; Moutiez, M.; Charbonnier, J.-B.; Ménez, A. *Nature* **1998**, *391*, 301-304.
- (286) Altamirano, M. M.; Blackburn, J. M.; Aguayo, C.; Fersht, A. R. *Nature* **2000**, *403*, 617-622.
- (287) MacBeath, G.; Kast, P.; Hilvert, D. *Science* **1998**, *279*, 1958-1961.
- (288) Matsui, H.; Tanaka, Y.; Brewer, C. F.; Blanchard, J. S.; Hehre, E. J. *Carbohydr. Res.* **1993**, *250*, 45-56.
- (289) Kuroki, R.; Weaver, L. H.; Matthews, B. W. *Nat. Struct. Biol.* **1995**, *2*, 1007-1011.
- (290) Kuroki, R.; Weaver, L.; Matthews, B. W. *Science* **1993**, *262*, 2030-2033.
- (291) Kuroki, R.; Weaver, L. H.; Matthews, B. W. *Proc. Natl. Acad. Sci. USA* **1999**, *96*, 8949-8954.
- (292) Leatherbarrow, R. J. *GraFit 4.014*, Erithacus Software, Ltd., 2001.

- (293) Konermann, L. *J. Phys. Chem. A* **1999**, *103*, 7210-7216.
- (294) Lindsay, D. G.; Reese, C. B. *Tetrahedron* **1965**, *21*, 1673-1680.
- (295) Wohl, R. A. *Synthesis* **1974**, 38-40.
- (296) Gelas, J.; Horton, D. *Carbohydr. Res.* **1978**, *67*, 371-387.
- (297) Namchuk, M. *Spontaneous and Glycosidase Catalyzed Hydrolyses of Deoxy and Deoxyfluoro  $\beta$ -Glycosides*, Ph.D. Thesis, Department of Chemistry, University of British Columbia, 1995.
- (298) Berven, L. A.; Withers, S. G. *Carbohydr. Res.* **1986**, *156*, 282-285.
- (299) Iversen, T.; Johansson, R. *Synthesis* **1979**, 823-4.
- (300) *LoggerPro 1.1*, Vernier Software and Tufts University ([www.vernier.com](http://www.vernier.com)), 1999.
- (301) Wolfram, S. *Mathematica 3.0*, Wolfram Research, Inc. ([www.wolfram.com](http://www.wolfram.com)), 1996.
- (302) Ortner, J.; Albert, M.; Weber, H.; Dax, K. *J. Carbohydr. Chem.* **1999**, *18*, 297-316.
- (303) Vincent, S. P.; Burkart, M. D.; Tsai, C.-Y.; Zhang, Z.; Wong, C.-H. *J. Org. Chem.* **1999**, *64*, 5264-5279.
- (304) McCarter, J. D.; Adam, M. J.; Braun, C.; Namchuk, M.; Tull, D.; Withers, S. G. *Carbohydr. Res.* **1993**, *249*, 77-90.
- (305) Gill, S. C.; von Hippel, P. H. *Anal. Biochem.* **1989**, *182*, 319-326.
- (306) Jünemann, J.; Thiem, J.; Pedersen, C. *Carbohydr. Res.* **1993**, *249*, 91-94.
- (307) Csuk, R.; Glänzer, B. I. *Adv. Carbohydr. Chem. Biochem.* **1988**, *46*, 73-177.